Factors Limiting the In-Service Lifetime of CrMoV Steels and Weldments for Pressure Equipment

Giustino Manna

Submitted to the University of Wales in fulfilment of the requirements for the Degree of Doctor of Philosophy

University of Wales Swansea

2004

Supervisors: Prof. B. Wilshire and Prof. R. Hurst

This work was granted by the European Commission and conducted at the Institute for Energy of the Joint Research Centre of the European Commission, Petten, The Netherlands, while the author was registered as student of the School of Engineering, The University of Wales Swansea.

MISSING PAGE/PAGES HAVE NO CONTENT

ORIGINAL COPY TIGHTLY BOUND

The following have been redacted at the request of the awarding university:

On page 2-1 (Figures)

Figure 2.2-1:Variation of methane pressure with fugacity in the temperature range from 473 to 873K [Odette, 1982].

On page 2-2 (Figures)

Figure 2.2-4: Stress Rupture Curves for SAE 1020 Steel at 811K (1000F) in argon atmosphere and in hydrogen atmosphere at 20.67MPa (900 psi) pressure [Allen, 1962a].

On page 2-3 (Figures)

Figure 2.2-5: Ductility loss due to hydrogen attack, given as variation in reduction in area. The specimens had been exposed to hydrogen at 873K (600°C) and pressures of 15MPa (150bar) or 23MPa (230bars) [Bocquet, 2001].

Figure 2.2-6: Schematic Illustration showing the process of bubble growth and failure of grain boundary [Sakai, 1981].

On page 2-4 (Figures)

Figure 2.2-7: Activity of carbon and dilatometric strain rates at 823K (550°C), as function of the tempering parameter [Shewmon, 1985].

Figure 2.2-8: Ductile shearing of ligaments between cavities in a carbon steel after exposure of 245 hours at 6.2MPa $H2$ and 810K (537°C) [Allen, 1961].

On page 2-5 (Figures)

Figure 2.3-2: Carbides transformation occurring in 2.25Cr-1Mo steel, as result of ageing phenomena [Tsai, 2003].

On page 2-6 (Figures)

Figure 2.4-1: Stress dependence of rupture life of 2.25Cr-1Mo base metal, weld metal, course-grain HAZ, fine-grain HAZ, intercritical HAZ and weld joint at 823 K [Laha, 2000].

On page 2-8 (Figures)

Table 2-1: Materials of construction for hydroprocessing reactors [Antalffy, 1994].

On page 4.4-1 (Figures)

Figure 4.4-1: Scheme of the second coupon of 2.25Cr-1Mo-V

On page 4.5-1 (Figures)

Figure 4.5-1: Drawing of the uniaxial sample.

Summary

"Factors Limiting the In-Service Lifetime of CrMoV Steels and Weldments for Pressure Equipment"

PhD, 2004, University of Wales Swansea

Giustino Manna

This research project addresses the factors limiting the lifetime of industrial components for pressure equipment used in particular in the petrochemical industry but also strongly linked conventional energy production plants.

Hydrogen attack, and the combined effect of both creep and hydrogen attack, are the key phenomena forming the object of study. These are frequently the cause of damage and catastrophic failures, with huge economic impact on the affected plants.

As the study is of industrial relevance, tests representative of the industrial reality have been carried out under simulated conditions. Three steels have been selected: the standard 2.25Cr-1Mo steel, which is the conventional commercial steel used for the construction of pressure vessels for petrochemical plants; the V-modified 2.25 Cr-1Mo steels, which represents the steel of new generation pressurized equipment; and the V-modified 3Cr-1Mo, which is also a newly designed alloy for pressure equipment use. Each of these materials was supplied with an industrial scale weldment and each test piece contained weld material.

The experimental part of the thesis, which included, among the others, tests on tubular specimens pressurized with high-temperature hydrogen or argon, has been realized using the unique hydrogen creep facilities available at the Institute for Energy of the Joint Research Centre. Moreover, interrupted creep tests, mainly carried out in hydrogen, allowed to gain more insight into the evolution of the damage in the different metallurgical zones of the chosen weldments. The tested specimens underwent extended microstructural characterization by means of optical microscope, scanning electron and transmission electron microscopes.

Whilst the sample made of V-modified 3Cr-1Mo steel failed in the base metal, those made with standard 2.25Cr-1Mo steel, or with its V-modified grade, exhibited Type IV failure, in both hydrogen and air. Based on the synergies between hydrogen attack and creep, conclusions on the evolution of the damage and the steps leading to failure are drawn. Hydrogen attack, however limited for more resistant steels, is still expected to contribute to premature failure in the weldments, and great care should be taken when introducing even improved steels into hydrogen bearing environments.

DECLARATION

This work has not previously been accepted in substance for any degree and is not being concurrently submitted in candidature for any degree.

Signed (candidate)

Date

STATEMENT 1

This thesis is the result of my own investigations, except where otherwise stated.

Other sources are acknowledged by footnotes giving explicit references. A bibliography is appended.

Signed (candidate)

Date

STATEMENT 2

I hereby give consent for my thesis, if accepted, to be available for photocopying and for inter-library loan, and for title and summary to be made available to outside organisations.

Signed (candidate)

Date

To Karla and our Lois Maria,
and also to my father and my mother

Table of Contents

List of Figures and Tables

Acknowledgements

This thesis is one of the achievements of a period of my life lived with great passion and enthusiasm. It had been possible thanks to a research fellowship granted by the European Commission. I really loved what I had been doing, and enjoyed doing it with the people I met at the Institute for Energy of the Joint Research Centre, whilst I was registered as Ph.D.-student at the University of Wales Swansea.

From each of these people I got a contribution to my research project and, more broadly, to my human experience and development. Towards each of them, I feel gratitude.

In particular I feel indebted towards:

Prof. Roger Hurst, my supervisor at the Institute for Energy of the Joint Research Centre, for the valuable scientific advice during the entire research project and for the strong and incisive support provided during the drafting of this manuscript.

Prof. Brian Wilshire, whose persuasion and support have been decisive for the finalization of my work. Prof. Wilshire taught me "in one hour" how to write a Ph.D. Thesis, let us hope I followed his advice.

Dr. Paolo Castello, for the great scientific support provided since the beginning of this study as co-supervisor at the Institute for Energy. I really appreciated the rigour of his approach and the tact always used in dealing with people.

Dr. Jean-Bernard Veyret, my previous Unit Head, Juha-Pekka Hirvonen, the Director of the Institute for Energy of the JRC, Prof. Kari Törrönen, for the deployment of all the resources necessary for this research. Furthermore, I am grateful to Jean-Bernard for his always energizing and motivating words.

Freek Harskamp, for the invaluable technical support for the set up of the experiments in hydrogen; Rene` Van der Aat, for the technical support for the set up of the creep tests in air; Rob Smit, for the general support during the set-up of the experiments. From Freek I learned the complex procedures for the operation of the creep rigs in hydrogen; from Rene`, the procedure for setting up a creep test in air.

Mark Wallendorf, Jesus Pozuelo Moreno, Klaas Smit, Ari Schipper, Paul Green, for the drawing and preparation of the test pieces, and for

Dr. Pietro Moretto, for the scientific advice on microstructural investigations; Elsa Conceiçao, for the support during SEM investigations; Paul Tambuyser and Miguel Prieto, for the support provided during the TEM investigation; Peter Frampton, for the preparation of the innumerable samples for SEM and optical microscope observation.

A particular thanks goes to Kurt Schuster, for the effective training on scanning electron microscopy and, again, to Peter Frampton, for the training on optical microscopy. Without these skills, the main findings of this thesis would have been not achieved.

Lango Metten, Alan van de Sande, JoJo Oudaert, for the performance of X-ray inspection on the tubular and uniaxial test pieces.

This study was also enriched by the co-operation with the other research groups, in particular the AMES [1] group. Explicitly, I want to thank:

Dr. Soraia Pirfo, for the passionate and enthusiastic co-operation on the applicability of the Magnetic Barkhausen Noise technique to the detection of hydrogen attack in steels.

Dr. Beatriz Acosta, for the application of the STEAM (Seebeck and Thomson Effect on Aged Materials) method for the detection of the hydrogen attack damage.

Arlindo Rito de Abreu, Chris McGirl, Mart Beers, for the support they gave for carrying out some Charpy V-notch tests and the Vickers hardness measurements.

Dr. Luigi Debarberis, Project Leader of SAFELIFE [2], for the enthusiastic active support to the realization of joint proposals of exploratory research, for fostering my development, and, most of all, for his friendship.

My research benefited also of the scientific discussions with:

Henrik J. Rantala, of whom I appreciate the scientific curiosity and the generosity in sharing his knowledge and experience with others.

Dr. Ferenc Gillemot, Dr. Milan Brumoski and Dr. Alexander Kryukov, for the scientific discussions concerning impact tests. I am also grateful to Dr. Gillemot and Dr. Kryukov, for the encouragements to complete and submit this thesis.

Dr. Peter Haenher for the scientific discussions on the tensile properties of the steels, and Stephan Ripplinger, for the assistance during the performance of some preliminary tensile tests.

I am grateful to Usinor Industeel, for having provided the materials tested in this study.

I am also grateful to my Unit Head, Dr. Michel Bièth, and to the TSSTP [3] Coordinator of the on-site assistance nuclear safety projects for Russia, Jean-Louis Monjaret, for their encouragement to finalize this work, and for inspiring the enlargement of my views to other research fields.

I am greatly indebted towards Luciano Fabbri, who influenced my life to such great extent. Luciano believed I would have succeeded, and his beliefs strengthened mines. To him go my friendship and my limitless gratitude.

I want to thank my mother and my sister, Melissa, and the friends of always, in particular Paolo Fabbri and Vito Faretina, for their constant presence, in spite of the distance. Thanks also to Franco di Persio, Luca Gandossi, Lois Brett and everyone else within the social circle.

Finally, most of all, I want to thank Karla Gramberg, the woman who is enriching my life since 4 years, for her love and constant support, for her deep understanding of human nature and for what I learned from her during these years of great achievements.

[1] AMES=Ageing Materials European Strategy
[2] SAFELIFE (EC Framework Programme 6, WP2004, Action n. 3132), is an integrated project, including AMES
[3] TSSTP= Technical and Scientific Support to TACIS and PHARE

1 Introduction

This section summarizes the main material issues found in the petrochemical industry and in the production of reactor pressure vessels, placing particular emphasis on the need for new materials.

~o~

Processes such as hydrocracking, desulphurisation, hydrogen treating and chemical synthesis of ammonia operate in conditions where the structural steels of hydroprocessing equipment are exposed to high pressures of hydrogen at temperatures above 573K (300°C). The industrial need to continuously improve productivity and efficiency of plant operations, and to meet environmental controls, increases the demand for large size reactors and more severe service conditions [Tahara, 1994]. In particular, the construction of coal gasification and liquefaction processes, proposed as an answer to the energy crisis, resulted in heavier requirements for the structural steels [Norris, 1976]. Coal conversion processes may require massive pressure vessels (40 m high, 6 m in diameter, 300-400 mm wall thickness), to be suitable for processes involving hydrogen and hydrogen sulphide gases at pressures up to 20 MPa and temperatures in the range 723-1173K (450-900 °C) [Todd, 1983]. Moreover, the construction of ultra super critical fossil power plants requires structural steels able to withstand a temperature of 873K (600 °C), which would produce, as additional beneficial effect, a considerable reduction in CO_2 emissions [Albert, 2004].

The structural steels of hydroprocessing equipment, exposed to high pressures of hydrogen and temperatures above 573K (300°C), may appear unaffected for long periods, even for years. Then, in a relatively short time, they can exhibit degradation of mechanical properties, mainly toughness and ductility, and, as a consequence, fail without warning [Kim, 2002]. The cause of this behaviour is a phenomenon of degradation called "hydrogen attack", which arises from the nucleation, growth and coalescence of methane bubbles to form fissures, mainly along the grain boundaries [Shewmon, 1985].

The phenomenon of hydrogen attack was discovered about 80 years ago in Germany, during the development of the process for the chemical synthesis of ammonia. Since then,

it has been a subject of major concern to the petroleum industry, which started to build large pressure vessels for the hydrogenation of feedstock. Afterwards, the construction of large plant for the gasification of coal extended the interest in the subject to another sector [Shewmon, *ibidem*]. In this way, the industrial failures due to hydrogen attack are an integral part of the wider category of failures due to hydrogen damage, where related accidents had been estimated in the USA as equivalent to about 100 billion dollars/year and are responsible for several deaths and many injuries of workers [Timmins, 1997; Kim, 2002].

The basis of the steel selection for the design of equipment operating in the presence of hot, high-pressurized hydrogen, are the Nelson curves, published for the first time in 1951 and occasionally updated. They collect data available from industrial experience and indicate the pressure-temperature ranges in which certain steels may be used without experiencing hydrogen attack [API, 1997]. These empirical curves are occasionally revised and, as a consequence, service equipment earlier considered safe could be unsafe. Besides, the Nelson diagrams give no information about new materials.

Selected on the basis of its overall characteristics, the standard (or conventional) 2.25Cr-1Mo steel, had been the material used for almost all the hydroprocessing reactors built during the 30 years up to the end of the 1990's. This structural steel is not suitable for design temperatures beyond 727K (454°C). For pressure vessels designed for temperatures higher than 727K (454°C), in accordance with ASME Sec. VIII, the design stress value is governed by creep rupture stress and rapidly decreases at higher temperatures, leading to the need for very thick walls, in some cases more than 500mm thick, which make it difficult for welding, NDE, transportation and erection. The transportation is mainly made by barge or ship, but the transportation from the fabrication shop to the ship loading facilities is usually made by multi-wheeled transport. Even then, most ports do not have facilities to lift a 9MN (~895 tonne) load off a ship [Antalffy, 1994].

Another problem found in heavy structures made of 2.25Cr-1Mo steel is the variation in microstructure and mechanical properties on quenching, due to the limited rates of heat

transfer. The formation of polygonal ferrite at the quarter and centre thickness locations, causes the deterioration of hardenability and mechanical properties.

The need for higher design stress intensity values, resulting in reduced wall thickness reactors, had been the driving force to develop new structural steels. Besides, the operating conditions of the new industrial processes require steels having good resistance to creep, hydrogen attack, hydrogen embrittlement and fatigue, combined with good weldability and toughness. For these applications, new grades of vanadium modified 2.25%Cr and 3% Cr steels were introduced during the 1990's.

The knowledge about the in-service behaviour of these alloys and particularly their respective weldments is still incomplete, so further study is necessary to define the boundary of the service conditions in which the use of the industrial components made of these materials is safe. These needs led several partners, representative of all the chain, from the steel producer to the end user (the petroleum companies), to integrate their research efforts in the Brite/Euram Project 1835 (PREDICH). The aim of this European consortium, conducted by Usinor Industeel (the previous name was Creusot-Loire Industrie), was to acquire data for the evaluation of the lifetime of pressure vessels made with new steels.

The scientific contribution of the Institute for Energy (the previous name was Institute for Advanced Materials) of the Joint Research Centre of the European Commission to the PREDICH Project consisted mainly in the work of Baker [1999; 2000] on the synergistic effects of creep and hydrogen attack in the standard 2.25Cr-1Mo steel, now extended through the present work. Whilst Baker's research was focused on the behaviour in creep and hydrogen attack conditions of the 2.25 Cr-1Mo steel, as base metal, the present study explores the damage mechanisms which intervenes in the prescribed conditions in the welded joints made of conventional and new structural low-alloy steels.

This thesis was prepared for a Doctoral Dissertation at the University of Wales Swansea. The thesis may be useful as a reference book for scholars aimed at investigating the degradation of steels in high-temperature conditions and, in particular, in presence of hydrogen. This study is also intended for a broader audience in the engineering sciences.

It is hoped that researchers in fields such as materials science, metallurgy, fossil and petrochemical plant engineering, NDT methodologies, as well as field engineers and plant managers, will find this work useful.

2 Literature Review

2.1 Evolution of Structural Steels for Hydroprocessing Reactors

The previous section introduced the main issues of the petrochemical sector and its need for more advanced materials. The following section will brief the reader about the evolution of hydroprocessing reactors, which is not limited to material advances but includes advances in design, fabrication, inspection and testing. Some of the alloys hereafter mentioned had been tested in the present work.

~o~

2.1.1 Historical Background

The evolution of modern reactor technology is in general traced back to the mid 1920's, when quenched and tempered chrome-molybdenum steels came in use in Germany for the production of reactors of high-pressure hydrogenation plants for the conversion of coal in transport fuels and of plants for ammonia synthesis. In the former process, the service temperatures ranged between 673 and 823K (400-550°C) with hydrogen pressures up to 69 MPa (690 bars). In the latter process, the temperatures ranged between 573 and 873K (300-600°C), and the pressure of hydrogen ranged between 21 MPa (210bars) and 96 MPa (960 bars) [Shewmon, 1985]. Since that period, the maximum pressures have been decreased and the lifetime of the equipment increased.

After a few decades of experience, the 2.25Cr-1Mo steel, mainly in the annealed conditions, appeared to be the most suitable for such industrial applications. The first large hydrocracking reactors, made of annealed 2.25Cr-1Mo steel, were built in 1955. During the 1960's, Chevron, together with several pressure vessels suppliers, carried out a development programme, with the purpose of assessing the suitability of 2.25Cr-1Mo, in quenched and tempered conditions, for the production of hydrocracking reactors. In 1966, eight reactors built with this material were put into service.

The 2.25Cr-1Mo steel had been predominantly used for reactor fabrication up to the end of the 1990's. In the 1980's, in the framework of worldwide programmes such as

API/MPC [4] in USA, NEDO [5] and JWES [6]/ECM in Japan, studies on Cr-Mo steels with higher design stress and excellent resistance to hydrogen attack were carried out [Tahara, 1990s]. In the middle of the 1980's, the Japan Steel Works started the development of the 3Cr-1Mo-0.25V alloy and, in 1989, the first two commercial reactors had been put into service in Alberta, Canada. Meanwhile, the development work on 2.25Cr-1Mo-0.25V steel was carried out. In 1997, Nuovo Pignone completed the fabrication of the first two hydroprocessing reactors made with this steel. Today, more than 100 reactors, already built or in the fabrication stage, are made of V-modified 3Cr-1Mo and 2.25Cr-1Mo alloys, which are expected to dominate the market of the hydroprocessing reactors for the next several decades [Antalffy, 2002].

The fifth generation of hydroprocessing reactor technology, that of the 1990's, uses operating conditions ranging from 673K (400°C), with 10.3MPa hydrogen partial pressure to above 755K (482°C), with corresponding hydrogen partial pressures up to 34.5MPa [Antalffy, 1994]. The newly developed hydroprocessing processes, most of which are not yet commercialised, require more severe operating conditions. In the petro-chemical industry, an issue is the increase of the efficiency of conventional chemical plants and build up of coal liquefying plants [Tsuchida, 2004]. Higher temperatures are already in use in the power generation sector, where the steam operation equipment works at temperatures higher than 811K (538°C). For these applications, alloys with higher chromium content had been developed and used, in particular the 9Cr-1Mo-V (Grade 91), the 9Cr-2W and the 12Cr-2W steels.

2.1.2 Performance of Cr-Mo Steels

On the basis of what has been mentioned, it is evident that the petrochemical sector achieved up to now a wide experience of the performances of the 2.25Cr-1Mo in the current hydroprocessing conditions. Wide experience had been also accumulated with respect to the material fabrication and welding technology. Antalffy *et al* [2002] report that, at the present time, the toughness at 233K (–40°C), measured on the standard

[4] API=American Petroleum Institute; MPC=Materials Properties Council
[5] NEDO=New Energy and Industrial Technology Organization
[6] JWES=Japan Welding Engineering Society

2.25Cr-1Mo steel by the Charpy V- Notch (CVN) test, is 54J for the base metal, the weld metal and the heat-affected zone (HAZ). For the new generation 2.25Cr-1Mo-0.25V and 3Cr-1Mo-0.25V steels, the authors refer that the same requirements are met for the base metal and the HAZ, whilst for the weld metal the minimum achievable toughness is at 244K (–29°C). For hydroprocessing applications, and taking in consideration the hydrogen attack phenomenon, the American Petroleum Institute (API) prescribes the temperature limitations of 755K (482°C) for 2.25Cr-1Mo steel, and 783K (510°C) for 2.25Cr-1Mo-0.25V, 3Cr-1Mo and 3Cr-1Mo-0.25V.

2.1.3 In-service Degradation Phenomena Affecting Cr-Mo Steels

Two main forms of hydrogen degradation occur in the hydroprocessing reactors, and they are universally known as hydrogen attack and hydrogen embrittlement [Antalffy, 1994, 2002].

The hydrogen embrittlement is a phenomenon occurring below 422K (149°C), during shutdown conditions. The consequent cracking, also called delayed cracking, is due to the hydrogen concentration accumulated in the reactor steels at service temperatures and pressures, and may occur when the reactor is cooled down too quickly to allow the outgassing of the steel. The 2.25Cr-1Mo and 3Cr-1Mo steels with high strength (higher than 758MPa) are more sensitive to the phenomenon than lower strength steels. Conversely, the hydrogen attack is a phenomenon registered at higher temperatures, above 573K (300°C).

These forms of hydrogen degradation set limits for the maximum operating temperature and strength level of the steels used for the vessel fabrication. The publication API 941 [1997] sets the safe limits for 2.25Cr-1Mo hydroprocessing reactors at 727K (454°C) and at partial pressures higher than 13.8MPa. For the 3Cr-1Mo and the V-modified 2.25Cr-1Mo and 3Cr-1Mo steels, the temperature limit is set at 783K (510°C), whilst the 9Cr and 12Cr alloys mentioned above are not susceptible to hydrogen attack at the design temperature of 839K (566°C).

The V-modified steels are less sensitive to hydrogen attack and, in a certain measure, to hydrogen embrittlement [e.g. Bocquet, 2001; Gingell, 2001]. The reason for this is that the finely dispersed vanadium carbides, precipitated into the alloy, tend to trap the hydrogen, reducing its diffusivity into the steel. This effect is more apparent in the low Cr alloys than in the 9Cr and 12 Cr steels. Besides, the vanadium addition to the 2.25Cr-1Mo and 3Cr-1Mo steels reduces their inherent susceptibility to the phenomenon of temper embrittlement, which occurs when alloy steels are held within or cooled slowly through the embrittling temperature range of 643-828K (370-555°C), and whose major effect is the increase in ductile to brittle transition temperature.

2.1.4 Thermal Treatments

During the fabrication of components for hydroprocessing plants, the Cr-Mo steels undergo different thermal treatments: dehydrogenation heat treatment (DHT), intermediate stress relieving (ISR) and post-weld-heat-treatment (PWHT). The DHT and ISR remove the hydrogen absorbed in the weld metal during the welding process and, in addition, the ISR reduces the weld metal stresses. For low Cr-Mo steels a DHT at 589K (316°C) is practised for unrestrained joints such as circumferential girth joints. An ISR at 894K (621°C) is usually carried out for restrained joints, such as nozzle to shell welds. For vanadium-modified steels, the ISR is necessary to prevent cold cracking.

The PWHTs both relieve weld metal stresses and temper the steels in such a way to confer the required properties. For the standard 2.25Cr-1Mo alloy, the final PWHT is usually set at 964K (691°C) whilst, for vanadium-modified low-chrome alloys, it is set at 991K (718°C). The welding experience on 2.25Cr-1Mo steel taught that the toughness in the weld metal could be improved by increasing the time for PWHT [Berzolla, 1994]. However, other authors [e.g. Bocquet, 2001] warn that increasing the PWHT has a detrimental effect on other mechanical properties (e.g. creep resistance).

2.1.5 *Pressure Vessels Protection Against the Internal Corrosion*

To be suitable to operate in aggressive service conditions, the hydroprocessing reactors must be protected from high-temperature corrosion, due to the presence of sulphur in the process. The most common form of protection adopted in thick wall reactors is a stainless steel weld overlay over the base metal, having a nominal 18%Cr 8%Ni composition. Different combinations of overlay compositions have given good results. The current industry practice, in the production of Cr-Mo reactors, is the use of a two-pass stainless steel overlay combination of type 309L and a type 347 final pass [Antalffy, 2002].

A sensitive related problem, encountered in the hydroprocessing reactors, is weld overlay debonding. The phenomenon, observed in some cases of reactor cool-down, is characterized by a cracking along the interface transition zone between the weld overlay and the Cr-Mo base metal. The tendency for debonding seems to increase when the hydrogen partial pressures, the operating temperatures and the cooling rates are increased. The crack propagation is mainly registered in zones where the carbide precipitation mostly occurs, i.e. along the grain boundaries in the overlay near the interface with the base metal. Differently from the conventional low Cr-Mo steels, the modern vanadium-modified 2.25Cr-1Mo and 3Cr-1Mo steels do not exhibit a great susceptibility to the weld overlay debonding. This is another advantage of these steels, and underpins their use and exploitation.

2.1.6 *Details of Construction of hydroprocessing Reactors*

Because the welds exhibit lower creep rupture strength than the base metal, to eliminate any potential risk due to this difference, the purchase specifications of the steel reactors usually incorporate the following requirements [Andersson, 1994; Tahara, 1994].

- Heavy wall pressure vessels are one-piece and fabricated from forged shell rings, in order to minimize weld seams. In this way, the delivery time and the shut down time for maintenance inspection are reduced. Besides, the machined shell forging, which allows fully mechanized welding processes, permits more accurate

dimensional control, which is an advantage for weight control, since it has to respect transportation restrictions

- The shell forging allows the elimination of highly stressed longitudinal weld seems.
- Girth joints of cylindrical shells and heads are usually welded by means of narrow gap submerged arc welding techniques
- The PWHT is targeted to achieve a good balance between strength, toughness and hardness of the finished reactor.
- The hardness should be controlled: the maximum acceptable value for hydrogen service is HV250 (238 BHN) [Andersson, 1994].

Most of these requirements are also adopted for the construction of reactor pressure vessels (RPV) for nuclear power plants [AMES, 1997]. All the RPVs of nuclear power plants built in eastern as in western European countries use low-alloy ferritic steels with bainitic microstructure [AMES, *ibidem*].

2.2 Hydrogen Attack: A Comparative Review

The previous section provides some information about the design of the reactor pressure vessels and the evolution of their structural materials. This section presents a review of the hydrogen attack, one of the two forms of hydrogen degradation in reactor steels. The combined effect of hydrogen attack and creep constitute the subject of the present work.

~ o ~

2.2.1 The Effect of Hydrogen on Steels

Hydrogen plays an important role in hydroprocessing reactors. This element may be introduced into steel during pickling, electroplating, melting, heat treating and welding. It may also enter during the operation of structures in hydrogen atmosphere at elevated temperatures. Two different forms of steels degradation had been identified: the attack at low temperature, below 422K (149°C), which affects mainly high-strength steels, and the high-temperature hydrogen attack, or simply hydrogen attack. Both these forms of degradation produce embrittlement of the steel and reduction of strength. Whilst the low-temperature hydrogen attack produces a reversible embrittlement, which can be recovered by annealing, the high-temperature hydrogen attack, from now reported in the present work as hydrogen attack, may damage the material permanently [Allen, 1961].

Recent studies have pointed out suitable hypotheses concerning the effect of hydrogen on the mobility of the dislocations. By performing compression test at 923K (650°C) on 2.25Cr-1Mo steel, hydrogenated up to 4.5wt.ppm, and strain rates of 5%/h and 10%/h, it has been found that, at the lower strain rate, a remarkable decrease of the compressive mechanical properties of the steel is observed, which led to a surprising softening effect. It is suggested that the presence of hydrogen in the 2.25Cr-1Mo steel favours the movement of dislocations and, consequently, the process of recovery [Zander, 2003]. These findings may add further understanding of the processes occurring in CrMoV steels, during exposure to hot high-pressurized hydrogen, in the presence of superimposed stresses.

2.2.2 *Generalities on Hydrogen Attack*

Early fundamental work had been performed on this subject by: Inglis, Naumann, Schuyten, Nelson, Ciuffreda, Weiner [Inglis, 1933; Naumann, 1937; Schuyten, 1947; Nelson, 1955; Ciuffreda, 1957, Weiner, 1961]. The main aspects of the damage are:

- Loss of strength and ductility
- Decarburisation
- Formation of microscopic cracks and fissures
- Blistering

The formation of fissures and blisters is believed to be due to the formation of methane, which cannot diffuse through the steel and, consequently, is trapped giving rise to high localized pressures. Hydrogen attack exhibits two main features: the surface decarburisation and the internal decarburisation. The latter leads to [Sundararajan, 1980, 1981; Erwin, 1982]:

- The formation along the grain boundaries of cavities, which are believed to be methane-filled bubbles
- The bubble growth, driven by the methane pressure
- Their link-up into fissures

With respect to the formation of creep cavities in metals, an extensive recent review is that of Kassner and Hayes [2003], to which the present work will refer further. The authors conclude that the mechanism by which cavities nucleate (independently of environmental factors) is still not well established, although it is universally accepted that the grain boundaries, in particular those oriented transverse to the acting stress, represent preferential sites for the nucleation. Kassner and Hayes also mention that, according to recent studies, the creep cavitation of metals appears to be a continuous process without incubation time. The same authors conclude that it is still not clear if the cavity growth, at high temperature and along the grain boundaries, is controlled by diffusion and flow of vacancies, even though much of the earlier literature has suggested the vacancy diffusion

is involved in the process of cavity growth [Kassner, *ibidem*]. The growth and link-up of cavities, in the presence of hydrogen attack, are governed by the so-called *methane reaction*.

2.2.3 *The Methane Reaction*

It is well known that hydrogen attack occurs in the presence of carbon in the steel. In the absence of carbon, the attack cannot occur [Thoma, 1966]. In fact, the driving force for cavity growth is essentially the internal methane pressure, because the internal and external hydrogen pressures are approximately equal, as a result of the high hydrogen diffusivity [Sagüés, 1978]. It is not possible to draw any valid conclusion about the mechanism of hydrogen-attack-induced bubble growth, if the pressure driving the bubble expansion is not known. The growth of the bubbles is a slow-rate phenomenon. Consequently, it is assumed that, at high temperature, the equilibrium methane pressure is achieved inside the bubbles. On the other hand, when the bubbles coalesce to form fissures, the existence of an equilibrium pressure is less clear [Shewmon, 1985]. The same consideration is valid at lower temperatures, when the formation of methane is slow.

The equation of the reaction

The methane formation is due to the reaction between carbon and hydrogen:

$$yC_{(s)} + 2yH_{2(g)} \rightarrow yCH_{4(g)} \qquad \text{Eq. 2.2-1}$$

Where y indicates the number of moles. However, within steel, most of the carbon is tied up in carbides and, thus the reaction equation should be written as:

$$^{1}/_{y}M_xC_{y(s)} + 2H_{2(g)} \rightarrow CH_{4(g)} + {}^{x}/_{y}M_{(s)} \qquad \text{Eq. 2.2-2}$$

where M_xC_y is the metal carbide present in the steel. This reaction can be split into two parts, to simplify the thermodynamic calculations:

1. That of carbide dissolution ($M_xC_y \rightarrow xM + yC$);

2. That of the methane reaction itself [Eq. 2.2-1].

The growth rate of bubbles increases monotonically with the methane pressure in the bubble at a given temperature and hydrogen pressure. The rate of methane formation varies linearly with carbon activity. Consequently, the bubble growth rate should be proportional to carbon activity [Sundararajan, 1980].

The methane pressure and the methane fugacity

The first kinetic models assumed the methane pressure to be equal to the methane fugacity. As a result of this assumption, the predicted methane pressures were very high and the common conclusion was that the bubbles grow by creep [Shewmon, 1985]. As reported by Shewmon, the equation of state for methane, developed by Odette and Vagarali, is described by the equation:

$$f_m = P_m \exp[C(T)P_m] \qquad \textbf{Eq. 2.2-3}$$

Where

$$C(T) = \frac{2.375}{T} + 1.78\times10^{-3} \qquad f_m > 10^4\,MPa$$

$$C(T) = \frac{1.187}{T} + 3.09\times10^{-3} \qquad 10^3 < f_m < 10^4\,MPa$$

$$C(T) = 0.005 \qquad f_m < 10^3\,MPa$$

The relationship between methane pressure and methane fugacity is plotted, for different temperatures, in Figure 2.2-1. This shows that at low hydrogen pressures and high temperatures the log-log plot approaches the slope of $P_m \sim P_H^2$, which is indicative of an ideal gas behaviour. In contrast, at high hydrogen pressures and low temperatures, methane behaves as a non-ideal gas and its pressure becomes independent of P_{H2}, which means that there is a nearly pressure-independent behaviour for hydrogen attack. For Fe_3C, the fugacity of methane is given by the equation

$$\ln f_m = -13.3 + \frac{13700}{T} + 2\ln P_H \qquad \text{Eq. 2.2-4}$$

Where P_H is the hydrogen pressure and hydrogen is assumed to behave ideally.

Rate controlling factors of the methane reaction

Hydrogen diffusion is not expected to be a rate-controlling factor, because it is too rapid and it takes only a few seconds for the element to diffuse from the surface to the centre of the samples. The rapidity of the hydrogen diffusion explains the simultaneous attack throughout the entire volume of the sample [Allen, 1962b]. The rate of diffusion of carbon, and the rate at which the carbides are decomposed, are expected to control the rate of methane reaction.

2.2.4 *Surface Decarburisation*

Steels exposed to hot high-pressurised hydrogen experience the phenomenon of decarburisation. As shown by Figure 2.2-2, the surface directly exposed to hydrogen environment experiences a phenomenon of pure decarburisation and, as a consequence, a low density of cavities is registered. It is argued by some scholars [e.g. Baker, 2000] that surface decarburisation and cavitation are competitive processes. In fact, in the case of pure cavitation, the bubbles contain the equilibrium methane pressure, methane forms slowly and there is little decarburisation of the surrounding matrix. For the surface exposed to hydrogen, the formation of methane can take place outside the steel. Furthermore, if there are fissures, especially if the fissures communicate with the external surface, the methane can vent to the surface and forms as rapidly as carbon can diffuse to the fissure surface. In this case, the decarburisation of the regions around the fissures proceeds rapidly [Shewmon, 1985]. The decarburised layer has a thickness depending on:

- The operational (or testing) conditions
- The composition of the steel
- The history of the steel (treatment received, eventual cold work, etc.)

- The geometry of the component (e.g. the thickness)
- Surface finish

Assuming that surface decarburisation due to hydrogen attack is limited by carbon diffusion to the free surface, Erwin [1982] used the following equation, solution for one-dimensional diffusion in a semi-infinite medium, to determine the diffusion coefficient:

$$C(x,t) = C_o \times erf(\frac{x}{2\sqrt{Dt}}) \qquad \textbf{Eq. 2.2-5}$$

Where

x = distance from free surface
t = time
D = diffusion coefficient
C_o = initial carbon concentration in the steel
C(x,t) = carbon concentration at a distance x, for time t
erf = mathematical error function

The temperature dependence of decarburisation is included in Eq. 2.2-5 within the diffusion coefficient:

$$D = D_o \exp(-\frac{Q}{RT}) \qquad \textbf{Eq. 2.2-6}$$

Where

D = diffusion coefficient
D_o = constant
Q = activation energy
T = absolute temperature
R = ideal gas constant

A value for the diffusion coefficient of carbon in iron is provided by the work of Wert [1950], who finds Q equal to 84100 J/mole and D_o equal to 0.02 cm^2/s.

The equation for a semi-infinite medium is applicable to thick-wall reactor vessels, in which diffusion is really one-dimensional and the ratios of vessel length (or circumference) to wall thickness are approximately infinite. In the real situation of a reactor pressure vessel, the structural steel does not come in direct contact with the aggressive environment. The thick-wall reactor pressure vessels are usually internally clad with stainless steel, up to 7 inch thick (~18cm). However, Erwin [1982] showed that the presence of the stainless steel cladding does not prevent decarburisation at temperatures where it is expected to occur.

2.2.5 *Bulk Decarburisation*

Bubble and fissure formation

The other effect of hydrogen attack is internal decarburisation. For example, 2.25Cr-1Mo steel exposed at 20.67 MPa pressurized hydrogen, at temperatures of 769 and 783K (496 and 510°C), exhibited a decrease in the carbon content of the bulk, which produced a reduction of the yield and tensile strength [Erwin, 1982]. Furthermore, Yokogawa *et al* [1989], registered a marked decrease in the carbon content of a low carbon steel (0.011%C, 0.01%Si, 0.32%Mn), exposed to hydrogen at 773K (500°C) and a pressure of 9.9MPa (99 bars), until a final constant value was reached.

The internal decarburisation leads to the formation of methane that cannot escape outside the steel and, for this reason, is trapped to form cavities which are methane-filled bubbles. The formation of cavities takes place mainly along grain boundaries. The growth and coalescence of bubbles nucleated along grain boundaries produces fissures, which are much larger than the original bubbles and can be also detected by naked-eye inspection, especially in the case of severe attack [Sakai, 1980; Erwin, 1982]. The strength of the steel matrix and the cohesion of the grain boundaries, due to the presence of suitable alloying elements, account for the incubation time before the bubbles grow to a size sufficient to degrade the mechanical properties and to be reliably detected by non-

destructive examination techniques [Shewmon, 1985]. On the basis of its morphology and effects, this form of attack had been divided into three different stages.

1. *First Stage*. The first stage does not affect the mechanical properties of the steel and is characterized by the nucleation and growth of bubbles, without coalescence. This stage is referred, after Vitovec [1982], as *the incubation period.*

2. *Second Stage*. In the second stage, the bubbles coalesce to form grain boundaries fissures which initially are about as long as the grain diameter and can then extend to many diameters in length forming fracture paths that produce a substantial loss of mechanical properties [Sundararajan, 1980].

3. *Third Stage*. In the third stage, the material is heavily deteriorated and a saturation of the degradation is registered.

Several investigations have been devoted to the incubation stage, because it is generally believed that the hydrogen attack kinetics depends strongly on the bubble density [Parthasarathy, 1987]. The first investigations go back to the end of the 1970's and the early 1980's, when very sensitive dilatometers (strain sensitivity less than 10^{-5}) and high magnification microscopes became available.

- Hakkarinen *et al* [1980] reported that the nucleation may occur in a few hours and they proved that at most the nucleation can happen in a few weeks, depending on temperature, hydrogen pressure and applied stress.

- Sundararajan and Shewmon [1980], who measured the sample expansion rate due to the methane-filled bubble formation, found that, for all the steels they tested, the expansion started immediately, once the example was exposed to high hydrogen pressures and temperatures. Consequently, they argued for the presence in the samples of pre-existing voids, which start to grow in less than 1-2 hours, when the samples are exposed to hydrogen. The work of Sundararajan and Shewmon provides the first data available in the literature on the kinetics of the incubation period.

- Hakkarainen *et al* [Hakkarainen, *ibidem*][7], with the transmission electron microscope, observed bubbles having dimension of 0.02-0.1 μm, then too small to be detected even with the scanning electron microscope

- Shewmon [1985] reports that a sensitive nucleation of bubbles was registered in carbon steels exposed to a pressure of hydrogen of 20MPa at temperatures higher than 648K (375°C). He also agrees on the pre-existence of voids in samples made of quenched and tempered (QT) 2.25Cr-1Mo steel, which become filled with methane, if exposed to a hydrogen pressure of 20MPa at 773K (500°C). The author did not register nucleation of additional bubbles in the base metal, weld metal and heat affected zone (HAZ) of this steel [Shewmon, *ibidem*]. According to this reference, the only work that shows evidence of nucleation of bubbles in 2.25Cr-1Mo steel, is the work of Thygeson and Molstad who exposed the steel at 773K (500°C) and a pressure of 100MPa.

- Also Yokogawa *et al* [1989] support the thesis that methane forms in micro-pores already present into the steel.

As a result of what has been reported, it is possible to argue that the nucleation of additional bubbles can take place in the Cr-Mo steels, but under pressures significantly higher than those able to induce nucleation in carbon steels. Because the hydrogen attack resistance of a steel is shown by the density of bubbles formed, when exposed in hot hydrogen environment, the higher resistance of the 2.25Cr-1Mo steels, with respect to carbon steels, is attributed to the fact that the former steels develop less bubbles than the latter ones [Parthasarathy, 1987].

Erwin [1982] pointed out that an important factor to be considered is the grain size: as the bubbles tend to form preferentially along grain boundaries, the smaller the grain dimension, the higher the planar grain boundary area and the higher the extent of the nucleation. Differently from other scholars, Erwin believes that the key issue is not the nucleation of bubbles, but rather the bubble density, the bubble size and the rate of bubble growth. According to this author, the major question is to understand under which

[7] The reader will note the limitations imposed by the SEM technology of 24 years ago!

conditions in steel the bubbles grow so slowly that they never coalesce to form fissures, so that the steel is always in the incubation stage. He used two parameters to characterize the extent of the bubbles formation: the average diameter and the average planar density (total number of bubbles on the total sampled area). Figure 2.2-3 shows the variation of the average bubble diameter as function of the time of exposure, for two different temperatures.

In the bare specimens exposed by Erwin, the bubble size was found to increase with the temperature and the exposure time. The cladding did not affect the size of the bubbles. In the case of steels having a ferrite and pearlite structure, the density of bubbles on ferrite/pearlite grain boundaries was higher than the density of bubbles along the ferrite/ferrite grain boundary. In the case of steels having an upper bainite structure, the bubbles formed along the prior-austenite grain boundaries.

Rate of Bubble Growth.

With the purpose of extrapolating the testing results to long times, several authors correlate the rate of bubble growth to the strain attributable to the bubble growth [Sagüés, 1978; Sundararajan, 1980; Erwin, 1982]. For this strain, Erwin suggests the relation:

$$E = D\pi \cdot \left(\frac{d}{2}\right)^2 \qquad \textbf{Eq. 2.2-7}$$

Where

E = strain attributable to bubble growth
D = planar bubble density
d = average bubble diameter

The equation measures a two-dimensional strain, whilst Sundararajan and Shewmon measure a linear strain and Sagüés a volume strain. The mentioned investigators [Sagüés; Sundararajan; Erwin; *ibidem*] report that the bubble growth exhibits two forms of behaviour. In a first stage, the growth of isolated bubbles is registered. In this stage, the strain is linearly proportional to time. In the second stage, the strain increases

exponentially with time. Sundararajan and Shewmon [1980] believe that this stage corresponds to the bubble coalescence. Because, in the first stage, the bubbles grow isolated, their growth is not influenced by neighbour cavities. For this reason, the bubble growth rate, Ė, is expected to depend only on temperature and hydrogen pressure. Assuming the bubble growth be a thermally activated process, Erwin used the equation suggested by Yu and Shewmon:

$$\dot{E} = A(P_{H_2})^n e^{(-\frac{Q}{RT})}$$

Eq. 2.2-8

Where:

Ė = linear bubble growth rate with time
P_{H2} = hydrogen partial pressure
T = absolute temperature
Q = activation energy
R = ideal gas constant
A,n = constants

In the reported testing conditions, Erwin found for Q the value of 113kJ/mole, a value which is in disagreement with the value found by Yu and Shewmon: 209±37.6 kJ/mole. Erwin found also that the presence of cladding does not change the bubble growth rate [Erwin, *ibidem*] and, since the clad is expected to decrease the concentration of hydrogen in the steel, the author suggested that the methane bubble formation is not rate-limited by the hydrogen concentration in the steel.

The total driving force for the bubble growth is [Shewmon, 1985]:

$$F = (P_m + \sigma_n - \frac{\gamma}{a})$$

Eq. 2.2-9

Where

P_m = the pressure of methane

σ_n = the static stress acting normally to the grain boundary and due to the applied stress

a = the bubble radius

γ = is the surface tension

γ/a = is the tension pressure

If the material undergoes creep, this will accelerate the bubble growth. According to Shewmon [1985], Dyson found that in a sample undergoing creep the voids form only on a fraction of the grain boundaries, and, if this fraction is small, there is a "cage" of grains with uncavitated boundaries surrounding the cavitated boundary. This group of uncavitated grains may act as a constraint for the cavitated boundaries. This is called the "cage effect". Shewmon argues that, in case of hydrogen attack of Cr-Mo steels, more resistant to the attack and to creep than the carbon steels, the cage effect may be present. But he reports that, on the contrary, Parthasarathy believes that for hydrogen attacked commercial Cr-Mo steels, the fraction of boundaries with bubbles is sufficiently high that the cage effect does not exist.

Shewmon also reports that, by means of very sensitive dilatometer, the growth rate of the bubbles had been found to be:

$$\dot{\varepsilon} = CP_H^n \exp(-\frac{Q_H}{RT}) \qquad \textbf{Eq. 2.2-10}$$

Where

P_H = the pressure of hydrogen. If the pressure of methane is used, the equation becomes:

$$\dot{\varepsilon} = CP_m^a \exp(-\frac{Q_m}{RT}) \qquad \textbf{Eq. 2.2-11}$$

Where P_m is the methane pressure. Q_m contains only the temperature dependence of the diffusion process limiting the motion of iron atoms, while Q_H contains both the temperature dependence and the dependence of methane pressure on temperature at constant hydrogen pressure [Shewmon, *ibidem*].

The Effect of Microstructure and Composition on the Bubble Formation

As reported by Erwin [1982], two important factors are responsible for low rates of methane bubble growth in 2.25Cr-1Mo steel:

1. The presence of stable carbides.
2. The high creep strength of quenched and tempered bainitic steel containing 1 % molybdenum.

As reported by other authors [Van der Burg, 1996], the presence of carbides in the steel subtracts carbon to the matrix, and, the higher the carbide thermodynamic stability, the lower the carbide rate of dissolution in the matrix. Thus, stable carbides tie up the carbon, which is then not available for the reaction of methanation. Furthermore, the fully bainitic microstructure of the quenched and tempered 2.25Cr-1Mo steel exhibits higher creep resistance than normalized and tempered steels, where a significant amount of ferrite is present. In this respect, Lundin *et al* [1984] found in the literature enough evidence about the contribution of Mo to the formation of the bainitic phase of the steel, and on the fact that one weight percent molybdenum in solution is sufficient to saturate the dislocation network, which is expected to have an additional impact on the creep properties.

According to Erwin [1982], the growth of methane-filled bubbles may be hindered by the development of an elastic back-stress around isolated bubbles. The higher the creep strength, the higher the magnitude of this resisting stress. Moreover, Erwin reports the rate of stress-induced bubble growth in quenched and tempered 2.25Cr-1Mo to be about 10 times slower than in the normalized and tempered conditions. Sundararajan and Shewmon [1981] interpreted the link between Mo additions and the increase in creep strength on the basis of the assumption that Mo does not have an effect on the activity of carbon in the steel. This assumption appears refuted by the WRC Bulletin 315 [Lundin, 1984], which underlines the high affinity of Mo for C, which makes the molybdenum a strong carbide former.

2.2.6 *The Kinetics of Hydrogen Attack*

Up to the beginning of the 1980's, two main works had been carried out with the purpose of characterizing the kinetics of hydrogen attack also in the incubation period:

1. The work of Sagüés *et al* [1978].
2. The work of Sundararajan and Shewmon [1980].

The former authors built and used a highly sensitive dilatometer to study the rate of hydrogen attack, measured by the swelling rate, for specimens exposed to various hydrogen pressures and temperatures; the latter studied the kinetics of the early period in three high-strength low alloy (HSLA) steels, in 2.25Cr-1Mo steel and in carbon steel, using a high-sensitivity capacitance dilatometer. The main findings of these authors can be summarized as follows:

- The early period is characterized by a linear dependence of the expansion rate from the exposure time. According to Sundararajan and Shewmon, this period is due to the growth of isolated methane-filled bubbles.
- After the early period, the accelerating expansion period (or accelerating swelling period, as it was called by Sagüés *et al*) proceeds at a rate that is approximately exponential in time. Sundararajan and Shewmon correlate this behaviour to the link-up of bubbles.
- The point of passage between the early stage and the accelerating stage is termed breakaway expansion after Sundararajan and Shewmon, whereas Sagüés and co-workers arbitrarily defined it as the time required to reach a swelling value of 10^{-4}.
- Under the testing conditions, respectively P=6.2MPa, T=748K (475°C), and P=21MPa, T=623-783K (350-510°C), the breakaway expansion is found respectively after 40 hours and less than 40 hours.
- If the hydrogen pressure or the temperature is changed, the expansion, after a transition period, continues at a new rate without any delay. If the temperature is

brought back to the same initial value, after some variation, substantially the same expansion rate is obtained.

Sagüés *et al* ascribe three regimes:

1. *Low T (~548K) or high P_{H2} (3.10MPa)*. The calculated methane pressures are below the equilibrium value and the cavities grow by creep;
2. *Intermediate T (~648K) and P_{H2} (1.55MPa).* The calculated methane pressure is the equilibrium pressure and decreases with T. The growth rate is creep-controlled and decreases as the temperature increases;
3. *High T (748K) and P_{H2} (3.10MPa).* Methane is present at low equilibrium pressures. The rate-controlling mechanism, especially when the bubbles are small, is the grain-boundary diffusion.

The existing models proposed up to the beginning of the 1980's, to explain the kinetics of hydrogen attack, can be divided into:

- Grain boundary diffusion controlled models.
- Power-law dislocation-creep-controlled bubble growth model.

Grain boundary models predict bubble growth rates which vary linearly with methane pressure, suggesting that the creep strength of the material has no effect on the growth rate itself. The material between bubbles remains elastic and the bubble growth occurs by diffusion of the material away from the bubble. The creep-controlled models predict growth rates that are strongly dependent on both methane pressure and bubble radius. These models are inadequate to explain the data obtained for both the carbon and low alloy steels, with respect to the incubation period [Sundararajan, 1981]. According to the reference, this is because the models are not complete and they assume that the surface diffusion of Fe atoms along the cavity surface, and the thickening of the cavitated grain boundary, are too rapid to be rate controlling. The difference between the two models, is that, for the former, the bubble growth rate is not influenced by the creep of the material; differently, for the latter, the bubble growth is by creep of the surrounding material, not only by diffusional growth [Chen, 1995].

2.2.7 *The Nelson Curves*

The limits of hydrogen pressure and temperature at which carbon and certain low alloy steels could be employed safely are defined by the Nelson diagrams [API, 1997], published for the first time in 1951 and occasionally updated [Norris, 1976]. They are empirical diagrams, based on the data available from industrial experience, and indicate, for different steels, the range of temperature and pressure in which hydrogen attack has been observed. These diagrams are still the main reference for the design of systems and components that operate in presence of hydrogen, and are revised to more conservative limits every time new failures are reported. These revisions have a huge economic impact on the industry and, besides, the Nelson curves are not applicable to the design of systems employing newly developed alloys. To overcome the inherent weaknesses of these empirical curves, a mechanistic understanding of the hydrogen attack is required. For this purpose, it is necessary to characterize the effect of hydrogen pressure, temperature and stress on the incubation and development of the attack [Sagüés, 1978].

2.2.8 *Factors Influencing the Effect of Hydrogen Attack on Steels*

Dependence of Hydrogen Attack on Pressure

The dependence of hydrogen attack on hydrogen pressure is clearly expressed by the Nelson curves, which, as said, describe for a given steel the Temperature/Pressure domain where the hydrogen attack occurs. The line bounding this region changes slope remarkably by passing from low to high pressures. In fact, hydrogen attack has been not observed in carbon steel for hydrogen partial pressures lower than 1MPa [Shewmon, 1985]. Shewmon *et al* [1980] devoted a study to this topic80]. They showed that the increase in pressure speeds up the attack and can change the morphology of the initial stage of it. As reported by Erwin [1982], the hydrogen attack process is dependent on pressure. Allen [1961] considers that the effect of pressure on the rate of the hydrogen attack is temperature dependent, and given by the equation:

$$t = \frac{K}{P^n} \exp(\frac{Q}{RT}) \qquad \textbf{Eq. 2.2-12}$$

Where

t = exposure time for 50 per cent of the property change

K,n = constants

P = hydrogen partial pressure

Q = activation energy

R = gas constant

T= absolute test temperature in degrees Kelvin

In case of creep tests in hydrogen, it was observed, as a general trend, the decrease of ductility with increasing hydrogen pressure and, at high stresses, the small influence on strength caused by variations of hydrogen pressure [Allen, 1962a]. This finding is consistent with the more recent views of Zander *et al* [2003], who suggest that hydrogen favours the movement of dislocations.

Sutherland *et al* [1965] also carried out a systematic study on the effect of pressure on hydrogen attack. They investigated the effects of pressure and applied stress on the rate of attack in 0.5% Mo steel and 1%Cr-0.5%Mo steel, reporting that the rupture lives of the Mo-steel specimens are progressively reduced by an increase of the hydrogen pressure on all the range of pressure investigated, up to 9.6 MPa (96bars). This effect is marked in the presence of low-applied stresses and small in the presence of high-applied stresses. The behaviour of the 1Cr-0.5Mo steel is found similar, but slightly different, to that of the 0.5% Mo steel, because no further reduction of the rupture time is registered by the authors for hydrogen pressures higher than 6.2MPa (62 bar).

The testing of SAE 1020 steel shows the dependence of the incubation period on the hydrogen pressure. It is found that, at 811K (538°C), and at a hydrogen pressure of 2.8MPA (28bars), the incubation period for this steel extends beyond 250 hours, whereas it becomes 30 hours in hydrogen at 6.2MPA (62 bars) [Coombs, 1965].

More recently, Chen and Shewmon [1995] showed that the pressure of hydrogen plays a determinant role on the growth of cracks in steel samples exposed to hydrogen, and that the crack rate drops when the hydrogen pressure is reduced, whilst maintaining constant temperature. More recent studies, carried out at the Institute for Energy of the Joint Research Centre on tubular specimens made of 2.25Cr-1Mo pressurized with hydrogen, provided further coherent data on the influence of stress and hydrogen pressure on the steel, confirming that stresses enhance the hydrogen attack [Baker, 2000].

The dependence of hydrogen attack on pressure is, of course, influenced by temperature. This is expressed by the equation of Odette and Vagarali [1982], which graphically shows that for hydrogen pressures higher than 2MPa (20bars) and for low temperatures, just above 573K (300°C), the methane pressure is high but about independent from the hydrogen pressure. Consequently, also for hydrogen attack, a pressure independent behaviour is expected [Shewmon, 1985].

Dependence of Hydrogen Attack on Temperature

The incubation time of the attack decreases rapidly when the temperature increases. Corresponding to a certain hydrogen pressure, there is a temperature below which the incubation time exceeds the life of the component, so no hydrogen attack is detected [Shewmon, 1985]. Chen [1995] reports that prior studies show that the processes of creep and diffusion, producing crack growth, are thermally activated and exhibit an exponential dependence on temperature and a linear dependence on time. As already mentioned (see Eqs. 2.2-5,6), the exponential dependence of the carbon diffusion on temperature was reported by Erwin [1982]. Furthermore, the Eqs. 2.2-8,10,11 [Shewmon, 1985] show that an increase in temperature determines an increase in the growth rate of the bubbles, and Eq. 2.2-12 [Allen, 1961] presents an exponential dependence on the inverse of temperature of the time needed for a marked reduction of the mechanical properties of the steel.

Dependence of Hydrogen Attack on the Applied Stress

Some alloy steels, resistant to hydrogen attack in the unstressed condition, are readily attacked when a stress is applied. In many sections of engineering structures, high stresses are concentrated in small regions, resulting in non-uniform stress distributions. At temperatures ranging between 700K (427 °C) and 873K (600°C), the application of stresses between 10.1 and 23.5MPa to low alloy steels is found to promote bubble nucleation and coalescence [Sakai, 1980]. Erwin [1982] reports the increase of bubble density of normalized and tempered 2.25Cr-1Mo steel, hydrogen exposed at high temperature, in combined conditions of creep and hydrogen attack. Chen and Shewmon [1995] register a higher density of bubbles along the grain boundaries of samples that experience higher stress. Besides, they proved that the stress/strain field around the crack tip accelerates the nucleation and growth of methane filled bubbles [Chen, *ibidem*]. Conversely, Yokogawa *et al* [1989], who performed on low carbon steel stress-free exposures at 873K (500°C) 9.9MPa (99bars), and creep tests in presence of an applied load of 94MPa, find that the applied stress has a little effect on the bubble density.

In the presence of applied stresses, the voids and fissures are still located along grain boundaries, as in the unstressed situation, but the time to produce them can be shorter by a factor of several hundred, as in the case of 0.5Mo steel and 1Cr-0.5Mo steel [Sutherland, 1965]. Sutherland *et al* suggest that the movement of dislocations plays an important role in the hydrogen attack, arguing that dislocation motion could aid the transport of hydrogen to reaction sites, favouring in this way the nucleation and growth of fissures. This can be interestingly correlated to the more recent studies of Zander *et al* [2003], who state that the hydrogen increases the mobility of dislocations. Other investigators [Allen, 1962a; Coombs, 1965] suggest that the applied stress may promote the initiation of grain boundary microfissures, which may explain the intergranular fracture occurring in the presence of hydrogen attack. These fissures are expected to be methane-filled, which means that the methane pressure contributes, together with the applied stress, to the coalescence and link up of bubbles.

In the case of carbon steel, the rate of the methane reaction is high, and the only pressure of methane may drive the growth of the bubbles into fissures, although the

application of stresses is expected to increase the growth rate. In the case of the 2 ¼ Cr-1Mo steel, and more so of its vanadium-modified grade, the rate of the methane reaction is low and the hydrogen attack may become marked only in the presence of applied stress whilst, in the unstressed situation, low or no attack would be observed. The effects of hydrogen pressure and applied stress on the rupture live of the steels are represented (in particular, for the SAE 1020 steel) by Figure 2.2-4. The curve shows three stages:

1. *First Stage*. The first stage could be associate to the incubation period, during which no microstructural changes can be detected.
2. *Second Stage*. The second stage is characterized by significant hydrogen attack and the rupture stress becomes markedly reduced.
3. *Third Stage*. In the third stage, hydrogen attack and decarburisation are essentially complete and they result in a reduction of the slope of the curve [Coombs, 1965].

The same authors report that, in hydrogen, the stress reduces drastically the incubation period and that, compared to what is observed in argon, higher stresses enhance the extent of the third stage creep at the expense of the second stage creep. The applied stress also seems to increase the process of decarburisation. Sponseller *et al* [1966] find a strong reduction of the bulk carbon concentration (from the initial value of 0.13% to the final average value of 0.10%) of samples made of 2.25Cr-1Mo steel, creep-ruptured after 163 hours in hydrogen at a temperature of 811K (538°C), a hydrogen pressure of 6.2MPA (62 bars), and a stress of 365 MPa. Similarly, they find a reduction of the average bulk carbon concentration of 0.5%Mo-0.006%B steel, failed after 78.8 hours, in the same conditions of temperature and pressure, and under an applied stress of 358 MPa, from the initial concentration of 0.14% to the final 0.065%. This effect could be related to the role that, according to Sutherland *et al*, the movement of dislocations plays on the hydrogen attack [Sutherland, *ibidem*]. Similarly, Yokogawa *et al* [1989] agree that the decarburisation occurs more quickly in creep specimens than in specimens exposed to hydrogen in the absence of superimposed stresses. However, they find that, after a certain time, very similar for both cases, the creep samples and the stress-free exposed tend towards the same limiting carbon content (0.004%).

Dependence of Hydrogen Attack on the Alloy elements of the Steel

In principle, because hydrogen attack is due to the reaction of hydrogen with carbon, one would think that by reducing the carbon content of a steel it is automatically reduced its susceptibility to attack. In reality, the reduction of the carbon content, as suggested by Thoma *et al* [1966], is not an effective way for increasing the hydrogen attack resistance, because steels with a few hundredths per cent of carbon are still attacked [Shewmon, 1985]. It is sound, instead, to opt for a solution which ties up the carbon in the steel, in such a way the element is less available for the reaction of methanation. This solution involves the addition of appropriate alloy elements, which exhibit high affinity for carbon. The molybdenum addition, for instance, increases both the rupture stress and the time necessary for its complete decarburisation [Coombs, 1965]. The same source states that:

- In the same testing conditions, the 0.5%Mo steel has an incubation period more extended than the commercial SAE 1020 steel and 1Cr-0.5Mo steel has an incubation period still more extended.
- The number of cracks registered in tested specimens made of 1Cr-0.5Mo steel is smaller than that registered in specimens made of 0.5Mo steel.

The higher resistance of the 2.25Cr-1Mo steel, with respect to the 1Cr-0.5 Mo steel and the 0.5Mo steel, is due to the higher concentration of Cr and Mo. It is well known that the two elements exert a carbide-stabilizing action into the steel, in this way lowering the internal pressure which provides the driving force for bubble growth, and increasing the resistance to the attack [Sakai, 1980].

As reported by Sponseller *et al* [1966], a previous work of Naumann shows that the increase in the Cr content alone, from 1% to 2.25%, shifts up the limiting service temperature approximately 29K, and the increase in the Mo content alone, from 0.5% to 1%, produces a comparable increase of 24K. Besides, as suggested by Rosenthal [1963], the segregation of Mo to grain boundaries reduces the grain boundary energy, in this way making more difficult the formation of new surface areas associated with cavities and microfissures. Also the paper of Song *et al* [2000] mentions the evidence in the literature

of the role of Mo in increasing the grain boundary cohesion. Another mechanism by which Cr and Mo may reduce hydrogen damage is through the reduction of carbon diffusion [Sponseller, 1966].

The addition of boron (~ 0.006%) to the 0.5%Mo steel, is reported to increase the hydrogen attack resistance of the steel. According to the author, the result is consistent with information reported by Rosenthal on steel containing 0.004%B and 0.14%C. The B tends to segregate at grain boundaries, reducing the interfacial energy and opposing to the creation of bubbles and, consequently, microfissures. Besides, the B in Mo-containing steels leads to the formation of bainitic ferrite in place of polygonal ferrite during air-cooling. The bainitic ferrite has a fine grain size and high dislocation density, in this way improving the yield and tensile strengths of the steel. This strengthening mechanism is expected to maintain its effectiveness, also in presence of a partial decarburisation of the bulk, because it does not require the presence of carbides.

Vanadium is also reported to improve the hydrogen attack resistance, in particular due to the formation of stable VC carbides [Todd, 1983]. Also Nagae *et al* [1987] find in the literature evidence of the beneficial effects of V, Cr, Mo, W, Ti on the hydrogen attack resistance, whilst the effects of Nb are controversial, even though it is a strong carbide former. Bocquet *et al* [2001] show that the tensile properties of the V-modified 2.25Cr-1Mo steel are less degraded by hydrogen attack than the homologous properties of the standard steel. Moreover, they observe that the ductility of the V-modified steels remains unchanged even for the longest exposures to hydrogen at temperature up to 923K (650°C) and pressure of 18MPA (180bars), whilst the standard steel shows a remarkable reduction in ductility (Figure 2.2-5).

Alloy elements can act as trapping sites for hydrogen. This happens if the elements are metallic and have a higher affinity for hydrogen than Fe. For example, V, Ti, Nb, Ta, Zr, and Y. These elements form in Fe effective trap sites, influencing solubility and diffusivity. For instance, the addition of vanadium to the steel reduces the diffusion coefficient and increases the solubility of hydrogen [Brouwer, 1992]. As a result of the higher solubility of hydrogen in the V-modified steels, the hydrogen activity (and the hydrogen fugacity) is also expected to be lower than in V-free steels. On the basis of what

has been reported, Brouwer considers too conservative for V-modified steels the limit of concentration of 3 ppm wt% for hydrogen in the V-free alloys, set by the American Petroleum Institute (API). The present section relates to the hydrogen attack resistance of steels. It is well established in the literature the connection in service conditions between the hydrogen attack resistance and the creep resistance of steels. For this reason, and with respect to the creep properties of steels, it is worth mentioning that the addition of Cr reduces the alloy creep resistance [Lundin, 1984; Shewmon, 1985], whilst the addition of Ti or V enhances the creep strength [Shewmon, *ibidem*]. Bocquet *et al* [2001] report that the addition of vanadium increases the creep strength of the steel, both in air and in hydrogen.

Dependence of Hydrogen Attack on the presence of Impurity Elements in the Steel

Impurity elements, mainly P, As, Sn, Sb and Si, may influence the grain boundary embrittlement of the steel termed "temper embrittlement". Step cooling treatment (SCT) is known to favour the segregation of impurities along grain boundaries, enhancing the effect that these elements may have on the temper embrittlement. Because hydrogen attack is characterized by the formation of bubbles, which nucleate mainly at carbides along grain boundaries, the presence of impurities along grain boundaries has been shown to affect the resistance of the steel to hydrogen attack (Figure 2.2-6) [Sakai, 1981].

In the case of the 2.25Cr-1Mo steel, exposed to hydrogen at a temperature of 843K (570°C), a pressure of 31.4MPa (314bars), and up to 320, 400 and 500 hours, it had been found that:

- P and As decrease the bubble density and SCT reduces the bubbles diameter;
- Sn increases the bubble density and diameter, but SCT does not enhance this effect;
- Sb increases the bubble density but reduces the bubble diameter;
- Si increases the bubble density and diameter.

These effects are influenced by the time of exposure, the increase of the exposure time enhancing the effect of some elements while reducing that of others. In particular, the respective effects of P and Sn had been explained in this way:

- The adsorption of P to the bubble surface promotes the nucleation by lowering the surface energy. Additionally, its presence on the bubble surface hinders the adsorption of C and H, in this way inhibiting the methane reaction.
- Sn does not segregate along grain boundaries and does not produce temper embrittlement. The strong repulsive interaction between Sn and C reduces the presence of the element in solution; in this way C is more available to participate in the methane reaction.

Dependence of Hydrogen Attack on the Surface Conditions

Hydrogen attack is a complex phenomenon involving several different mechanisms: hydrogen adsorption, dissociation, absorption, diffusion, desorption, recombination or reaction with carbon, carbon diffusion and creep [Allen, 1961]. Dissociation and adsorption of hydrogen are phenomena happening at the metal surface. Allen *et al* [1962b] studied the effect of the surface finishing on SAE 1020 and Ferrovac 1020. They found that specimens polished with diamond are more rapidly attacked than those having surface ground with 400-grit emery paper, also showing more extensive surface decarburisation and fissuring.

Dependence of hydrogen attack on the deoxidation of the steel

It is worthwhile to quote the study of Shewmon *et al* [1980], concerning two plain carbon steels, having similar composition, fully deoxidised, one electroslag-refined (ESR), the other aluminium-killed, exposed to hydrogen, at 688K (415°C) and respectively 6.4 and 17MPa. At low pressure, the Al-killed steel was more resistant to hydrogen attack than the ESR one. The modes of development of the attack registered in the two steels became different in the case of the application of a pressure of 17MPa. In the ESR-steel, the hydrogen attack produced the nucleation, growth and coalescence of bubbles to form

fissures. Together with fissures, the grain boundaries of the ESR steel showed the presence of arrays of bubbles. Conversely, the attack in the Al-killed steel consisted of a distribution of intergranular fissures, randomly oriented, with no presence of arrays of bubbles detected at the grain boundaries. This difference is attributed to the presence of impurities at grain boundaries that may favour the nucleation of bubbles in one case, and, in the other, the growth of one or a few bubbles along grain boundaries, before other bubbles can nucleate and grow.

Dependence of Hydrogen Attack on the Prior Thermal Treatment of the Steel

Both industrial experience and research work indicate that the post-weld-heat-treatment (PWHT) of Cr-Mo steels for hydrogen service improves the resistance to hydrogen attack, because it leads to the formation of more stable carbides in the steel, reducing the activity of carbon and, then, the equilibrium methane pressure [Parthasarathy, 1984; Berzolla, 1994; Timmis, 1997]. In particular,

- Berzolla *et al* report that the reduction of the tempering parameter produces an increase of the hydrogen attack sensitivity for both 2.25Cr-1Mo steel and 2.25Cr-1Mo-¼V steels. The authors did not study the analogous behaviour of the 3Cr-1Mo-V steel, but expect the same effect for it.

- Timmis proposes that both high temperatures and longer times are beneficial. In fact, 2.25Cr-1Mo steel, post weld heat treated for 16h at 963K (690°C) became more resistant to hydrogen attack than the same steel post-weld-heat-treated for 24h at 903K (630°C). The same beneficial effect, produced by the higher treatment temperature, was observed in 1Cr-0.5Mo steel and 1.25Cr-0.5Mo steel.

Also Shewmon [1985] confirms that part of the literature supports the thesis that the resistance to hydrogen attack of quenched and tempered 2.25Cr-1Mo steel increases appreciably with tempering, due to the replacement of the M_3C carbide with the more stable $M_{23}C_6$ and M_7C_3. Unfortunately, a work of Parthasarathy and Shewmon, who measured the carbon activity and the dilatometric strain rates of quenched and tempered 2.25Cr-1Mo steel, at 823K (550°C) and as a function of the tempering parameter, shows

that the carbon activity - and the hydrogen attack - drops continuously with the increasing of the tempering time, but with an asymptotic trend (Figure 2.2-7) [Shewmon, *ibidem*]. In addition to this, Bocquet *et al* [2001] find that increasing the tempering time deteriorates the creep strength of the weldment. These findings suggest a need to limit the tempering parameter in order to confer enough creep strength to the steel weldment.

In conclusion, the optimal tempering treatment (TP parameter) is the one that offers the best ratio (*beneficial effects*)/(*treatment*), where "*beneficial effects*" include both the resistance against hydrogen attack and the creep strength, and "*treatment*" means its typology, its duration and its cost.

2.2.9 *Degradation of Steel Mechanical Properties due to Hydrogen Attack*

General Issues

The major effect of hydrogen exposure on the tensile properties is the decrease in strength, which can be explained by bulk decarburisation. The coalescence of bubbles along grain boundaries (without formation of fissures) is believed not to affect the room-temperature tensile properties, whereas they may affect the creep properties, because they can act as sites to initiate premature intergranular creep fracture. In fact, grain boundary sliding and cavity formation is one possible creep deformation mechanism. The work performed by Allen *et al* [1961, 1962b] on steels such as the high-purity carbon steel, Ferrovac 1020, and the commercial SAE 1020, investigates the effect of the attack on specific mechanical properties, including: yield strength, ultimate strength, true fracture stress (defined as load at fracture divided by the minimum cross-sectional area), strain to fracture, reduction of area, in the case of tensile tests, critical bending moment and angle of bend at initiation of a crack, in the case of notched bend test and hardness. Their work shows that:

- The mechanical properties under consideration are reduced by hydrogen attack. In particular, the true stress at fracture and the reduction of area appears as the most sensitive to the occurrence of the hydrogen attack.

- The variation with time of exposure to hydrogen is similar for all the properties considered and is due to: 1) the formation and growth of fissures, 2) decarburisation, 3) recovery and recrystallisation.
- The rapid change of properties is preceded by an induction period. At an advanced stage of attack, the rate of attack decreases and the property changes becomes asymptotic to a final value, depending on the composition of the steel and on the testing conditions.
- The rate of drop in properties increases with the increase of the degree of cold work.
- The reduction of the mechanical properties is promoted by the development of fissures along the former austenite grain boundaries and at the interface between ferrite grains and pearlite colonies.
- The growth of fissures is found to occur by increasing separation of the grain boundaries, rather than by lengthwise increase along grain boundaries.

The final shape of the fissures appears to be dependent upon the history of the steel, i.e. prior thermal treatments and cold work. In particular, the fissures of the annealed SAE 1020 showed a spheroid shape, and the bridges between the blisters fracture only after large plastic strain has occurred, indicating an expansion by creep and a high ductility of the material under the test conditions (Figure 2.2-8). In contrast, the previously cold-worked steel exhibits fissures of more prismatic shape, resulting from the alignment of the nucleation sites for the fissures after cold work. The fissuring and the cold work may produce channels in the steel through which methane or hydrogen can escape, limiting the maximum gas pressure in the fissures. Yokogawa *et al* [1989] comment that, for low carbon steels, hydrogen attack degrades the reduction of area more than the elongation, in the case of both tensile and creep tests.

Hydrogen Attack and Creep

The understanding of the mechanisms of hydrogen attack in steels is, according to Shewmon [1985], "*another way to study the processes that limit creep ductility in alloys*".

In fact, hydrogen attack affects the tensile, bending, hardness and specific gravity of steels [Allen, 1961], and also the creep properties. In particular, the hydrogen attack is combined with phenomena of decarburisation, recovery and recrystallisation, which are expected to influence the creep behaviour. Reciprocally, creep plays an important role in the process of growth of bubbles, blisters and fissures, and, as result of the creep of the steel, it is expected to enhance bubble growth rate and nucleation of bubbles. The creep strength of the metal matrix is a constraint for the bubble growth under the action of the maximum equilibrium methane pressure that develops within the steel. In addition, the atomic processes leading to the growth of methane bubbles present many similarities to the slow growth of grain-boundary voids in the creep of alloys, and the formation of fissures due to hydrogen attack corresponds to the fracture of the creep sample. For these reasons, the models explaining the methane bubble growth owe much to the creep models [Shewmon, 1985].

The creep and rupture testing of solid specimens, in a controlled gas environment at high temperature and pressure, dates back to the end of 1950's and the beginning of the 1960's. In that period, special equipment was built to carry out the tests [Allen, 1962; Coombs, 1965]. Allen *et al* [1962a] performed one of the first studies on creep and testing in hydrogen and argon at high pressure and temperature. Their findings are the following:

- Hydrogen attack decreases the creep properties. This reduction is due to the internal decarburisation, which leads to the formation of fissures along grain boundaries.
- The effect of hydrogen attack is higher in the presence of low applied stresses, which means long testing times, and is lower in presence of high-applied stresses, which means shorter testing times.
- The ductility reduces with hydrogen attack, and the general trend is towards lower ductility with increasing hydrogen pressure.
- The hydrogen attack promotes the initiation of inter-crystalline cracking.

Sutherland *et al* [1965] report for the 1Cr-0.5 Mo steel an initial increase of ductility when the hydrogen pressure is increased up to 6.2MPa. The metallographic investigations

show that, in spite of the increased stability of the carbides in the steel, due to the addition of Cr and Mo, decarburisation of the ferrite occurs, producing this change of ductility in hydrogen [Coombs, 1965]. Coombs suggests that, in the hydrogen environment, the stresses necessary to obtain the same value of minimum creep rate are lower. These findings are in agreement with those reported by Allen *et al* [1962a], who registered an increase in the ductility of the steel with increasing hydrogen pressure. The experimental results of Yokogawa *et al* [1989] also denote an increase in secondary creep rate, while the conclusions of Zander *et al* [2003] suggest that the hydrogen favours the movement of dislocations. Moreover, as observed by Sutherland *et al* [1965], the increased mobility of the dislocations is expected to facilitate the transport of hydrogen to the reaction sites.

Yokogawa *et al* [1989] carried out creep tests on low carbon steel in hydrogen and in argon, at a temperature of 773K (500°C), a pressure of 9.9MPa (99 bars) and under an applied stress of 94MPa. They report in hydrogen a shorter rupture time, creep elongation and extent of the secondary creep stage, with respect to the test carried in argon, whilst the secondary creep rate is higher. The creep samples of Yokogawa *et al* show dimpled transgranular fracture in argon for all testing times (from ~10 hours to ~ 3000h), whilst, in hydrogen, transgranular fracture occurred only for very short rupture times (less than 13 hours). After that time, dimpled grain boundary fracture was observed together with the transgranular fracture, and the amount of the first type of fracture increased with the rupture time. Void formation in the creep specimens was observed in the tertiary creep stage.

In the context of the reported Brite/Euram Project 1835 (PREDICH), Bocquet *et al* [2001] performed creep-rupture tests on either parent metal and cross-weld specimens made of standard 2.25Cr-1Mo steel, V-modified 2.25Cr-1Mo steel, 3Cr-1Mo-V-Ti-B steel, in air and hydrogen, in the range of temperatures between 803-903K (530-630°C). In the case of the standard 2.25Cr-1Mo steel, the applied stress was 100MPa. For its V-modified counterpart, three stresses had been applied, namely 120, 150, 190 MPa. The hydrogen pressure was in all cases 18MPa (180 bars). Their results show that hydrogen has an effect on the creep behaviour of the steels, but the creep properties of the V-modified 2.25Cr-1Mo steel are less degraded than the properties of the standard steel.

Moreover, the hydrogen effect is more apparent towards the lower temperatures. The same authors found that the 3Cr-1Mo-V-Ti-B steel shows similar creep strength in air and in hydrogen, which means that it is even less sensitive to hydrogen attack. The cross-weld specimens tested by Bocquet *et al* failed in the following zones [Bocquet, *ibidem*]:

- Fine-grain heat-affected-zone (FGHAZ), for the standard 2.25Cr-1Mo steel and its V-modified counterpart;
- Base metal (BM), for the V-modified 3Cr-1Mo steel.

In Chapter 5, these results will be compared with the findings of the present work.

The Effect of Hydrogen Attack on Impact Properties

Hydrogen attack is manifested by the formation of fissures at grain boundaries and at inclusion interfaces, which cause the reduction of the mechanical properties, in particular impact properties and ductility [Coombs, 1965]. With reference to the early works of Naumann [1937] and of Wiener [1961], Shewmon [1985] reports that the mechanical properties first and most affected by hydrogen attack are the impact properties, and next the ductility. The "*last and least*" affected are the ultimate tensile strength and the yield stress.

The impact tests, carried out by Sponseller *et al* [1966] on miniature Izod-type specimens, show that specimens made of 2.25Cr-1Mo steel, exposed for 148 hours in hydrogen at 811K (538°C), a hydrogen pressure of 6.2MPa (62 bars), absorbed, at all testing temperatures, quantities of energy slightly higher than their unexposed counterparts. The authors attribute the increase in energy absorption to the decarburisation of the steel. The same authors find that specimens made of 0.5%Mo-0.006%B steel, exposed in hydrogen at the same temperature and pressure for up to 515 hours, exhibit a reduction in energy absorption, due to the reduction of the carbon content from 0.14% to 0.011%.

In the work of Todd and Chung [1983], quenched and tempered 2.25Cr-1Mo steel, exposed in hydrogen at 823K (550°C), 10MPA (100 bars), up to 1000 hours, present a shift in the 67J (50 ft-lb) impact transition temperature of 40K. Scanning electron

micrographs of 2.25Cr-1Mo steel, fractured at 77K, show mixed cleavage and intergranular fracture, but no presence of methane bubbles at prior austenite grain boundaries. The authors conclude that the change in impact properties is attributable to tempering and segregation of impurities during the isothermal ageing, more than to hydrogen attack. By increasing the pressure to 13.8MPa (138 bars), the authors register a reduction in the upper shelf toughness level and a shift of the 67J impact transition temperature of more than 130K, which is interpreted as due to hydrogen attack methane bubbles formation on grain boundaries.

The 2.25Cr-1Mo steel, exposed for 1000 hours at 873K (600°C) and 29.4MPa (294 bars) hydrogen pressure, shows a huge reduction in the shelf energy, as does the standard 3Cr-1Mo steel. This reduction is completely eliminated by the addition of 0.32% vanadium to the steel, whilst the addition of Nb up to 0.04% slightly reduces this improved hydrogen attack resistance [Nagae, 1987].

2.2.10 The Role of Carbides on the Resistance to Hydrogen Attack

The driving force for the hydrogen attack is the reaction of methanation, which allows the hydrogen to link with the carbon of the steel to form methane (see §2.2.3). An effective way of increasing the resistance of the steel to hydrogen attack is the formation of stable carbides (see §2.2.5), which limits the availability of carbon for the methane formation. The formation of stable carbides is achieved by the addition of elements are V, Mo, Ti, Cr, W, B, which present high affinity to carbon and are consequently strong carbides formers (see §2.2.8). According to Allen [1962b], the effect of alloy elements on the stabilization of carbides had been demonstrated by an early work of Naumann. Afterwards, several authors investigated the role of carbides on the hydrogen attack of steels, and the literature suggests that the distribution of bubbles depends on that of the carbides [Sakai, 1980].

Hydrogen is expected to adsorb, to dissociate and to absorb into the metal, where it migrates to the reaction sites to form methane. The carbon, necessary for the reaction, is present within the ferrite matrix and in the form of carbides. It is assumed that hydrogen does not react directly with carbides [Allen, 1962b]. Initially, the carbon of the ferrite

matrix is used in the methane reaction. This leads to the depletion in carbon of the matrix, which introduces a non-equilibrium condition that causes the driving force for the decomposition of carbides. As reported by Todd [1983], the elimination of Fe_3C from the microstructure contributes to improve the hydrogen attack resistance of the steel. The author suggests that high resistance to hydrogen attack could be achieved by tempering times long enough to replace Fe_3C in the microstructure with a stable alloy carbide distribution.

2.3 The CrMoV Steels

The current section is devoted to the steels mainly used in the construction of reactor pressure vessels: the CrMoV steels. The section is divided in two parts: the first introduces the standard 2.25Cr-1Mo steel, which is the steel most used in the world for this application; the second considers the V-modified low Cr-Mo steels, which constitute the second generation of steels for reactor pressure vessels for the (petro)chemical industry.

~O~

The use of CrMoV steels started in the 1950s, for applications requiring high creep resistance, as casings and rotors of high-pressure turbines for power plants. Currently, the choice of the pressure vessels fabricators fells between the following steels (Table 2.3-1):

- Conventional 2.25Cr-1Mo alloy
- Enhanced 2.25Cr-1Mo alloy (Code Case 1960-2)
- 2.25Cr-1Mo, ¼ vanadium alloy (Code Case 2098-1, introduced in August 1990 in the ASME Code)
- Conventional 3 Cr-1Mo alloy
- 3Cr-1Mo, ¼ V, Ti, B alloy (formerly Code Case 1961, introduced in December 1984 in the ASME code)
- 3Cr-1Mo,V, Cb, Ca alloy (Code Case 2151)

The creep resistance of the new CrMoV steels is remarkably higher than that of the conventional and enhanced 2.25Cr-1Mo steels, and of the old CrMoV steels, produced during the 1960's, probably due to higher V content and lower Si content [Berzolla, 1994].

2.3.1 *The 2.25Cr-1Mo Steel*

Introduction

The 2.25Cr-1Mo steel had been favourably considered for a number of applications in the energy field. For example, in recent decades it has been widely used for the production of hydroprocessing reactors, including the pressure-containing shell of the thick-wall reactor vessel. The good creep resistance, conferred by elements as Cr and Mo to the steel, also make it suitable for high temperature power-generation applications, such as steam headers, which are thick-walled manifolds (~0.1m), of large diameter (~1m) gathering steam from sets of boiler tubes.

The steel has been used in the construction of several European fast breeder reactors and for the superheaters in the Russian BOR-350 project [Lundin, 1984]. In more recent times, and for the first time in its history, the 2.25Cr-1Mo steel has been selected by the Japan Atomic Energy Research Institute (JAERI) for the construction of the High Temperature engineering Test Reactor (HTTR), a precursor to the development of the High Temperature Gas Cooled Reactor (HTGR), as example of the new generation of multi-purpose nuclear reactors [Sato, 1997]. The reasons for this large variety of applications are the strength of the steel for high-temperature applications, its satisfactory resistance to corrosion and oxidation, its good formability, weldability and its reasonable cost [Lundin, 1984].

Thick-wall reactor vessels generally use water-quenched and tempered 2.25Cr-1Mo steel, with a bainitic microstructure. In general, they meet the composition and mechanical property requirements of ASME Code Specifications SA-387, Grade 22, Class 2, or SA-336, Grade F22. On the other hand, many components of the high-pressure hydroprocessing plants, such as piping and thin-wall vessels, use annealed 2.25Cr-1Mo steel. The first improvement to the 2.25Cr-1Mo steel was obtained with the practice of the water quenching and tempering, together with the reduction of impurities (mainly S and P) and the vacuum treatment of the molten steel [Berzolla, 1994]. The conventional 2.25Cr-1Mo alloys and the enhanced 2.25Cr-1Mo alloy (ASME Code Case 1960-2) are the steels mostly chosen for construction of hydroprocessing reactors. The difference

between the two steels is given by the different final tempering (PWHT) that, for the enhanced steel, is carried out at a lower temperature to assure higher tensile strength. The limitations due to the enhancement consist of:

- Higher hydrogen embrittlement.
- Higher susceptibility to hydrogen attack.

As a result of the potentially adverse effects of hydrogen, the following limits have been set for this category of steels:

- Maximum operating temperature of 727K (454°C) (by API 941, limitation imposed by hydrogen attack).
- Maximum strength level of steel 689 MPa (for conventional 2.25Cr-1Mo steel, limitation imposed by hydrogen embrittlement).
- In absence of outgassing procedures at shutdown, the maximum safe hydrogen content in the steel of 3ppm is suggested.

The conventional steel has been widely used, whilst a limited number of reactors have been built using the Code Case 1960-2 (Figure 2.3-1) [Antalffy, 1994; Tahara, 1994].

Resistance to Hydrogen Attack of 2.25Cr-1Mo Steel

The 2.25Cr-1Mo steel is widely used for reactor vessels operating in high temperature and hydrogen pressure, because of its good general properties. The work of Sponseller *et al* [1966] seems to be the first on the resistance of 2.25Cr-1Mo steel to hydrogen attack. In spite of the short testing times, respectively 163 and 78.8 hours for the 2.25Cr-1 Mo in normalized-and-tempered condition and for the 0.5%Mo-0.006%B steel, their results prove the former steel to be more resistant to hydrogen attack than the latter. Furthermore both are more resistant than the 1Cr-0.5Mo steel and the 0.5Mo steel studied in previous works [Sutherland, 1965; Coombs, 1965].

Up to the end of the 1970's, the literature reported only decarburisation effects in 2.25Cr-1Mo steel exposed to hot hydrogen. For instance, the work of Norris and Sticha [1976] on quenched and tempered (Q&T)-2.25Cr-1Mo steel, tested in hydrogen at 693K

(420 °C) to 783K (510°C), and pressures of 13.8MPa (138 bars) and 20.7MPa (207 bars), under stresses from 248 to 434 MPa, does not refer to evident effects of hydrogen attack (with the exception of decarburisation), although the lifetimes range from several hundreds to several thousands hours. On the other hand, the work of Hakkarainen *et al* [1980] documents the formation of methane bubbles in the steel, after exposure to hydrogen for 20 days at a temperature of 873K (600°C) and a pressure of 13.8MPa. The bubbles were 200 to 1000Å in size and had been detected via TEM analysis. Their preferential sites of nucleation were Fe/Fe-Mo on grain boundaries and MnS inclusions. As consequence of the methane reaction, almost all the cementite (Fe_3C) disappeared.

Evolution of the Mechanical Properties of the 2.25Cr-1Mo after Thermal Treatments

Several authors have studied the change of the mechanical properties of the 2.25Cr-1Mo steel, due to the evolution of the steel microstructure during ageing. Yang and Kim [2001] exposed the steel at 803K (530°C) up to 500, 1000 and 5000 hours. They compared the exposed material with in-service aged material, part of the elbow tube of a steel pipe, used at 803K up to 10000 hours. Their findings are the following:

- A rapid decrease of the tensile properties with ageing: the decrease was more pronounced in the case of the in-service aged material.
- An about linear decrease of the hardness as function of the ageing time.
- An evolution of energy transition temperature, obtained from Charpy V-notched impact tests, given by the function

$$To = -37 + 0.1027 \times t^{0.6} \qquad \text{Eq. 2.3-1}$$

suggested by the authors for the estimation of the degradation of the steel after exposure at high temperature.

The fatigue crack growth rate versus the intensity factor did not change remarkably with the ageing, both artificial and in-service, in spite of the changes occurring in the

morphology and distribution of carbides. The authors argued that the changes in carbides population are not relevant to fatigue cycling.

Microstructural Changes Induced by Ageing in 2.25Cr-1Mo Steel

The knowledge of the microstructure of steels is fundamental for understanding the evolution of the mechanical properties during the operating conditions of components of petro-chemical plants and of plants for energy production. It is necessary to gain a better insight, if accelerated testing is to be confidently applied. More recently, the precipitate characterization has been used as source of valuable information for remnant life assessment [Senior, 1988].

The ageing of 2.25Cr-1Mo steels has been extensively studied, although most of the work had been performed, for practical reasons, on material that underwent accelerating ageing at temperatures higher than those used in service. Because temperature strongly influences the kinetics and thermodynamics of carbide evolution, the limiting aspect of this approach is that the resulting microstructure cannot be representative of that encountered in the real service conditions. On the other hand, to perform research studies on part of in-service equipment offers certain advantages, as it allows exploring realistic situations, but also presents evident disadvantages. First, the materials available usually differ slightly in composition, the thermal processing histories are different, and also the operating regimes may differ. As a consequence, meaningful test certificate and operational data of the components are absent. These issues had been identified as limiting factors in the assessment of operational plants [Mitchell, 2001].

The good creep resistance of Cr-Mo steels make them suitable for high-temperature applications as steam headers. These components are usually forged, welded and underwent, after welding, PWHT. As reported by Mitchell and Ball [*ibidem*], the tempering of 2.25Cr-1Mo at 973K (700°C) for 10h, converts all the M_3C in alloy carbides. This treatment is usually adopted for PWHTs. For the considered industrial applications, the microstructure of 2.25Cr-1Mo steel usually consists of pro-eutectoid

ferrite and bainite, conferring good creep resistance in the short term. In fact, this microstructure is unstable and changes quite slowly during service lives beyond 20 years and at a range of operating temperatures from 793K (520 °C) to 833K (560°C). These microstructural changes modify the mechanical properties, affecting the creep resistance, which is of particular concern in the steam headers, because it is their life-determining factor. The carbides in the pro-eutectoid ferrite are mainly M_2C's, whilst the bainite shows various carbides, as M_7C_3 and $M_{23}C_6$ type [Mitchell, *ibidem*].

In the normalized-and-tempered 2.25Cr-1Mo steel, Kleuh [1974] has found a creep resistance unexpectedly higher than that registered in quenched-and-tempered 2.25Cr-1Mo steel .The reason for this difference, with reference to the work of Baker and Nutting [1959], is in the different kinetics of the carbide reactions occurring in the constituents of the steel. In the former case, the steel microstructure shows a considerable amount of proeutectoid ferrite whilst, in the latter case, it is mainly made of bainite. For both constituents, the reaction kinetics are different. In fact, whilst in bainite the first carbide to be formed is cementite (which changes in Mo_2C and Cr_7C_3, with the subsequent formation of $M_{23}C_6$ and M_6C), in ferrite the first precipitate to be formed is Mo_2C (or M_2X, if also it includes other alloy elements), which directly changes in M_6C. Baker and Nutting [*ibidem*] refer that mainly the Mo_2C is responsible of the enhancement of the creep strength of the steel.

In the bainitic phase of the 2.25Cr-1Mo steel, the $M_{23}C_6$, usually of globular shape, forms at the expense of the Mo_2C and does not improve considerably the creep strength. In bainite, the intermediate reaction of the Mo_2C in $M_{23}C_6$ is rapid and, as consequence, the disappearance of the former carbide in bainite is faster than in ferrite. The $M_{23}C_6$ carbide is found mainly along the grain and lath boundaries [Lundin, 1984; Senior, 1988]. In general, the ageing phenomena confer to the grains more spherical shape and cause the growth of carbides at the grain boundaries. This produces an increasing sensitivity of the grain boundaries to the crack initiation and the steel may become brittle.

Depending on the previous thermal history, the carbides in the as-received and aged condition may be M_2C, M_3C, $M_{23}C_6$, and M_7C_3 [Yang, 2001]. The volume fraction of M_7C_3 and $M_{23}C_6$ is expected to increase with the ageing time, according to the work of

Baker and Nutting [1959]. In the bainitic phase of the 2.25Cr-1Mo steel, the M_7C_3 carbide is usually rod-like, whilst M_3C is circular-shaped and the M_2C appears as a very tiny acicular particle scattered within the bainitic sub-units [Tsai, 2003]. Tsai *et al* [*ibidem*], who also studied the effect of ageing phenomena on 2.25Cr-1Mo steel, conclude that the carbide transformation sequences in bainite and martensite are similar. They report for $M_{23}C_6$ a shape similar to that of M_7C_3, but with a slightly smaller size. In the same phase, the Cr content in $M_{23}C_6$ carbides had been found lower than that in M_7C_3 carbides and vice versa for the Mo content. The carbide transformation occurring in 2.25Cr-1Mo, as result of ageing phenomena, are summarized in Figure 2.3-2.

Probably, one of the few studies investigating the influence during ageing in air of exposure time, temperature and applied stress on the microstructural evolution of 2.25Cr-1Mo steel, is that of Gope *et al* [1993]. The authors carried out TEM investigations on the shoulders and the gauges of samples that underwent creep-rupture tests in air at 813K (540°C) and 853K (580°C). In both cases, the superimposed stress was calculated in such a way to have two values of rupture time: one close to 7000 hours, the other close to 16000 hours. The results confirm for the 2.25Cr-1Mo steel the carbide evolution reported by Baker and Nutting [*ibidem*]. In particular, the authors conclude that the ageing of the steel in stress-free conditions produces an increase in size of the M_2C carbides, whilst the superimposition of stresses accelerates the dissolution of these carbides and promotes the formation of M_6C carbides. Baker *et al* [2000] who carried out TEM investigations on samples exposed to hot high-pressurized hydrogen at 873K (600°C), pressures ranging from 19.5 to 26MPa, and durations from 123 to 715 hours, in absence of applied external stresses, report the presence of M_6C-type carbides in the decarburised layer underneath the surface exposed to hydrogen, together with the presence of M_6C, M_7C_3 and of traces of M_2C in the bulk material.

2.3.2 The Vanadium-modified Steels

Introduction

The increased use of heavy oil in refineries and the development of new processes, such as for coal liquefaction, require steels of improved strength at temperatures up to 755K (482°C) and higher resistance to hydrogen attack than the standard 2.25Cr-1Mo steel. Similarly, modern fossil fired power plants require improved high temperature strength [Tsuchida, 2004].

In 1983, the API/MPC "Program to Study Material for Pressure Vessels Service with Hydrogen at High Temperature and Pressure" was started in USA. The purpose was to develop and standardize to ASME and ASTM, modified 2.25Cr-1Mo steel, with higher strength and resistance to hydrogen attack [Nagae, 1987]. The ASME Boilers and Pressure Vessels Code, Sec. VIII Div. 2, prescribes for the standard 2.25Cr-1Mo steel the acceptable stress at temperatures up to 755K (482°C), but this stress decreases rapidly for temperatures higher than 727K (454°C).

Tests carried out by Nagae *et al* on steels exposed for 1000 hours at 873K (600°C) and 29.4MPa hydrogen pressure, showed that the standard 2.25Cr-1Mo steel is strongly attacked under this testing conditions. The addition of 0.32%V to the standard 2.25Cr-1Mo steel confers higher resistance to hydrogen attack even under these test conditions, while the addition of Nb up to 0.04 % slightly decreases this hydrogen attack resistance, even though both steels display attack resistance better than the standard 2.25Cr-1Mo and 3Cr-1Mo steels [Nagae, 1987].

The 2 ¼ Cr-1Mo-V steel

The steel has been fabricated to operate in a range of temperatures up to 755 (482°C) and under hydrogen partial pressure as much as 20.7MPa. Up to this temperature, the steel shows high creep rupture strength [Tsuchida, 2004]. For this reason, it is regarded as a candidate material for the construction of fossil power plants, coal liquefying plants and conventional chemical plants with higher efficiency.

Tsuchida *et al* report that the creep rupture strength of the V-modified 2.25Cr-1Mo steel is similar to that of the V-modified 9Cr-1Mo steel and 9Cr-1Mo-W steel, up to a temperature of 823K (550°C), but decreases for higher temperatures and longer rupture times. Conversely, the creep rupture elongation increases under these conditions, showing a reduced susceptibility to brittle creep rupture [Tsuchida, *ibidem*]. The authors attribute the lower creep strength of the V-modified 2.25Cr-1Mo steel, with respect to the modified 9Cr-1Mo steels, to the larger interspacing of the grain-boundary carbides registered in the former steels.

The use of the modified 9Cr-1Mo steel had been limited by reheat cracking of the HAZ, but this matter had been solved by means of calcium treatments that stabilize the impurities, such as sulphur which segregates mainly to grain boundaries. These impurities reduce the grain bonding, in this way giving rise to grain boundary fracture [Shinya, 1998].

The 3Cr-1Mo-¼V-Ti-B Steel

After an extended test campaign, this steel was found to be an excellent material for heavy wall pressure vessels for hydrogenation processes. In 1986, the material was certified by TÜV in Germany. Then, in 1989, it was authorized as a material specified in ASME Section II and Section VIII, Division 1 and 2. The distribution in 1993 of reactors built with this steel is given in Figure 2.3-3. The advantages presented by this steel, with respect to the 2.25Cr-1Mo steel, are:

- Higher allowable stress at the design temperature of 727K (454°C) per ASME Section VIII, Div. 2, than 2¼Cr-1Mo quenched and tempered steel in the 517MPa UTS conditions. This improvement resulted in more reactor volume within the rail transport weight restrictions.
- Higher resistance to hydrogen attack.
- Higher resistance to hydrogen embrittlement, with comparable resistance to temper embrittlement.

- Higher resistance to debonding, due to the hydrogen trapping effects of precipitated VC carbides.

These metallurgical characteristics allow lower pressurizing temperatures, reducing the start-up time. Besides, the possibility to use the material at higher temperatures provides more operating flexibility and time to react to an eventual temperature excursion of the process, before depressurising the unit [Andersson, 1994].

2.3.3 Creep Strengthening Techniques in Low-alloy Ferritic Steels

Two main mechanisms are considered: Carbide Dispersion Strengthening and Solid Solution Strengthening.

Carbide Dispersion Strengthening

When alloy elements are present in the steel in low concentration, they can go into solution in the ferrite matrix or in cementite. In higher concentrations, they can form alloy carbides thermodynamically more stable than cementite. The elements that contribute to the formation of carbides with enthalpies of formation higher than cementite are Cr, Mo, V, W, Nb and Ti. In particular, at 973K (700°C), the affinity of some of these alloys elements for carbon can be written as V>Mo>Cr>Fe [Senior, 1988]. Mn is a weak carbide former and Ni, Cu and Co do not form carbides. In contrast, Mo, V, Nb and Ti are strong carbide forming elements [Kuzuku, 1998]. Ni is reported to increase the austenite stability and speed up the precipitation of VC-type carbides [Slugen, 1999].

The sites where carbides preferentially form are dislocations, grain boundaries and sub-boundaries, which provide paths for the rapid diffusion of solute elements. Usually, the precipitation does not lead to the formation of the equilibrium carbide [Thomson, 2000]. As reported by Tsai *et al* [Tsai, 2003], Honeycombe and Bhadeshia suggested in 1995 two mechanisms of carbide formation: "in-situ transformation" and "separate nucleation". In the former case, the new alloy carbide nucleates at the interface between the original carbide and matrix, and grows at the expense of the original carbide, which tends to disappear. In the latter case, the new alloy carbide nucleates separately at new

sites, mainly dislocations, and it grows whilst the original carbide dissolves in the ferrite matrix. The carbides that are usually found in alloy steels are [Senior, 1988; Thomson, 2000]:

- *MC type*, which is considered among the most stable compounds in nature. It is a vanadium-rich carbide, frequently referred to as M_4C_3 or V_4C_3. Its structure is fcc, similar to that of NaCl, but with covalent bonding. The most common are TiC, NbC, VC. Senior [*ibidem et passim*] reports that several studies have shown that the carbide may contain a large amount of Mo, dependent on alloy composition and initial heat treatment. The same author states that, in austenitized and tempered 1Cr-Mo-V steel, the MC type carbides are plate-like and nucleate preferentially on dislocations within prior bainite lathes. At high temperatures – around 873K (600°C) – the carbides tends to be coarse, with the replacement of V by Mo. According to Senior, the MC carbides may give rise to the nucleation of M_2C. The formation of the Mo-rich carbide depletes the matrix in Mo and may lead to the re-solution of Mo from MC. This suggested mechanism results in a very low coarsening rate, or partial dissolution, of the MC carbides.

- *$M_{23}C_6$ type*, usually Cr-rich carbide with the complex cubic structure of $Cr_{23}C_6$. In steels containing Mo, it can have the formula $Fe_{21}Mo_2C_6$ whilst, in steels containing both Cr and Mo, the carbide formula can be between the two reported values. This carbide can also contain Mn and W, leading to the formation of $Cr_{21}W_2C_6$. In low-alloy CrMoV steels, its formation has been registered mainly along grain and lath boundaries [Lundin, 1984; Senior, 1988].

- *M_7C_3 type*, usually Cr-rich carbide with the trigonal structure of Cr_7C_3 [Thomson, 2000]. Senior reports a pseudohexagonal structure [*ibidem*]. In it, Fe is soluble up to 60% and more. Other elements soluble in these carbides are, in order of solubility, Mn, V and Mo. The formation of M_7C_3 is expected to happen "in situ", close to cementite or at the interface cementite/ferrite, with some scholars suggesting there is not enough Cr in the ferrite matrix for the precipitation of M_7C_3.

- *M_2C type*, Mo-rich carbide. Thomson reports for it a fcc structure [Thomson, *ibidem*], whilst Senior a close-packed hexagonal structure [*ibidem*]. In M_2C, significant quantities of Cr, V, Fe, W are soluble. Usually, its morphology in low-alloy CrMoV steels is acicular and its nucleation during tempering and ageing is reported at lath boundaries, close to M_3C or at the ends of M_4C_3, where it produces the characteristic H-carbide. M_2C is reported to be the main responsible of the creep strengthening of the steel [Baker & Nutting, 1959].

- *M_6C type*, which is Mo-rich carbide with fcc structure. Dependent on the Mo content, it can exist in the range of compositions between Fe_2Mo_4Cr and Fe_3Mo_3C. In this carbide, Cr and V are soluble in small quantities. Usually, it forms "in situ" at grain boundaries, where it grows rapidly at the expense of neighbouring carbides, such as $M_{23}C_6$ and M_2C. Oh *et al* [1999] suggest that the presence of coarse M_6C carbides in the inter-critical heat-affected-zone (ICHAZ) of 1Cr-1Mo-0.25V, extracted from a turbine rotor after 20 years of service, are preferential sites for the formation of cavities during creep tests. Consequently, they are responsible for the Type IV failure of creep samples cut from this steel.

The strengthening action exerted by the carbides depends on several factors [Lundin, 1984]:

- The shear strength of the carbides. In fact, these particles must be resistant to the shearing action of an impinging dislocation, otherwise the dislocation could cut through the particle leaving it permanently sheared.

- The particle spacing. Lundin *et al* refer that the strength of the steel is proportional to the square root of the volume fraction of precipitates, divided by the radius of the particle. Consequently, the strength increases with increasing volume fraction and decreasing particle radius, which reduces the particle spacing.

- The magnitude of the strain field around the particle. This strain field influences the effectiveness of the interaction of the particles with the dislocations. According to Lundin [1984], the particles coherent with the surrounding matrix generate a larger strain field than those that are not coherent. But, at creep

temperatures, the coherent precipitates are not stable and, by growing, they may lose their coherency with the matrix. What is reported by Lundin *et al* [*ibidem*] in this respect is surprising. One would expect the strain field generated in the surrounding matrix by a coherent particle to be lower than that generated by a non-coherent one, and not vice-versa. In addition, at creep temperatures, one would expect the growth of non-coherent particles, possessing high particle/matrix interface energy, to be higher than that of a coherent particle.

- The difference in specific volume between the particle and the matrix. The higher this difference, apparently the better the particle will be a source of vacancies. Vacancies help climb of dislocations that have been stopped by an obstacle.

- The particle stability. This means that, at the service temperatures, the particle will neither modify its size and composition with time, nor will do it at slow rate. Because the changes in size and composition of a particle are influenced by the diffusion rate of atoms through the matrix, factors that influence the diffusion rate (e.g. surface energy and particle composition) have an impact on the stability of the particle.

The distribution of precipitated carbides depends on the composition of the steel, on the time (e.g. tempering time) and on previous thermomechanical treatments. For instance, an extended tempering produces a reduction in the volume fraction of intra-lath carbides and a coarsening of grain boundary carbides [Senior, 1988]. Finally, there is a counter effect implied by the precipitation of carbides: the fact that their presence in the matrix may give rise to cavitation. In fact, second-phase particles may be sites for stress concentration upon application of a stress, and may increase the nucleation of cavities along the grain boundaries through the increase of its free energy, and facilitating, in this way, the concentration of vacancies [Kassner, 2003].

Solid Solution Strengthening

The strengthening of low-alloy ferritic steels is mainly achieved by means of carbide precipitation. Another, but less influential mechanism, is by means of solid solution strengthening. This mechanism is due to the interactions among interstitial elements (e.g.

carbon and nitrogen) and substitutional alloying elements able to form carbides and nitrides. The interactions among interstitial and substitutional elements, as well as those among only substitutional elements, may lead to the formation of clusters which are too small for precipitation, but big enough to produce a strain field in the surrounding matrix, that inhibits the movement of the dislocations. This movement may be also inhibited by the mechanism of solute drag, which is caused by a strong interaction between the dislocations and the interstitials, and by the consequent formation of solute atmospheres around dislocations [Lundin, 1984]. According to the referred Lundin *et al*, the related literature states that, at about 866K (593°C), the binding energies of Mo atoms with dislocations are about 10 times higher than those of the Cr atoms, whereas the interaction energies of both atoms with carbon are comparable. Song *et al* [2000] report that the segregation of Mo to grain boundaries may enhance the grain bonding, an effect that had been confirmed both theoretically and experimentally.

Carbides in Cr-Mo(-V) Steels

In 2.25Cr-1Mo steel, the carbide that mainly produces creep strengthening is the acicular M_2C type [Baker & Nutting, 1959]. Under typical in-service conditions, this carbide may undergo changes due to the initial microstructure, the service temperature, the duration of the permanence in the service conditions. As a consequence, the M_2C carbides may coarsen and dissolve, affecting the creep properties of the steel. In fact, as reported above, the increase of the inter-particle spacing between the precipitates produces a decrease in creep strength.

An industrial example shows that the weld metal of a pipe, in service at 839K (566°C) for 31 years, showed coarse Cr-rich carbides, namely $M_{23}C_6$, M_6C and M_7C_3, along the ferrite grain boundaries. Besides, some intragranular M_2C carbides were detected. Creep rupture and creep crack-growth tests, carried out on specimens extracted from the weldment, illustrated the detrimental role exerted by the coarse carbides precipitated along the grain-boundaries with respect to the creep properties of the steel. These carbides appeared as preferential sites for the nucleation of voids [Liaw, 1991].

The addition to the steel of strong carbide formers, such as V, Ti and Nb, leads to the formation of carbides of the MC type, which are more stable than M_2C and similarly effective in promoting the creep strength. In Cr-Mo-V steel, the V-carbides are usually dispersed within the grains and are very stable. In fact, the coarsening of these carbides is slight, so does not affect the creep properties of the steel even in the case of a steam pipe kept in service up to 15 years of service at 813K (540°C) and a hoop stress of 70MPa [Singh, 1997]. The precipitation of carbides is obviously influenced by the diffusion rate of alloying elements in the matrix. For instance, vanadium has a higher affinity to carbon than chromium or molybdenum. In spite of this, the precipitation of VC happens at higher temperatures and at lower rate than the precipitation of Cr carbides [Slugen, 1999].

In other studies, devoted to Cr-Mo-V steels thermally treated at temperatures ranging between 773K (500°C) and 973K (700°C), it was confirmed that M_3C is metastable at all temperatures investigated. $M_{23}C_6$ is stable for the lower temperatures of the range, whilst the carbide M_7C_3 exists in equilibrium and MC is the carbide of equilibrium of all steels containing vanadium over the range of temperatures considered, [Výrostková, 1998]. The addition of strong carbide-forming elements inhibits and in part prevents the formation of $M_{23}C_6$, because the carbon is subtracted for the formation of MC. Moreover, if Mo is added to Cr steel, the first element tends to replace the second in the structure of $M_{23}C_6$. It had been found that the reported strong carbide-forming elements reduce the thermodynamic stability of $M_{23}C_6$ and decrease their dissolution temperatures and energies [Kuzuku, 1998]. In particular, the addition of Nb to standard 2.25Cr-1Mo and 3Cr-1Mo steels produces the formation in the grains of fine Nb carbides, having dimension of 100-200 Å.

In the V-modified 2.25Cr-1Mo steel, coarse carbides of Fe, Cr, Mo, as $M_{23}C_6$, M_7C_3, M_6C, and acicular Mo_2C carbides are scarce, and fine precipitates of 500 Å diameter are uniformly dispersed in the grains. The carbides consist mainly of Mo, V and Cr. The addition of Nb to the V-modified steel makes these carbides finer and substitutes, in the chemical composition, the Nb with the Cr [Nagae, 1987]. In general, the amount of Cr, Mo and V in carbides before post-weld-heat-treatment (PWHT) is significantly smaller

than the bulk content. The amounts of these elements precipitated as carbides increases after PWHT, as the tempering parameter increases.

2.3.4 *Effect of Thermal Ageing on the Impact Properties of Cr-Mo Steels*

The ageing of 2.25Cr-1Mo steel at 803K (530°C) up to 500, 1000, 5000 hours, had been found to increase the ductile-brittle transition temperature (DBTT) according to the relation [Yang, 2001]

$$To = -37 + 0.1027 \times t^{0.6}$$

Eq. 2.3-2

The ageing of Cr-Mo steels is expected to lead to the formation of $M_{23}C_6$, and, afterwards, of M_6C, which precipitates as coarse particles along grain boundaries. These carbides are detrimental to the toughness of the steel [Kuzuku, 1998]. The addition of strong carbide-forming elements to the steel reduces the amount of carbon in solution, so less is available for the formation of coarse $M_{23}C_6$ carbides.

2.4 Weldments

The large-scale pressurized components used in the (petro)chemical and power generation sectors inevitably contain weldments. For this reason, the structural steels used in the production of these components are not only present as base metals but also as welded joints. The present section introduces the main features of weldments and the differences in mechanical behaviour between the weldments and the base metal.

2.4.1 *Design of Pressurized Components*

The majority of creep failures in pressurized components are associated with welds [Smith, 2003]. Weldments are critical parts of the industrial components, mainly due to the microstructural changes which give rise to marked variations in creep properties. Pressurized components of electricity generating stations and petro-chemical plants

operate for long periods at temperatures where creep may occur. At the design stage, the appropriate wall thickness of these components can be calculated by using the expression:

$$t = \frac{PD}{(2SE + P)} \qquad \textbf{Eq. 2.4-1}$$

Where

t = wall thickness.
P = internal pressure.
D = outside diameter.
E = efficiency factor.
S = allowable component stress.

The allowable stress is calculated via different procedures, depending on the considered code (e.g. ASME B31.1). The stress values are determined by extrapolation of the uniaxial creep data of the structural materials under consideration, and, in spite of the uncertainties due to the extrapolation process, the industrial experience gives evidence that the long-term operation of the components is usually guaranteed without failure if the operating conditions are kept within the designed limits. This evidence proves that, in general, the component design is conservative, justifying the practice of extending the operation of large-scale plants beyond the original design life [Parker, 1995].

The design of industrial components operating in creep regime takes in consideration that the cross-weld material exhibits rupture strength lower than the parent material and dependent on the applied stress and temperature. For this reason, it is common practice to introduce weld reduction factors (WRF) which, for CrMoV steels, are in the range 20-60%, reflecting the degree to which the presence of cross-welds lowers the rupture strength with respect to the parent metal [Middleton, 2001]. The choice of WRF values is based on the available test data, but, as reported by Middleton *et al* [*ibidem*], the available laboratory cross-weld data are insufficient to define precisely the WRFs at long times for each alloy.

2.4.2 Relevance of Weldments for the Service Life of Components

The satisfactory performance of low alloy steel weldments often determines the safe operation of high-energy piping systems and pressure vessels in electricity generating systems and petrochemical plants. Service experience indicates relatively short-term failures are a consequence of microstructural features, which exhibit high strength and low ductility or low strength and high ductility [Parker, 1994]. Design recommendations in general do not take into consideration the presence of weldments, whilst most of the service failures of industrial equipment made of Cr-Mo steels have been reported to occur in the welds, mainly in the HAZ. The performance of weldments had been identified as the limiting factor in applications where creep is important. Consequently, much research has been devoted to the correlation between the weld microstructure and its mechanical properties, with the purpose of achieving improved in-service performance, via developed welding practices and fabrication procedures. In particular, research and development work has been devoted to the standard 2.25Cr-1Mo, and, as a consequence, current welding and fabrication technology confer good impact properties to the weld metal and HAZ after a minimum post welding heat treatment (PWHT) cycle. As far as the V-modified 2.25Cr-1Mo and 3Cr-1Mo steels are concerned, it is reported that the vanadium present in the low chrome steels does not affect the hardenability and weldability of the steel, and the effects in terms of susceptibility to reheat or stress relief cracking are not relevant [Antalffy, 1994, 2002].

The chemical composition and the microstructure of the weldments are influenced by different factors, namely:

- The chemical composition of the electrode.
- Its flux coating (if flux coated electrodes are used).
- The welding process.
- The process parameters.

Thus, the microstructure of the HAZ depends on the composition of the alloy in use and is controlled both by the thermal fields, produced by the thermal input occurring during

the welding process, and by the phase transformations of the material being welded. In particular, very important are the time at peak temperature and the cooling rate. The HAZ is usually divided into different sub-zones, each with a different type of microstructure and different mechanical properties [Mannan, 1996].

- The coarse-grain heat-affected zone (CGHAZ), which is near the fusion boundary and experiences temperatures well above AC_3. The exposure to these temperatures dissolves the carbide dispersion, which is the main obstacle to the growth of the austenitic grains, and the formation of coarse-grained austenite occurs. On cooling, because the cooling rates are relatively high, the austenite tends to transform to bainite within the prior coarse austenite grains.
- The fine-grain heat-affected zone (FGHAZ), which experiences lower temperatures, although still above AC_3. The growth of the austenite grains is limited by the rate of dissolution of the carbide population.
- The intercritical heat-affected zone (ICHAZ), which experiences temperatures between AC_1 and AC_3, and, for this reason, partially transforms to austenite. In this region, the cooling rates are relatively low and, consequently, the austenite transforms to ferrite surrounded by untransformed material, which has been tempered.
- Overtempered zone, also called subcritical heat-affected zone (SCHAZ), which experiences temperatures below AC_1.

According to Parker [1995], for low alloy steels, the prior austenite grain size could be related to the peak temperature by the equation:

$$D_t^{2.8} - D_o^{2.8} = kt \exp\left[\frac{-Q}{RT}\right] \qquad \textbf{Eq. 2.4-2}$$

Where

D_o = initial grain size.

D_t = grain size developed after time t at temperature T.

k, R = constants.

Q = activation energy for grain growth.

The equation describes the formation of a coarse grained region where the peak temperature is the highest, which means close to the fusion boundary. Moving towards regions which experiences lower peak temperatures, the grain size decreases.

It is not only the HAZ which is characterized by different zones: a range of microstructures also characterizes the weld metal. Industrial components, having a multipass structure, contain regions made of columnar grains, limited by the grain boundaries of prior austenite grains and by coarse and fine zones, which result from the HAZs of overlapping beads. For this reason, weldments have inhomogeneous microstructures and, consequently, non-uniform mechanical properties. Thus, as reported by Mannan and Laha [1996], there is limited information about the types of carbides in the different zones of the HAZ. For the low Cr-Mo steels themselves, some information is given in paragraph 2.3.3.

To reduce the residual stresses introduced by the welding process, and to stabilize their microstructures, a post-welding heat treatment (PWHT) is usually carried out. To maximize the *effectiveness/cost* of the PWHT, it is necessary to understand its effects on the mechanical properties of the steel, and to interpret these effects in the light of the microstructural changes it induces. By increasing the PWHT (i.e. by increasing its duration), the resistance of the steel to hydrogen attack and to creep cavitation increases, as a result of carbide stabilization; but some researchers have pointed out that the increase of the tempering parameter of a PWHT produces a detrimental effect on the mechanical properties of the material [Bocquet, 2001].

2.4.3 *Creep of Weldments*

The creep behaviour of weldments is traditionally investigated by testing cross-weld specimens. In fact, the damage obtained during laboratory tests is, in general, considered representative of the damage developed in service conditions. However, the weldments are not homogeneous and exhibit a range of structures, so the evaluation of their creep

strain is not an easy matter. One aspect emerges clearly: namely, damage development is linked to strain accumulation. The current section refers to the major features which characterise the creep behaviour of weldments, in particular of low Cr-Mo steels.

The Testing of Weldments

Fusion welding of low alloy steels produces different heterogeneous microstructures. The microstructure determines the properties of the steel, so the weldments present variations in strength and ductility (see Figure 2.4-1 and Figure 2.4-2). By testing cross-weld specimens, it is thought possible to understand the creep behaviour of weldments. In general, laboratory tests are carried out under conditions more severe than the operating ones, and a process of extrapolation is required to foresee the behaviour of weldments under service conditions. This approach is valid if the creep ductility of the different structures of the tested samples is similar to those encountered in the plant conditions [Parker, 1996].

Creep rupture and creep crack growth tests performed on the weld metal of ex-service pipes, which had been operating for 31 years at the temperature of 839K (566°C), showed creep rates and creep crack propagation rates significantly higher for the weld metals than for the base metals [Liaw, 1991]. It is also found that the creep deformation and the rupture data of the weld metal of the ex-service pipe are inferior to those of the base metal. The equation proposed by Liaw *et al* [*ibidem et passim*] for the creep rate is

$$\dot{\varepsilon} = 9.5 \times 10^{-2} \sigma^{9.36} \exp(-\frac{337500}{8.32T}) \qquad \textbf{Eq. 2.4-3}$$

Where T is the temperature in degree Kelvin. Because the exponent of the stress is higher than 5, it is argued that dislocation climb is the rate-controlling process for creep deformation of the weld. Instead of the Monkman-Grant relationship, Liaw *et al* report that the equation that best fits the experimental data for the tested steel is:

$$\dot{\varepsilon}^{-1.0} \frac{(t_p + t_s)}{(\varepsilon_p + \varepsilon_s)} = 0.9 \qquad \text{Eq. 2.4-4}$$

For the crack propagation rate, the same authors refer the equation:

$$\frac{da}{dt} = 8.38 \times 10^{-5} C_t^{0.77} \qquad \text{Eq. 2.4-5}$$

Where da/dt is measured in (mm h^{-1}), and C_t in (J m^{-2} h^{-1}). C_t is the creep crack driving force parameter developed by Saxena and co-workers. The investigation showed that the degradation of the mechanical properties was due to the formation of voids close to the coarse carbides precipitated along grain boundaries. It is arguable that a contribution to the loss of properties was also due to the partial dissolution of M_2C carbides present in the grains.

Effect of the prior thermal treatment on the creep of weldments

Cross-weld specimens made of 1.25Cr-0.5Mo steel, in the as-received (normalized and tempered) conditions and after two-hour PWHT at 970K (700 °C) or 1023 (750°C), tested in the temperature range of 833 to 873K (560 to 600°C) and in the stress range of 80 to 162MPa, showed that [Parker, 1996]:

- The level of reduction of area at rupture was linked to the degree of tempering.
- The high-ductility ruptures, registered in samples that underwent severe PWHT, occurred in the base metal. This behaviour was attributed to the high-tempering treatment, which led to a homogenisation of the structures. Although the failure was due to a localized necking, considerable strain was detected in the HAZ and in the weld metal, not only in the base metal.
- The more brittle fractures, registered in the samples that underwent lighter or no PWHT, occurred in the HAZs, as a consequence of the formation of creep cavities

along grain boundaries. This grain-boundary creep damage was found similar to the Type IV damage detected in service welds.

Clearly, the fracture behaviour of parent metal and cross-weld samples is sensitive to the PWHT, which influences both the ductility of the steel and the location of the registered failure. However, the work of Albert *et al* [2003] on 11Cr-0.5Mo-2WVNb, tested at 923K (650°C) and 70MPA, after a PWHT at 1013K (740°C) for 15 minutes to 4 hours, suggested that the duration of the PWHT does not influence significantly the rupture time. Even so, the different PWHTs produce differences in creep properties, hardness and microstructure. For instance, after creep-rupture testing, the weldments that underwent long-duration PWHT exhibited a number of creep cavities close to the fracture surface sensibly higher than the weldments that underwent short-duration PWHT. Similarly, after interrupted creep testing, the former weldments showed a large number of microcracks and, for the latter, the HAZ is practically crack-free [Albert, *ibidem et passim*]. With reference to the results reported by Lundin *et al* [1984], the findings of Albert *et al* are consistent with reports which point out that the microstructure obtained by means of relatively low tempering parameters is less stable. Consequently, microstructural changes are expected during the in-service conditions, which may induce a sensitive decrease in the mechanical properties.

Redistribution of stress in the creep of weldments

Finally, it is important to consider hoop stress redistribution during the creep of weldments, which allows regions of low strength to shed this stress to more resistant zones. The redistribution of the stress is more limited when the axial stress is considered. In this case, the creep rate of the weld metal increases as its creep strength decreases [Parker, 1995].

2.4.4 *Failure of Weldments*

Different kinds of failure occur in weldments. They are [Parker, 1994; Mannan, 1996]:

- *Type I failure*, which is a transverse weld metal cracking.

- *Type II failure*, with cracking originating in the weld metal but extending in the HAZ.
- *Type III failure*, which is a heat-affected-zone cracking.
- *Type IV cracking*, cracking registered in the intercritical region of the HAZ.

A more detailed description of these failures is reported by Mannan and Laha [1996].

- The Type I and Type III affect mainly low alloyed Cr-Mo steels, whilst the Type IV, which is a major maintenance and inspection problem of utilities worldwide, is registered also in high chromium Cr-Mo steel weldments, although it is more pronounced in low Cr-Mo steels.
- The Type III initiates in the CGHAZ, and nucleates on prior coarse grain boundaries. The Type I forms along the prior austenite grain boundaries in the coarse columnar weld, while Type IV forms mainly in the intercritical zone (ICHAZ).
- The occurrence of Type IV is attributed to the reduction of creep strength of the ICHAZ, after depletion of the zone in fine acicular M_2C carbides and the formation of coarse high-order carbides. Because the ICHAZ is the softer zone of the weldment, strain tends to accumulate in it, decreasing the creep strength of the weldment.
- The occurrence of the Type III and I can be avoided by using small diameter electrodes and low input welding, and by performing an adequate PWHT to relieve the welding stresses and fully refine the CGHAZ or reduce its width.
- The occurrence of the Type IV can be avoided by reducing the width of the ICHAZ, which can be achieved by using lower heat input during the welding process, and by reducing the difference in creep strength among the base metal, the ICHAZ and the CGHAZ. This latter target can be obtained by modifying the composition of the steel.

At least three catastrophic in-service failures of components with longitudinal weldments are reported in literature [Parker, 1995]. To give a measure of the severity of the failure, that occurred in January 1986, in a hot reheat steam line, was 7 m long and 2 m wide. Because the consequences of catastrophic failures are usually very serious, the design of pressure vessels has been modified in such a way to eliminate longitudinal weldments and to reduce in general the presence of weldments in pressurized components (See paragraph [2.1.6]).

The failure of weldments can be also influenced by an anomalous presence of inclusions. Thus, Parker [*ibidem*] states that the catastrophic failure of January 1986 was due to the "abnormal high concentration of non-metallic inclusions near to the fusion line of the submerged arc weldment".

Type IV Failure

It seems appropriate, at this point, to dedicate a separate section to the Type IV failure. This is a major maintenance and inspection problem of utilities worldwide, resulting from the creep damage accumulation in the ICHAZ of ferritic steel pipes during long-term service [Smith, 2003]. In particular, it has been registered in low Cr-Mo weldments. In fact, in the case of low Cr-Mo steels, especially 2.25Cr-1Mo steel, weldments creep at a faster rate than the base and weld metal and, at all stress levels, the weldments exhibit the lowest rupture life [Mannan, 1996]. In the ICHAZ, which is the softer zone with lower strength, the creep strain becomes progressively more localized.

The Type IV cracking is, then, a consequence of the low creep strength of a metallurgical zone at the edge of the HAZ. The reason for this weakness had been attributed to the scarce presence of finely dispersed M_2C carbides, which are considered to govern the creep strength of these steels. The dissolution of the M_2C carbides and the consequent formation of coarse carbides, $M_{23}C_6$, M_7C_3 and M_6C type, decreases the mechanical properties of the steels, particularly the creep strength, i.e. the severe coarsening of the carbides dispersion minimises their precipitation-strengthening role [Mannan, *ibidem*]. Another factor, occurring as consequence of the welding process, influences the weakness of this zone. During welding, the Type IV zone experiences a

peak temperature lower than AC_3, and very slow cooling rates, which result in the formation of a mixture of fine-grained ferrite, with grain diameter lower than 5μm, some large ferrite grains and untransformed base metal. The presence of the fine grains of ferrite is expected to lower the creep strength [Parker, 1996]. Furthermore, the zone will contain a high density of fine grains, which reduces the creep strength [Kimmins, 1993].

As pointed out by Parker and Stratford [Parker, *ibidem*], if during testing of cross-weld specimens the displacement measurements are carried out by using the standard specimen gauge length, the samples exhibiting Type IV failures show small total extensions. This fact may lead to the wrong conclusion that the Type IV is a brittle fracture mode. In reality, a strain-based approach for the assessment of the creep behaviour of the weldments, combined with an accurate investigation of the microstructural features, demonstrates that Type IV is a high-ductility failure [Kimmins, 1993], and the low displacement is a result of the localization of the strain accumulation, with local strains higher than 30%.

One distinctive aspect of the Type IV failure is the combined distribution of stresses. For instance, the analytical studies show that when a cross-weld sample is subject to a uniaxial load, if the weld presents a weak zone constrained by stronger zones, the weak zone experiences a multiaxial stress state [Smith,'03]. In detail, in a cross-weld uniaxial sample including a Type IV zone, the strong and weak zones are loaded in series. In this case, the soft zones try to deform transversely and, if possible, neck-down. However, if the weak zone is sufficiently thin, the constraint exerted by the stronger zones inhibits this effect and the resultant triaxial stress state reduces the equivalent stress and suppresses the yielding [Kimmins,'93]. For this reason, Kimmins *et al* [Kimmins, *ibidem*] suggest that a multiaxial creep rupture criterion should be considered in the modelling of the creep behaviour of cross-weld specimens.

Moreover, under low applied stresses (<100MPa) the creep strength of the Type IV zone is appreciably lower than that of the parent steel; on the other hand, under higher applied stresses (>140MPa, for 1/2CrMoV steel), the creep strength of the cross-weld joint and that of the parent metal coincide [Smith, *ibidem*]. Middleton *et al* [2001] suggest that this behaviour is an effect of the hydrostatic stresses induced within the Type IV

zone, as a result of the support offered by the parent metal. According to these authors, the hydrostatic stresses inhibit the flow processes which govern the rupture in the short-term (high-stress regime). Conversely, in the long-term (low-stress regime), the rupture is controlled by damage processes which are accelerated by hydrostatic tension.

Smith *et al* [2003] highlight that limited work was carried out on creep cavity accumulation in the Type IV zone, although recent investigations on the accumulation of cavities on grain boundaries of low alloy steels has been published by Walker and by Walker *et al.* These studies conclude that the Type IV failure is anticipated by the formation of cavities at grain boundaries, and mainly develops on the grain boundaries of fine grains. In general, the cavities are not uniformly distributed in the Type IV zone, nor is there a systematic gradient of distribution in the zone. The abundant nucleation of cavities, registered in cross-welded samples, is thought to be due to the grain boundaries sliding. In fact, the multiaxial state of stress, induced by the constraint, is relaxed by means of grain boundary sliding, which is mainly relevant at lower stresses, because in this condition the grain boundaries exhibit low resistance to sliding [see also Kimmins, 2003]. The mentioned authors report also that the Type IV zone deforms independently from adjacent stronger material; then, it is not constrained. For this reason, it is meaningful to test simulated Type IV specimens (The fact that no constraint is acting is confirmed by the Von Mises equivalent stress governing the failure). Besides, the Type IV specimens show proportionality between the number of cavities and the reduction of area (The authors in the case of cross-weld specimens perform no measurements). Several investigators report the close association between creep cavitation and strain (more than time) [e.g. Kassner, 2003].

2.4.5 *Hydrogen Damage in Welds*

The limited work carried out up to now on the weld metal shows that it is more sensitive to hydrogen attack than the base metal. This sensitivity is due to the higher density of methane-filled bubbles, which is assumed to be an effect of the higher presence in the metallurgical zone of pre-existing voids [Parthasarathy, 1987].

As reported by Shewmon [1985], the previous data concerning the HAZ of Cr-Mo steels, in particular of quenched and tempered 2.25Cr-1Mo steel, are few and contradictory. Consequently, it is not possible to formulate final conclusions concerning the hydrogen attack of the HAZ. For example, Sakai and Kaji exposed in the same conditions base metal and its weld heat-affected zone, stress relieved for 10 hours at 950K (677°C). They report that the dimensions of the bubbles in the HAZ are similar to those found in the base metal, but the bubble density is about 16 times higher. To have more understanding of the scarce data concerning the HAZ, Parthasarathy and Shewmon [1987] performed specific studies on this metallurgical zone in quenched and tempered 2.25Cr-1Mo steels. They exposed samples to increasing pressures, respectively 20.5, 24.5, 28, 31 MPa, and afterwards to the initial pressure of 20.5MPa, while the temperature was kept constant at 823K (550°C). The same experiment was carried out at a temperature of 853K (580°C), adopting values of pressure slightly different from those mentioned. After each jump, the authors waited until that the strain rate of expansion had reached a steady value. Their main conclusions were:

- Agreeing with previous studies, the HAZ of the quenched and tempered 2.25Cr-1Mo steel is more susceptible to hydrogen attack than the base metal, but less than the weld metal.
- In presence of high pressures, the nucleation of bubbles can be induced in this metallurgical zone.
- The nucleation is not homogeneous and due to the growth of a number of pre-existing voids which appear to grow only under the action of higher pressures of hydrogen.

Bocquet *et al* [2001] for cross-welded samples made of 2.25Cr-1Mo steel, 2.25Cr-1Mo-¼V steel, 3Cr-1Mo-V-Ti-B steel and Grade 91, 9Cr-1Mo-V steel, report that all samples tested in air and hydrogen ruptured in the FG-HAZ. These findings are in agreement with their model, which predicts higher creep strain in the FGHAZ than in other regions, and, consequently, higher local axial stresses, which accelerate the growth of voids in this metallurgical zone.

2.5 Conclusion of the Literature Review

1. Histories of failures, registered worldwide, have pointed out the weakness of weldments in pressurized components of (petro)chemical plants. Several failures have been registered in welded joints, mainly in the HAZ.

2. Type IV failure is a major maintenance and inspection problem of utilities worldwide. Some recent studies on the creep behaviour of cross-welded samples made of 2.25Cr-1Mo and V-modified 2.25Cr-1Mo failed in the FGHAZ, whilst those made of 3Cr-1Mo-V steel failed in the base metal.

3. A lack of experimental data, in particular under complex state of stresses, is noted with respect to the behaviour of welded joints in hot high-pressurized hydrogen. This is a result of the high costs and difficulty of the necessary experiments under these severe conditions. Consequently, the prediction of the lifetime of industrial components operating in hydroprocessing conditions is still based on the Nelson curves, an empirical tool which is not rigorous and certainly not applicable to the design of components which use newly developed steels.

4. The petrochemical sector has a wide experience of the performances of the 2.25Cr-1Mo in the current hydroprocessing conditions, because this steel has been used for more than 40 years. Unfortunately, there is a lack of operational data on the performances of the 3Cr-1Mo-V steel and, in particular, the V-modified 2.25Cr-1Mo steel.

5. Under uniaxial stresses the mechanical properties of steels are degraded, because applied stresses enhance hydrogen attack. This conclusion has been extended by the work of other researchers to the case of components under multiaxial stresses. However, very little information is available on the behaviour of welded joints in hot high-pressurized hydrogen and in presence of complex state of stresses.

3 Aim of the Thesis

The review of the available literature reveals numerous topics for which new information is required, in order to understand hydrogen attack in steels and contribute towards the design and safe and economic operation of petro-refinery reactors. The present programme was therefore designed to fulfill the following aims:

1. To investigate the creep behaviour of welded joints of commercial low alloy CrMoV steels developed for petro-refinery applications in hot high-pressurized environment, allowing comparison with data obtained in air or inert gas..
2. To achieve some insight into the mechanisms governing damage accumulation and failure.
3. To evaluate the effects of alloying elements, namely Cr and V in Cr-Mo steels, on the strength of the welded joints, particularly in the presence of hydrogen attack.
4. To study the effect of applied stresses, both uniaxial and multiaxial, on the evolution of hydrogen attack damage.

4 Experimental Techniques

4.1 Uniaxial Creep Testing in Air

Uniaxial creep testing in air was completed to provide data reference against which the data from hydrogen testing could be interpreted, comparing creep behaviour in air and in hydrogen. Rigorously, one should compare the data from uniaxial creep tests in hydrogen with equivalent data from uniaxial creep tests in inert gas, in order to eliminate the influence of oxidation on specimen lifetime. In the framework of the present work, it has been assumed that this influence was small [8] and the reference uniaxial creep tests have been performed in air, using standard rigs. The following section describes briefly the testing set-up and procedures used for carrying out the tests at the Institute for Energy of the Joint Research Centre, which is Certified ISO 9001 and ISO 14001.

[8] It has been observed that, for the considered test durations, the thickness of the oxide layer is about 200μm.

4.1.1 The Uniaxial Creep Rigs

Loading System

The rigs used for testing were MAND™ constant load, dead-weight lever-arm machines, shown schematically in Figure 4.1-1. The machines used were labelled in the laboratory as Machine 1 and Machine 2. With Machine 1, the loading was applied through a 39.4:1 lever-arm ratio whilst, with Machine 2, the lever arm ratio was 40.3:1. The loading was kept constant by maintaining the lever in a horizontal position throughout the test. Specifically, as the specimen elongates, the loading weights move downwards until they trip a switch which causes the motor to turn, lifting the weights a small amount to maintain the lever position. When the first tests were carried out, the set-up did not cater for the automatic turning off of the furnace after failure of the specimens. For this reason, the fracture surfaces of some of the first tested specimens were covered by an oxidized layer. To overcome this inconvenience, the machines were equipped with a further switch, which automatically turns off the furnace. Calibration of the loading lever was performed with a Rein™ proving ring.

Heating System

Specimen heating was applied with a three-zone 3 kilowatt Mike Lockwood™ furnace. Three 'S' type control thermocouples were connected to Eurotherm™ temperature controllers. The specimen temperature was measured with three 'K' type thermocouples: one was positioned about in the middle of the gauge-length, the others were touching the two extremes of the specimen gauge-length. The thermocouples had been respectively labelled as: Top, Middle, Bottom. Normal temperature control of ±0.9K was obtained at 873K (600^{0}C). This was only obtained by careful insulation at the top and bottom of the furnace. To ensure accuracy, the thermocouples were usually replaced after about 1500 hours testing. In addition, each new batch of thermocouples was checked in a highly accurate calibration furnace prior to use.

Measurement of Specimen Elongation

Aluminium oxide extension rods were connected to the top and bottom of the specimen gauge length by means of grips that were machined to fit the specimen knife-edges. These rods were led out of the bottom of the furnace via holes cut into the insulation material. LVDTs with a 50mm range were used to measure the relative displacement between those rods connected to the top and bottom of the specimen. The use of two LVDTs allows averaging of their values, which gives more accurate strain results. The LVDTs were regularly calibrated against high-accuracy ceramic spacer blocks. A typical calibration sheet is shown in Figure 4.1-2.

4.1.2 Testing Procedures

Initial Specimen Loading

Before loading, the specimen gauge diameter was measured with a micrometer in five different positions, so that the average cross sectional area could be calculated. Next, the extension arms were attached to the specimen, followed by the thermocouples. Finally, the specimen was screwed into the load train and mounted in the rig, ensuring that the lever arm was horizontal and that the specimen was in the middle of the furnace. A small 20N load was applied to the specimen, to take up any slack in the system.

Specimen Heating

Temperature set-points were initially set at about 773K (500^0C). The motor on the rig was set to "*automatic*", to ensure that movements caused by thermal expansion were accounted for. Once stable, the temperature controllers were adjusted independently, until the test temperature of 873K (600^0C) was reached. It was normally necessary to leave the rig overnight to allow the temperatures to settle.

Specimen Loading

When the specimen temperature had stabilised, the load could be applied. This was done by first lowering the loading pan until it rested on an aluminium spacer. The weights could then be applied without the risk of shock loading the specimen. Once the correct amount of load was added for the required stress (gravity taken as 9.813 ms^{-2}), the motor was turned on so that the weights were slowly lifted away from the aluminium spacer. The motor was then set to "*automatic*" and the test start time recorded.

Data logging

Both the LVDT voltage signals and the temperature were logged on a Dell™ computer, with a data acquisition programme written in-house with the Labview™ programming language. In addition, the programme converted the LVDT voltages into strain measurements, recording all the data to file for later manipulation. Data was normally saved to file every half-hour, or every hour for longer-term tests. A log book was also kept and updated daily for manual data

4.2 Uniaxial Creep Testing in Hydrogen

To carry out these tests, two identical uniaxially-loaded creep testing rigs, for use under high-pressure hydrogen, have been used. The rigs are a unique facility of the Institute for Energy, designed and built in the framework of the European Project Brite/Euram 1835 (PREDICH). The rigs are designed to be capable of measuring creep strain under hydrogen pressures up to 22MPa, temperatures reaching 923K (650°C) and loads of up to 10KN. A schematic diagram of the rigs and a photograph of them are given in Figures 4.2-1 and 4.2-2 respectively. For the design, fabrication and running of such rigs, much technological innovation and investment has been necessary, especially in terms of safety. Few laboratories in the world have been capable of building similar rigs. Consequently, there are very few guidelines for their construction. The following section aims to describe the design and function of these hydrogen creep rigs (HCR).

4.2.1 Rig Design

The rigs are designed in such a way as to be capable of loading two specimens in series, so that a greater volume of test data could be obtained in a given time. This aspect was desired in the context of the project PREDICH, to allow the testing of a large number of specimens. However, another reason prompted the opportunity of testing two samples in the same testing conditions and in parallel. In fact, both specimens would be under the same load until one would register failure. For the other specimen, the test would be stopped when the specimen is in a seriously damaged state but a little before the failure. In this way, metallographic examination of the unfailed samples would provide information on the damage processes. As far as the specimen size and dimensions are concerned, the PREDICH partners agreed to use specimens having a gauge length of 50mm and a gauge diameter of 8mm. This choice influenced the rig design. The specimens used in the experimental part of the current work were smaller than those used in the PREDICH project. Consequently, it was necessary to build small adapters to allow these specimens to fit into the HCR load train.

4.2.2 Active Gas Containment and Safety in the Hydrogen Creep Rigs

Hydrogen Gas Pressure Chamber

The pressure chamber containing the specimens, extensometer gauges and load train are designed to withstand a total internal pressure of up to 22MPa (220bar) at temperatures reaching 923K (650^{0}C). Type 316 stainless steel is chosen for the construction, because of its' resistance to hydrogen environment, its good weldability and ready availability. The pressure chamber is also designed to withstand any compressive force applied by the load train, due to the fact that the load train is anchored to the top of the pressure chamber. The internal diameter is made as small as possible, compatible with the accommodation of the extensometers and the load train, to minimise the volume of hydrogen gas present. The load train is sealed with water-cooled rubber o-rings at the point where it passes out of the bottom of the pressure vessel, and a swaged type stainless steel seal prevents leakage at the top of the vessel, where the load train is bolted on. Separate active gas inlet and outlets are built into the chamber to allow greater control of the internal pressure, and to allow a small flow past the specimens during a test. This ensures continuous refreshment of the hydrogen environment.

Safety Blanket Gas

Just under the hydrogen pressure chamber is located another smaller chamber filled with a slightly higher pressure of argon. This provides a low-pressure gradient across the rubber o-rings around the load train, so lowering the risk of hydrogen leakage past those rings. Furthermore, in case of hydrogen leakage, the gas goes into an inert environment where it cannot react explosively with oxygen. To enhance safety, the whole pressure chamber is surrounded by a large steel bell housing, filled with low-pressure argon. The oxygen and hydrogen content of the argon is constantly monitored so that any leak could be detected, keeping the risk of subsequent explosion as low as possible. In addition, the argon is kept in constant flow through the bell housing, thereby flushing away any potential build up of hydrogen or oxygen. As a further design safety feature, the volume of the housing is large enough to contain a catastrophic leak from the pressure chamber

without the risk of bursting. In the unlikely case of bursting, the concrete safety cell which surround the rigs provide a further safety boundary.

Compensation of the induced Axial Load on the Load Train

The high pressures used in the gas chamber exert an axial load on the load train, which must be considered in load calculations. To compensate for the additional load, an equalising device was constructed, based on an idea that, according to Baker [1999] had been used in a similar rig by Yokogawa *et al.* The same device had also been used successfully in a compact tension specimen testing rig previously constructed at the Institute for Energy of the JRC [Looney'94], and is shown in Figure 4.2-3. The device is a piston, which is fed with high-pressure argon from the argon chamber. The piston is designed to work against, and exactly balance, the internal test pressure. This is achieved by making the surface area of the piston head equal to the cross sectional area of the load train as shown in the figure.

Installation for the hydrogen supply

A diaphragm compressor, capable of pressurising hydrogen to over 27MPa (270bar), provides the high-pressure hydrogen, required for the tests. A rack of two 50 litres bottles, containing gas at 20MPa (200bar), supplies the compressor. The bottles are connected via hand-operated pressure regulators and high-pressure pipeline, capable of supporting up to 400MPa (4000bar). In case of accidental over pressurization, pressure relief burst valves are incorporated into the system. Both the compressor and the bottles are stored in a separate well-ventilated room outside the laboratory area. All the high-pressure rigs are situated within concrete cells with steel doors, which are designed to stop debris in the event of an explosion. The high-pressure gas is pumped into the rigs via a series of manual and automatic valves, the layout of which is shown in the control panel for the rig (Figures 4.2-4a and 4.2-4b). The hydrogen pressure is also controlled by the high-pressure argon, which produces a low-pressure differential across the seal at the bottom of the exposure chamber. Thus, if the argon supply is cut off for any reason, the hydrogen will also be cut off.

The argon blanket gas is fed through both oxygen and hydrogen monitors. In case of hydrogen leakage and of unacceptable oxygen presence in the bell housing, pre-set alarm levels of these gases allow the active gas to be dumped through the exhaust valve, and the furnace to be automatically turned off. In addition, hydrogen detectors are located in the compressor room, in the test cells and in the control room. All of them are connected to alarms, which automatically stop the test and dump the pressure if dangerously high hydrogen levels are detected. To perform leak tests, the hydrogen gas supply can be switched to helium. A highly sensitive "Leybold UL100 Plus" helium detector is used to check the presence of helium leaks, especially at joints and seals, before hydrogen pressurisation. Extra checks are also carried out with "Snoop"™ soap solution, which bubbles in case of leak presence.

4.2.3 Specimen Heating and Temperature Control

Specimen Heating Method

The work of Baker [Baker, *ibidem et passim*] showed that the use of Thermocoax sheathed resistance wire allows the test temperatures to be reached quickly. The temperatures chosen were 843K (570°C) for the 2.25Cr-1Mo steel and 873K (600°C) for the V-modified 2.25Cr-1Mo and 3Cr-1Mo steels. A good control of the temperature had been obtained by winding the wire into spiral grooves around the pressure chamber. The temperature gradient along the specimen is minimised by fixing anti-convection buffers at either side of the specimen. To provide even greater temperature stability and control, the furnace is split into four heating zones consisting of two long (16cm) zones with 2kW power around the specimens, and two shorter (8cm) zones with 1kW power at the top and bottom of the furnace, to control thermal gradients. The longer zones are designed to be long enough to account for specimen extension during creep, and thus are slightly offset towards the top of the specimens. Finally, heat loss from the thermocoax wire is limited by surrounding the four heating zones with Thermiculite insulation. A schematic illustration of the completed furnace is shown in Figure 4.2-5.

Temperature Measurement and Control

To measure the temperature, four sheathed 'S' type thermocouples are used, directly attached to the centre of the four heating zones. These thermocouples send the input into four Eurotherm 2208e controllers, which could be given independent set points. The specimen temperatures are measured with two sheathed 'N' type thermocouples, positioned close to the top and bottom shoulders of each specimen. It is not always possible to measure directly the temperature of the specimen gauge length, because of the extensometer design. However, according to Baker, previous experiments had shown that the position of the thermocouples on the shoulder sections gave a good representation of the true gauge temperature. Moreover, it was found that the temperature gradient across the length of the specimen could be controlled to within 1K or less.

4.2.4 Creep Specimen Extensometry

The Design Problem

Traditional methods of strain measurement in creep involve the use of extension arms connected to the top and bottom of the specimen gauge length. In this way, the gauge length strain can be measured in terms of displacement between those arms using an LVDT. However, when high-pressure gas is being used, the arms should pass through the seals, which would induce friction and compromise the reliability of the strain readings. An alternative method is to measure the displacement of the load train somewhere outside of the furnace. Of course, this technique cannot be used in the case of two specimens being tested in series, as the strain rate of each may differ. A first solution adopted at the Institute for Energy of the JRC consisted of an in-situ capacitive displacement transducer, described in the work of Baker below. The advantages of this system were the small size, the possibility to be used in-situ and the high accuracy. This produces a change in capacitance, which is converted to a voltage. Several problems had been encountered during the initial work on development of the capacitive gauges, particularly when operating under high temperatures. These were generally associated with concentricity of the specimen and electrical shorting between either the two halves of the capacitor, or one

part of the capacitor with the shielding. It was therefore decided to carry out the majority of creep tests with single specimens (not two specimens in series in the load train), so that displacement could be measured with an LVDT attached to the load train.

4.2.5 Creep Specimen Loading

The Loading Device

In the context of the PREDICH project, it was considered that a maximum load of 10KN would be sufficient for all planned tests. Moreover, in the work of Looney [Looney,'94], the use in previous rigs of pneumatic loading devices produced good results. This device had been chosen for the rigs for uniaxial creep tests in hydrogen [Baker, *ibidem*]. The main advantage of such a system is the small size and elimination of the need for difficult dead-weight loading procedures. In addition, the maximum free movement offered by the device was 100mm, more than enough for the expected combined strains of two specimens in series. A HBM load cell, calibrated with a Rein proving ring, was used to measure the applied load, while Coreci PID controllers meant that the load was controllable to within approximately ±5N over the range of interest.

Load Train Description

The load train is constructed from 16mm thick stainless steel. Rubber o-ring type seals are located at all junctions with pressure chambers of argon or hydrogen. The length of the load train had been calculated on the basis of the expected strain of the two samples, and to be long enough beneath the furnace to help cooling before passing through the first set of seals. A knuckle-eye joint within the high-pressure argon chamber allows the assembly of the load train and confers some flexibility. In addition, the seals through to the hydrogen chamber were designed to accommodate some lateral movement.

Frictional Load Effect of the O-rings

Baker [Baker,'99] noted that the load applied to the specimen is slightly lower than that given by the load cell due to the frictional force exerted on the load train by the o-rings.

This effect is enhanced under high pressures, due to o-ring compression. During Baker's work, the frictional effect was carefully assessed and it was found that the frictional force exerted by the o-rings at an internal pressure of 22MPa (220bar) is approximately 200N.

4.2.6 Testing Procedures

Before Specimen Fitting

Before fitting the specimen in the rig, it is ultrasonically cleaned in ethanol. Then, micrometer measurements are taken in at least five different locations. Afterwards, the average cross-sectional area is used for the calculation of the load necessary to give the required stress.

Calibration of the Thermocouples

Before fitting the specimen, calibration of the thermocouples is carried out by means of Isotech Blok Calibrator, type Jupiter 650S, serial nr. 19560/1, with reference sensor PT-100, serial nr. S317 / 2.

Calibration of the Load Train

Calibration of the load of both machines used Proofing Ring Rein 2Mp (Mega Pounds), Serial Nr. 1084, calibrated once a year by NMi (Nederlands Meetinstituut), Cert. Nr 3806279-01, with Digital Dial Indicator: 1082 Millitast Mahr Nr. 4142 serial number 10115.

Calibration of the LVDTs

The LVDTs of both rigs are calibrated with respect to the displacement. The calibration is carried out against highly accurate ceramic spacer blocks, namely Mitutoyo Cera Block Set serial n. 948866. The LVDTs have a range of ± 25mm. The range had been initially explored by 1.4mm to 50mm using steps of 5mm. The results are reported in figure 4.2-6. In the figure, the range between 15mm and 25mm had been chosen as more convenient,

because the corresponding signal looks linear. A more detailed calibration of the LVDT had been devoted to this range. The calibration is based on steps of 1mm.

Specimen Fitting

Thermocouples are then attached to the top and bottom shoulders, and the specimen is mounted in the load train. In this phase of the work, only one specimen at a time was tested, never two specimens in series. The rig was then assembled and the LVDT for external measurement of the creep strain was placed in position and zeroed. Figure 4.2-7 shows the two halves of a tested specimen, in the load train. The two thermocouples are also visible.

Calibration of the Load Train

Calibration of the load of both machines used the Proofing Ring Rein 2Mp (Mega Pounds), Serial Nr. 1084, calibrated once a year by NMi (Nederlands Meetinstituut), Cert. Nr 3806279-01, with Digital Dial Indicator 1082 Millitast Mahr Nr. 4142, serial number 10115. The measuring load cell of both the machines are type Mill U4000, and have a Range up to 1000 kg. The calibration is carried out with respect to the range 4.5-5.5kN, a range that includes the loads used for the planned tests. The calibration procedure starts with zeroing the offset and setting the gain equal to 1. The load is increased from 4.5kN to 5.5kN in steps of 0.1kN. In this way, the load system has the possibility of following the set load progressively. The calibration allows calculation of the true value of the gain. An example of the Load Calibration curve is shown in Figure 4.2-8.

Leak Testing

Before proceeding with the tests, the pressure chamber and gas infrastructure was leak tested by passing approximately 2MPa (20bar) of helium through the system. For this purpose, the valves, which allow the flow of argon and hydrogen in the gas distribution rack, are closed (Figure 4.2-9) and the valves permitting the flow of helium are opened (Figure 4.2-10). Particular attention was paid to the seals on the load train. Leak detection was carried out with a combination of the helium detector, Snoop soap solution, and pressure drop tests, which involve observing the change in pressure within the pressure

chamber when both the inlet and outlet valves are closed. Once the rigs were confirmed leak free, the bell housing was put into place, and evacuation of the air commenced.

Evacuation of the Bell Housing

Evacuation of the bell housing involved lowering the pressure to approximately 0.05MPa (0.5 bar), and back filling with argon gas. This procedure was repeated up to five times, until the oxygen content of the bell housing was around 0.3%. To further reduce the oxygen content, a steady flow of argon at about 0.12MPa (1.2 bar) was fed through the bell housing. After a few hours, the oxygen content was normally reduced to 0% (within the resolution limits of the detector).

Heating

Once the oxygen content was sufficiently reduced, the furnace was turned on and allowed to heat up to around 773K (500^{0}C). Using the thermocoax heating system, the required temperature was reached relatively quickly (normally within a couple of hours). The final heating to 873K (600°C) was then carried out in small, well-controlled steps, in which the four individual temperature controllers were independently adjusted.

Alarms

Before pressurisation, the safety alarms had to be checked and set (see Figure 4.2-11) Both forewarning and critical alarm levels were set, with only the critical alarm able to cause shut down of the experiment. The oxygen alarm levels of the bell housing were set at 3% and 4.5% respectively. In addition, hydrogen alarms connected to the bell housing exhaust, the garage, the gas trunking and the control room were set at 5 and 10%.

Pressurisation

Hydrogen pressurisation was performed by increasing the pressure of argon in the high-pressure argon chamber. A mechanical device allowed a slightly lower (-0.15MPa) pressure of hydrogen to be introduced into the hydrogen pressure chamber. In this way, the hydrogen was controlled by the safety gas, so that if the safety gas supply was cut off,

so would the hydrogen. All hydrogen detectors were carefully monitored during pressurisation, and the pressure was introduced slowly, over a period of several minutes.

Loading

Once pressure and temperature were stable, the uniaxial creep load was applied. This was applied slowly, using the Coreci PID controllers, over several minutes to avoid accidental overloading (Figure 4.2-12). Once at the desired test load, the test start time was recorded.

Data Logging

A reference book for each reinforced concrete cell was used to store information about each test, including start time, temperature, pressure, material, etc. In addition, periodic readings of the actual temperature, pressure, load and strain from the LVDT were recorded. However, the majority of data logging took place on a Siemens™ computer running a data acquisition programme written in the Labview™ programming language. This programme read the time, temperature, pressure and extensometer signals every few minutes, and wrote the data to file at specified intervals (normally every ½ - 1 hour).

4.3 Internally Pressurised Tube Testing

To perform the testing of internally pressurized tubular components, the rig available at the Institute for Energy of the Joint Research Centre has been used. This rig had been set up and upgraded during previous works performed at the Institute [Looney, 1994; Baker, 1999]. Figure 4.3-1 shows how the rig appears when open, and Figure 4.3-2 provides a schematic representation. The rig had been used for tests in both hydrogen and argon environments. Of course, when argon is used, there is no need for the specific safety features required whilst using hydrogen. To the author's knowledge, only a limited number of results have been published as yet on tests of hydrogen-pressurised tubes where the hoop strain has been continuously measured.

4.3.1 Active Gas Containment and Control in the Tubular Testing Rig

Lay-out of the Equipment

The rig is located in a bunker within the laboratory, called Cell 1, surrounded by thick concrete walls. The room is closed by means of doors made of thick steel. The compressor and the bottles supplying the pressurizing gas are located outside the laboratory, in a separate room.

Specimen Pressurisation

The compressor allows a pressure of over 27MPa (270bar) to be reached. The gas is fed directly into the top of the specimen via a Tescom PID regulator, and flows away from the bottom, in such a way to have a continuous flow through the specimen to allow better control of the pressure. Figure 4.3-3 shows the so-called gas distribution rack, through which the supply of gas to the rig is achieved, and Figure 4.3-4 shows part of the rig control panel.

The Bell-Housing

As the performance of pressurization tests by means of hydrogen requires very strict safety measures, the testing rig, included the furnace, is enclosed in a thick-walled

aluminium bell-housing. In this way, in case of failure of the specimen, the outflow of hydrogen is contained to prevent catastrophic consequences. As additional safety measure, the bell housing is filled with argon at a pressure of about 0.15MPa (1.5 bars) and the oxygen content of the bell housing is constantly monitored to exclude the occurrence of a chemical explosion. Previous work performed at the Institute for Energy of the JRC (JRC-IE) [e.g. Baker, 1999] showed that the rate of hydrogen diffusion through the specimen wall during a test was significant, and could cause a build-up of hydrogen within the bell housing, if not removed. For this reason, the rig is equipped with an extraction system, which keeps the specimen in a constant flow of argon. The hydrogen content of this flow is monitored, and the content increase indicates that the tube is close to bursting

Gas Supply Infrastructure

The gas supply infrastructure is much the same as that for the hydrogen creep rigs (HCR) rigs, described in section 4.2. The main difference is in the extraction system, which draws away any hydrogen that has diffused through the specimen wall, as mentioned above.

4.3.2 Heating System

Heating of the specimen is achieved by means of a three-zone 3 kilowatt Mike Lockwood furnace. The temperature in each zone of the furnace is measured with a 'S' type thermocouple, for a total of three thermocouples for the entire furnace. These sensors provide the input for independent Eurotherm PID controllers. The specimen temperature is monitored with three sheathed 'N' type thermocouples, positioned at the top, middle and bottom of the gauge length. The previous experience at the JRC-IE showed that the best temperature control is achieved by inserting rings of insulating material into the so-called "measuring tube", above and beneath the specimen, to reduce heat loss by convection. Additional insulation rings placed on top of the furnace further improved the temperature control. In this way a satisfactorily stable temperature is guaranteed, with a maximum drift of ± 0.5K, which is within the recommended practice set out by the

HTMTC [1989]. The temperature differences between the three specimen thermocouples were normally less than 1K.

4.3.3 Hoop Strain Extensometry

The 12-Gauge Capacitance Transducer

Considering the complexity of the deformation of pressurized pipes, which is characterized by a partial bulging, a capacitance system of extensometers was designed and fabricated at the JRC-IE, jointly with SJB Engineering Bristol, during the previous work of Baker [1999]. In this system, the specimen forms one plate of the capacitor, and the gauges form the other plate. The system is made of twelve independent gauges, arranged in three horizontal rings of four. The system is shown schematically in Figure 4.3-5, and realistically in Figure 4.3-6. A more detailed schematic version is given in Figure 4.3-7. When an alternating voltage is applied across the plates, the capacitive reactance becomes linear with the gap between the plates. The tube strain is measured by determining the change in distance between the two plates of each capacitor. In this way, it is possible to achieve comprehensive monitoring of the tube deformation, and the position of maximum hoop strain can be distinguished. However, the measurement provided by each individual gauge is subject to potential error due to concentricity problems; so, for accurate strain measurements, the average of each set of four gauges is taken. The gauges, each measuring approximately 1.5 x 1 cm, are mounted into a three-section stainless steel pipe, which forms the so-called "measuring tube". However, for a proper operation of the gauges, they must be isolated from this pipe. Isolation was obtained by spraying the stainless steel housing with aluminium oxide. In this way, the assembly of the measuring tube became easier, and also the electrical isolation of its three sections was obtained.

Calibration of the Gauges

The reliability of the capacitance gauge transducers had been validated during the previous work at the Institute for Energy. The calibration performed during the present work provided some inputs for the improvement of the system itself. The calibration had

been made initially at room temperature, using a set of calibration tubes with diameter ranging between 40mm and 65mm. The respective diameters of the pipes are 40, 45, 50, 55, 60 and 65mm. The range of our interest is between 50 and 60mm. The calibration consisted of two rounds: in one, the diameter was increased from 40 to 65mm, in the other, it was reduced back to 40. Figure 4.3-8 shows a reference tube positioned in the measuring tube of the rig, during the calibration.

For the calibration, the gain of the acquisition system is set to 1 and the offset to zero. Before starting the calibration, the oven had been kept for 24 hours at 323K (50°C), to remove possible traces of humidity, which could affect the signal output. The position of the sensors inside the measuring tube had also been measured, in such a way that each reference tube could be positioned in a correct way with respect to all the sensors. Each time that a reference sample is inserted into the measurement tube, five measurements are taken for that value of diameter. The time elapsed between a measurement and the next is ~3-7 minutes. It had been noted, by comparing the two results for each tube, that their value can be influenced by two main factors: firstly, the position of the tube inside the measuring tube, and, secondly, the slight movement of the measuring tube when a tube is inserted and then removed after calibration. For this reason, particular care had been taken by creating constraints for the measuring tube, in such a way as to avoid its movement.

During the initial calibration of the system, the signal was not constant. This behaviour was due to the lack of insulation of the cables. For this reason, the cables had been substituted with cable THERMOCOAX, sheath Inconel 600 and conductor Inconel 600. The dimensions of the cables are outer diameter 2±0.03mm, sheath thickness 0.32±0.05mm and conductor diameter 0.34 ±0.04mm. In the phase of calibration with the new cables, a signal between 0V and roughly 0.5V had been obtained, whilst a signal of 10V maximum amplitude was expected. Some improvement was made to the sensor device. Specifically, a cement mixed with water had been used to fill the gap between the sensor and the external metal plate, to increase the resistance of the capacitive sensor; and the metal plates had been substituted with another having a larger surface area to improve the magnetic field. The cement (Isolationisms SKA 90 produced by HALDENWANGER -

Germany) was made mainly of Al_2O_3 (95%) and SiO_2 (4.75%). It was heated up to remove any water it contained. In spite of the mentioned modifications, the achieved signal was still too low. The as-received cables were not coaxial, so they had been converted to coaxial. The signal continued to be low. It was suspected that the weakness of the signal was due to the moisture accumulated in the cement. The measurement tube was therefore heated to 473K (200°C) and maintained for 48 hours at that temperature. After this thermal treatment, the desired amplitude of the output signal was obtained.

Another calibration was performed and, to have more certainty of the signal reliability, each calibration tube of the series was kept in the measuring tube for 24 hours at 473K (200°C). In this way, the stability of the output signal, as a function of the time, could be also observed. Furthermore, the stability of the signal had also been verified at 873K (600°C). In this case, the calibration tubes had been kept at least for 16h inside the oven and the constancy of the signal had been observed. This procedure had been followed for the calibration tubes having respectively diameter of 45mm, 50mm, 55mm and 60mm. After this step of calibration, the system was cooled down to room temperature and kept in this condition for a few days.

Next, some other problems had been noted in the data acquisition system of the multiaxial rig. This trouble was due to the exposure of the measuring tube in air at 873K (600°C), which caused the formation of a layer of oxide between the cables, which prevented the passage of the signal. It was necessary to dismount the measuring tube and remove the oxide layer. Besides, the contact between tube and cables had been guaranteed by welding a wire of Pt-Rd on tube and cables via spot welding. After this intervention on the measuring tube, the calibration had been again carried out by means of tubes of 50, 55, 60 and 65 mm diameter. As starting value, 50mm had been chosen, because the external diameter of the specimen gauge is 50.3mm. The three sets of 4 values were averaged during each sequence and, again, the values coming from the two sequences were compared and, if satisfactorily similar, averaged. The final average values were used to set the most suitable values for the experiment of the gain and of the offset. The results of the averaging are presented in Figure 4.3-9, where it appears evident that the use of a tube 65mm in diameter does not guarantee a constant signal. For this reason it was

decided to limit the calibration to the range 50-60mm which is, considering the values of strain expected, the range of our interest.

Calibration of the Control-Pressure

To give a reference value for the applied pressure, the Druck PV 411 hand-pump was used, which can generate either pneumatic pressure and vacuum or hydraulic pressure. The range of hydraulic pressure in which it can be operated is 0-70MPa (0-700bar). The reading is taken by means of Druck DPI 610 Portable Pressure Calibrator. For the calibration, the range 16.5-19.5MPa (165-195bar) was chosen, because the working pressure was 18MPa (180bar). Initially, for the pressure were chosen a "zero point" equal to zero and a gain equal to 1. The calibration had been made in such a way as to have a deviation of 0.035% in correspondence of the value of the applied pressure (18MPa).

4.3.4 Testing Procedures

Specimen Fitting

To the specimen are connected, firstly, the gas inlet and outlet tubes, and, then, the thermocouples (for details about the specimen preparation, see § 4.5). Before mounting the specimen, the ceramic spacers are positioned around the shoulders, as shown in Figure 4.3-7. Finally, insulation material is positioned around the gas supply pipes, to help keep good temperature control during the test.

Leak Testing

At this point, the bell housing is closed. Afterwards, a leak test of the testing tube is performed. For this purpose, it is pressurized with helium up to 2MPa (20bar) at room temperature. The pressure is maintained for 24h and no traces of a leak were detected. For this purpose, a combination of the helium detector, Snoop soap solution, and pressure drop tests is used, the latter involving the observation of the change in pressure within the specimen when both the inlet and outlet are closed. When the leaks had been fixed, the bell housing is mounted and evacuation of the air commences.

Evacuation of Bell Housing

The bell housing is then flushed by means of Argon, to reduce the presence of oxygen underneath the safe limit of the detector. For this purpose, six cycles of flushing with argon are usually carried out, during which the pressure is kept between -0.03MPa (-0.3bars) and +0.045MPa (0.45bars) in the bell housing. The flushing is performed to reduce the presence of oxygen in the bell housing to 0.3%. To further reduce the oxygen content, a steady flow of argon at about 0.15MPa (1.5 bars) is created through the bell housing. After a few hours, the oxygen content is reduced to minimal traces

Flushing with hydrogen

After the tube is flushed three times by means of hydrogen, hydrogen is introduced into the tube and pressurized up to 1MPa (10bar). Then, the outlet valve is open and the gas evacuated. After the third flushing, the tube is charged with hydrogen and pressurized up to 1MPa (10bar).

Heating and Pressurization

The temperature is increased up to about 843K (570°C) with a ramp rate of 1K/min, to avoid overshooting and to avoid stressing the steel by the induced temperature gradient. Final adjustment up to 873K (600°C) is usually made with a higher ramp rate (e.g. 5K/min), in order to reach the set-point rapidly. When the final temperature is reached and stabilized, the pressure is increased to 18MPa (180 bars) at a speed of 0.25 MPa/min (2.5bar/min). Afterwards, eventual changes in temperature are carried out to accommodate any changes in temperature produced by the pressurization.

Alarms

As for the uniaxial creep tests, the alarms are part of the safety system adopted for the test rig. Different types of alarms are distinguishable:

1. Fore-alarm and critical alarms: the first is a warning, the second causes the shut down of the experiment. They monitor the oxygen levels in the argon present in the bell housing, and their thresholds are set at about 3% and 4.5% respectively.

2. The hydrogen alarms connected to the extraction tube, the bell housing, the garage and the control room have their thresholds set at 5 and 10%.

The alarm for the hydrogen gas pressure shows two set points: a high set point and a low set point, i.e. about 0.5-1MPa (5-10 bars) above and below the test pressure. In this way, it is sensitive enough to shut down the hydrogen supply, in case of a sensitive drop in pressure, which could be due to the failure of the specimen or accidental over-pressurisation, caused by compressor or controller failure. The threshold guarantees that the alarm is not sensitive to small fluctuations in pressure.

Data Logging

The data logging is carried out by means of an Olivetti™ computer, running a data acquisition programme written in the Labview™ programming language. This programme reads the time, temperature, pressure and extensometer signals every few minutes, since the starting of the heating up phase. The data are written to file at specified intervals (normally every ½-1 hour). In addition, a traditional reference book is used to store information about each test, including start time, temperature, pressure, material, etc., and periodic readings of the actual temperature, pressure, and voltage signals from the capacitance transducer.

4.3.5 Strain Measurements after Test

The methodology, adopted for the strain measurement of pressurized tubular specimens after testing, has been conceived, modified and improved during the course of the present research work.

Measurements on the Cross-welded Tube, made of 2.25Cr-1Mo Steel

The measurements are carried out by means of calliper vernier on the external surface of the specimen. For this purpose, 9 parallel lines, spaced of 20° from each other, had been drawn on the surface. On each line, the variation of measurement of diameter is taken every 5mm. In correspondence of each point of measurement, a marker is traced (Figure 4.3-10).

Measurements on the Longitudinally-welded Tubes, made of 2.25Cr-1Mo-V Steel

At this point, the methodology of measurement registers a remarkable improvement. The measurements are no longer measurements of diameter but measurements of strain. The measurements are carried out by means of a machine tool. This equipment guarantees high precision and accuracy in setting rotating angles and translational movements along the axis X and Y. The translational movements are digitally controlled, with an accuracy of 0.1mm. The angles are set with the accuracy of 1 degree (Figure 4.3-11). The machine is equipped with a sensor that lightens, when it touches the surface of the tube (Figure 4.3-12 and Figure 4.3-13). The measurements are carried out along lines spaced of determined angles. Along each line, the spacing of the measurements is of at 5mm. With the purpose of having a detailed mapping of the strain of the tube, high numbers of measurements (along lines spaced at small angles) are performed in the zones which registered higher deformation (Figure 4.3-14). However, fewer measurements (along lines separated by bigger angles) are carried out in zones that registered very low (or no) strain (Figure 4.3-15).

PAGE MISSING IN ORIGINAL

4.4.2 The 2.25Cr-1Mo-V welded Joint

The material was received from the same producer, in the form of two coupons: the first coupon, having dimensions equal to 80mm × 150mm × 250mm, was received and tested in the framework of the PREDICH Project; the second coupon (see Figure 4.4-1), requested for the purposes of the present work, had dimensions equal to 56mm × 351mm × 396mm. The ingot contained four equidistant weldments, all obtained in the 351mm dimension: three with prismatic section, and the fourth with rectangular section. The weldments were submerged-arc multipass weldments: 9 passes for the weldment with rectangular section, 12 passes for the others. Both coupons underwent similar thermal treatments, consisting of water quenching from 1223K (950°C) and tempering of the base metal at 923K (650°C), with PWHT consisting of 10 h at 978K (705°C). Again, the base metal was bainitic, with some fine carbides precipitated mainly along the grain boundaries at the edges of bainite plates. The HAZ was also mostly bainitic, with some precipitates of proeutectoid ferrite, while the weld metal was a mixture of ferrite and a lath arrangement of upper bainite.

4.4.3 The 3Cr-1Mo-V welded Joint

This material, also received in the form of a welded coupon, was a leftover of the PREDICH Project. The coupon was a parallelepiped, measuring 70mm × 130mm × 280mm, which had a cross-weldment at about middle-length. This material also underwent a thermal treatment consisting of water quenching from 1223K (950°C) and tempering at 923K (650°C) of the base metal, with PWHT consisting of 10h at 978K (705°C). The resulting microstructure was similar to those encountered in the 2.25Cr-1Mo standard steel and in its V-modified grade.

4.5 Specimen Preparation

In this section, the procedure adopted for the preparation of both the uniaxial and multiaxial test-pieces is described

4.5.1 Specimens for Uniaxial Creep Testing

The creep specimens were designed in accordance with British Standard 3500 "Creep and Rupture Testing of Metals" [BS3500, 1969], which states several dimensional ratios designed to reduce the effect of stress concentrations (Figure 4.5-1). The first stage of the specimen preparation involved cutting of 14mm diameter cylinders from the original block, by means of wire erosion. After machining, the specimens were cleaned, given a polish with 800-grit emery paper and washed again with acetone prior to testing. The storage of the samples was accomplished by immersing them in acetone to prevent corrosion.

4.5.2 Specimens for Multiaxial Creep Testing.

Specimens for internally pressurized tubes testing had been obtained from the coupons made of 2.25Cr-1Mo standard steel and from 2.25Cr-1Mo-V steel. In the former case, one tube was bearing a circumferential weldment at about middle-length of its gauge length. In the latter case, two tubes having a longitudinal weldment were obtained, one for hydrogen pressurization and the other for pressurisation by means of argon. More details about the testing are to be found in section 4.6.

The Design of the Tubular Specimen

On the basis of the work of Baker on tubular specimens [1999] and of the uniaxial creep results of PREDICH, it was decided to test the tubes in the presence of an internal pressure of 18MPa (180bars) and at temperatures that would realize a state well above that described by the Nelson Curves [API, 1997] (see §4.6). The design of the tubes refers to the code of practice suggested by the High Temperature Mechanical Testing Committee [HTMTC, 1989]. In addition, the wall thickness is set to ensure a shallow hydrogen concentration gradient across it, such that the effect of the hydrogen could be clearly seen. To conform to the PREDICH project, a temperature of 843K (570°C) was chosen for the tests on welded 2.25Cr-1Mo standard steel, and a

temperature of 873K (600°C) for tests on its V-modified grade. It was decided to apply to the tube made of standard 2.25Cr-1Mo steel a stress of 100MPa, in order to have evidence of hydrogen attack in the different metallurgical zones of the weldment. From the results of the first uniaxial tests carried out on the V-modified 2.25Cr-1Mo steel, a stress of 120MPa was selected for the tubular specimens made with this steel. This stress was expressed as mean diameter hoop stress given by

$$\sigma = \frac{Pd_m}{2t} \qquad \text{[Equation 4.5-1]:}$$

where P is pressure, d_m is the mean diameter, and t is the thickness. Table 4.5-1 gives the comparison between the adopted design parameters and the recommended ones for all the tested tubes [HTMTC, 1989]. It is normal practice to use a gauge length somewhat longer than the minimum value suggested. The stress raising effect of the shoulders is minimised when the shoulder thickness is 1.2 times the gauge thickness. However, JRC experience demonstrates that a ratio of 1.5 is better, as it reduces strain in the shoulder area. It should also be noted that the shoulder length may also be shorter than the recommended $2d_o$, without adversely affecting the test.

Filler Bars

The inside of the tube is occupied by a filler bar, having diameter of 37mm, slightly lower than the inner diameter of the tube (44mm). In this work, the filler bars are obtained from the same coupon used to produce the tube, i.e. with the weldment. This design feature has a twofold purpose:

- To minimise the volume of hydrogen gas and, hence, the explosive potential inside the tubes.
- To have the same welded joint exposed in the absence of superimposed stresses. By comparing the pressurised tube and the filler bar, it is possible to speculate on the role of the applied stress on the enhancement of the damage in the different metallurgical zones.

Tube Preparation Procedure

A cylinder having an internal diameter of 51mm, with an external diameter of 55mm and 327mm long, is cut from the received coupon by means of spark erosion. The

cutting procedure allows a bar having a diameter of 37mm and length 295mm to be provided from the same ingot. From the first piece, a tubular specimen is machined in conformity with the Code of Practice suggested by the High Temperature Mechanical Testing Committee, and its surface is finished to 800-grit paper. (Figure 4.5-2). The second piece is also surface finished with 800-grit paper (Figure 4.5-3). The hole on the base, and the narrow cut on the lateral surface, are both produced by the wire erosion. From the base metal of the ingot, two end caps are machined, and their geometrical features are given by Figure 4.5-4, Figure 4.5-5, Figure 4.5-6. To have good fit of the end cap, the inside ends of the tube are machined (Figure 4.5-7) and the local inner diameter of the tube thickness is increased from 43mm to 44mm. In correspondence of the shoulders the tube diameter is reduced from 54mm to 44mm (Figure 4.5-2). Figure 4.5-8 shows the complete set for a tubular specimen: tube, filler bar and end cups.

On the other end of the filler bar a groove is introduced, together with some narrow channels that put the groove in contact with the outer surface (see Figure 4.5-9). Afterwards, the holes produced by the wire erosion are closed as well as the lateral cut of the filler bar by welding (see Figure 4.5-10 and Figure 4.5-11). In this way, the filler bar becomes a solid bar. The groove produced at one end allows the stable vertical positioning of the filler bar on the end cap when the tube will be positioned vertically during the test (see Figure 4.5-12, Figure 4.5-13). The gas is injected via the end caps, and the design detail produced on one base of the cylinder leaves open some lateral windows, which allow the gas to flow on the external surface of the filler bar (see Figure 4.5-14). In this way, hydrogen can diffuse from the external surface toward the inner of the steel filler bar. This allows the investigation of the eventual gradient of the damage due to hydrogen attack. The groove and its lateral mini-channels are a design detail which had been devised for the 2.25Cr-1Mo-V tubes. The tube made of the standard grade, previously manufactured, did not exhibit this feature. Figures 4.5-15, 4.5-16, 4.5-17, and 4.5-18, show the assembly sequence for the tubular specimen. Figure 4.5-19 shows the twin tubular specimens.

Welding of the Tube

For preparation of the tube made of 2.25Cr-1Mo standard steel, the end-caps were attached to the tubes using electron beam welds, producing a high-quality weld with a

minimum of specimen distortion. This weldment technique had been also adopted in the previous work of Baker, who found that:

- In some cases, the electron beam weldments could leak hydrogen, due to lack of penetration of the weld, which creates a stress concentration at the weld root.
- Having three welds next to each other created tensile residual stresses, which may have contributed to the premature weld failure.

As a result, many of Baker's tubes were welded with only one electron beam weld. In the present work, the weldment of the standard steel was also made with only one electron beam weld, and the results have proved completely satisfactorily. Nevertheless, for the tubes made of 2.25Cr-1Mo-V steels, it was decided to adopt the usual multi-pass argon-arc welding, which gives a strong and reliable weldment. The weld material used was 309 LHF, DIN 8556, SG X2CrNi24.

The Gas Supply Pipes

In order to provide gas tight ends on the specimens, end-caps were designed, machined and welded to the tube. In addition to the end caps, gas supply pipes made from 14mm × 8mm stainless steel tube were welded onto the end caps at either end. These pipes were joined with high-pressure fittings, to allow safe connection to the gas supply infrastructure. After welding, the outside of the tube was polished with 800-grit paper and cleaned with acetone.

Positioning of Thermocouples on the Tube

The temperature to which the tube was exposed during the test has been measured by means of three thermocouples type "N". These thermocouples were spot welded on the external surface of the tube gauge length, respectively in correspondence of the two ends of the gauge and on the middle of it. The thermocouples had been positioned in such a way to be not on the weldment, but on the base metal.

4.5.3 Specimens for Exposure in Absence of Applied Stress

In the case of the standard 2.25Cr-1Mo steel, the specimens for exposure in the absence of applied stresses (so-called stress-free exposures) had been obtained from leftovers and were not regular. However, the specimens made of V-modified 2.25Cr-1Mo steel had been cut from a well-defined section of the original block and, for this reason, have the same geometry, i.e. parallelepipeds having dimensions 7mm × 10mm × 48mm.

4.6 The Test Conditions

The conditions chosen for the tests performed in the present work are given in Table 4.6-1 and in Table 4.6-2. For the tests on the standard (or traditional) 2.25Cr-1Mo steel, a temperature of 843K (570°C) was selected, consistent with the temperature adopted for the tests carried out in PREDICH project. For the tests on V-modified 2.25Cr-1Mo and 3Cr-1Mo steels, the temperature of 873K (600°C) was selected. The tables show that the testing on V-modified 2.25Cr-1Mo steel had been carried out by considering two different batches. One batch was a leftover of the PREDICH project, which allowed comparisons to be made with the results of that project. The other batch had been requested from the same producer specifically for the present work.

4.6.1 Uniaxial Creep Tests in Air

The tests on the V-modified 2.25Cr-1Mo and 3Cr-1Mo steels have been performed under applied stresses of 100, 120 and 140 MPa. In addition, a test at 170MPa had been carried out on the first batch of 2.25Cr-1Mo-V and on 3Cr-1Mo-V. For the standard 2.25Cr-1Mo steel, uniaxial tests have been completed only at 100MPa, but at 843K (570°C) and 873K (600°C).

4.6.2 Uniaxial Creep Tests in Hydrogen

As shown in Table 4.6-2, the uniaxial creep tests in hydrogen environment have been carried out at 843K (570°C) under an applied stress of 100MPa in the case of the standard 2.25Cr-1Mo steel, but at 873K (600°C) and for stresses ranging from 100 to 170MPa for theV-modified 2.25Cr-1Mo and the V-modified 3Cr-1Mo steels. The hydrogen has been kept at a pressure of 18MPa (180bars) with the exception of the test performed on the first batch of V-modified 2.25Cr-1Mo under a stress of 120MPa. In this specific case the hydrogen pressure has been kept at 22MPa (220bars).

4.6.3 Internally Pressurized Tubes (Multiaxial Creep Tests)

Creep tests were undertaken for tubes made of 2.25Cr-1Mo standard steel and on V-modified 2.25Cr-1Mo steel. For the pressurization, hydrogen and argon have been used.

4.6.4 Exposure in the Absence of Applied Stresses

These tests have been carried out in an appropriate furnace for the exposure in air, and in a high-pressure autoclave for exposure to hydrogen. The temperature and hydrogen pressure adopted is the same as that chosen for the respective creep testing.

5 Results and Discussion

5.1 Outline of the Work Performed

The current chapter reports the results of the experimental work performed on the tested steels and weldments, together with the discussion of the results. The experimental work consists of

- Ageing tests, in air and in controlled atmosphere (hot high-pressurized hydrogen). The ageing exposures are tests in absence of applied external stresses. They are also referred to as "stress-free" exposures, which does not exclude the presence of some residual stresses in the material, but these stresses are assumed to be very small in comparison with those induced by the application of external loads.
- Creep testing, in air and in hydrogen, involves uniaxial tests on cross-weld specimens and tests under more complex states of stress, achieved via the pressurization of tubular specimens. In addition, hardness measurements are carried out on the test pieces.
- Microstructural investigations, by means of optical microscope, scanning electron microscope (SEM) and transmission electron microscope (TEM) are performed with the purpose of adding more insight to the observed phenomena.

5.2 Testing on the Standard 2.25Cr-1Mo welded Joint

The current section reports the results of the tests on the standard 2.25Cr-1Mo welded joint. The tests performed are:

- Tests in the absence of applied external stresses, i.e. stress-free exposures.
- Tests in the presence of an applied external stress, uniaxial or multiaxial.

5.2.1 Stress-Free Exposure in Hydrogen

The base material and its weldment have been tested in hydrogen at 843K (570°C) and 18MPA (180bars). Two steps of exposure are considered here: up to 2000h and up to 4000h. The results of microstructural observations are described and compared with those of the stress-free filler bar, also used as a stress-free reference during the corresponding experiment under multiaxial load. The situation after 2000h of exposure is presented in Figure 5.2-3, for the five metallurgical zones of the sample. The weld metal (WM) is the metallurgical zone most affected by cavitation, whilst the fine-grained-heat-affected-zone (FGHAZ), the inter-critical-heat-affected-zone (ICHAZ) and the base metal (BM) are all only slightly cavitated. The coarse-grained-heat-affected-zone (CGHAZ) can be considered not cavitated.

As shown in Fig. 5.2-4, after 4000h of exposure the FGHAZ is the most heavily cavitated zone; the ICHAZ exhibits a damage comparable with that of the FGHAZ; the weld metal is cavitated, but the extent of damage is similar to that registered in the 2000h case. The base metal is slightly cavitated, mainly along the grain boundaries, whereas the CGHAZ is still not cavitated, although it is possible to find exceptional areas with a few relatively large cavities (0.5-1μm). The cavities of the weld metal are in both cases round and conserve their shape while growing; the cavities of the FGHAZ coalesce and produce relatively large voids (2-4μm) of irregular shape along the grain boundaries. The cavities of the base metal also tend to coalesce to form elongated voids along the grain boundaries. In the base metal, an increase of the grain size with the increasing exposure time can be seen. In addition, bainitic laths appear after 4000h, in general of larger dimension and developing along preferential directions. The bainitic phase tends to result in a continuum extended from one side of the grain to the other [Lundin, 1984].

Comparison with the stress-free filler bar and the pressurized tube

The welded stress-free filler bar of the pressurized tube exposed to hydrogen, during the multiaxial test up to duration of 3230h, exhibits different damage features. The description of the damage of the pressurized tube is part of section 5.2.3. In this section, the results are recalled for an immediate and worthwhile comparison with the other results coming from the so-called "stress-free" samples.

As shown in Fig. 5.2-5, the FGHAZ also appears as the most cavitated zone after 3230 hours of exposure, with somewhat lower damage in the base metal and the CGHAZ, and with practically no damage in the weld metal. In the pressurized tube, the cavitation is more intense, but the sensitivity of the different metallurgical zones is compatible with what is found in the stress-free filler bar: i.e. very high cavitation in the FGHAZ, high cavitation in the base metal, much less cavitation in the CGHAZ, a few isolated voids are detected in the weld metal close to the CGHAZ and almost no damage is registered at the centre of the weld metal.

The different behaviour of the weld metal, in the two different stress-free cases, the filler bar and the stress-free exposures, is difficult to explain. It seems that the cavitation of the weld metal starts very early. In fact, the 2000h sample indicates that the cavitation, in the detected measure, shows up in the weld metal before other zones, including the FGHAZ. It is possible to argue than the nucleation is easier in the weld metal than in the FGHAZ and the rest of the HAZ. But, for some reason, the growth of the cavities slows down and, after 4000h of exposure, the cavitation extent is about similar to that registered after 2000h.The fact that nucleation of cavities appears very soon in the steel, and in its weldment, is well established. Already, the work of Sundararajan and Shewmon [1980]. which provides the first data available in literature on the kinetics of the incubation period, proves that the formation of methane-filled bubbles in the steel, once it is exposed to hot high-pressurized hydrogen, starts immediately.

The fact that the cavitation of the weld metal is more marked, at an early stage of attack, than the cavitation of the other zones could be explained by the work of Parthasarathy [1987]. This reports that the higher sensitivity of the weld metal to the hydrogen attack is due to the higher density of methane-filled bubbles, assumed to be an effect of the presence in the metallurgical zone of pre-existing voids. In addition,

the weld metal of a multipass weldment is a zone that exhibits a remarkable grain-boundaries development. Some zones present big columnar grains, some others – which are interfaces among two or more passes – present relatively small equiaxed grains. It is well documented [e.g. Sakai, 1980; Erwin, 1982] that grain boundaries offer preferential locations for the nucleation and growth of cavities.

As observed before, growth of cavities in the weld metal is at a certain moment slowed down. In this respect, it is possible to assume that the high hardness of the weld metal (See Figure 5.2-13 for the as-received conditions) plays a constraint role on cavities growth. However, this role is apparently not exerted in the first 2000h. The carbide population of the weld metal is also expected to play some role. In fact, the literature concerning the standard 2.25Cr-Mo steel recognizes the stability of the carbides as one of the main factors influencing the hydrogen attack sensitivity of the steel [e.g. Erwin, 1982]. It is also possible that the weld metal contains some unstable carbides, whose sensitivity to hydrogen attack is apparent before that for the carbides of the other zones. Should the density of these carbides be relatively low, their contribution to the build-up of a methane pressure in the weld metal could progressively decrease during the second part of the experiment, thereby reducing the cavity growth rate. Other information about the weld metal is provided by the results of the measurements performed by means of electro-probe micro-analysis (EPMA), which show an increase of the Mn content in the weld metal with respect to the base metal (Figure 5.2-14; Table 5.2-2); and Mn is known as an element that stabilizes carbides, tying up carbon in the steel. Some indication of the consistency of these hypotheses will come through the publication of the findings of the Brite/Euram Project 1835 (PREDICH), the results of which are still confidential. However, at least three questions arise:

1. Why does the weld metal cavitation of the filler bar seem less than the weld metal cavitation in the exposed samples?

2. Why does cavitation appear in the CGHAZ of the filler bar, whereas in the CGHAZ of the stress-free exposed samples there is practically no cavitation?

3. Why does the damage observed in the FGHAZ, GCHAZ and the base metal of the filler bar after 3230 hours seem, in general, more advanced than that observed after 4000 hours in the samples presented here?

Regarding question 1, the filler bar was observed under relatively low magnification on deeply etched samples, so cavitation in the weld metal could simply have been not well assessed during the first observation. Alternatively, one may consider that the stress-free exposed samples have been obtained from leftovers of the original block. Thus, the weld metal section of them is much smaller than that present in the filler bar and tube and, more precisely, it is only the part of the weldment closer to the CGHAZ. If it is also considered that the observations on the stressed tube show that the weld metal close to the CGHAZ exhibits slight cavitation, the low cavitation detected in the weld metal of the "stress-free" samples is less surprising.

The question on the different sensitivity of the CGHAZ between the two cases (tube + filler-bar and stress-free exposure) remains open, as well as that concerning the apparent different damage levels in the FGHAZ and base metal.

Results of TEM Investigations on "Stress-Free" exposed 2.25Cr-1Mo Steel

In the context of the present work, no TEM investigations had been devoted to the 2.25Cr-1Mo steel. However, results are now reported for some investigations carried out at the Institute for Energy of the Joint Research Centre by Baker *et al* [2000], who analysed the filler bars of 2.25Cr-1Mo tubular specimens (from the same or a different batch) pressurized with hydrogen at 873K (600°C), a pressure ranging from 19.5MPa (195bars) to 26MPa (260bars), and durations from 123 to 715 hours. The authors detected the presence of M_6C-type carbides in the decarburised layer underneath the surface exposed to hydrogen, and the presence of M_6C, M_7C_3 in the bulk material. No M_2C had been detected in the decarburised layer, and only traces of this carbide-type had been detected in the bulk material. These findings indicate that the evolution of carbides in steels aged in hydrogen is consistent with the schemes suggested by Baker and Nutting [1959] and by Gope *et al* [1993]. Considering the short exposure times, it is possible to suggest that the hydrogen accelerates the dissolution of M_2C carbides, which, according to the referred authors, are responsible for the creep strength of the steel.

5.2.2 Uniaxial Creep Tests

Uniaxial Creep Results

Two uniaxial creep tests had been carried out in air on the 2.25Cr-1Mo welded joint:

- One test at 843K (570°C) and in presence of an applied initial stress of 100MPa.
- Another test at 873K (600°C) under the same applied stress.

A third test had been performed in hot high-pressurized hydrogen at a temperature of 873K (600°C), a pressure of 18MPa (180bars) and in presence of an applied initial stress of 100MPa. The full creep curves are shown by Figure 5.2-1, Figure 5.2-2 and the results are summarized in Table 5.2-1. In the case of the tests in air, the increase of the temperature from 843 to 873K (570 to 600°C) produces a decrease of the rupture time from 4646 to 560 hours and an increase of the minimum creep rate (MCR) of about one order of magnitude [9], which corresponds to a reduction of the secondary-creep stage. The strain at rupture and the reduction in area also increase sensitively, demonstrating an increase in ductility. These results are perfectly compatible with the well-established knowledge about creep of steels and welds

In hot high-pressurized hydrogen (P=18MPa and T=873K), the lifetime, the rupture strain and the reduction in area decrease drastically, with respect to the testing in air, whereas the minimum creep rate increases. The decrease in ductility is a hydrogen attack effect documented in earlier studies [e.g. Allen, 1962a]. In particular, Allen reports that the decrease in ductility becomes more relevant with increasing hydrogen pressure. Several workers document the increase of minimum creep rate in hydrogen [Coombs, 1965; Sutherland, 1965; Yokogawa, 1989], and others report that hydrogen in the 2.25Cr-1Mo steel facilitates the movement of dislocations, and promotes recovery [Zander, 2003].

[9] The author is aware that such observations on the minimum creep rate and on the rupture strain of a weldment assume the weldment as homogeneous and, consequently, are not rigorous. Anyway, in spite of their empirical aspect, they give the opportunity for some qualitative considerations.

Microstructural Investigations

The ruptured samples had been sectioned, put in resin, polished, etched and observed by means of optical and scanning electron microscopy. The optical observation of the sample tested in air at 843K (570°C), (Fig 5.2-6x[10] and 5.2-7y) shows that:

1. The fracture occurs in the ICHAZ.
2. High voiding is detected, in both samples, in the ICHAZ close to the fracture surface. Void formation is also detected in the base material close to the ICHAZ, where they coalesce along a direction approximately perpendicular to that of the applied stress.
3. Voids are also found in the HAZ, but their density decreases going towards the FGHAZ and the CGHAZ.
4. Smaller isolated voids are detected in the weld metal, which experienced slight reduction in area.

A further investigation had been performed by means of SEM. It was not possible to obtain information from the fracture surface, because it was covered by an oxide layer. Nevertheless, by examining the cross-section, it was possible to make some deductions about the typology of the damage.

1. In the ICHAZ, not only big voids of irregular shape are found, but also numerous small cavities of sub-micron size, nucleated mainly at interfaces (Ferrite/Cementite or Carbides/Matrix) (Fig 5.2-6g, -6h, -6k, -6l). The small cavities are often linked to each other by very narrow cracks, which develop at interfaces and follow circuital paths (Fig.5.2-6i, -6j). The growth of the voids appears to happen by assimilation of neighbouring cavities and microcracks (Fig. 5.2-6n).
2. The inner surface of the voids showed the formation of cavities and cracks linking along the grain boundaries (Fig. 5.2-6m).
3. The formation of big voids (20-100μm) was not detected in the surface layer, having a thickness ranging between 150 and 600μm (Fig. 5.2-6p).

[10] X and y are used to indicate all the letters of the array (e.g. a,b,c, d, ...).

4. The weld metal appears practically not to be cavitated (Fig. 5.2-6o).

On the basis of the reported results, it is possible to argue that:

a. The failure has intergranular features.

b. The lower creep cavitation, usually observed close to the surface in samples tested in hydrogen, is not only an effect of decarburisation, but also a consequence of the stress distribution, because less cavitation is found in the steel close to the surface of the samples tested in air. It is argued that the nucleation of cavities inside the sample produces a local relaxation of the stresses, and the more superficial layers of the sample become subjected to more intense stresses.

This thesis is supported by the recent work of Albert *et al* [2004] who studied the creep rupture properties of the HAZ of P122 steel using a Gleeble 1500 simulator. These authors observed that the cavity density in the specimen interior, close to the centre of the specimen, is higher than near the specimen surface. On the basis of FEM analysis, they explained the experimental finding as due to the presence of high hydrostatic stress and creep strain close to the specimen centre. Consequently, the quoted authors expect the cracks to initiate from the specimen interior by coalescence and linking of creep cavities, and propagate towards the specimen surface. Furthermore, it is here suggested that the formation of cavities in the specimen interior produces a local relaxation of the stresses [Kimmins, 1993] and a consequent shedding of stress to non-cavitated areas. The more external layers of the specimen experience states of higher stress, which inhibits the grain boundary sliding, which, according to Kimmins is mainly relevant at lower stresses, but triggers locally the plastic flow.

The other cross-welded uniaxial sample, made of 2.25Cr-1Mo steel, had been tested in air at 873K (600°C), under an initial stress of 100MPa. The test duration was 560 hours. The sample had been observed by means of optical microscope before and after etching (Fig. 5.2-7a, -7b, -7c, -7d). The two halves show a bigger reduction in area, with respect to the sample tested in air at 843K (570°C). This can be explained as an increase of ductility due to the higher temperature. Voids have been detected throughout the HAZ, with a few long voids stretched in the direction of the applied

stress and having axis about perpendicular to the fracture surface. Also in this case the fracture occurs in the ICHAZ.

Figures 5.2-8x[11] give the results of the microstructural investigation carried out by means of optical microscope on the third uniaxial cross-weld sample, tested in hydrogen. Failure again takes place in the ICHAZ, with small reduction in area and voids are detected in the ICHAZ close to the fracture surface. Less voids are detected in the FGHAZ, whereas no voids are encountered in the CGHAZ, weld metal and base metal. The lower ductility and reduction in area, registered in hydrogen are, as reported, a well-documented effect of the hydrogen attack [e.g. Coombs, 1965; Shewmon, 1985; Bocquet, 2001]. Conversely, the fact that the fracture happens in the ICHAZ contradicts the findings of the Project Brite/Euram 1835 (PREDICH), whose samples are reported to break in the FGHAZ, for tests performed in both air and hydrogen [Bocquet, *ibidem*]. This discrepancy is surprising because, as mentioned in section [4.4.1], the welded-joint tested in the present work is a coupon received by the Institute for Energy for its partnership in the project Brite/Euram 1835 (PREDICH). However, the literature on the creep of low alloy steel weldments reports the occurrence of failure in the ICHAZ, and this typology of failure is termed "Type IV cracking" [Mannan, 1996; Parker, 1996]. In particular, Parker and Stratford suggest that the low creep strength of the ICHAZ is due to the dissolution of M_2C Carbides, with consequent formation of coarse carbides of the $M_{23}C_6$, M_6C and M_7C_3 type. In addition, the presence in the zone of fine-grained ferrite is expected to lower the creep strength. Moreover, Gope *et al* [1993] report that the superimposition of stresses inhibits the growth of M_2C carbides, so that – as suggested in the present work – the creep strength is further reduced.

5.2.3 *Internally Pressurized Tube (Multiaxial Creep Test)*

One test had been carried out on a tube, made of 2.25Cr-1Mo steel and with a circumferential weldment at about middle-length. The tube had been pressurized by means of hot high-pressurized hydrogen (18MPa) at a temperature of 843K (570°C). The test has been interrupted, before bursting, after 3230 hours. The tube dimensions are drawn in Figure 5.2-9a, and the nominal composition of the tube base material and

[11] In this case, x is a generic letter which is used to indicate al the letters of the array (a,b,c,d,e).

consumable are given in Table 5.2-2. This table also shows a comparison of the nominal values and the results of electro-probe micro-analysis (EPMA) measurements. Table 5.2-3 provides information on the sample geometry and the stress conditions, and synthesizes the creep results.

Strain Measurement during Testing

The creep curves, recorded at the top, centre and bottom of the gauge length during the test, are presented in Figure 5.2-9b, with some results given in Table 5.2-3. After approximately 50 hours, the minimum creep rate at all three locations denotes that the ends deform at a slower rate ($8x10^{-10}s^{-1}$) than the central part ($3x10^{-9}s^{-1}$). The pressurised sample progressively bulges, approximately at mid-length, with this feature becoming increasingly evident as the test progresses. After 3200 h, the deformation rate increases abruptly, so the test was interrupted 30 hours later in order to prevent tube bursting.

X-ray Investigation and Naked-eye Inspection

After the test, the end caps and the filler bar were removed and the pressurized sample was inspected by means of X-rays. Figure 5.2-10 shows the tube, the filler bar and the end caps, as they appear after the test. Figure 5.2-12 presents the results of the inspection performed by means of X-rays. It gives evidence of the presence of two main cracks in the part of the weldment more affected by bulging. This is more apparent from Figure 5.2-17, which shows a detail of Figure 5.2-12, i.e. the cracks appear to propagate from the HAZ into the base metal. In addition, many other smaller cracks are detected close to both the fusion lines. Examination of the tube by naked eye was carried out after having cut it along its axis. Inspection of the tube internal surface confirmed the existence of the two big cracks and many small cracks propagating from the ICHAZ into the base metal (and, in some cases, propagating entirely into the base metal).

Strain Measurement after Testing

The measurements after testing of the strain in the tube is carried out by measuring the local variations of the tube gauge diameter. For this purpose, measurements of diameter are taken, by means of calliper, every 5mm along the whole gauge length.

This is repeated following 9 parallel lines spaced of 20° from each other, thus mapping deformation over the whole surface. The resulting strain values are shown in Figure 5.2-11 as a function of the distance from the central point of the weld, taken as x=0. Although the tube bulging is more pronounced on one side of the gauge surface than the other, in general the strain is quite symmetric around the circumference, but not along the length. The point of maximum deformation (~5%) is located in the weldment, very close to the HAZ. The strain value at the tube mid-length, ~ 4.5%, is in reasonable agreement with the maximum strain recorded by the central capacitance gauge (Table 5.2-3). Figure 5.2-10 shows the tube, the filler bar and the end caps as they appear after the test. On the tube surface, it is possible to see the markers corresponding to the positions where the strain measurements have been taken.

Metallographic Examination and Hardness Measurements

Different sections were cut from both the tube and the filler bar for post-exposure Vickers hardness measurements, so well as optical and scanning electron microscopic examination. The hardness results have been compared with those of the as-received material. Across the HAZ, and in both the base metal and the weld metal close to the HAZ, the spacing of the measurements has been about 0.45mm, in order to obtain a detailed profile. Most of sections were taken longitudinally from both the tube and the filler bar, mounted in bakelite, polished and etched with 3% Nital for 20 to 40 seconds and then examined. In the case of the tube, the longitudinal cut meant that the hoop stress direction was left perpendicular to the plane of observation (i.e. slice A). In order to investigate the effects of the main stress direction in further detail, additional transverse cross sections were also cut from the base metal, HAZ and weld metal, and mounted with the hoop stress axis lying parallel to the plane of observation (i.e. slice B). Finally, to localize the onset and their direction with respect to the direction of the hoop stress, a longitudinal section (including the base metal and weldment) was cut from the more deformed part of the tube, and mounted in resin in such a way as to have the surface directly exposed to hydrogen visible (i.e. Slice C).

Hardness Vickers Results

Vickers hardness data are presented in Figure 5.2-13, which compares the cross-weld hardness profile for the as-received coupon with those of the materials exposed in

stress-free condition and under multiaxial creep stress. The lower hardness of the as-received coupon is registered in the ICHAZ (~ 189 HV), whilst the higher hardness is registered in the weld metal (~ 210 HV). The filler bar presents a slight reduction in the hardness of all the metallurgical zones, but the trend of the hardness profile is in general maintained. A strong decrease in the hardness is found in the pressurised tube, especially in the zone that experienced the highest deformation, and affects all metallurgical zones. The zone which registers the highest reduction in hardness, is the weld metal (from ~219 to ~165). Moreover, the hardness profile appears flattened by the application of the multiaxial stress: the highest value is ~175 (Fusion Line) and the lowest value ~162 (ICHAZ and FGHAZ).

The high reduction in hardness, occurring in the weld metal, might be correlated with the general reduction of mechanical properties in the zone [Mannan, 1996]. This behaviour, especially in the case of thick-section weldments, could be emphasized by the stress redistribution during creep, which causes the region of low strength to shed the stress to the more resistant zones [Parker, 1995].

Microstructural Analysis: Filler bar (stress-free)

Although hydrogen-attack-induced cavitation in the filler bar is evident after 3230 hours of exposure, no fissuring is observed in any of the metallurgical regions of the HAZ. The voids form preferably along grain boundaries, at triple points and other interfaces, and remain isolated. Significant differences in the extent and morphology of damage are observed between the different metallurgical areas of the welded joint. As mentioned in section 5.2.1, and shown in Figure 5.2-5, the cavity density is maximum in the FGHAZ, lower in the CGHAZ and base metal, much lower in the weld metal, where cavities are in general smaller (less than 1μm in size) and rounded. The cross-weld distribution of cavities is approximately symmetrical along the length of the bar, with respect to the weld centre. No gradient of damage is observed along the base metal sections, although some locally higher concentration of cavities are observed in some regions, apparently distributed at random, which is possibly due to residual stresses in the welded joint.

Microstructural Analysis: Internally Pressurized Tube

X-ray examination of the tube clearly reveals the presence of cracks (Figures 5.2-12 and 5.2-17). These are located at the two sides of the weldment, apparently starting very close to the HAZ and propagating in the neighboring base metal, where they can join other formed microcracks. Microstructural examination of transverse sections reveal that cracks form close to the inner wall of the tube (Figures 5.2-15, 5.2-19), starting underneath a surface decarburised layer approximately 100μm thick. As shown by the figures, the cracks are intergranular and preferentially oriented perpendicularly to the hoop stress axis. Intergranular rows of voids are also present, which confirm the strong increase of damage due to the applied stress. Cavities are found to link-up into small cracks, apparently driven by the hoop stress, as previously suggested by recent studies carried out at the Institute for Energy of the Joint Research Centre [Baker, 2000; Castello, 2001]. As for the filler bar, strong differences are observed in the hydrogen attack sensitivity of the different metallurgical areas. Also in this case, if the bigger cracks are excluded, the rest of the damage is rather symmetrically distributed with respect to the point at x=0.

The welded joint is examined in correspondence with the bulging and with the opposite side where the material experiences lower strain. In this way, it is possible to compare the damage detected in correspondence of different strain levels. For this purpose, two slices containing all the metallurgical zones are cut longitudinally from opposite areas of the weldment, corresponding with the position where the gauge length presents the highest relative variation of diameter (~4.9%). These are hereafter called "slice A" and "slice B", with slice B being the one that experiences lower strain. A third slice, called "slice C", is cut from the same zone, in order to observe the surface directly exposed to the hot high-pressurized hydrogen. Figures 5.2-16 and 5.2-16' represent the damage registered in slice B, starting from the base metal and moving towards the weld metal. Cavities had been detected almost over the entire welded joint, with the exception of the weld metal, which exhibits light cavitation represented by the characteristic small round shaped cavities. The most cavitated zone is the FGHAZ (Fig. 5.2-16'g), followed by the ICHAZ (Fig. 5.2-16f) and CGHAZ (Fig. 5.2-16'h,i). The cavities nucleated mainly at grain boundaries. Less cavitation is in general detected in the base metal (Fig. 5.2-16a,b,c), but some areas exhibit thin necklaces of small cavities nucleated along the grain boundaries. Low cavitation is

detected in the sub-critical-heat-affected-zone (SCHAZ) (Fig. 5.2-16d,e) and near the fusion line (Fig. 5.2-16'l). An isolated case of cracking is found between the fusion line and the weld metal (Fig. 5.2-16'l,m). Apart from the base metal, no preferential orientation of damage is observed in the other metallurgical zones.

On the basis of the curves of Figure 5.2-11, slice A was cut between x= 7mm and x= 13mm, and had been taken from the part of the circumferential weldment where the X-ray investigations detect the presence of two main cracks, starting close to the HAZ and propagating into the base metal, along the axial direction of the tube (Figure 5.2-12). The cross section was polished to 1μm and etched by means of Nital 3%. Also, in the transverse cross-sections, cavitation is apparently not dependent on the hoop stress direction. Figures 5.2-19, 5.2-20a to -20h and 5.2-21 show the result of the microstructural investigation on the slice A, which experiences the bulging effect. Fig. 5.2-21 then confirms the presence of a decarburised layer, less affected by cavitation, around 100μm thick. The damage is not uniform and is prominent up to about 1mm underneath the surface exposed to hot high-pressurized hydrogen.

The investigation by means of optical microscope shows the thinning of the tube corresponding to the ICHAZ and to the FGHAZ (Figure 5.2-19). The damage appears in form of large voids in the base metal near to the ICHAZ, and in the SCHAZ and ICHAZ. Coalescence of voids of smaller dimension is also detected in the ICHAZ. A few isolated smaller voids are observed in the FGHAZ, with no voids apparent in the CGHAZ and weld metal. Using the scanning electron microscope, the base metal appeared highly cavitated, with cavities formed along grain boundaries and linking up along them (Figure 5.2-20a). This link up of cavities results in an intergranular separation of the grains. In the base metal, cavities are also registered at interfaces between different phases (Ferrite and Cementite) (Figure 5.2-20a). The SCHAZ is cavitated, with less tendency to formation of cavity necklaces (Figure 5.2-20b). The cavities are formed mainly at interfaces. The ICHAZ appears highly cavitated, with a tendency to formation of clusters of cavities (Figures 5.2-20c,d). Cavities are present at interfaces and, in some cases, short narrow cracks are detected between grains (intergranular). The FGHAZ is highly cavitated, as is the ICHAZ and the base metal (Figure 5.2-20e). In spite of this, in the FGHAZ zone, no tendency is registered to form localized clusters of coalescing cavities, as happens in the ICHAZ, nor the tendency to link-up along grain boundaries, as in the base metal. The CGHAZ shows

less cavitation than the rest of the HAZ (Figures 5.2-20f,g) and the weld metal is populated by very small cavities, although a few isolated large voids (3-7μm) are detected (Figure 5.2-20h). The dimension of the voids encountered in the FGHAZ is similar to that of the voids found in the ICHAZ and CGHAZ: a few microns in size. The voids found in the base metal are slightly smaller, and the cavities found in the weld metal are appreciably smaller (a few hundreds of nm in size) and round-shaped. As result of these findings, the most damaged zones are:

1. The base metal, due to the presence of necklaces of cavities along grain boundaries.

2. The ICHAZ, due to the formation of clusters of cavities of bigger size. The lowest cavitated zone is the weld metal.

Finally, the slice C (Figures 5.2-18a,b) clearly exhibits the presence of cracks on the surface exposed to hydrogen. Their onset is in correspondence with the ICHAZ and SCHAZ, and their direction of propagation is about the same for all of them and perpendicular to the hoop stress direction. The onset of cracks is also apparent in the base metal, in a range a few millimetres distant from the ICHAZ.

At this point, a dilemma emerges. As showed by Figure 5.2-17, the investigation carried out up to this point shows that the FGHAZ is the most cavitated and voided zone. In spite of this, no cracking is detected in this zone, whilst big cracks are found in the ICHAZ, SCHAZ and in the base metal close to it. For this reason the conclusion is that the ICHAZ and the base metal (but more the ICHAZ) are the most damaged zones, although the FGHAZ is the most cavitated. It is therefore inferred that, in presence of applied stresses, the failure of the 2.25Cr-1Mo welded joint, under the reported experimental conditions, starts in the ICHAZ, in the SCHAZ, and also in the base metal, but not in the FGHAZ, as suggested by other workers [e.g. Bocquet, 2001; Gingell, 2001].

To solve this dilemma and explain why the failure starts in the ICHAZ, a more detailed investigation had been carried out, using the scanning electron microscope at higher magnifications, also using the secondary electron mode. The results of this investigation show that, as for the uniaxial tests in air (Figures from 5.2-6h up to –6l) and in the case of multiaxial test in hydrogen, the ICHAZ is populated by very small

cavities. These form mainly at interfaces (Fig. 5.2-22), in particular at the interface carbide/matrix. They, then, become connected by very narrow cracks (Fig. 5.2-24), which may have locally a circuiting development but are also able to connect each other forming long ramified narrow cracks, which can be more than 100μm long (Fig. 5.2-23). The formation of long and narrow cracks seems to be facilitated by the presence of long carbides (or series of carbides), close to which sub-micron sized cavities form (Fig. 5.2-25a,b,c). It could also be due to the different intrinsic strength of the various zones, which may imply that even if the FGHAZ has more voids, it continues to be stronger than the ICHAZ.

5.3 Testing on the 2.25Cr-1Mo-V welded Joint

This section reports the results of the tests carried out on the V-modified 2.25Cr-1Mo welded joint, namely:

- Uniaxial tests, both in air and in hot high-pressurized hydrogen.
- Multiaxial tests, carried out by pressurizing tubes carrying a longitudinal weldment with either argon or hydrogen.

5.3.1 Uniaxial Creep Testing (Batch 1, PREDICH welded Joint)

This paragraph reports the results of the tests carried out, at a first stage of the present work, on some samples obtained as leftovers of the welded coupon used to carry out part of the tests of the PREDICH Project (Brite/Euram 1835) [Bocquet, 2001; Gingell, 2001]. The tests represent, in the context of the present work, preliminary investigations, performed whilst awaiting another welded coupon provided by the same producer (Usinor Industeel - CLI).

Creep Tests

The tests have been carried out in air and in hot high-pressurized hydrogen at testing temperature of 873K (600°C). The applied initial stress was in the range 120 to 170MPa, for the tests performed in air, and 120MPa for the test carried out in hydrogen. The hydrogen pressure was 22MPa (220bars) whilst, for all the other tests performed in this work, the set pressure was 18MPa (180bars, equal to that used in PREDICH). Figure 5.3-1 shows the creep curves obtained. A first feature of the curves is that the tertiary stage is rather short. Especially in air, at lower initial stress, the curves show a well-defined and extended secondary, and the sample fractures a short while after the beginning of the tertiary stage. It is evident that the exposure to hydrogen, at 873K (600°C) and 22MPa (220bars), of the sample carrying an initial stress of 120MPa, reduces remarkably (by about 74%) the lifetime of the weldment (from approximately 1300 hours to about 340 hours!). This result is similar to that found in the case of the standard 2.25Cr-1Mo cross-weld steel, where at 873K (600°C), 18MPa (180bars) and in presence of an applied stress of 100MPa, the lifetime of the welded joint is reduced by about 68% (from 560 hours to 185 hours)

with respect to the value registered in air. The stress-rupture plot (Figure 5.3-2) shows an evident linear trend for the results in air.

It is interesting to compare the single hydrogen result concerning this steel with the linear fit of the results, obtained in hydrogen at 18MPa, for the second batch of steel. It is evident, that a further reduction in lifetime is caused by increasing the hydrogen pressure from 18 to 22MPa. This finding is consistent with data reported in literature [e.g. Shewmon, 1980]. Moreover, the dependence of the stress from the minimum creep rate also shows a linear trend [12].

Microstructural Investigations

The results of the microstructural investigations, carried out on the ruptured samples, show that, in all cases, fracture occurs in the ICHAZ. Conversely, the samples obtained from the same batch tested under the Brite/Euram Project n. 1835 (PREDICH) are reported to fracture in the FGHAZ, in both air and hydrogen [Bocquet, 2001; Gingell, 2001]. A possible reason of this difference in results is the fact that, under high stresses, the weldment experiences flow processes [Middleton, 2001], which deform the grains of the zones where the strain is mostly accumulated (i.e. the ICHAZ [e.g. Kimmins, 1993] and the nearest layer of the FGHAZ). It is expected that, after the deformation of the grains, the boundary between the ICHAZ and the FGHAZ is difficult (even impossible) to distinguish. Finally, it is recalled that, even today, there is no standardized use of the terminology for the different zones of the HAZ, and it is opinion of the author that this absence of a "common language" might be misleading. As an example, Albert *et al* [2004] decide not to distinguish between ICHAZ and FGHAZ, because both these zones have a fine-grained microstructure after the PWHT. Hence, they use the acronym "FGHAZ" for both. The same is done by his colleagues, Watanabe *et al* [2004], who adopt the convention of calling the ICHAZ still FGHAZ, but, as this zone is close to the base metal, they found it more appropriate to use the designation FGHAZBM.

[12] The author is aware that the minimum creep rate does not have much meaning with cross-weld samples, and is cautious while interpreting the results of its measurements.

5.3.2 Uniaxial Creep Testing (Batch 2)

With the second batch of V-modified 2.25Cr-1Mo welded steel, the results of the tests performed in hydrogen - at equal temperature and in presence of equal applied initial stresses – also show a remarkable reduction in lifetime with respect to the tests in air (Figure 5.3-4). This reduction, at a temperature of 873K (600°C) and a pressure of 18MPa (180bars), shows dependence on the applied initial stress given by the equation:

$$\frac{\left(t^r_{air} - t^r_{hydrogen}\right)}{t^r_{air}} \times 100 = -0.346 \times \sigma + 102.7 \qquad \text{Eq. 5.3-1}$$

Where t^r indicates the rupture time (Figure 5.3-5). Furthermore, the elongation at rupture [13] of the cross-welded samples tested in hydrogen is lower than that experienced by the cross-welded samples tested in air. In both cases, the elongation at rupture increases with the applied initial stress. As already observed whilst discussing the results concerning the 2.25Cr-1Mo steel, the reduction in elongation (ductility) is an effect of the hydrogen attack well documented in literature [e.g. Sutherland, 1965; Coombs, 1965; Yokogawa, 1989]. Also for this steel, the stress-rupture graphs in air and in hydrogen show a linear trend

and, as expected, the exposure to hydrogen leads to lower values of the rupture-time for fixed values of the applied initial stress (Figure 5.3-6. The dashed line plotted in the graph gives the trend in air of the stress-rupture results of the cross-welded samples, obtained from the first batch). It is clear that both batches have about the same behaviour in air and over the range of stresses explored. In the considered range of values, the stress versus the minimum creep rate shows linear trends both in air and in hydrogen (Figure 5.3-7), with higher slope in hydrogen than in air This figure also includes data from two of the three additional interrupted uniaxial creep tests carried out in hydrogen in presence of applied stress at 94 and 106MPa. These results are not considered in the fitting, but it is clear that they are fully compatible with the other results obtained in hydrogen.

[13] The author is aware that the elongation at rupture does not mean too much with cross-weld samples, and is cautious whilst considering this property.

Tsuchida *et al* [2004], who studied the creep rupture properties of the V-modified 2.25Cr-1Mo steel with respect to its microstructure, confirm that creep rupture tests reduce the density of dislocations and induce the formation of sub-grains inside the martensite lath, with the size of sub-grains increasing as the testing temperature increases. The authors suggest that the coarsening of precipitates in the matrix and along grain-boundaries, in particular the formation of needle-like Mo_2C from globular M_7C_3, is the main reason for the increase in creep rupture elongation with increasing testing temperature.

Microstructural Investigation

Figure 5.3-8 gives the image – and a magnified detail – of a fractured sample. Evidently, the fracture is preceded by localized necking. In this specific case, the sample was tested in hot high-pressurized hydrogen. As result, the surface is rather shiny and it is possible to distinguish by naked eye the border of the interface between the weld metal and the HAZ (see lower arrow). On the basis of this naked-eye observation, it is possible to hypothesize that the failure happens in the HAZ. This assumption will be confirmed, for all the tested samples, by the microscope investigation. In the case of samples tested in air, it is not so easy to see the weld metal contour, because the sample surface is covered by an oxide layer.

Figure 5.3-9 shows, as example, the cross-section of the welded-joint tested in hydrogen in presence of an applied stress of 120MPa. The fracture indeed falls in the HAZ, but rather close to the base metal. Also, the fracture of the sample tested in air, under the identical initial-load and temperature conditions, exhibited the same feature (Figures 5.3-10a,b).

These investigations by means of optical microscope on samples tested in air and in hydrogen prove that, also in the welded joints made of 2.25Cr-1Mo-V steel, the fracture happens in the ICHAZ and not in the FGHAZ, as suggested in previous studies [Bocquet, 2001; Gingell, 2001]. It is, then, a Type IV-failure, which is notoriously combined with localized strain accumulation [Parker, 1996]. This feature is consistent with the testing results (e.g. Figure 5.3-8).

To acquire more information regarding the fracture mechanisms, some interrupted creep tests have been carried out in air and in hydrogen.

5.3.3 Interrupted Uniaxial Creep Tests (Batch 2)

The uniaxial creep-rupture test, performed in air under an applied initial stress of 100MPa, had been interrupted just before the failure (Figure 5.3-4). Similarly, three other interrupted tests had been carried out in hydrogen, at the same temperature and hydrogen pressure (Figure 5.3-11). In one case – that is Int I - an initial stress of 106MPa had been applied, and the test had been interrupted at the beginning of the *tertiary* stage. For the other two tests, an initial stress of 94MPa had been applied and the two creep tests had been stopped at the beginning of the *tertiary* (Int III) and at 2/3 of the *secondary* (Int II). The tests were designed to have practically the same duration for Int I and Int II. In this way, by comparing the damage in both cases, it could be possible to obtain information on the effect of the stress on the damage, after a fixed time of exposure to hydrogen. Furthermore, the comparison between Int II and Int III gives information about the effect of prolonged application of the stress to the welded-joint (test duration) under a fixed applied initial stress. The creep-rupture curve for the test performed in hydrogen, in the presence of an applied initial stress of 100MPa, has been chosen as reference for the interrupted tests in hydrogen.

Microstructural Investigations

The microstructural investigation, on the samples from the interrupted tests, have been carried out in the following order:

1. Cross-welded sample, tested in air, under an applied initial stress of 100MPa.
2. Cross-welded sample, tested in hydrogen, under an applied initial stress of 106MPa.
3. Cross-welded sample, tested in hydrogen, under an applied initial stress of 94MPa and up to 928 hours.
4. Cross-welded sample, tested in hydrogen, under an applied initial stress of 94MPa and up to 648 hours.

The findings of these investigations are reported in the above order.

1. Sample tested in air (σ_o= 100MPa, t=2453h)

Before starting the microstructural investigation, the sample had been inspected by means of X-rays. This characterization had been carried out in the NDT laboratory of the High Flux Reactor of the Institute for Energy of the Joint Research Centre. The outcomes clearly show that the test had been stopped at a very late stage of the test (Figure 5.3-12). The sample was, afterwards, placed entirely in resin, and longitudinally cut in the middle. Figure 5.3-13 offers a SEM image of the cross-section, before etching. The fracture appears oriented at about 65° respect to the direction of the applied stress. Observation by optical microscope of the welded-joint shows a fracture located entirely in the HAZ, nucleated very close to the base metal, in the ICHAZ, and propagating towards the sample surface through the HAZ (Figure 5.3-14).

2..Sample tested in hydrogen (σ_0=106MP, t=647h)

With the naked eye, a small crack, located at about middle-length of the specimen gauge, can be detected. Using an optical microscope, it is possible to measure the crack length, which is about 1.5mm (Figure 5.3-15). At higher magnification, it appears that the damage is a crack in formation, to be considered more as ongoing coalescence - still not complete - of rather large voids (Figure 5.3-16). The link-up of voids gives the crack a wavy appearance, which is oriented at about 65 degrees with respect to the direction of the applied stress. At the link-up tips, small cavities are detected, which facilitate the crack propagation [Chen, 1995].

Observation of the sample after etching proves that, as expected, nucleation of the crack takes place not in the FGHAZ but close to the base metal, in an area recognized as being part of the ICHAZ (Figure 5.3-17). Also, these findings refute the thesis that the fracture happens in the FGHAZ [e.g. Bocquet, 2001; Gingell, 2001]. In addition, the figure documents the presence of localized necking corresponding to the ICHAZ, which confirms that the zone experiences a localized strain accumulation, which is relevant to Type IV cracking [Parker, 1996]. Using the SEM, the area around the crack appears highly cavitated (Figure 5.3-18), and confirms the localization of the crack in the ICHAZ. An extended study by SEM had been carried out in the area around the crack. From these observations, the following mechanism of fracture is suggested:

1. NUCLEATION. The formation of cavities takes place at interfaces between different phases (e.g. carbide/matrix; inclusion/matrix; grain boundary).

2. LINK-UP. The methane and the hydrogen inside the cavity exert a pressure on the inner side of the cavity. This pressure does not have the time to cause the growth of the cavity by a creep mechanism, because the link-up of neighbouring cavities takes place. The link-up is facilitated by the formation of very narrow cracks at the bainite/martensite interface and along grain boundaries (Figure 5.3-19a).

3. MICROCRACKING. The narrow cracks link separated cavities and propagate by following circuital paths. In this way, pieces of material become isolated (Figure 5.3-19b).

4. MOSAICING. The network of micro-cracks becomes more defined and the narrow cracks wider. At a local level, the material begins to appear separated into small pieces by the cracks, giving an appearance similar to the texture of a mosaic (Figure 5.3-19c).

5. FRAGMENTATION. The mosaic texture becomes more evident and the crack width increases. The material loses its coherency and fragments (Figure 5.3-19d).

6. VOIDATION. The mosaic structure collapses and voids appear. The newly created void grows by assimilation of neighbouring cavities and micro-cracks (Figure 5.3-19e).

7. CRACKING. The voids link-up and form a crack. The crack grows by propagation of the crack tips, which produces plastic deformation in the surrounding material.

8. RUPTURE. The process ends-up with the failure of the welded component.

Areas of the ICHAZ more distant from the registered crack also appear cavitated (Figure 5.3-20), and the extent of the cavitation is higher than for the FGHAZ (Figure 5.3-21). The base metal, the CGHAZ, the fusion line (Figure 5.3-22) are practically not cavitated. The weld metal is populated by a non-uniform distribution of smaller cavities, round-shaped and isolated (Figure 5.3-23).

The distribution of carbides in the ICHAZ, FGHAZ and base metal had been observed by means of SEM in *secondary electron* mode, which guarantees the achievement of higher magnifications compared to the *back-scattered electron mode* (Figure 5.3-24a,b,c). The ICHAZ shows a distribution of relatively fine carbides dispersed in the matrix, whilst the carbides of the FGHAZ seem of bigger dimension. In the base metal, carbides of large size are found both in the matrix and along grain boundaries. Finally, as reported previously [Tsai, 2003], interfaces (in particular carbide/matrix interfaces) represent preferential locations for cavities nucleation (Figure 5.3-25).

3..Sample tested in hydrogen (σ_0=94MPa, t=928h)

Again, in this case, the cross-section of the sample before etching exhibits a highly cavitated area corresponding to a region of localized necking. The distribution of cavities covers a huge part of the sample section. Cavities form mainly inside the specimens and they propagate from the centre towards the surface layers. This feature seems compatible with the view that surface decarburisation and cavitation are competing processes; i.e., the higher the decarburisation of the zone, the lower the incidence of cavities [Rosenthal, 1963]. It is also in agreement with the recent conclusions of Albert *et al* [2004] about the gradient of cavity density, while moving from the interior towards the surface of specimens tested in air. These authors correlated the experimental finding to the presence of high hydrostatic stress and creep strain close to the specimen centre. Moreover, it is here suggested that the cavitated internal layers of the specimen shed stress to the non-cavitated and more external layers, which experience plastic flow. On the other hand, the high stresses that cause the plastic flow inhibit the nucleation of cavities, because they inhibit the grain boundary sliding. Consequently, it is concluded that the less presence (or even the absence) of cavities close to the surface exposed to hydrogen, is not only an effect of the decarburisation but, also, of the redistribution of stresses that takes place during the specimen creep deformation.

As with the cracking of the samples "1" and the cavitation of the sample "2", the distribution of cavities in sample "3" exhibits an orientation, which is at about 65° to the direction of the applied stress (Figure 5.3-26a). Hence, it is possible to argue, that, either in air or in hot high-pressurized hydrogen, under the imposed test conditions, the crack does not nucleate in one zone and propagate across the sample. Instead, the

crack forms by "*distributed nucleation*", (Figure 5.3-26b), i.e. cavities form, link-up and coalesce to produce voids, the voids then join to form "*elements of crack*", which connect to produce the main crack. For this reason, some of the cavities present in the more cavitated zone exhibit a more advanced stage of development. As appeared at higher magnification, these bigger cavities are interconnected by very narrow microcracks, and the whole link-up is extended to a length of some millimetres. Again, much lower levels of cavitation are found in layers close to the sample surface (Figure 5.3-26c). The etching of the sample by means of Nital, confirms that the damage is mainly located in the HAZ and close to the base metal, in the zone identified as the ICHAZ (Figure 5.3-27). Besides, in this sample, extended cavitation is found in the weld metal, along the grain boundaries (Figure 5.3-28).

The investigation of the damage by SEM shows that the most damaged zone, the ICHAZ, is populated by voids of irregular shape (Figures 5.3-29a,b,d), the formation of which is presumably due to the mechanism described before, for the presentation of the results of the test of sample "2". The origin of the damage seems due to the nucleation of cavities of sub-micron size (Figure 5.3-29c). The cavities and voids appear in general linked by microcracks. In particular, the more developed voids are connected by a sequence of narrow microcracks and cracks, which is extended for many hundreds of microns (Figure 5.3-29a). It is argued that this extended link-up will produce, at a more advanced stage of damage, the main crack that will cause the failure of the welded joint (e.g. see Figure 5.3-16). At the SEM, also the FGHAZ appears very cavitated, with cavities and voids of irregular shape; but no link-up of them, by means of microcracks, is detected (Figures 5.3-30a,b). For the weld metal, it is confirmed the presence of small round-shaped cavities in the grains, and, in some areas, the link-up of the cavities distributed along grain boundaries (Figures 5.3-31a,b). Finally, the base metal appears practically not cavitated (Figure 5.3-32a). The attack is found in rare locations as the interfaces inclusion/matrix (Figure 5.3-32b).

4.. Sample tested in hydrogen (σ_0= 94MPa, t=648h)

The test was interrupted at about 2/3 of the *secondary stage* (Figure 5.3-11). Using the optical microscope, neither cracking nor cavitation is detected in the welded joint. The SEM investigation also shows no significant cavitation in all the metallurgical zones.

The presence of damage, still in the embryonic phase, is detected only in the ICHAZ. It consists of sub-micron-sized cavities, mainly nucleated at the interfaces among different phases as between carbides and matrix (Figure 5.3-33a,b,c,d). On the basis of the reported results, it is suggested that these cavities of sub-micron sized cavities, ranging between about 40nm and 200nm, do not grow by creep but participate in a phenomenon of link-up.

5.3.4 Internally Pressurized Tubes (Multiaxial Creep Tests)

The tested tubular specimens, made of 2.25Cr-1Mo-V steel, have a longitudinal weldment along their entire length. Two samples had been pressurized, by means of argon or hydrogen, at a temperature of 873K (600°C) and a pressure of 18MPa, in such a way as to obtain an initial hoop stress of 120MPa. The measurement of the strain had been carried out by means of twelve capacitive sensors, distributed in groups of four around the top, middle and bottom positions of the gauge length. For each of these positions, the average signal had been calculated to give one signal for the top, one for the middle and one for the bottom of the gauge length. Figure 5.3-34 shows the three curves for the test, referred to the tube pressurized with Ar and the tube pressurized with H_2. The stress-rupture plot (Figure 5.3-35) shows that the tubular specimen pressurized with H_2 exhibits a lifetime longer than the uniaxial cross-welded specimens tested in hot high-pressurized hydrogen. In contrast, the tubular specimen pressurized with Ar has a lifetime shorter than that of the uniaxial cross-welded specimens tested in air. Because, for each test, the three average creep curves display very similar trends, one average curve could be constructed for each multiaxial test. This approach is useful for minimum creep rate calculations (Figure 5.3-36). Clearly, the minimum creep rate of the sample pressurized with Ar is practically the same as that for the corresponding uniaxial creep-rupture sample tested in air. However, the minimum creep rate of the sample pressurized with H_2 is lower than that of the corresponding uniaxial test. Surprisingly, it is very close to that of the corresponding samples tested in air and argon. This aspect will be discussed in the section dedicated to the microstructural investigations.

Both pressurized samples display, after bursting, a longitudinal failure about 120mm in length. With the naked eye it is possible to ascertain that the failures propagate at

the interface base metal/weld metal (Figures 5.3-37; 5.3-38). It is symmetrically positioned with respect to the middle of the gauge length of the sample pressurized with hydrogen, whilst is closer to one of the two shoulders of the sample pressurized with argon. In both tubular specimens, a movement outward of the whole weld metal is registered. This movement creates, on the external surface of the piece, a small step, which is just visible close to the shoulders and increases towards the middle of the sample (Figures 5.3-39; 5.3-40). On the external surface of the sample pressurized with hydrogen, it is possible to distinguish the borderline of the weld metal, as already noted in the case of the uniaxial creep tests carried out in hydrogen. After test, both samples underwent strain measurement, with the results presented in Figures 5.3-41, 5.3-42, 5.3-43. The strain measurement procedure allows the "*digitalisation*" of the gauge length. Hence, following the strain measurements, the gauge length is sectioned in rings 5mm thick. On their cross-section are performed the microstructural investigations.

Microstructural Investigations on the Tubular Sample pressurized with Hydrogen

Two rings have been examined using the optical microscope: one ring contains one of the tips of the fracture, the other contains the part of the HAZ which experienced a strain of 5%. As already mentioned, the value of the strain of the HAZ is an average of the values registered in the different metallurgical zones, and does not provide information on the true strain of the weaker zone, the ICHAZ, which is known to accumulate strain [Kimmins, 1993]. The examination of the first ring shows that the fracture starts in layers of the steel close to the surface directly exposed to hydrogen (Figure 5.3-44). The fracture onset is due to the nucleation and coalescence of cavities. The cross-section of the sample is characterized by a non-uniform distribution of cavities, with a zone, close to the surface exposed to hydrogen, where the cavitation is more active and, consequently, more dense. In this zone, cavities nucleate close to the surface and the nucleation process propagates through more inner layers of the material, towards the external surface, which is exposed to argon. The high-density distribution of cavities exhibits an orientation, which is neither perpendicular to the hoop direction, nor symmetric with respect to the initial hoop stress direction. As already observed by Baker [1999] for the tubes made of 2.25Cr-1Mo base metal, another feature of the fracture is the tearing of the tube wall, causing

a thinning of the wall which starts from the outside and works its way inwards. This produces a reduction of area more pronounced than in the corresponding uniaxial cross-weld specimen.

After etching, the ICHAZ appears as the zone with a higher density of cavities. In this case, the fracture starts in the ICHAZ, close to the surface exposed to hydrogen, and propagates catastrophically through the base metal, crossing about half of the ring thickness moving towards the outer surface, exposed to argon (This is an important aspect that will be discussed further). The ICHAZ is also the zone most affected by the thinning of the tube wall, whilst the weld metal and the base metal distant more than 2-3mm from the fractured surface experiences low reductions in thickness. On the basis of these findings, the registered damage seems to be the synergy of two phenomena:

1. A phenomenon of stress-assisted hydrogen-attack cavitation, which appears close to the surface exposed to hydrogen.
2. A phenomenon of creep-induced thinning of the tube wall. The latter phenomenon is more pronounced in the layers closer to the external surface of the tube, which is exposed to argon.

Both mechanisms act in tandem, and, whilst the first prevails close to the surface exposed to hydrogen, the second is more evident close to the surface exposed to argon, where the hydrogen attack is less evident. Observation of the other ring confirms these conclusions (Figure 5.3-45):

a. The ICHAZ, the FGHAZ and part of the base metal are the zones that experience tearing and consequent reduction in thickness. In contrast, the weld metal and the base metal more than 2-3mm from the ICHAZ exhibit practically no reduction in thickness.

b. The cavities are distributed along the ICHAZ, with a higher density in the layers underneath the surface directly exposed to hydrogen, whereas the density decreases towards the outer surface, exposed to argon.

c. Among the many cavities, a few larger voids are detected. These have an elliptical shape and are elongated in the direction of the hoop stress.

These observations suggested that the crack does not start from the surface but forms just inside the tube wall, as a consequence of the link-up of growing voids which nucleate mainly close to the surface exposed to hydrogen. This is coherent with what was suggested by Albert *et al* [2004], who performed uniaxial creep tests in air on simulated weldments, with the difference that for these tubes pressurised with hydrogen the crack appears to start more close to the surface. The cracking, therefore, represents a sub-surface phenomenon. This suggestion is in line with the condivision of Baker for tubular samples, of standard 2.25Cr-1Mo base metal, pressurized with hot hydrogen [19999]. Therefore, the sub-surface nature of the damage seems to be peculiar to the hydrogen attack of tubular specimens, seemingly independent of the presence of weldments. This feature should be considered in the choice of the NDT method for the detection of hydrogen attack damage.

Some considerations are at this point necessary. The gradient of damage, i.e. the denser cavitation observed close to the hydrogen-exposed surface, is a recognized effect of stress-assisted hydrogen attack and of the gradient of hydrogen concentration across the wall thickness. Kimmins [1993] suggests that a local relaxation of stresses is caused by the formation of cavities, and Parker [1995] concludes that low-strength regions shed stress to the more resistant ones. A cavitating area is a low-strength area, thanks also to the relaxation of stresses it experiences, and it is not surprising if a higher "share" of the applied stress is charged on the areas which are not cavitating and, therefore, able to oppose more resistance to deformation. It is, then, suggested that, because the regions close to the surface exposed to hydrogen experience higher cavitation, they shed stress to the regions less cavitated, in particular those closer to the surface exposed to argon. In these, two acting factors concur:

1. The lower concentration of hydrogen, if compared to the highly cavitated areas.

2. The higher applied stress.

In other terms, the onset of the damage (cavitation) is also the starting of ideal sub-division of the wall thickness in two types of areas:

a. The outer areas [14] (hereafter called "*O-areas*"), with higher applied stresses and lower concentration of hydrogen.

b. The inner areas (hereafter called "*I-areas*"), with lower applied stresses and higher concentration of hydrogen.

And this differentiation is independent of the presence of weldments. Already Baker [1999], who tested tubular specimens made with 2.25Cr-1Mo base metal, observed:

- Marked cavitation in the I-areas.
- Very low or no cavitation in the O-areas.
- Thinning of the tube wall, starting from the outer surface (The phenomenon was more evident for higher applied mean diameter hoop stresses).

Moreover, also the observation of the 2.25Cr-1Mo cross-welded tube, tested in the present work, revealed a gradient of damage across the tube thickness independently of the metallurgical zone (See Figures 5.2-15, 5.2-19). Therefore, it is a general behaviour that the I-areas experience stress-assisted hydrogen attack cavitation and cracking, whilst the O-areas mainly creep-induced thinning. Furthermore, the increase of the applied stress, experienced by the O-area, can change the mechanism of damage in the case these areas include welded joints. In fact, as suggested by some authors [Middleton, 2001; Smith, 2003] under relatively low stresses the creep strength of the ICHAZ is appreciably less that that of the parent material. On the contrary, under higher applied stresses, the creep strength of the cross-weld joint and that of the parent metal coincide. Probably, this can explain why, as said, the fracture starts in the ICHAZ (in a I-area) and propagates catastrophically through the base metal (O-area), crossing about half of the ring thickness towards the outer surface.

A point to clarify is that in the samples made of 2.25Cr-1Mo base metal tested by Baker [Baker, *ibidem*] in hydrogen, the local thinning of the tube wall is not as marked as in the samples of 2.25Cr-1Mo-V, with a similar longitudinal weldment, tested in the present work. Of course, it is not possible to carry out a quantitative comparison between the tube sections observed by Baker and those considered in the present work, since the respective local strains experienced by the steels might be

[14] The reference is the axis of the tubular specimen.

markedly different. A qualitative consideration is, instead, possible. Taking into account that the V-modified grade has higher creep resistance than the standard 2.25Cr-1Mo steel, the fact that the former steel exhibits high thinning in the ICHAZ confirms the poorer mechanical properties in this zone. In this respect some further elements of analysis come from the work of Middleton *et al* [2001], who point out that the addition of "refractory elements", as vanadium, to 9% and 12% Cr ferritic steels, increases its mechanical properties but does not increase the mechanical strength of the Type IV zone. Consequently the adoption of high weldment reduction factors is still compulsory in the design of industrial components made with these materials. Another reason of the difference in thinning between the 2.25Cr-1Mo, tested by Baker [1999], and its V-modified grade is that the former is less resistant to hydrogen attack. Therefore, it is not surprising that the steel exhibits higher reduction of ductility with respect to its V-modified counterpart. Furthermore, the pressures of hydrogen used by Baker for the standard steel were in the range 19.5 to 26.0 MPa, which is higher than the pressure used in the present work for testing the V-modified tubes (18MPa). On the other hand, those pressures corresponded to initial mean diameter hoop stresses in the range 85.1 to 113.5 MPa, which is lower than the initial stress applied on the V-modified tubes (18MPa).

Comparison between the Uniaxial and Multiaxial Creep Results

1. Some questions are still open: Why does the tubular specimen, pressurized with H_2, exhibit a lifetime longer than the uniaxial cross-welded specimens tested in similar conditions?

2. Why the minimum creep rate [15] of the same tubular specimen is lower than that of the corresponding uniaxial test, and very close to that of the corresponding samples tested in air and argon?

The difference between the uniaxial creep and the tubular pressurized tests is that in the former case the sample is entirely surrounded by hot high-pressurized hydrogen, whilst, in the latter, only one side of the sample is in contact with the hydrogen environment. Consequently, tubular specimens experience an asymmetric hydrogen concentration through the wall thickness, and the consequent damage is also

[15] As already pointed out, it is not rigorous to consider concepts as minimum creep rate while testing welded specimens

asymmetric. These differences might be the reasons of the registered differences in lifetime and in minimum creep rate.

Microstructural Investigation on the Tubular Sample pressurized with Argon

Two rings had been cut from the tested tube: the first, represented by Figure 5.3-46 contains the fracture, the second, not fractured, had been cut from a part of the tube which experienced a radial strain of ~6% (Figure 5.3-47). As for the test-piece pressurized with hydrogen, also this one failed in the ICHAZ and large voids are found in this zone, underneath the fracture surface. The second ring exhibits a remarkable accumulation of strain in the ICHAZ, and this finding is consistent with the literature on the subject [e.g. Kimmins, 1993]. Figure 5.3-47 also shows that, together with the ICHAZ, the base metal adjacent to it experiences high deformation, which agrees with the thesis that "*regions where deformation is relatively rapid will shed stress to regions of the component where deformation is relatively slow*" [Parker, 1995]. Furthermore, in the mentioned figure it is visible that the base metal close to the ICHAZ strains along a preferential direction (indicated by the yellow arrow), which is about normal to the ICHAZ line. Cavities are detected in this deformed base metal (Figure 5.3-48), whereas higher cavitation is found in the ICHAZ (Figure 5.3-49). Conversely, the ICHAZ close to the inner surface of the tube exhibits low cavitation (Figure 5.3-50), probably due to the redistribution of the stresses, which lead to multiaxial conditions [Kimmins, 1993; Middleton, 2001; Smith, 2003].

In conclusion, similarly to what was suggested by Baker [1999] for the tubes made with standard 2.25Cr-1Mo, base metal, the failure of tubular specimens manufactured of V-modified 2.25Cr-1Mo steel, longitudinally welded, is due to a crack propagating from the inner to the outer surface, for specimens pressurized with hydrogen, and is due to thinning of the tube wall, which appears to start in the more external layer and move inwards.

5.3.5 *TEM Investigations on the 2.25Cr-1Mo-V welded Joint (Batch 1)*

In the present research, the first preliminary uniaxial creep-rupture tests on the first batch (PREDICH Batch) had been combined, for fundamental purposes, with a investigation by means of TEM on the microstructure of the welded joint. The zones

investigated are the base metal, the FGHAZ and the weld metal. No investigation is made of the ICHAZ, because the TEM analysis was carried out at an initial stage of the study when the interpretation of the results was much influenced by the findings of the PREDICH project, which reports failure in the FGHAZ [Bocquet, 2001; Gingell, 2001]. The TEM investigation performed in the present work is aimed at exploring possible relationships between the detected damage and the microstructure of the welded joint, in particular its carbides population. The purposes are:

1. To link the damage with the identity of the carbides in the zones.
2. To characterize the carbides' identity in terms of chemical composition and morphology (Figure 5.3-51).

The procedures adopted are summarized in Figure 5.3-52. Replicas of the metallurgical zones had been extracted. For each zone, a separate investigation had been devoted to the carbides "*in the grain*" and to the carbides "*along grain boundaries*". Both *small* and *large* carbides had been analysed. The composition of each carbide had been determined, with carbide given an identification number to establish a link between the carbides' chemical composition (Figure 5.3-57) and their morphology (Figure 5.3-56). The results provide detailed information on the carbides population in the different zones (Figure 5.3-53, Figure 5.3-54, Figure 5.3-55) and their composition (Table 5.3-1). The main findings are summarized as follows:

- No M_6C is detected in the 2.25Cr-1Mo-V, batch 1, in the as-post-weld-heat-treated conditions. This finding is in agreement with the known stability of the carbide, which is expected after long-term in-service exposure of the steels [Baker & Nutting, 1959; Oh, 1999; Tsuchida, 2004]
- $M_{23}C_6$ is found, only in small numbers, along grain boundaries in the FG-HAZ. According to the evolutionary diagram of Baker and Nutting [1959], the presence of few $M_{23}C_6$ particles in the FGHAZ seems to be an effect of the thermal treatment undergone by the zone during the welding and PWHT. The location of the $M_{23}C_6$ carbides along grain boundaries agrees with results reported by Lundin *et al* [1984] and by Senior [1988].
- For all the three zones, MC type carbides are dominant inside the grains, whilst M_7C_3 dominates at grain boundaries.

- The analysis of the TEM images shows that the MC type carbides are present as a coarse dispersion inside the grains of the base metal, in form of fine dispersion inside the grains of the weld metal, and more rarely dispersed in the grains of the FG-HAZ (Figure 5.3-58). This wider spacing can be a result of the dissolution and coarsening of the carbides after the imposed thermal treatment.

These results can be compared to the findings of Tsuchida *et al* [2004], who give an explanation for the creep properties of the V-modified 2.25Cr-1Mo steel on the basis of its microstructure. Two points of interest emerge whilst comparing the processes of production and welding of the steel tested by Tsuchida *et al* [Tsuchida, *ibidem et passim*], and of that investigated in the present work:

1. Tsuchida *et al* studied steels normalized at 1253K (980°C), followed by accelerating cooling before tempering at 1003K (730°C). The V-modified 2.25Cr-1Mo steels tested in the present work had been cooled from 1223K (950°C) and tempered at 923K (650°C).

2. The steels of Tsuchida *et al* underwent a PWHT at 978K (705°C) for 6 or 30h, whereas the V-modified 2.25Cr-1Mo steel of the present work received a PWHT at 978K for 10h.

The findings of both studies are also consistent.

- No traces of M_6C carbides were found in the investigated steels. Moreover, the work of Klueh *et al* [1974] leads to the same result.

- Presence of a few $M_{23}C_6$ particles along the grain boundaries of the FG-HAZ had been detected during the present work, but not in the base metal. Similarly, Tsuchida *et al* [*ibidem*] do not report the presence of this carbide type. This convergence of results seems attributable to use of the same tempering parameters [16]: 21.1×10^3 (T=978K; t=30h), for the steels tested by Tsuchida *et al*, 20.5×10^3 (T=978K; t=10h), for the steel tested in the present work. In fact, these authors suggest that $M_{23}C_6$ form at an early stage of tempering and changes to M_7C_3 as consequence of the aging induced by the PWHT. For

[16] The tempering parameter is defined as TP=T(Log(t)+20) where T is expressed in K and t in h.

values of the tempering parameters equal or higher than 21.1×10^3, this change is expected to be completed.

- Both studies report the presence of needle-like M_2C carbides, mainly inside the grains of the steel. On the basis of their observations, Tsuchida *et al* [Tsuchida, *ibidem et passim*] suggest that Mo_2C nucleates close to the M_7C_3 carbide, and grow inside the grain by consuming the latter one. Their finding is supported by the work of Senior [1988]. In spite of this confirmation, their conclusion contradicts the relevant literature on the microstructural evolution of carbides in Cr-Mo steels (e.g. 2.25Cr-1Mo steel), which suggests that Mo_2C disappears in favour of the formation of M_7C_3 [e.g. Baker & Nutting, 1959; Klueh, 1974].
- Another point of convergence between the two studies is the finding that, in the as-PWHT material, the inside of the grains is populated by very small V and Mo carbides (diameter ~20nm). In the work of Tsuchida *et al*, the V-carbides are named V_4C_3, which is another way of indicating the MC carbides [Senior, 1988].

A particular feature of the MC type carbide is the fact that it is carbon deficient and is expected to be vacancy free [Senior, *ibidem*]. Because the carbide is rich in V, it ties up the carbon atoms, preventing reaction with hydrogen. However, because the carbide is carbon deficient, a high density of MC carbides is necessary to increasing its resistance against hydrogen attack.

Together with these data on the as-received V-modified 2.25Cr-1Mo welded steel, the results of TEM/EDS investigations carried out on the same welded joint, after exposure to hydrogen in stress-free and stress-applied conditions, are also available at the Institute for Energy of the Joint Research Centre. This work, jointly performed by the Institute for Energy and ISQ, concerned the welded joint in the following conditions:

1. As received.
2. Creep conditions, in hydrogen, at 873K (600°C), 18MPa, in presence of an applied stress of 150MPa and for a duration of 570h.
3. Creep conditions as above, but up to 2500h.
4. Autoclave exposed, in hydrogen at 873K (600°C), 18MPa, up to 4000h.

PREDICH project was mainly focused on the base metal, weld metal and FGHAZ, not on the ICHAZ. The major findings of the PREDICH TEM/EDS investigation on 2.25Cr-1Mo-V welded joint can be summarized as follow [BE 1835-4]:

- The exposure to hydrogen of the base metal, in presence as well as in absence of applied stress, reduces the presence of M_7C_3 carbides in favour of the formation of M_2C carbides.
- The exposure to hydrogen of the weld metal favourites the formation of large M_6C carbides, both along grain boundaries and in grains, either in the bulk or at the surface of the test pieces.
- The FGHAZ, in the as-received conditions, exhibits lower presence of MCs than the base metal together with M_6C carbides. The exposure to hydrogen of the FGHAZ favourites the formation of large M_6C carbides, both along grain boundaries and in grains, either in the bulk or at the surface of the test pieces.
- After exposure, the presence of M_6C is registered in the surface of all the metallurgical zones, and, as said before, in some of them this carbide is dominant.
- The exposure to hydrogen enriches in molybdenum the M_2C carbides of the FGHAZ and in vanadium its MC carbides. Vice-versa, the vanadium content of the former, the molybdenum content of the latter, and the iron content of both, decrease.

At this point, two major questions are still open:

- How can the Type IV failure of the cross-weld specimens made of 2.25Cr-1Mo steel, and of those made of V-modified 2.25Cr-1Mo steel, be explained on the basis of the microstructural features?
- Why does the ICHAZ zone register the highest strain accumulation?

The ICHAZ experiences a peak of temperature lower than AC_3 and very slow cooling rates. This results in the formation of a mixture of untransformed material and fine grain ferrite. The ferrite is expected to lower the creep strength [Parker, 1996]. In addition, the presence of fine grains implies a very high grain boundary area, which

can also lower the creep strength [Kimmins, 1993]. No acicular M_2C's, and a few coarse M_2C's, have been found in the grains of the FGHAZ, during the TEM investigation carried out in the present research, as well as in the PREDICH project [BE 1835-4]. Also the ICHAZ is expected to exhibit low or no presence of M_2Cs, and the literature suggests that a major cause of the weakening of the zone is just the rare presence of finely dispersed M_2C's [Parker, *ibidem*], which are expected to contribute markedly to the creep strength of the steel [Baker & Nutting, 1959]. The formation of sub-grains with low dislocation density, and the coarsening of carbides, have been observed in the ICHAZ of 2.25Cr-1Mo welded steel, aged at 823K (550°C), both in stress-free and stress-applied conditions [Watanabe, 2004]. A large interspacing among carbides is expected to be detrimental for the creep strength of the V-modified 2.25Cr-1Mo alloy [Tsuchida, 2004].

The study of Smith *et al* [2003] concluded that Type IV failure is intergranular and is anticipated by the formation of cavities at grain boundaries. The dissolution and coarsening of "in-grain" carbides, which is expected to take place during in-service exposure [Senior, 1988], is usually linked to the precipitation of carbides along grain boundaries. These carbides may offer sites for stress concentration upon application of stresses and may increase the nucleation of cavities along grain boundaries [Kassner, 2003]. In particular, the precipitation and coarsening of Mo-rich carbides ($M_{23}C_6$) and, for longer service times, M_6C type carbides, are expected to promote cavitation [Oh, 1999]. Possibly, their formation is combined with the depletion of the grain boundary in Mo, which is well known to increase the cohesion of the grain boundary by decreasing its free energy [Rosenthal, 1963; Song, 2000]. The findings of the PREDICH project show that the exposure to hydrogen enhances the ageing of the steel and anticipates the formation of M_6C carbides, which are expected to enhance the nucleation by becoming of large dimension. In addition, the mechanical properties of the HAZ are also decreased by the registered enrichment in molybdenum of the M_2C carbides, which cause the depletion of the surrounding metal. Finally, the literature reports that the depletion in Mo of the matrix of Cr-Mo-V steels can be also an effect of the tempering, during which the vanadium of the V-rich MC carbides could be replaced by molybdenum, so that Mo is the prevalent element present in the carbide [Výrostková, 1998].

5.4 Testing of the 3Cr-1Mo-V welded Joint

For the 3Cr-1Mo-V steel, uniaxial creep tests were conducted in air and in hot high-pressurized hydrogen. This section reports the results of the uniaxial tests in relation to the microstructural studies of the tested samples.

5.4.1 Uniaxial Creep Tests

Uniaxial Tests in Air

A large elongation, that increases when the applied initial stress increases, characterizes the failure of the cross-weld specimens made of 3Cr-1Mo-V steel, tested in air at 873K (600°C). Similarly, when the applied stress increases, the time of rupture decreases. The creep curves show a pronounced tertiary phase (Figure 5.4-1), and a heavy reduction in area is displayed by the failed specimens (Figure 5.4-4). The high rupture elongation and lower creep resistance, compared to the V-modified 2.25Cr-1Mo steel, supports the view that the creep strength decreases on increasing the Cr content from 1 to 3 weight percent [Lundin,'84].

In the case of the tested samples, failure takes place in the base metal. Yet, while the elongation of the different metallurgical zones was not measured, it is possible to state qualitatively that a very high share of the elongation occurs in this metallurgical zone. The Vickers hardness profile (Figure 5.4-5) indicates that the CGHAZ is the hardest zone, and presents an increase in hardness of about 12 (twelve) per cent with respect to the base metal. The weld metal is also hard, with a hardness which is about 8 per cent higher than that of the base metal. Again, for the 3Cr-1Mo-V, as for the other tested steels, the softer zone is the ICHAZ, which has a hardness which is slightly (about the 3 per cent) lower than that of the base metal. Finally, the FGHAZ shows a substantial increase in hardness when moving from its interface with the ICHAZ to the interface with the CGHAZ.

The cross-weld 3Cr-1Mo-V steel is characterized by a sequence of hard and soft zones similar to those found during previous studies [e.g. Kimmins, 1993; Parker, 1995; Mannan, 1996; Parker, 1996; Smith, 2003]. The rupture time, on logarithm scale, depends linearly on the stress (Figure 5.4-2), with a similar linear stress dependence of the minimum creep rate (Figure 5.4-3). The microstructural investigations carried out

on the broken samples show that fracture occurs in the base metal. Moreover, the reduction in area increases quickly on passing from the weld metal to the FGHAZ (Figure 5.4-6), and increases progressively going towards the fracture surface, which shows ~0.5mm deep dimples (Figures 5.4-7a,b).

In the base metal just underneath the fracture surface, it is possible to find large voids elongated in the direction of application of the stress. Their density and size decrease significantly when moving more deeply into the base metal. Very rare large voids, probably due to the presence of inclusions, are detected in the HAZ, but no voids are detected in the weld metal. The failure of the base metal has also been reported by partners in the European project Brite/Euram 1835 (PREDICH) [Bocquet, 2001], who tested the same steel at 873K (600°C) under stress from 120 to 190MPa. Bocquet *et al* did not provide an explanation of this finding, which should be really interpreted in the light of the studies of Kimmins *et al* [1993] and of Smith *et al* [2003]. These authors suggested that the failure of the base metal in laboratory tests is not representative of real in-service conditions, when lower applied stresses are expected to cause Type IV failure.

Uniaxial Tests in Hydrogen

The cross-welded samples tested in hot high-pressurized hydrogen exhibit a lower rupture time than the equivalent tests in air, and a slightly lower elongation at rupture (Figure 5.4-1). This reduction in rupture time, and slight reduction in elongation, decreases as the applied initial stress increases. This is consistent with the fact that hydrogen attack increases as the time of exposure of the steel to hot high-pressurized hydrogen increases. Furthermore, the stress-rupture times and the minimum creep rate, as functions of the applied initial stress, exhibit trends similar to those found in air, except that the stress-rupture curve in hydrogen is shifted towards lower values of rupture time, and the minimum creep rate curve correspondingly towards higher values (Figures 5.4-2,3).

In hot high-pressurized hydrogen, the failure of the samples again occurs in the base metal, but the fracture surface shows smaller dimples than the fracture surface of the specimens tested in air (Figures 5.4-8, -9a and b, -10). As with the samples tested in air, large elongated voids, having the direction of the applied initial stress, are observed using an optical microscope, and their density decreases on going towards

deeper layers of the material. The samples tested in hydrogen also display a fast increase in reduction of area, on passing from the weld metal to the FGHAZ, and a progressive increase in reduction of area moving along the base metal towards the fracture surface.

In contrast to the observations recorded for the 2.25Cr-1Mo and 2.25Cr-1Mo-V welded joints, failure of the V-modified 3Cr-1Mo welded joint appears in the base metal. The welded joint made of standard steel underwent a PWHT consisting of 30 hours at 963K (690°C), whilst the two V-modified steels had been exposed for 10h at 978K (705°C). The two PWHTs present very similar tempering parameters: respectively, 20.5×10^3 and 20.7×10^3. Consequently, it is difficult to conclude that the PWHT is the reason of the markedly different behavior among the tested welded joints. The occurrence of the failure in the base metal seems to be due more to the magnitude of the applied stress. Considering that the creep resistance of the 3Cr-1Mo-V is markedly lower than that of the 2.25Cr-1Mo-V, it is suggested that the stresses adopted in the present work, as well as in the PREDICH Project [Bocquet, 2001], may be high enough to cause the failure of the welded joint in the base metal. Hence, at stresses similar to those encountered in-service, Type IV failure would be found [Smith, 2003].

6 Conclusions of the Research

Three types of Cr-Mo steels have been tested in the present work:

a. The standard 2.25Cr-1Mo steel, used for more than 40 years of operation in different hydroprocessing conditions.

b. The V-modified 2.25Cr-1Mo Steel, which had been used since the middle 1990's.

c. The 3Cr-1Mo-V steel, used since the end of 1980's.

For hydroprocessing applications of these steels, and taking in consideration the hydrogen attack phenomenon, the American Petroleum Institute prescribes the temperature limitations of 755K (482°C) for 2.25Cr-1Mo steel and 783K (510°C) for 2.25Cr-1Mo-0.25V, 3Cr-1Mo and 3Cr-1Mo-0.25V.

The conclusions of the present work are as follows:

1. Weldments are confirmed to be a major concern in the industrial pressurized components for the (petro)chemical industry. Weldments are a weak point of these components, both with respect to the resistance to creep and hydrogen attack. These deficiencies are more marked in the 2.25Cr-1Mo steel and its V-modified counterpart than in the 3Cr-1Mo-V steel, and may be the cause of unexpected catastrophic failures.

2. For all metallurgical zones of the welded joint, the superimposition of stress has a synergistic effect on the development of hydrogen attack, under the test conditions of the present work. This result is complementary to and consistent with the work of Baker devoted to the same issue but limited to the 2.25Cr-1Mo base metal.

3. The addition of vanadium to the 2.25Cr-1Mo steel increases, as expected, the resistance of the steel to hydrogen attack and its creep strength, but does not change the mechanism of damage of the welded joint. In fact, in air or in hydrogen, under uniaxial or more complex states of stress, fracture of the welded joints occurs in the ICHAZ as a result of the formation of small cavities at the interfaces (ferrite/bainite, carbide/matrix, grain boundaries), and

their link-up by narrow cracks, which propagate mainly at ferrite/bainite interfaces. This result contradicts those of previous researchers who suggested the fracture takes place in the FGHAZ.

4. It is suggested, possibly for the first time, that the failure of the ICHAZ is due mainly to the formation of very narrow microcracks at interfaces. A possible mechanism is hypothesized and outlined.

5. In the case of the 2.25Cr-1Mo-V welded joint tested in hydrogen, the formation of the main crack does not follow a mechanism of local nucleation and propagation. On the contrary, crack nucleation is distributed across a large fraction of the specimen section. In addition, in its development, the crack seems to conserve a particular orientation with respect to the applied stress direction. This orientation, found in samples tested in both air and hydrogen, seems linked to the orientation of the HAZ in the sample, which was not perpendicular to the direction of application of the stress. The fact that the damage (cracking) of different samples, extracted from the same part of the welded coupon, exhibits similar orientation, underpins the hypothesis that, in air as in hydrogen, under the imposed test conditions, the catastrophic damage develops in one specific metallurgical zone, namely, the ICHAZ.

6. A distinctive feature of the present programme was the assessment of the increase in Cr content on the hydrogen attack resistance of the steel. The 3Cr-1Mo-V steel shows an enhanced hydrogen attack resistance of the welded joint, but reduced creep strength, when compared to the 2.25Cr-1Mo-V steels. The ductility increases and the lifetime decreases; the failure is registered in the base metal, which experiences high elongation and reduction in area. It is therefore suggested that, under the lower stresses encountered in service, failure of the welded joint would be Type IV.

7. The mechanisms of failure of tubular specimens, made of standard 2.25Cr-1Mo or its V-modified grade, pressurized by means of hot hydrogen or argon, are independent of the presence of weldments. Tubes pressurized with hydrogen fail because cracks form underneath the surface exposed to hydrogen and propagate towards the outer surface. On the contrary, tubes pressurized with argon fail because a progressive thinning of the tube wall moves from the

more external layers inwards. In reality, tubes pressurized with hot hydrogen exhibit both mechanisms: cavitation-induced cracking, in areas close to the internal surface, and ductile tearing in areas close to the external surface.

8. The in-house built facilities and the expertise available at the Institute for Energy of the Joint Research Center allow studying hydrogen attack in conditions similar to the service ones. The calibration and testing procedures, as the work instructions related to the use of any kind of equipment, are consistent with the national and international safety practices, as well as with the ISO 9001 and ISO 14001 standards. This guaranteed the safe and accurate execution of the reported research project.

7 Suggestions for Future Work

Further Testing

- The present work, on welded uniaxial and tubular specimens, achieves results which are satisfactorily representative of the in-service conditions. Due to time constraints, tests had been carried out at a temperature and in presence of applied initial stresses markedly higher than those encountered in service conditions. Consequently, it is necessary to produce data still closer to the industrial reality, with respect to the temperatures, stresses and times involved.

- In particular, the testing of the V-modified 3Cr-1Mo welded joint, under stresses lower than those considered in the present work, should allow to explain why the alloy fails (under the selected conditions) in the base metal, while all the others tested exhibit Type IV failure.

Material Characterization and Mechanical Properties

- The cracking of the ICHAZ of 2.25Cr-1Mo and V-modified 2.25Cr-1Mo steel is due to the formation of microcracks which link each other forming well-developed textures. The formation of these cracks is noted mainly at interfaces. Further investigation should be devoted to obtaining more insight on the formation of these microcracks. One could, for instance, carry out microhardness measurements on the appropriate interfaces, as well as dedicate a study to eventual changes of the composition of these interfaces during testing in hydrogen environment, in the presence or in the absence of applied stresses.

- This research offered the opportunity of co-operation with researchers in other disciplines, namely NDT damage assessment. Although not included in the scope of the present work, first trials of characterizing the hydrogen attack damage, in standard 2.25Cr-1Mo and V-modified 2.25Cr-1Mo steels, by means of Magnetic Barkhausen Noise (MBN), have been carried out at the Institute for Energy. The results are very promising and already presented to several specialised conferences. A research programme should be devoted to

the verification and qualification of the applicability of the MBN technique to the hydrogen attack detection for plant life assessment.

Microstructural Characterization and Mechanical Properties

- The work of Tsuchida *et al* [2004] is one of the few devoted to microstructural evolution in V-modified 2.25Cr-1Mo, but does not characterize the microstructure of the weldment. Further work is therefore needed to clarify the evolution of carbides in the different metallurgical zones of the weldments of the 2.25Cr-1Mo steel and of its V-modified counterpart. This investigation should focus mainly on the carbides of the zones (ICHAZ, FGHAZ), which exhibit, both in hydrogen and in air, the highest damage. The evolution of carbides in the base metal should be also investigated for comparison.

- In particular, Tsuchida *et al* [Tsuchida, *ibidem*] suggest that Mo_2C nucleates close to the M_7C_3 carbide and grows inside the grain by consuming the neighbouring M_7C_3 carbide. Their conclusion is underpinned by the work of Senior but conflicts with the relevant literature on the microstructural evolution of carbides in Cr-Mo steels like 2.25Cr-1Mo steel, which sees the Mo_2C disappearing in favour of the formation of M_7C_3 [e.g. Baker & Nutting, 1959; Klueh, 1974]. Considering the role plaid by the M_2C type carbides on the creep properties of these structural steels, the reported inconsistency should be clarified by investigating the evolution of carbides in the V-modified 2.25Cr-1Mo steel and the effects of V addition on the thermodynamic stability of the Mo_2C and M_7C_3 carbides.

- The mechanical properties of the 3Cr-1Mo-V welded joint should be studied in relation to the distribution of carbides in the different metallurgical zones of the weldment and their evolution during PWHTs. This study could provide a foundation for development of more advanced PWHTs for improving the performances of welded joints.

The Experimental Set-up

- The facilities available at the Institute for Energy of the Joint Research Centre, and used in the context of the present work to perform tests in hydrogen

environment, could be easily adapted to perform similar tests in different environments.

- Most of the insight achieved through the present work came from the execution of interrupted tests, in particular in hydrogen atmosphere. In some cases it has been possible to stop the test just before the failure, and important information has been obtained (e.g. see the multiaxial test on the tubular specimen made of standard 2.25Cr-1Mo steel). In other cases, the plan to stop the test close to the end life failed. It is suggested to modify the experimental set up (and the software of control) to facilitate the performance of successful interrupted tests.

Underpinning the Safety and Security of Energy Supply

- This work has been conceived in connection with the technical and scientific needs of the petrochemical sector. On the other hand, the CrMoV steels are traditionally used in the fossil fuel powered and nuclear sectors (e.g. the reactor pressure vessels of the Russian-designed nuclear power plants). In recent years the 2.25Cr-1Mo steel has been used for the development of prototypes of High Temperature Gas-cooled Reactors. Future work could be addressed to the concerns related to the structural use of these alloys in innovative nuclear power plants but also in advanced, high-efficiency fossil fuel fired plants.

References

Albert S.K., Matsui M. Watanabe T., Hongo H., Kubo K. and Tabuchi M. (2003): "*Variation in the Type IV cracking behaviour of a high Cr steel weld with post weld heat treatment*", International Journal of Pressure Vessels and Piping, vol. 80, pp. 405-413.

Albert S.K., Matsui M., Hongo H., Watanabe T., Kubo K., Tabuchi M. (2004): "*Creep rupture properties of HAZs of a high Cr ferritic steel simulated by a weld simulator*", International Journal of Pressure Vessels and Piping, Article in Press, accepted on January 20, 2004 and available on-line.

Allen R.E., Jansen R.J., Rosenthal P.C., and Vitovec F.H. (1961): *"The Rate of Irreversible Hydrogen Attack Of Steel At Elevated Temperatures"*, Proc. API, vol. 41 [III], pp. 74-85.

Allen R.E., Rosenthal P.C., and Vitovec F.H. (1962): *"Creep Rupture Behaviour of Mild Steel Under Conditions of Hydrogen Attack"*, Proc. API, vol. 42 [III], pp. 464-471.

Allen R.E., Jansen R.J., Rosenthal P.C., and Vitovec F.H. (1962): *"Analysis of Probable Mechanisms of High Temperature Hydrogen Attack of Steel"*, Proc. API, vol. 42 [III], pp. 452-462.

Davies L.M. (1997): *"A Comparison of Western and Eastern Nuclear Reactor Pressure Vessel Steels"*, AMES Report No.10, European Commission Report EUR 17327 EN, IE/JRC, Petten, The Netherlands.

Andersson J, Prager M. (1994): *"Design margins and production of a 3Cr-1Mo-V steel built to ASME Section VIII, Div. 2"*, Proc. of the Second International Conference on Interaction of Steels with Hydrogen in Petroleum Industry Pressure Vessels and Pipeline Service, October 19-21, Vienna, Austria, vol. 2, pp. .555-576.

Antalffy L.P., Chaku P.N. (1994): *"Metallurgical Design & Fabrication Aspects of Modern Hydroprocessing Reactors"*, Proc. of the Second International Conference on Interaction of Steels with Hydrogen in Petroleum Industry Pressure Vessels and Pipeline Service, October 19-21, Vienna, Austria, vol. 2, pp.619-657.

Antalffy L.P., Chaku P.N., Canonico D.A., Pfeifer J.A., Alcorn D.G. (2002): *"The potential for using high chromium ferritic alloys for hydroprocessing reactors"*, International Journal of Pressure Vessels and Piping, vol. 79 (8-10), pp. 561-569.

API (1997): *"Steels for Hydrogen Service at Elevated Temperatures and Pressures in Petroleum Refineries and Petrochemical Plants"*, API recommended practice 941, Fifth Edition.

Baker A. (1999): *"Combined creep and hydrogen attack of petro-refinery steel"*, PhD Thesis, Swansea University, UK.

Baker A., Manolatos P., Castello P. and Hurst R. (2000): "*Role of Stress on Hydrogen Attach*", Proc. EUROMAT 2000, "Adv. in Mech. Behaviour, Plasticity and Damage, Eds.

Baker R.G. and Nutting J. (1959): "*The tempering of 21/4%Cr-1%Mo steel after quenching and normalizing*", Journal of The Iron and Steel Institute, vol. 192, pp. 257-268.

(BE 1835-4) JRC/IE, ISQ: BRITE-EURAM Project BE-1835: "*Proposal of Final Report on Task 4.4 (Microstructural Analysis)*"

Berzolla A., Bertoni A., Bocquet P., Hauck G. (1994): *"The new 2 1/4 Cr and 3Cr 1Mo 1/4V steels for pressure vessels operating in hydrogen environment. A Joint European Research Contract"*, Proc. of the Second International Conference on Interaction of Steels with Hydrogen in Petroleum Industry Pressure Vessels and Pipeline Service, October 19-21, Vienna, Austria, vol. 2, pp. .577-606.

Bocquet P., Castello P., De Araujo C.L., Ohm R., Van Wortel H., Schloegl S. (2001): *"Prediction of Pressure Vessel Integrity in Creep Hydrogen Service (PREDICH)"*, Proc. European Symposium on Pressure Equipment-ESOPE 2001-Paris 23-25 Oct..

Brouwer R.C. (1992): *"Hydrogen Diffusion and Solubility in Vanadium Modified Pressure Vessel Steels"*, Scripta Metallurgica et Materialia, vol. 27, pp. 353-358.

(BS3500) British Standard BS 3500 (1969): British Standard Methods For: *"Creep and Rupture Testing of Metals"*, Part 3. Tensile Creep Testing,

Castello P., Baker A., Manna G., Manolatos P., Hurst R. and Parker J.D. (2001): "*Creep of 2.25Cr-1Mo steel tubular test pieces under hydrogen attack conditions*", Proc. of the 9th International Conference on Creep & Fracture of Engineering Materials & Structures, University of Wales Swansea, 1-4 April, pp. 699-708.

Chen, L.C. and Shewmon P. (1995): *"Stress-Assisted Hydrogen Attack Cracking in 2.25Cr-1Mo Steels at Elevated Temperatures"*, Metallurgical and Materials Transactions A, vol. 26A, pp. 2317-2327.

Ciuffreda A.R. and Rowland W.D. (1957): "*Hydrogen attack in reformer service*", Proc. API, vol. 37, pp. 116-128.

Coombs J.W., Allen R.E., Vitovec F.H. (1965): *"Creep and rupture behaviour of low alloy steels in high pressure hydrogen environment"*, Trans. ASME, Journal of Basic Engineering, vol. 87, pp. 313-318.

Erwin W.E. (1982): *"Mechanism of hydrogen attack in 2.25Cr-1Mo reactor steel"*, Proc. 4th Midyear Refining Meeting on Services in Hydrogen Operations, API, NY, pp. 120-134.

Gingell A., Bocquet P. and Balladon P. (2001): "*Creep Behaviour of CrMo(V) Steel Grades and their Welds in Hot Hydrogen Environment*", Proc. of the 9th International Conference on Creep & Fracture of Engineering Materials & Structures, University of Wales Swansea, 1-4 April, pp. 709-722.

Gope N., Chatterjee A., Mukherjee T., Sarma D.S. (1993): *"Influence of Long-term Aging and Superimposed Creep Stress on the microstructure of 2.25Cr-1Mo Steel"*, Met. Trans., vol. 24A, pp. 315-326.

Hakkarainen T., Wanagael J. and Li C-Y (1980): *"Direct observation of Methane Bubbles in a 2.25Cr-1Mo Steel after hydrogen exposure"*, Met. Trans. 11A, pp. 2035-2036.

(HTMTC) High Temperature Mechanical Testing Committee (1989): *"A Code of Practice for Internal Pressure Testing of Tubular Components at Elevated Temperatures"*, Prepared by the Internal Pressure Testing Working Party, HTMTC/IP/6/89.

Inglis N.P. and Andrews, W. (1933): "*The effect on various steels of hydrogen at high pressures and temperatures*", Journal of the Iron and Steel Institute, vol. 128, pp. 383-408.

Kassner M.E., Hayes T.A. (2003): "*Creep cavitation in metals*", International Journal of Plasticity, vol. 19, pp. 1715-1748.

Kim T.-G. (2002): *"Failure of piping by hydrogen attack"*, Engineering Failure Analysis, vol. 9 (5), pp. 571-578.

Kimmins S.T., Coleman M.C., Smith D.J. (1993): *"An overview of creep failure associated with heat affected zones of ferritic weldments"*, Proc. of the 5th International Conference on Creep & Fracture of Engineering Materials & Structures, pp. .681-694.

Klueh R.L. (1974): *"The effect of carbon on 2.25Cr-1Mo steel (II). - Creep-rupture properties"*, Journal of Nuclear Materials, vol. 54, pp. 55-63.

Kuzuku V., Aksoy M., Korkut M.H. (1998): *"The effect of strong carbide-forming elements such as Mo, Ti, V and Nb on the microstructure of ferritic stainless steel"*, Journal of Materials Processing Technology, vol. 82, pp. 165-171.

Laha K., Rao K.B.S. and Mannan S.L. (1990): *"Creep Behaviour of post-weld heat treated 2.25Cr-1Mo ferritic steel base, weld metal and weldments"*, Mater. Sci. Eng. A, vol. 129, pp 183-195.

Laha K., Chandravathi K. S., Rao K. B. S., Mannan S. L. and Sastry D. H. (2000): *"Prediction of creep deformation and rupture behaviour of 2.25Cr–1Mo weld joint"*, International Journal of Pressure Vessels and Piping, vol. 77, pp 761-769.

Liaw P.K., Rao G.V., Burke M.G. (1991): *"Creep fracture behaviour of 2.25Cr-1Mo welds from a 31-year-old Fossil power plant"*, Mater. Sci and Eng., vol. A131, pp. 187-201.

Looney L. (1994): *"The Effect of High Pressure Hydrogen on the Creep Fracture of Ferritic Steel Components"*, PhD. Thesis, University of Dublin, Trinity College, May.

Lundin C.D., Kelley S.C., Menon R. and Kruse B.J. (1984): *"Stress Rupture Behavior of Post Weld Heat Treated 21/4 Cr-1Mo Steel Weld Metal"*, Welding Research Council Bullettin, No 315, pp. 1-66.

Mannan S.L. and Laha K. (1996): *"Creep Behaviour of Cr-Mo Steel Weldments"*, Trans. Indian Inst. Met., vol. 49 (4), pp.3 03-320.

Middleton C.J., Brear J.M., Munson R and Viswanathan R. (2001): *"An Assessment of the Risk of Type IV Cracking in Welds to Header, Pipework and Turbine Components Constructed from the Advanced Ferritic 9% and 12% Chromium Steels"*. Proceedings of Third Conference on Advances in Materials Technology for Fossil Power Plants, The Institute of Metals, London, pp. 69-78.

Mitchell D.R.G., Moss C.J., Griffiths R.R. (1999): *"Optimisation of post-weld heat treatment of a 1.25Cr-0.5Mo pressure vessel for high temperature hydrogen service"*, International Journal of Pressure Vessels and Piping, vol.76, pp. 259-266.

Mitchell D. R. G., Ball C. J. (2001): *"A quantitative X-ray diffraction and analytical electron microscopy study of service-exposed 2.25Cr–1Mo steels"*, Materials Characterization, vol. 47 (1), pp. 17-26.

Naumann F.K. (1937): *"Einwirkung von Wasserstof unter hohem Druck auf unlegierten Stahl"*, Stahl und Eisen, 32, pp. 889-899.

Nelson G.A. and Effinger R.T. (1955): *"Blistering and Embrittlement of Pressure Vessel Steels by Hydrogen"*, Welding Journal, vol. 34 (1), pp. 12-21.

Nomura T., Imanaka T. (1994): *"Ultrasonic Detection of Hydrogen Attack in Hydroporcessing Equipment"*, Proc. of the Second International Conference on Interaction of Steels with Hydrogen in Petroleum Industry Pressure Vessels and Pipeline Service, October 19-21, Vienna, Austria, vol. 2, pp. .521-528.

Norris E.B., Sticha E.A. (1976): *"Effect of hydrogen on the stress-rupture strenght of 2.25Cr-1Mo steel"*, ASME Pub. MPC-2"Metals Properties for the petroleum & Chemical Industry", Ed. Schoefer, pp. 1-14.

Odette G.R., Vagarali S.S. (1982): *"An Equation of State for Methane for Modeling Hydrogen Attack in Ferritic Steels"*, Metallurgical Transactions, 13A, pp. 299-303.

Oh Y. K., Kim G. S. and Indacochea J. E. (1999): *"Creep rupture behaviour due to molybdenum rich M6C carbide in 1.0Cr-1.0Mo-0.25V bainitic steel weldment"*, Scripta Materialia, vol. 41 (1), pp. 7–1.

Osage D., Buchheim G.M., Warke W.R., Prager M., Chell G., Anderson T. (1994): *"Fitness for Service Evaluation of Hydrogen Process Vessels"* Proc. of the Second International Conference on Interaction of Steels with Hydrogen in Petroleum Industry Pressure Vessels and Pipeline Service, October 19-21, Vienna, Austria, vol. 2, pp. 813-823.

Parker J.D., Parson A.W.J. (1994): *"The tempering performance of low-alloy steel weldments"*, International Journal of Pressure Vessels and Piping, vol. 57, pp. 345-352.

Parker J.D. (1995): *"Creep behaviour of low alloy steel weldments"*, International Journal of Pressure Vessels and Piping, vol. 63 (1), pp. 55-62.

Parker J.D., Stratford G.C. (1996): *"Strain localization in creep testing of samples with heterogeneous microstructures"*, International Journal of Pressure Vessels and Piping, vol. 68 (2), pp. 135-143.

Parthasarathy T.A., Shewmon, P.G. (1987): *"Hydrogen Attack behaviour of the Heat Affected Zone of a 2.25Cr-1Mo Steel Weldment"*, Metallurgical Transactions A, vol. 18A, pp. 1309-1312.

Peddle B.E. and Pickles C.A. (2001): *"Carbide Development in the Heat Affected Zone of Tempered and Post-Weld Heat Treated 2.25Cr-1Mo Steel Weldments"*, Canadian Metallurgical Quarterly, vol. 40 (1), pp. 105-126.

Rosenthal P.C., Schroeder W.L., Vitovec F.H. (1963): *"Effect of Low-Alloy Additions on the Resistance of Carbon Steels to Hydrogen Attack"*, Proc. API, vol. 43 [III], pp. 98-105

Ryu K.S., Park J.S., Nahm S.H., Yu K.M., Kim Y.B. and Son D. (2000): *"Dependence of magnetic properties on isothermal heat treatment time for 1Cr–1Mo–0.25 V steel"*, Journal of Magnetism and Magnetic Materials, vol. 222 (1-2), pp. 128-132.

Ryu K.S., Park J.S., Nahm S.H., Yu K.M., Kim Y.B. and Son D. (2001): *"Nondestructive evaluation of aged 1Cr–1Mo–0.25 V steel by harmonic analysis of induced voltage"*, Journal of Magnetism and Magnetic Materials, vol. 231 (2-3), pp. 294-298.

Sagüés A.A., Okray Hall B. and Wiedersich H. (1978): *"On the mechanism of Hydrogen Attack"*, Scripta Metall., vol. 12, pp. 319-326.

Sakai T. and Kaji H. (1980): *"Nucleation and growth of bubbles formed by hydrogen attack in low alloy steels"*, Proceedings JIMIS-2, hydrogen in Metals, Jpn. Inst. Met., pp. 489-492.

Sakai T. and Kaji H. (1980): *"Effect of impurity elements on the formation of bubbles by hydrogen attack in 2.25Cr-1Mo steel"*, Proc. Conf. On Hydrogen effects in Metals, Moran, Wyo, TMS/AIME 1981, pp. 903-911.

Sato I., Suzuki K. (1997): *"Manufacturing and material properties of forgings for the reactor pressure vessel of the high temperature engineering test reactor"*, Nuclear Engineering and Design, vol. 171 (1-3), pp. 45-56.

Schlögl S.M., Svoboda J. and Van der Giessen E. (2001): *"Evolution of the Methane Pressure in a Standard 2.25Cr-1Mo Steel during Hydrogen Attack"*, Acta Materialia, vol. 49, pp. 2227-2238.

Schuyten J. (1947): *"Hydrogen Attack on Metals at High Temperatures and Pressures"*, Corrosion and Material Protection, vol. 4, pp. 13-18.

Senior B.A. (1988): "A Critical Review of Precipitation Behaviour in 1Cr-Mo-V Rotor Steels", Materials Science and Engineering, vol. A103, pp.263-271.

Shewmon P.G. (1985): *"Hydrogen attack of pressure-vessel steels"*, Materials Science and Technology, vol. 1, pp. 2-11.

Shinya T. and Tomita Y. (1998): *"Effect of Calcium Treatments and Strain Rate on Reheat Cracking of Vanadium-Modified 2.25Cr-1Mo steel"*, Materials Characterization, vol. 40, pp. 221-225.

Singh R. and Singh S.R. (1997): *"Remaining creep life study of Cr-Mo-V main steam pipe lines"*, International Journal of Pressure Vessels and Piping, vol. 73 (1), pp. 89-95.

Slugen V., de Bakker P.M.A, De Grave E., Magula V., Van Hoecke T., Van Waeyenberge B. (1999): *"Annealing behaviour of reactor pressure-vessel steels studied by positron-annihilation spectroscopy, Mössbauer spectroscopy and transmission electron microscopy"*, Journal of Nuclear Materials, vol. 274, pp. 273-286.

Smith D.J., Walker N.S. and Kimmins S.T. (2003): *"Type IV creep cavity accumulation and failure in steel welds"*, International Journal of Pressure Vessels and Piping, vol. 80, pp. 617-627.

Song S. -H., Faulkner R. G. and Flewitt P. E. J. (2000): "Quenching and tempering-induced molybdenum segregation to grain boundaries in a 2.25Cr–1Mo steel", Materials Science and Engineering A, vol. 281 (1-2), pp. 23-27.

Sponseller D.L. and Vitovec F.H. (1966): *"Resistance to hydrogen Attack at 1000 F of 2.25%Cr-1%Mo and 0.5%Mo-0.006%B Steels"*, Proc. Symp. On Heat-treated steels for elevated temperature service, pp.74-85.

Sundararajan G. and Shewmon P. (1980): *"The hydrogen attack of HSLA Steels"*, Metallurgical Transactions 11A, pp. 509-516.

Sundararajan G. and Shewmon P. (1981): *"The kinetics of hydrogen attack of steels"*, Metallurgical Transactions, 12A, pp. 1761/1775

Sutherland C.W., Vacca P.J., Rosenthal P.C. and Vitovec F.H. (1965): *"Effect of Stress Concentration and Gas Pressure on the Creep Strength of Steel in Hydrogen Environment"*, Proceedings of the Annual Meeting of the American Petr. Instit., vol. 45 (III), n. 325A, pp. 181-189.

Tahara T., Ishiguro T., Iga H. and Motoo A. (1994): *"Application of Advanced Cr-Mo Pressure Vessel Steel for High Temperature Hydrogen Service"*, Proc. of the Second International Conference on Interaction of Steels with Hydrogen in Petroleum Industry Pressure Vessels and Pipeline Service, October 19-21, Vienna, Austria, vol. 2, pp. 541-554.

Thoma P.E., Vitovec F.H. and Mullendore J.A. (1966): *"Effect of Hydrogen on the Creep Rupture Properties of Iron"*, Proceedings of the Annual Meeting of the American Petr. Institute. Institute. Institute, vol. 46 (III), pp. 345-351.

Thomson R.C. (2000): *"Characterization of Carbides in Steels using Atom Probe Field-Ion Microscopy"*, Materials Characterization, vol. 44, pp. 219-233.

Timmis P.F. (1997): *"Solutions to Hydrogen Attack in Steels"*, ASM International, 1997.

Todd. J.A. and Chung D.W. (1983): *"Developmental 2.25Cr-1Mo Steels for Coal Conversion Vessels"*, Proc. Conf. Specialty Steels and Hard Materials, Pretoria, South Africa, Pergamon Press, pp. 207-212.

Tsai M.C. and Yang J.R. (2003): *"Microstructural Degeneration of simulated heat-affected zone in 2.25Cr-1Mo steel during high-temperature exposure"*, Materials Science and Engineering, vol. A340, pp. 15-32.

Tsuchida Y., Inoue T. and Suzuki T. (2004): "Creep rupture strength of V-modified 2 ¼ Cr-1Mo steel", International Journal of Pressure Vessels and Piping, in press, available on-line since 2/2/04.

Van der Burg M.W.D. and Van der Giessen E. (1996): *"Hydrogen Attack in Creeping Polycrystals due to Cavitation on Grain Boundaries"*, Hydrogen Effects in Materials, Edited by Thompson A.W. and Moody N.R., The Minerals, Metals & Materials Society, pp.314-322.

Vitovec F.H. (1982): *"Modelling of hydrogen attack of steel in relation with material and environmental variables"*, Proc. On Conf. On Current solutions to hydrogen problems in steels, Washington DC, 1-5 Nov.

Výrostková A., Kroupa A., Janovec J. and Svoboda M. (1998): *"Carbide reactions and phase equilibria in low alloy Cr–Mo–V steels tempered at 773–993 K. Part I: Experimental measurements"*, Acta Materialia, vol. 46 (1), pp. 31-38.

Watanabe T., Yamazaki M., Hongo H., Tabuchi M., Tanabe T. (2004): *"Effect of stress on microstructural change due to aging at 823k in multi-layer welded joint of 2.25Cr-1Mo steel"*, International Journal of Pressure Vessels and Piping, In press.

Weiner, L.C. (1961): *"Kinetics and Mechanism of hydrogen attack of steel"*, Corrosion-NACE, March 1961, pp. 109-115.

Yang H. and Kim S. (2001): *"A study on the mechanical strength change of 2.25Cr–1Mo steel by thermal aging"*, Materials Science and Engineering A, 319-321, pp. 316-320.

Yokogawa K., Fukuyama S., Kudo K. and Shewmon P. (1989): *"Effect of hydrogen attack on tensile and creep properties of low carbon steel"*, International Journal of Pressure Vessels and Piping, vol. 37, pp. 365-385.

Zander D., Maroef I., Olson D., Elizier D. (2003): *"Positive effects of hydrogen on the plasticity of 2 1/4 Cr-1Mo steel"*, Journal of Alloys and Compounds, vol. 356-357, pp. 809-812.

Figure 2.2-1: Variation of methane pressure with fugacity in the temperature range from 473 to 873K [Odette, 1982].

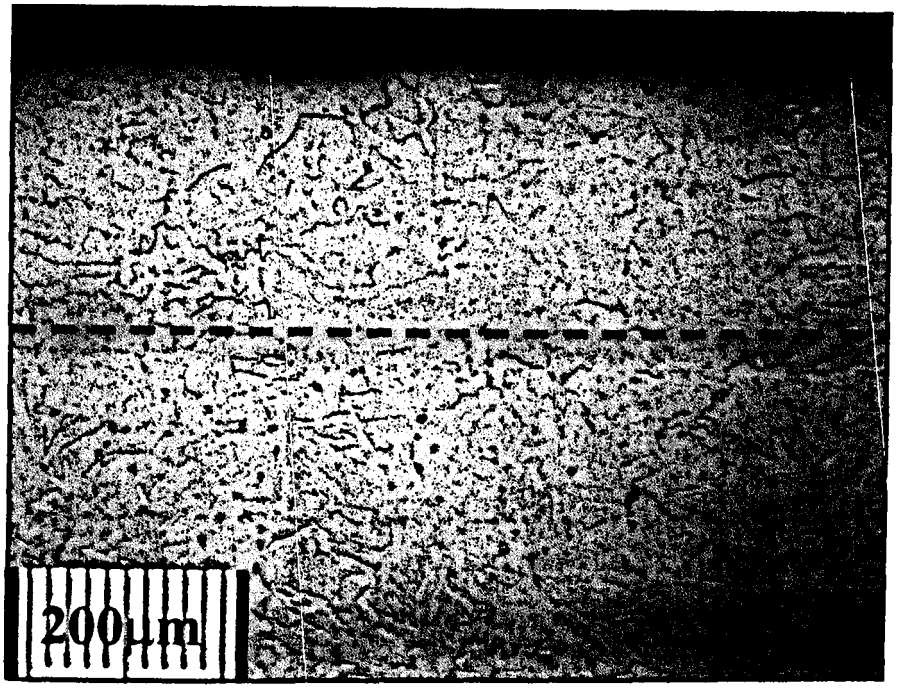

Figure 2.2-2: 2.25Cr-1Mo steel exposed to hydrogen at 843K (570°C), 18MPa, up to 3230h and in presence of a stress of 100MPa. The steel underneath the surface directly exposed to hydrogen experiences the phenomenon of decarburization. The decarburized layer shows low cavitation.

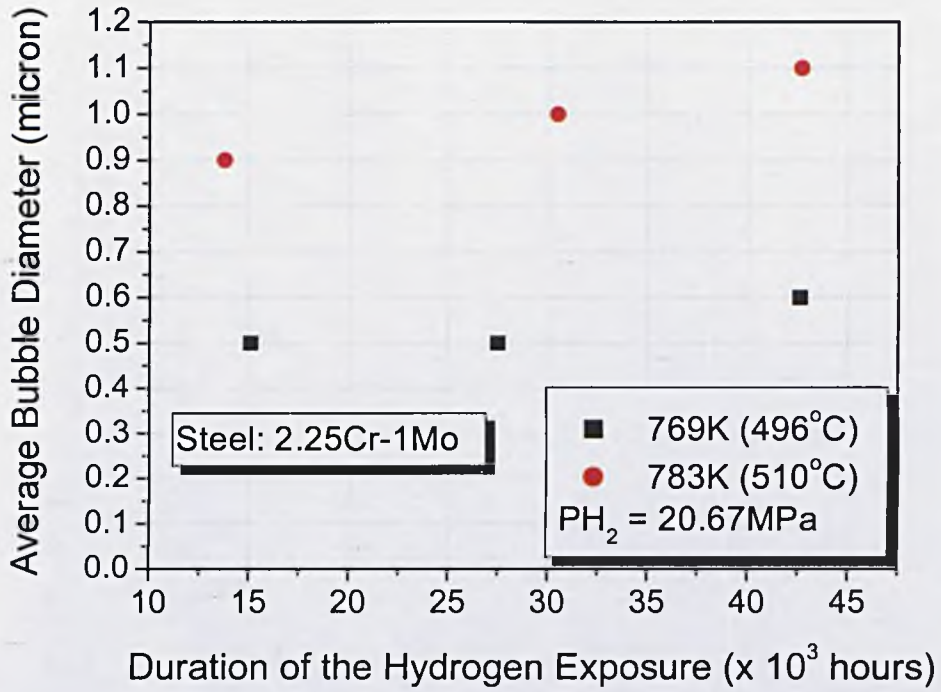

Figure 2.2-3: Variation of the average bubble diameter as function of the time of exposure, for two different temperatures. Data from Erwin [1982].

Figure 2.2-4: Stress Rupture Curves for SAE 1020 Steel at 811K (1000F) in argon atmosphere and in hydrogen atmosphere at 20.67MPa (900 psi) pressure [Allen, 1962a].

Figure 2.2-5: Ductility loss due to hydrogen attack, given as variation in reduction in area. The specimens had been exposed to hydrogen at 873K (600°C) and pressures of 15MPa (150bar) or 23MPa (230bars) [Bocquet, 2001].

Figure 2.2-6: Schematic Illustration showing the process of bubble growth and failure of grain boundary [Sakai, 1981].

Figure 2.2-7: Activity of carbon and dilatometric strain rates at 823K (550°C), as function of the tempering parameter [Shewmon, 1985].

Figure 2.2-8: Ductile shearing of ligaments between cavities in a carbon steel after exposure of 245 hours at 6.2MPa H_2 and 810K (537°C) [Allen, 1961].

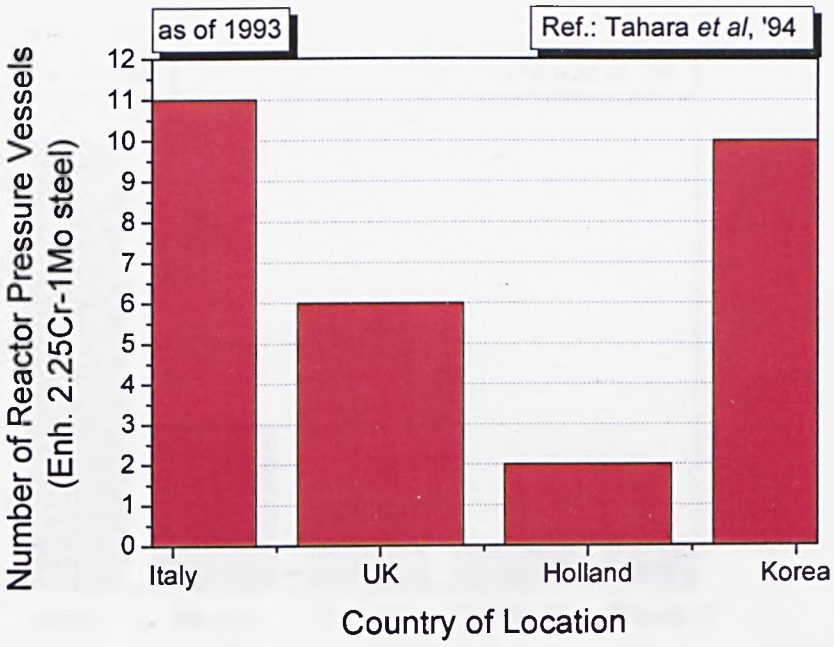

Figure 2.3-1: Distribution of reactor pressure vessels made of Enhanced 2.25Cr-1Mo steel (as for 1993)

Figure 2.3-2: Carbides transformation occurring in 2.25Cr-1Mo steel, as result of ageing phenomena [Tsai, 2003].

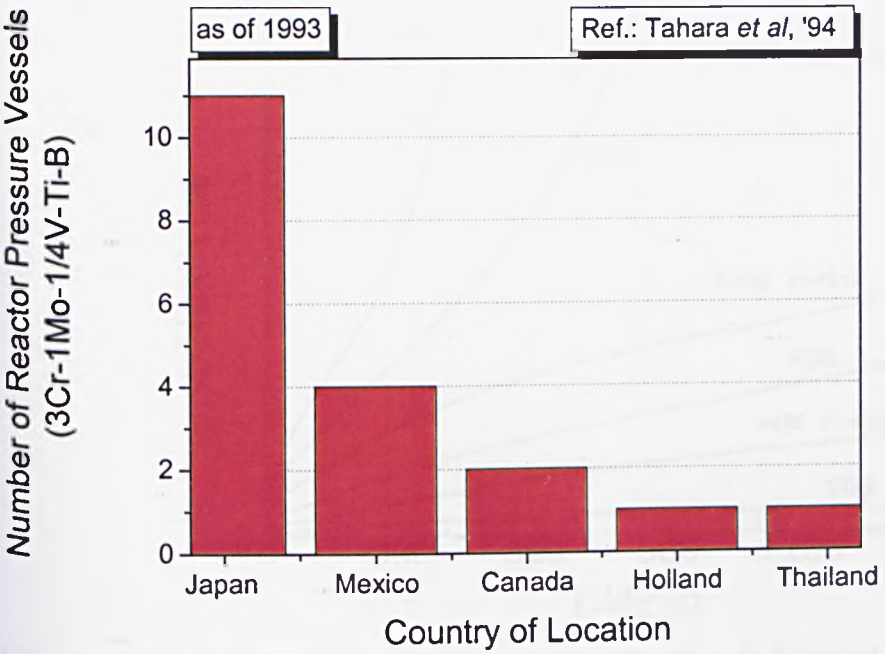

Figure 2.3-3: Distribution in the world of reactors made of 3Cr-1Mo-V-Ti steel

Figure 2.4-1: Stress dependence of rupture life of 2.25Cr-1Mo base metal, weld metal, coarse-grain HAZ, fine-grain HAZ, intercritical HAZ and weld joint at 823 K [Laha, 2000].

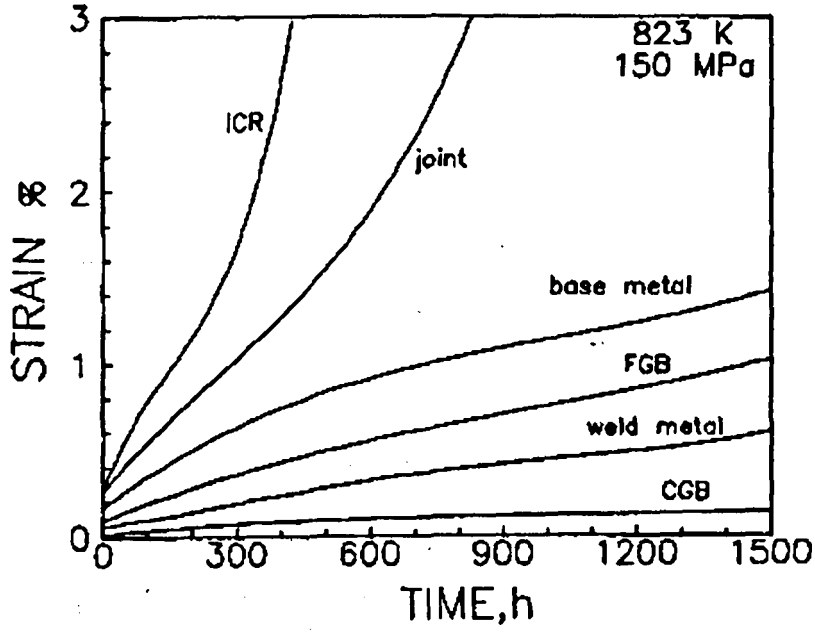

Figure 2.4-2: Creep curves of different constituents of 2.25Cr-1Mo weld joint at 150 MPa and 823 K [Laha, 2000].

Table 2-1: Materials of construction for hydroprocessing reactors [Antalffy, 1994].

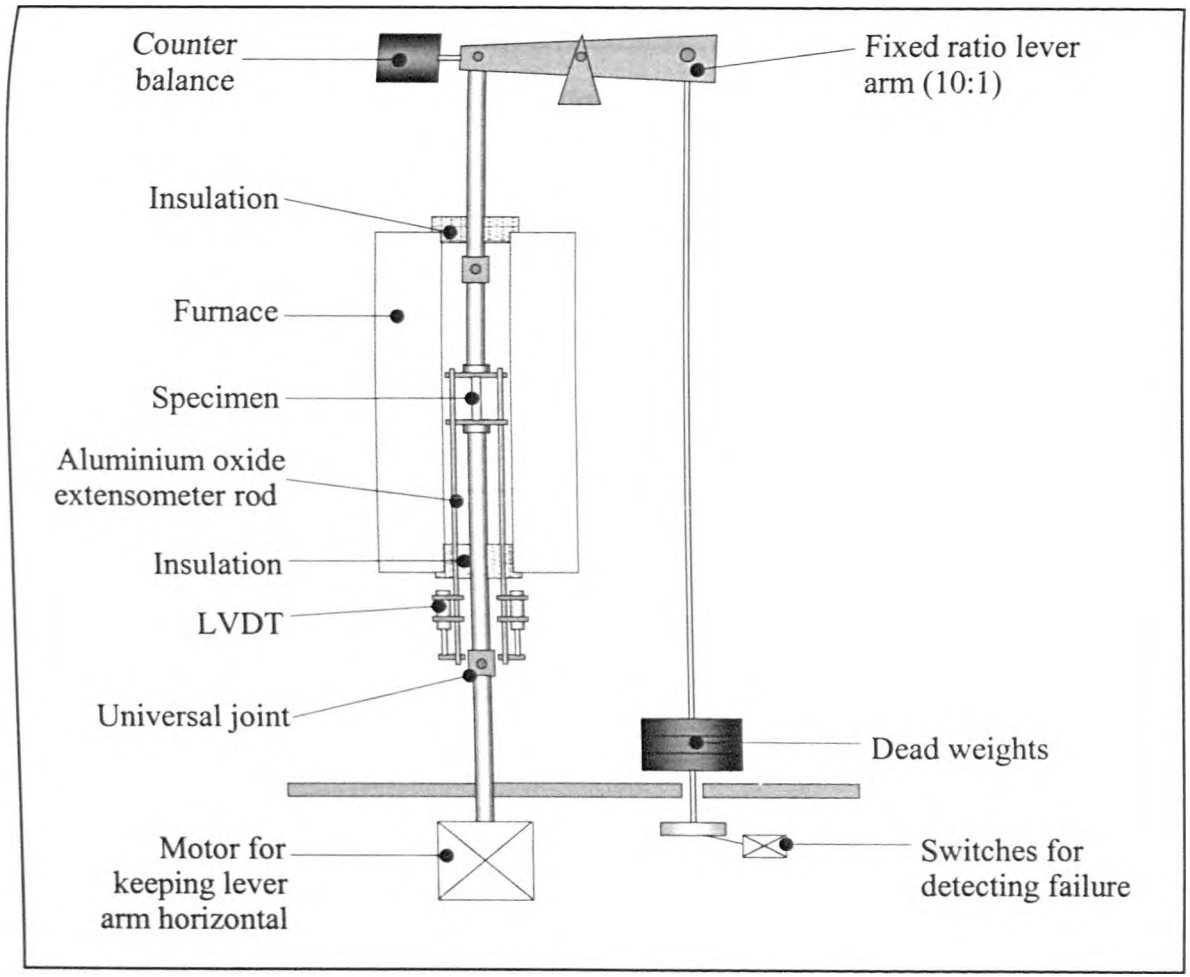

Figure 4.1-1: Schematic of the creep rig for uniaxial creep testing in air

operator: F.Harskamp **LVDT 1** **Date 20-8-01**

LVDT A Solartron AX 5.0 S/N M922505A543-06
Transmitter Solartron OD2 S/N 953115

Gauge block	Reading [mm]	deviation %
0	0.01	-0.03
1	1.00	0.00
2	2.00	0.00
3	3.00	0.00
4	4.00	-0.01
5	5.00	-0.01
6	5.99	0.02
7	7.00	0.01
8	8.00	0.00
9	9.00	0.00
10	9.98	0.03

Zero = 0.993 **Gain = 2.502**

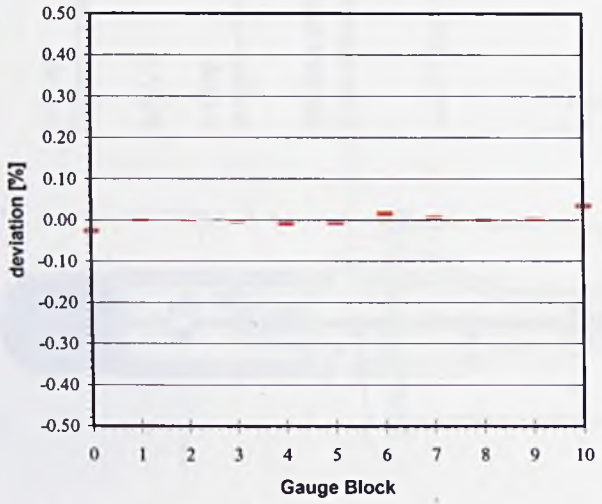

Measurements

up	down	average
0.9983	0.9983	0.9983
1.3933	1.3927	1.3930
1.7926	1.7926	1.7926
2.1928	2.1928	2.1928
2.5936	2.5933	2.5934
2.9929	2.9926	2.9927
3.3897	3.3863	3.3880
3.7899	3.7893	3.7896
4.1907	4.1901	4.1904
4.5900	4.5894	4.5897
4.9883	4.9776	4.9830

Calibration Report

LVDT's are calibrated by inserting Ceramic gaugeblocks under the measurement Tip of the LVDT
Mitutoyo Code 516-367 Set number BM3-32-1 Serial nr.948866 Grade 1 Last calibrated 10-1998 Certificate Nr GMA-98-10089

Figure 4.1-2: Typical LVDT calibration sheet of extension vs output voltage, for uniaxial creep testing

4.2 – Uniaxial Creep Testing in Hydrogen - Figures

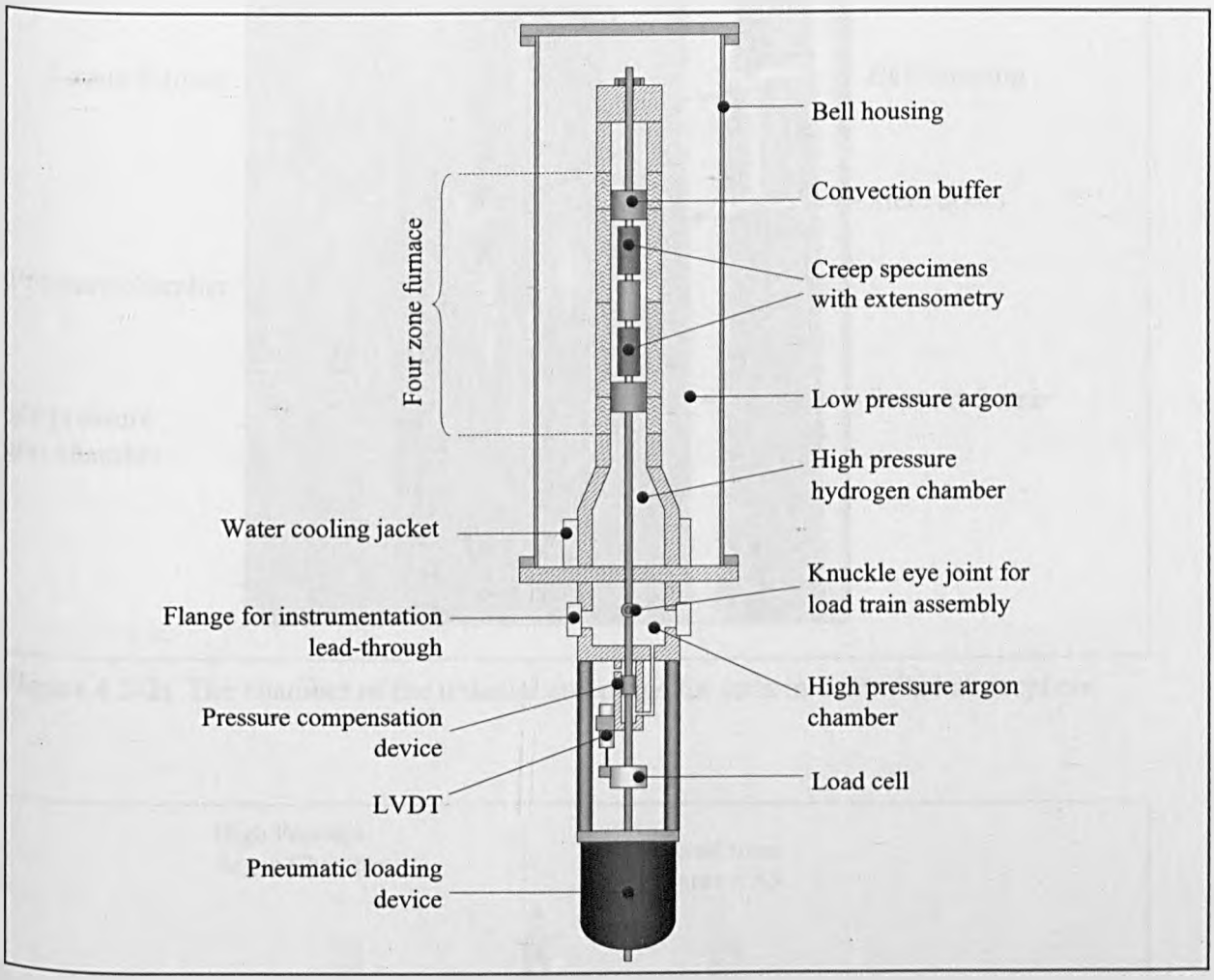

Figure 4.2-1: Scheme of the creep rig used for uniaxial creep-rupture tests under high-pressure hydrogen environments

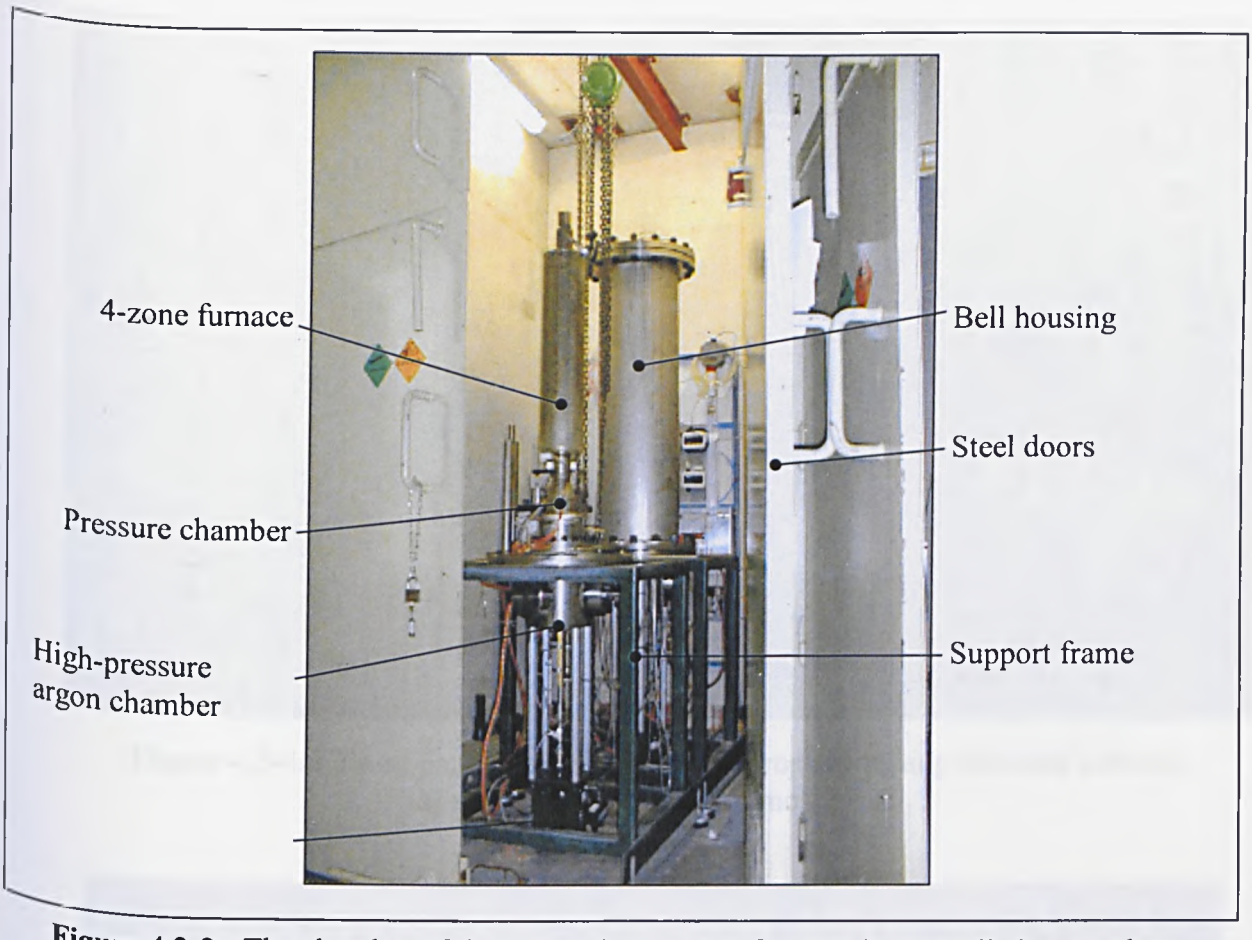

Figure 4.2-2: The chamber of the uniaxial creep rigs for tests in controlled atmosphere

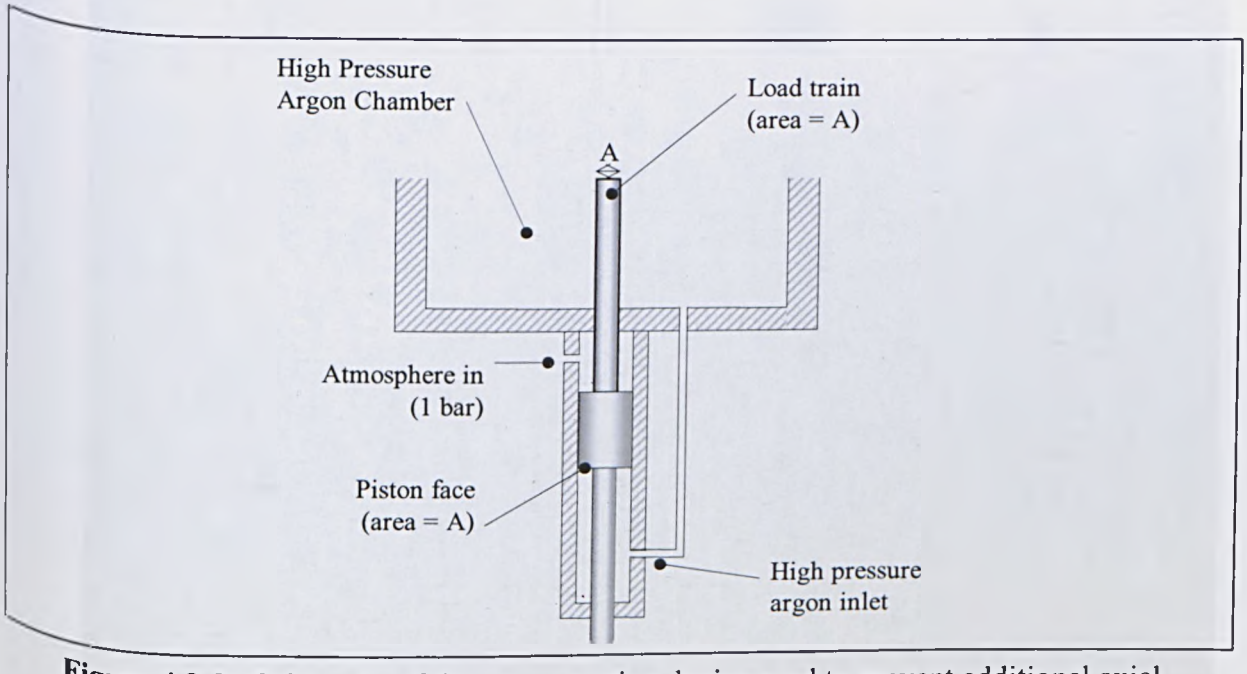

Figure 4.2-3: Schematic of the compensation device used to prevent additional axial loading due to the internal test pressure

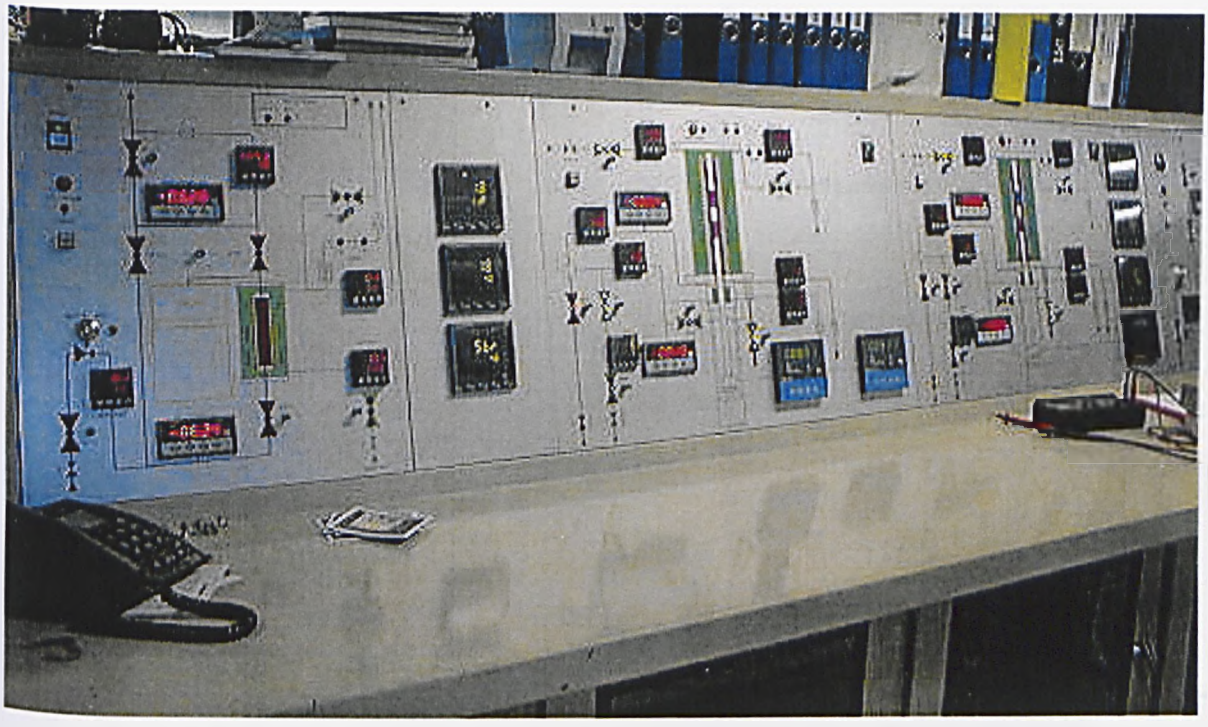

Figure 4.2-4a: Front panel of the rigs for creep-rupture testing tube and uniaxial specimens in controlled atmosphere.

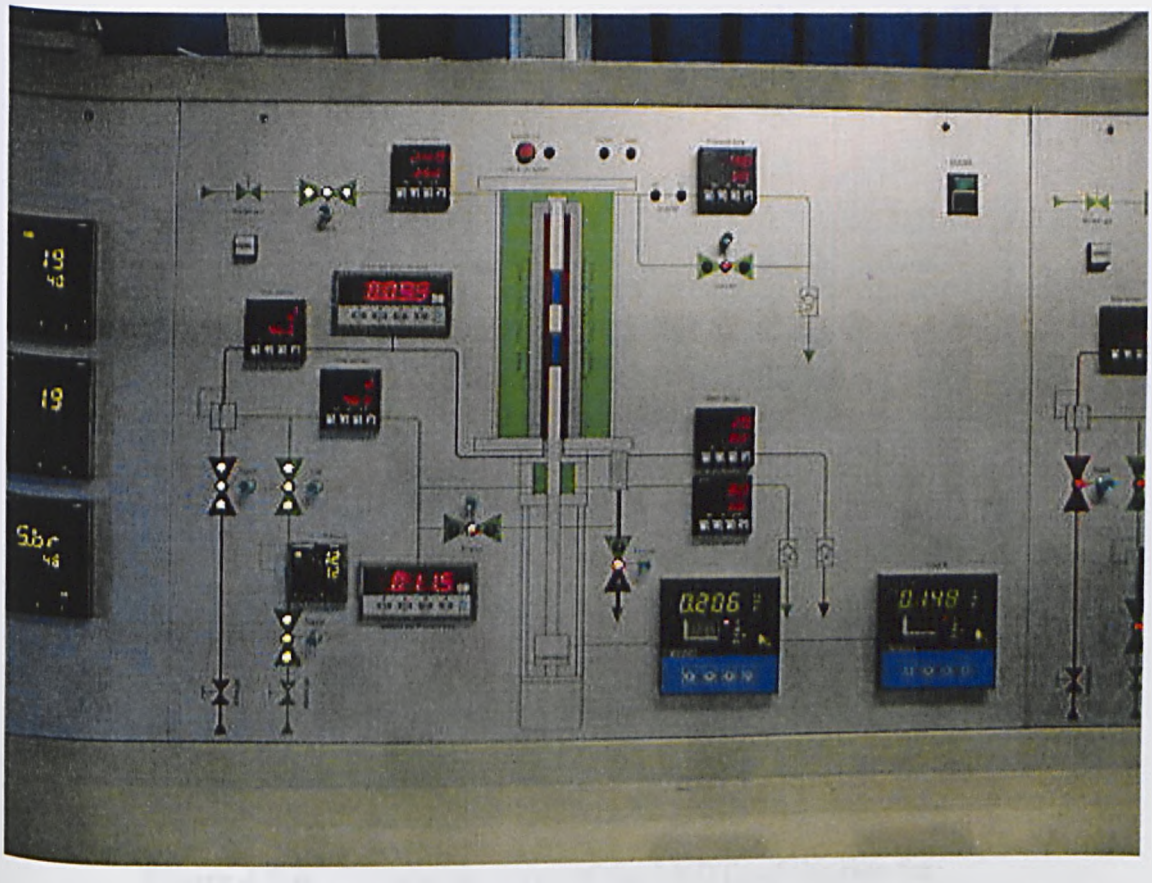

Figure 4.2-4b: The front panel of the rigs for uniaxial creep-rupture testing in controlled atmosphere. The displays below, on the right, are for the application of the load.

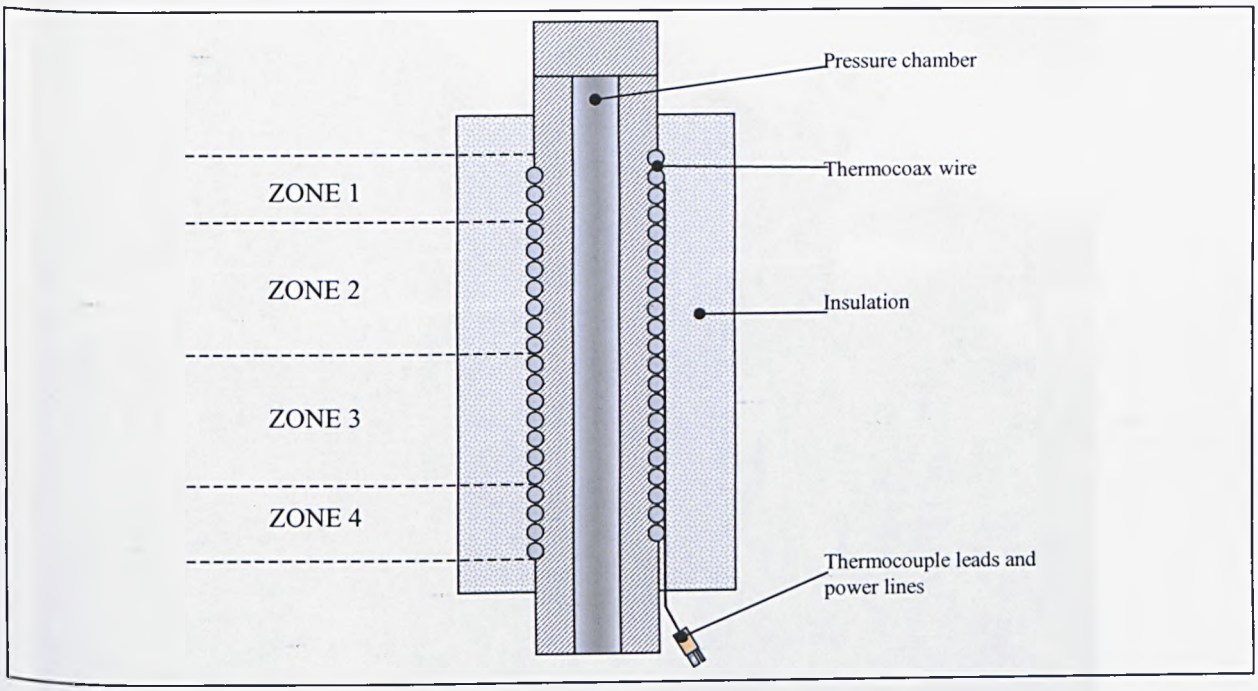

Figure 4.2-5: Schematic representation of the furnace.

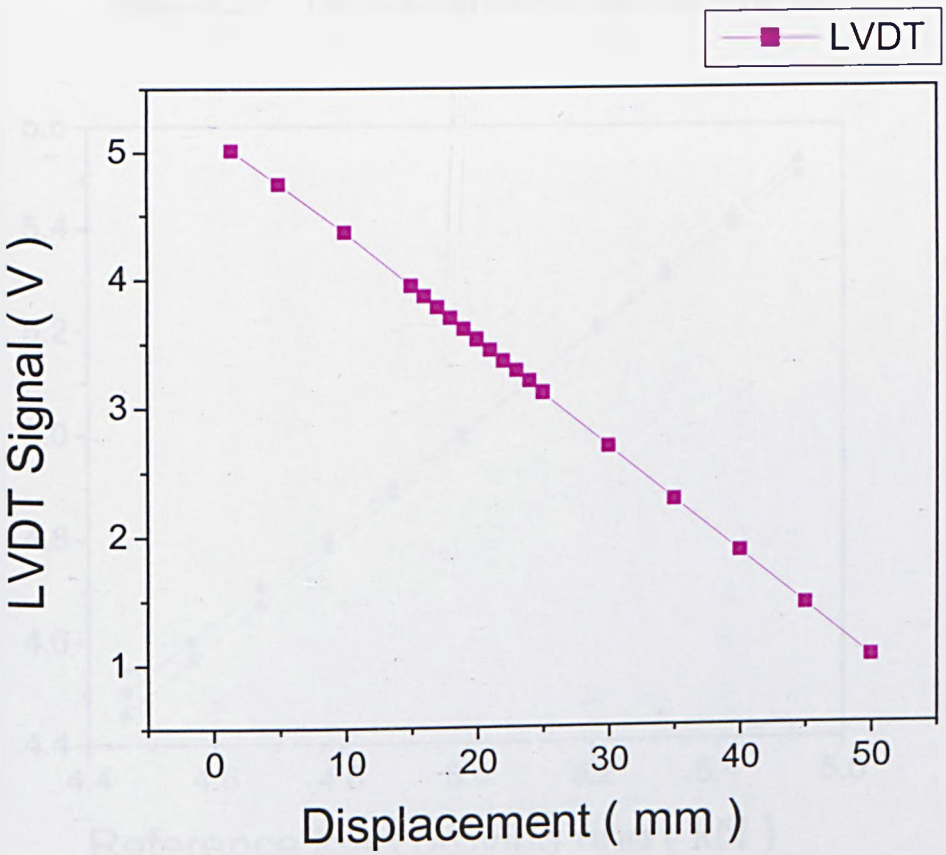

Figure 4.2-6: Calibration curve of the LVDTs of the rigs for creep-rupture testing in controlled atmosphere.

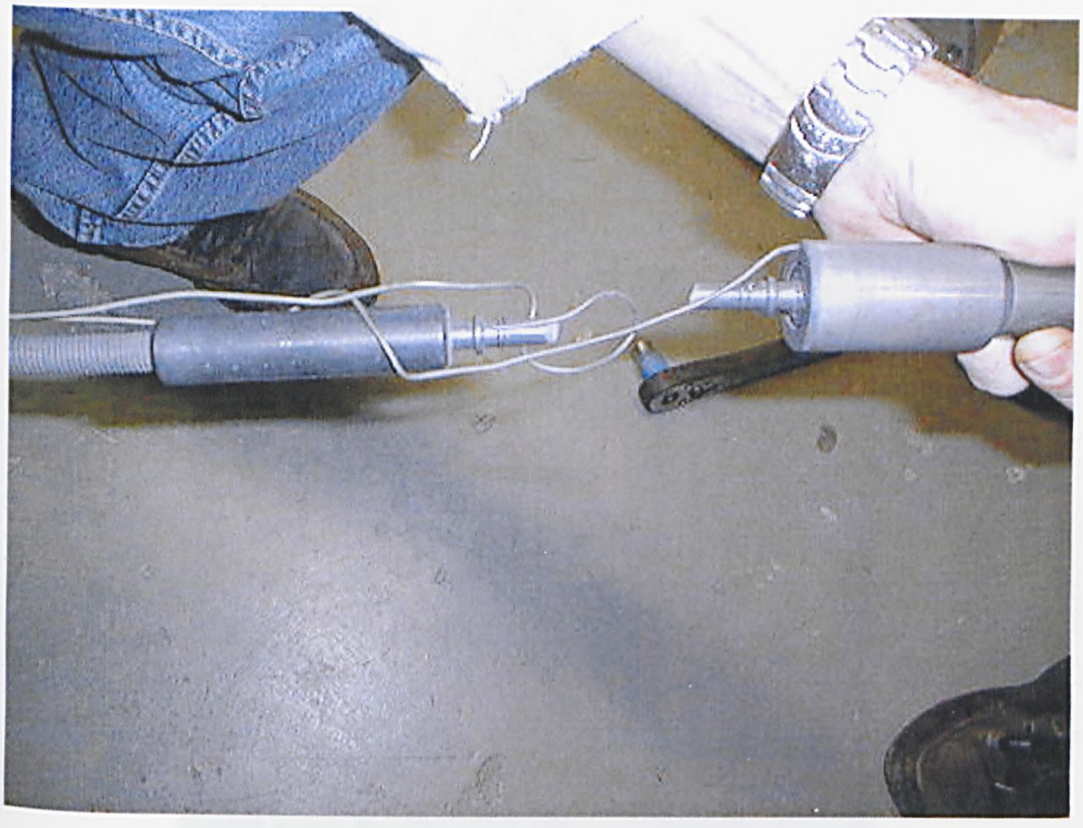

Figure 4.2-7: The load-train with a specimen, after test.

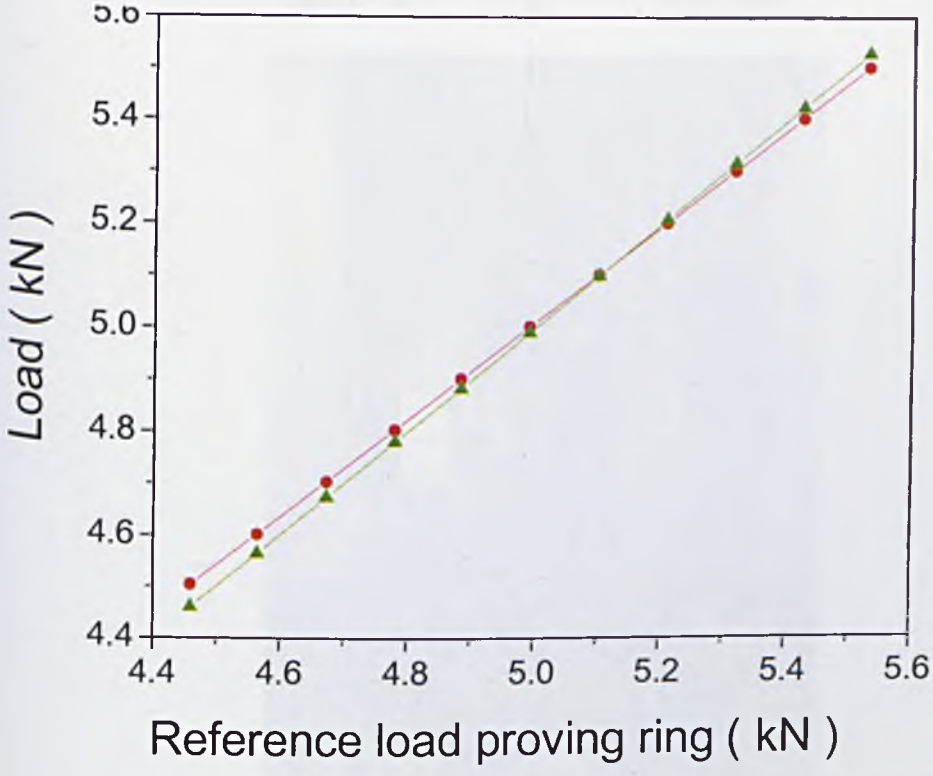

Figure 4.2-8: Calibration curve for the load of the uniaxial creep-rupture rigs in controlled atmosphere.

Figure 4.2-9: The gas distribution rack.

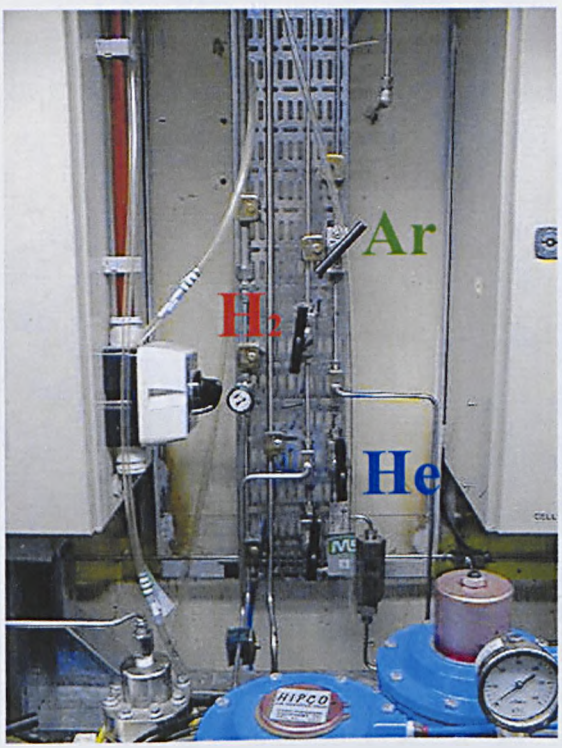

Figure 4.2-10: Manifolds for the flow of gas (H_2 or Ar or He) in the supply system.

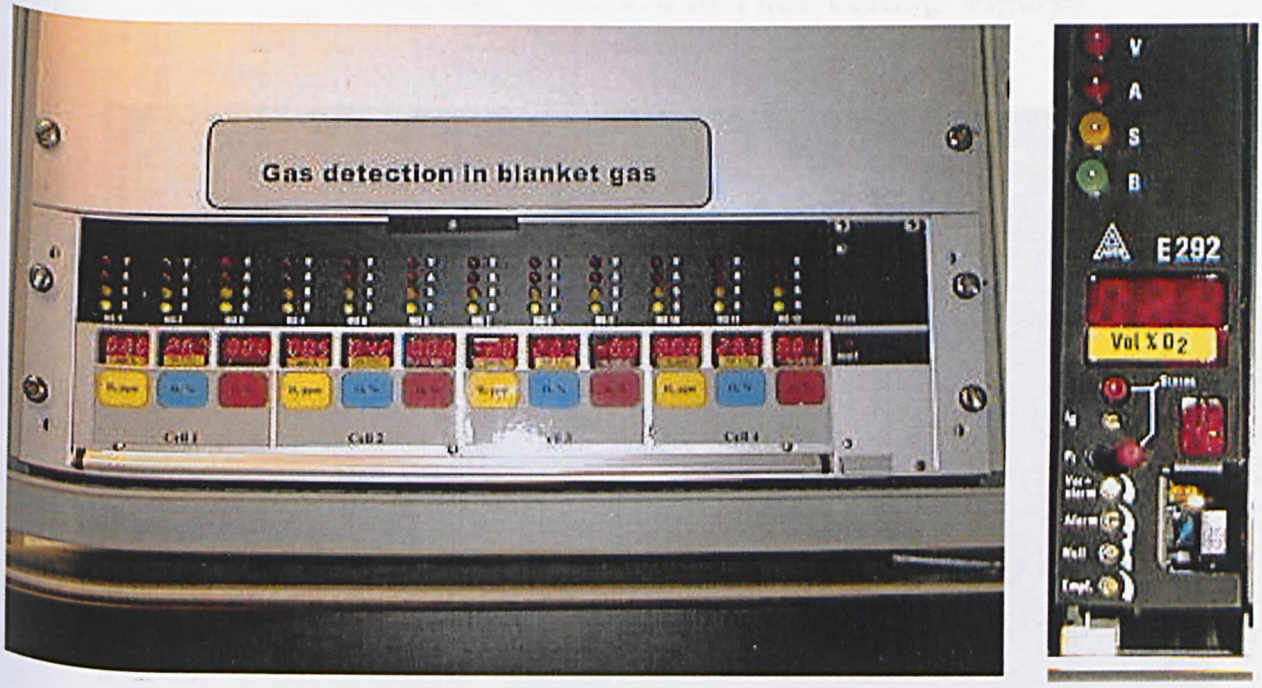

Figure 4.2-11: Safety alarm system. It is used for setting the threshold for the oxygen in the blanket system.

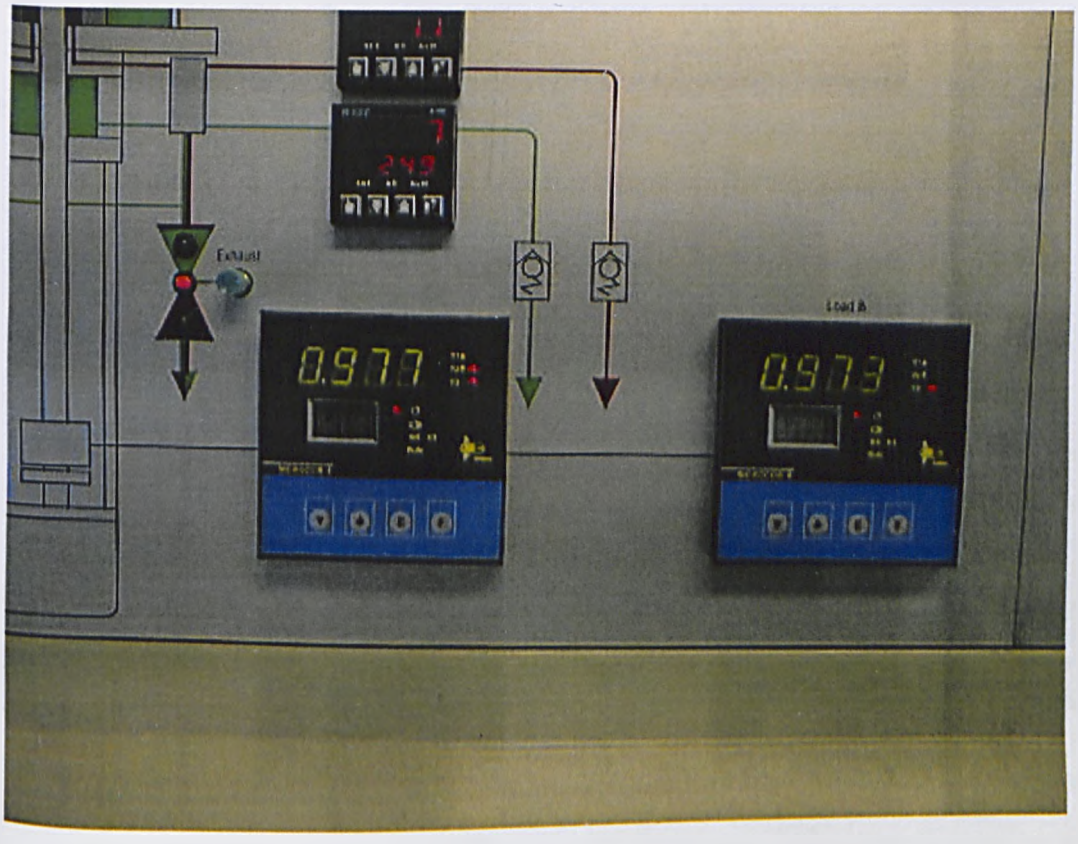

Figure 4.2-12: Controllers for the application of the load to the uniaxial creep specimens.

4.3 Internally Pressurized Tube Testing- Figures

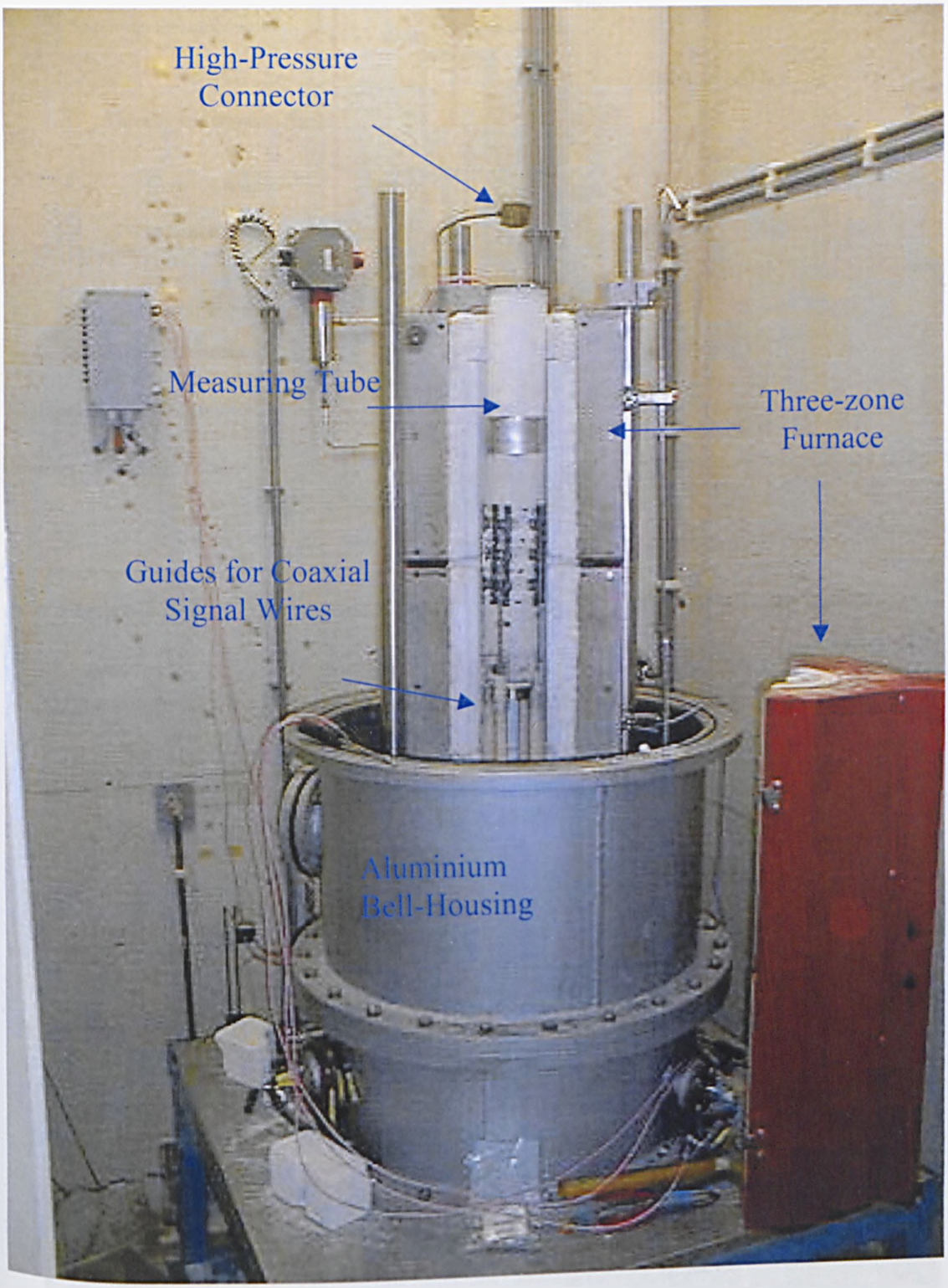

Figure 4.3-1: The rig for creep-rupture testing of tubular pressurized specimens.

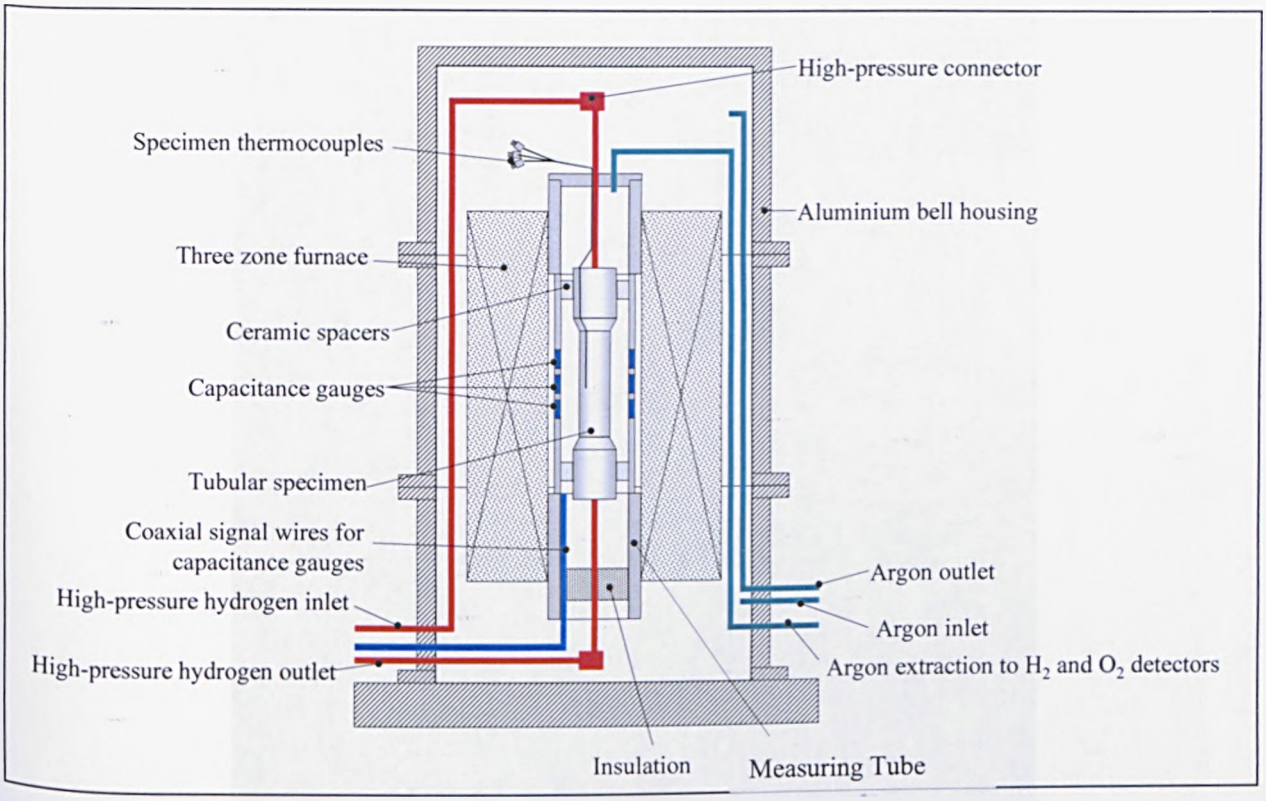

Figure 4.3-2: Cross-section scheme of the rig for testing of tubular specimens.

Figure 4.3-3: Gas distribution rack for the rig for tubular specimens.

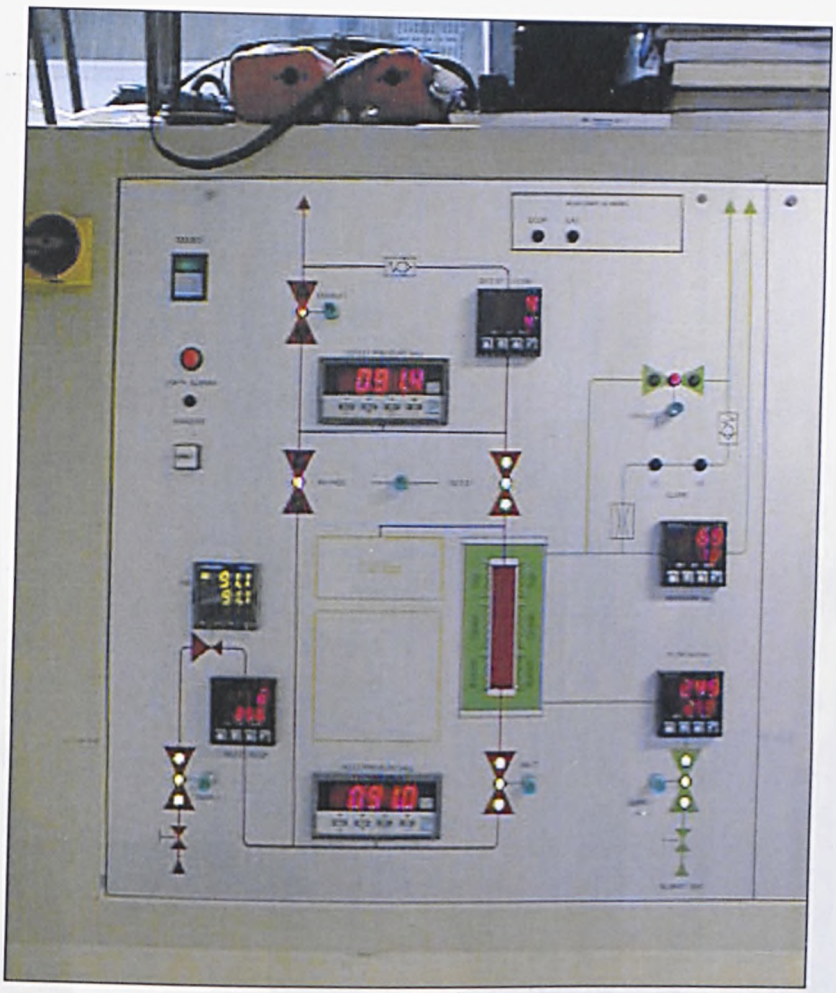

Figure 4.3-4: The control panel of the rig for tubular specimens.

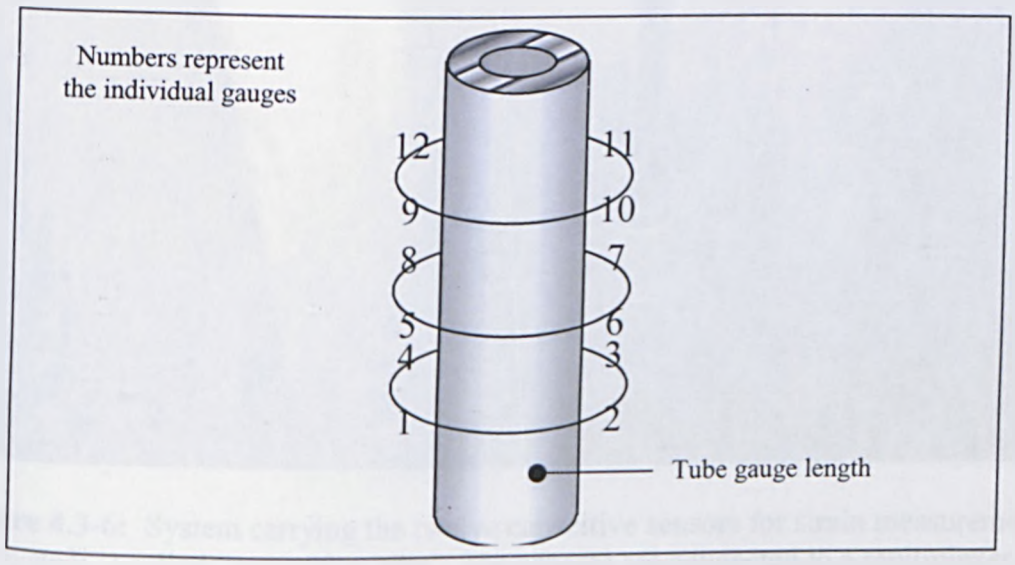

Figure 4.3-5: Scheme of the distribution of sensors around the tube gauge length. Twelve sensors are positioned, divided in groups of four sensors. Four sensors are located at the top, four in the middle and four at the bottom of the gauge length.

Figure 4.3-6: System carrying the twelve capacitive sensors for strain measurement. The system is called "measuring tube". The sensors are connected to a multiplexer via coaxial cables.

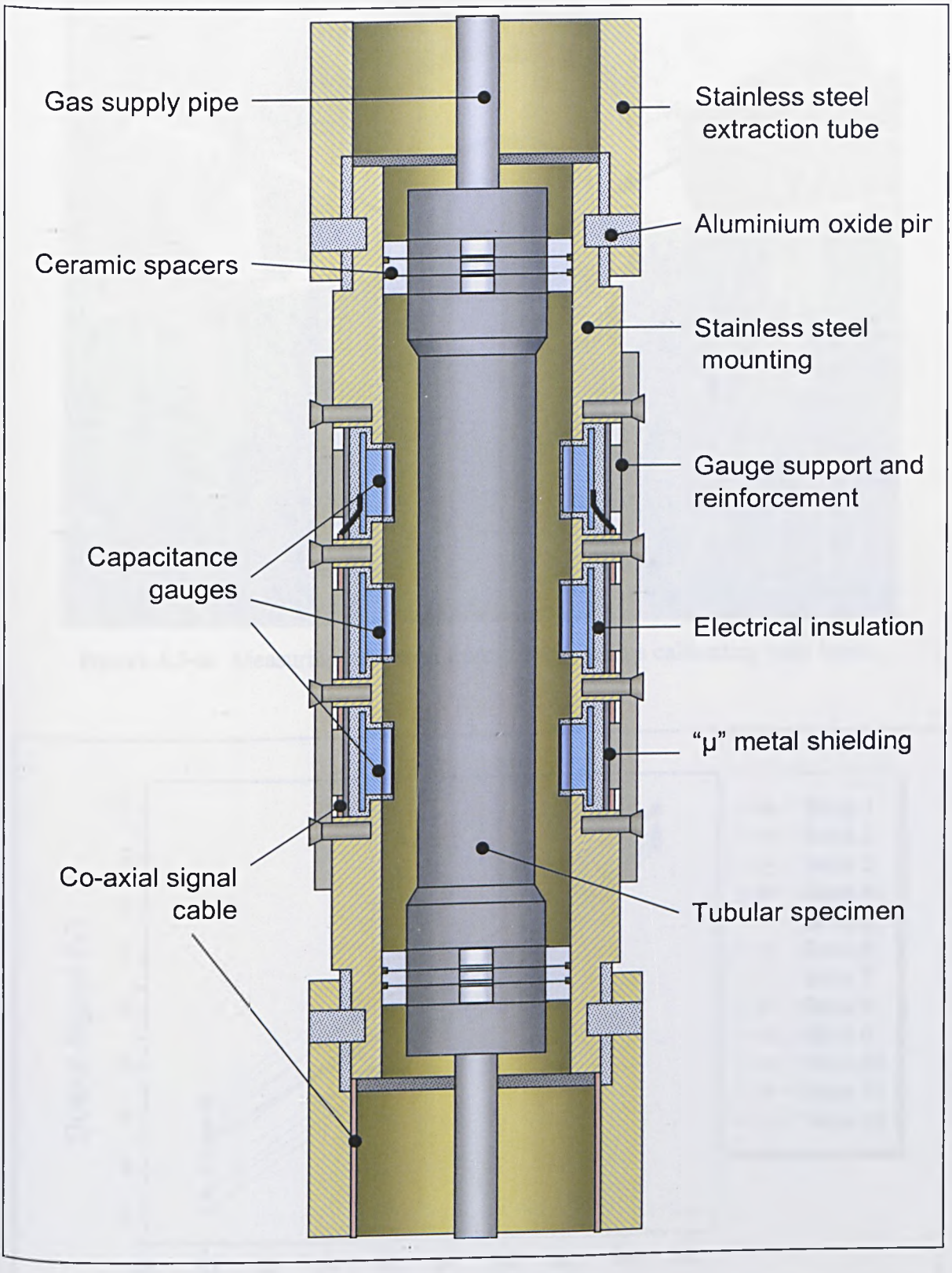

Figure 4.3-7: Detailed cross-section of the measuring tube

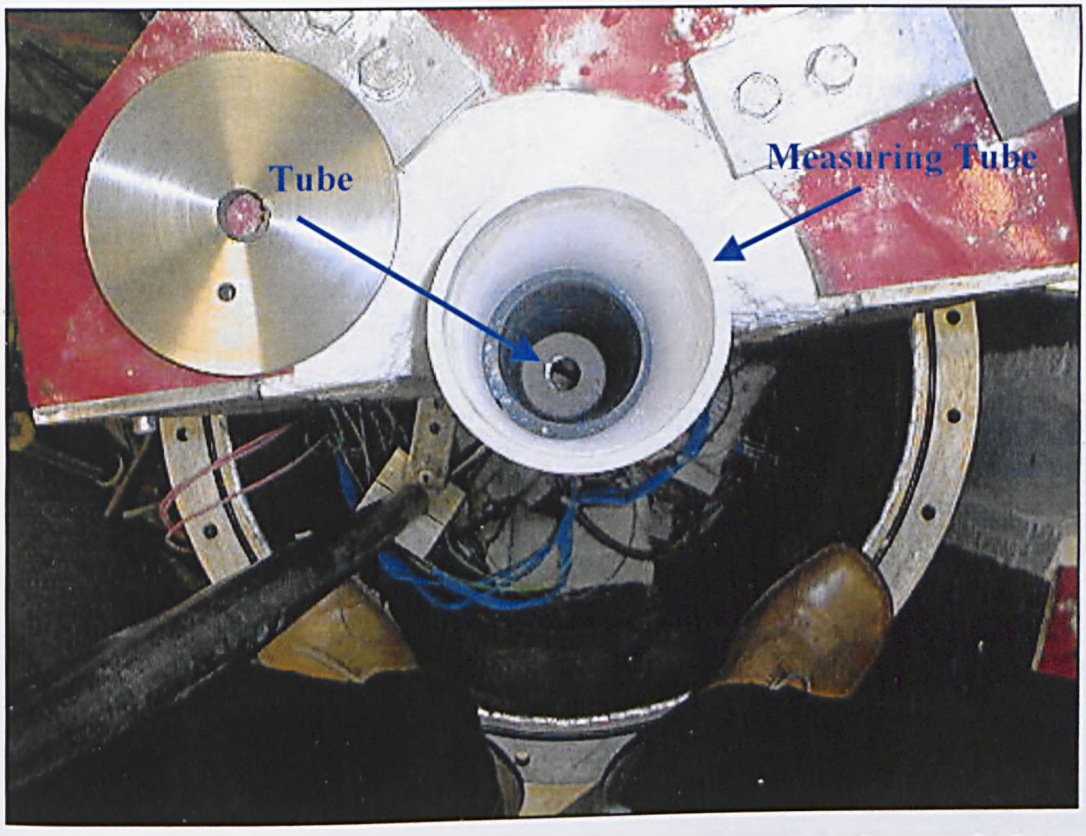

Figure 4.3-8: Measuring tube seen from the top, with a calibrating tube inside.

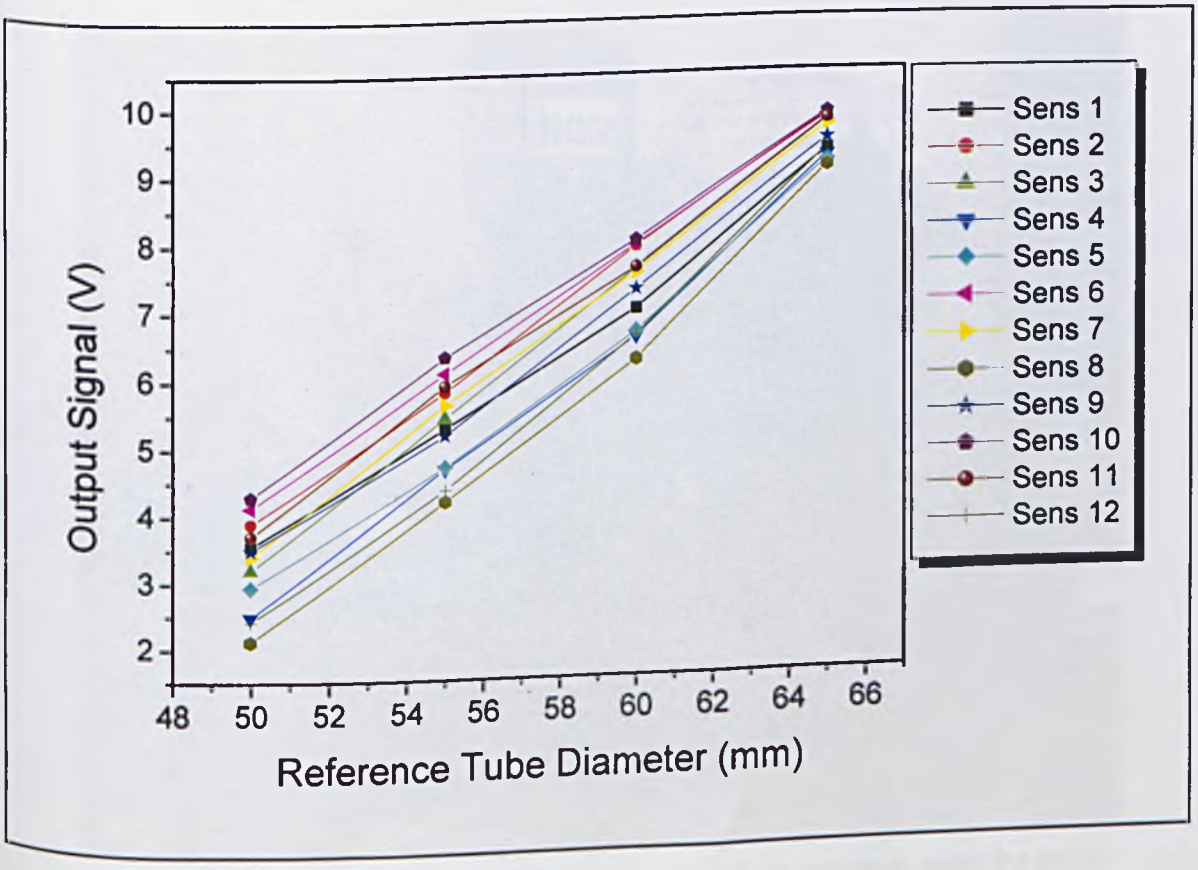

Figure 4.3-9: Calibration of the measuring tube for strain measurement.

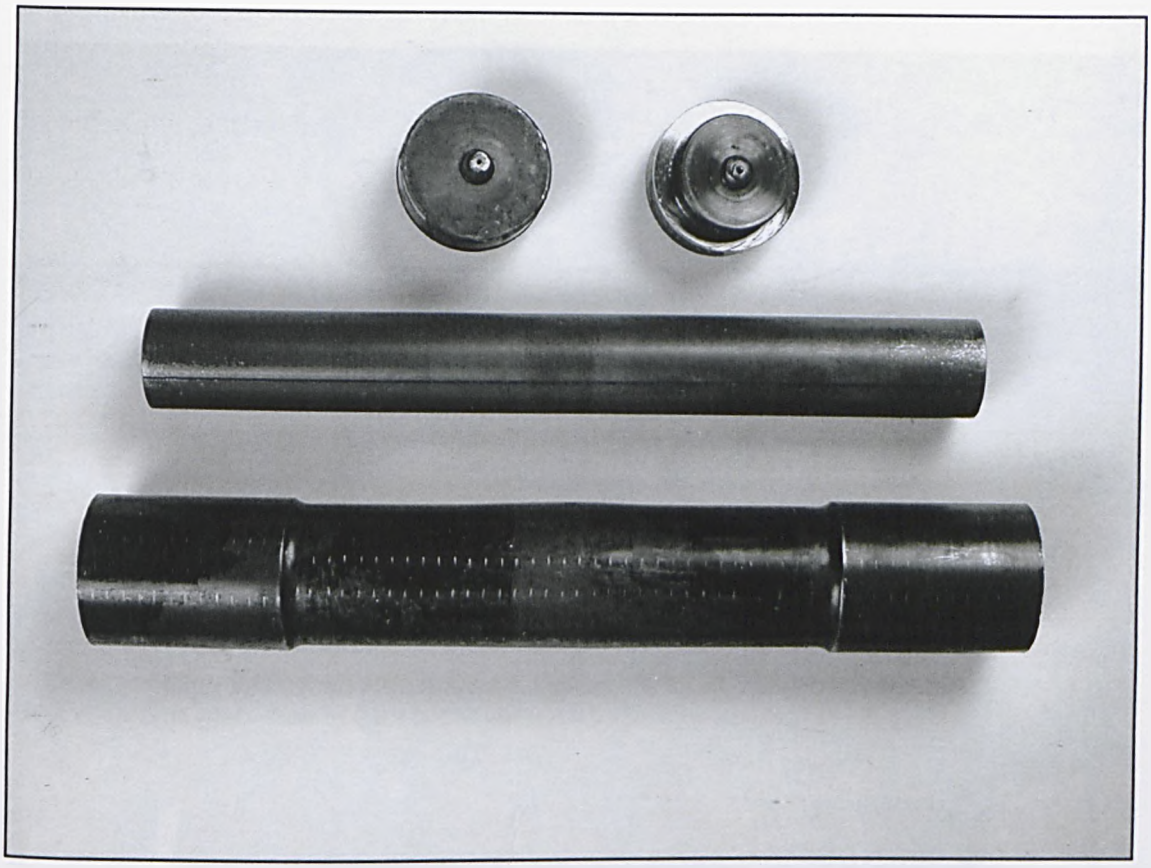

Figure 4.3-10: Cross-welded tubular specimen, made of 2.25Cr-1Mo steel, with filler bar and end caps, after test.

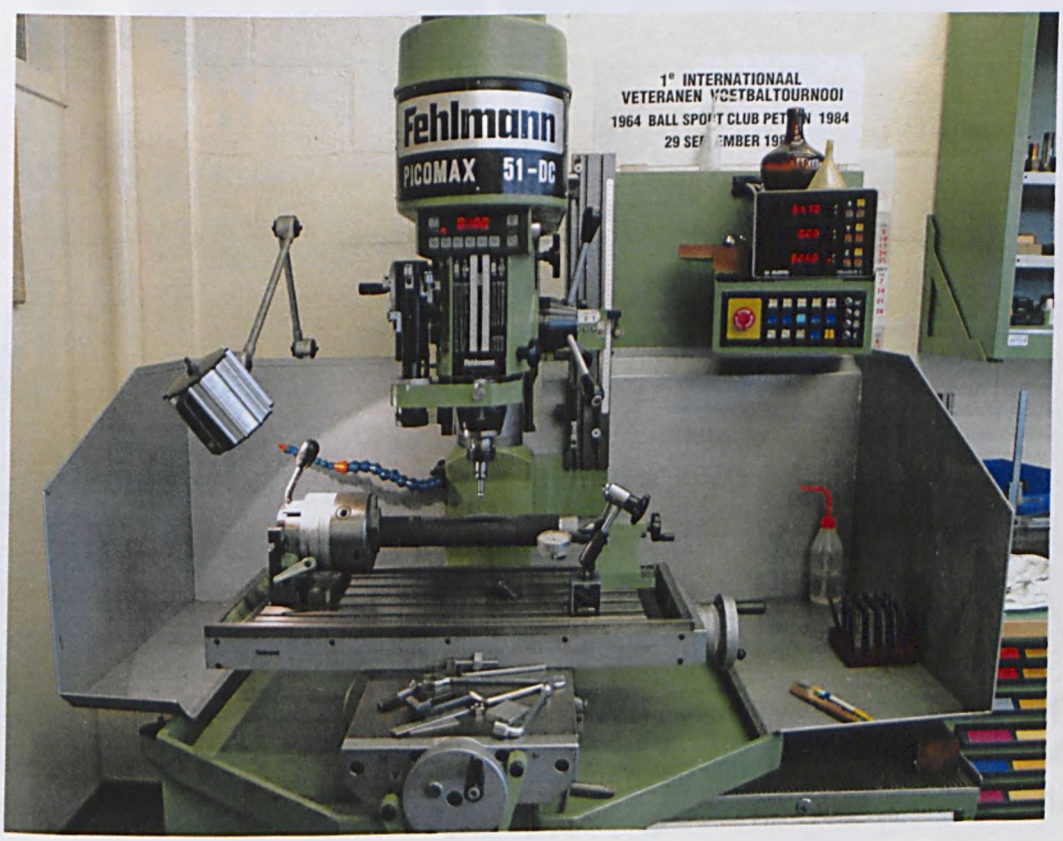

Figure 4.3-11: Machine tool with four-jaw chuck on one side, used for strain measurement on the tubular specimen.

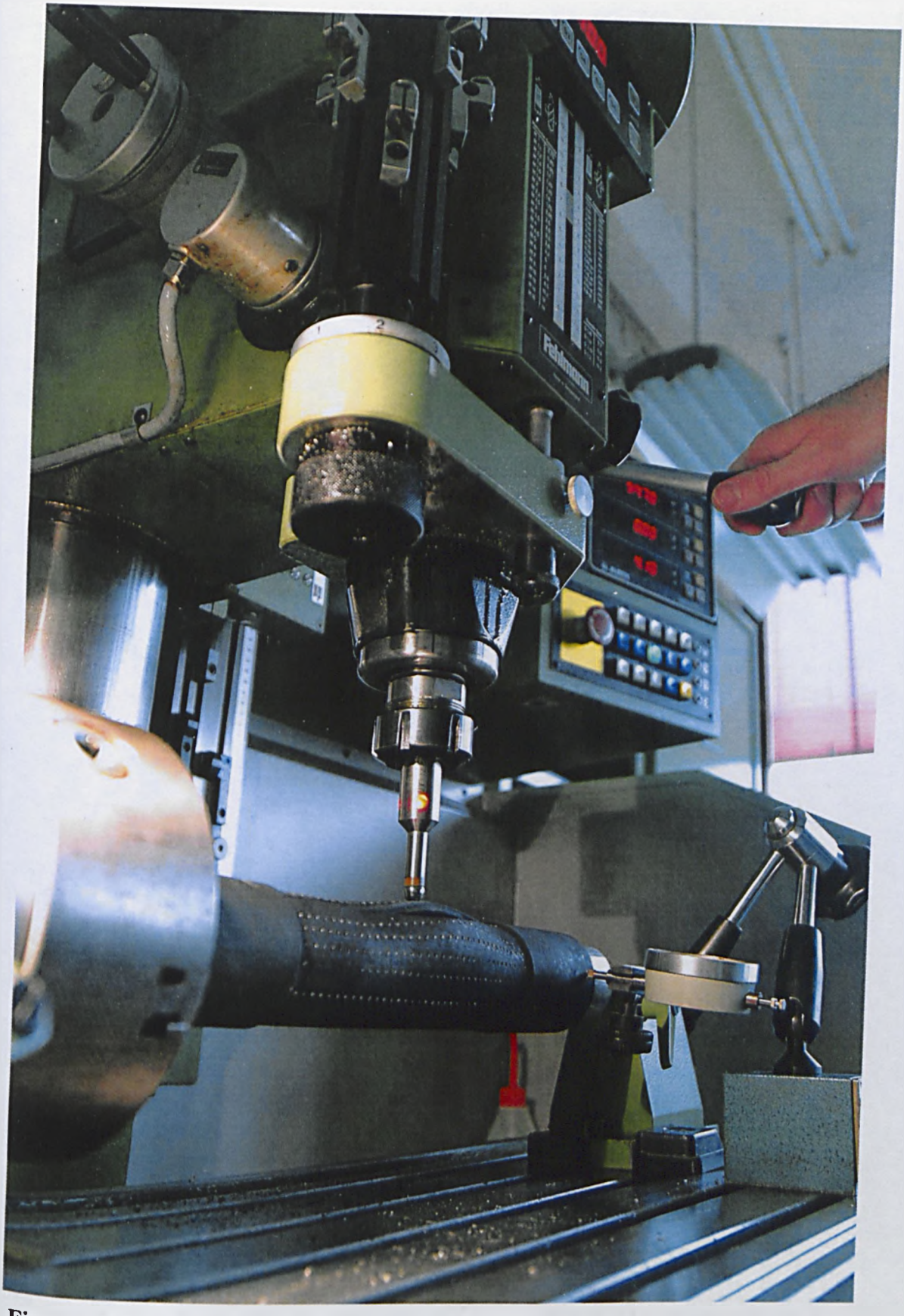

Figure 4.3-12: The machine is equipped with a sensor that lights when it touches the surface of the tube.

Figure 4.3-13: Performing strain measurements on the tubular specimens, following the original procedure set-up in the current work.

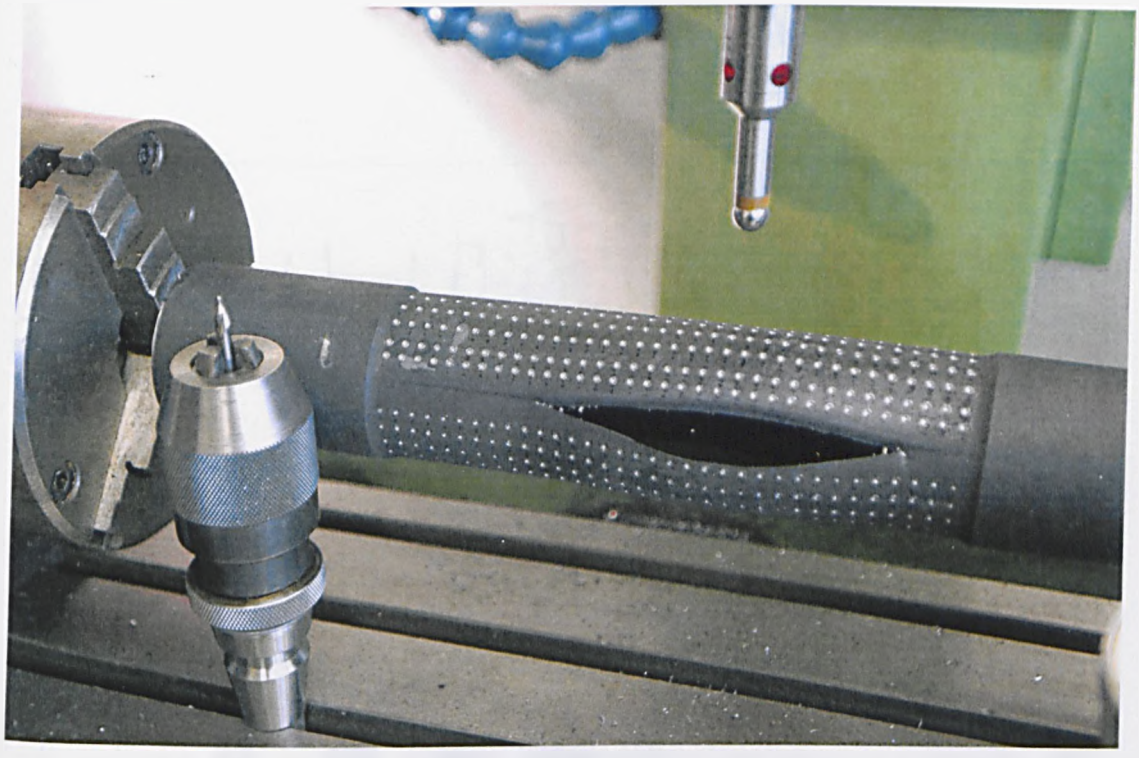

Figure 4.3-14: The measurements are more dense where the strain is higher (close to the fracture)

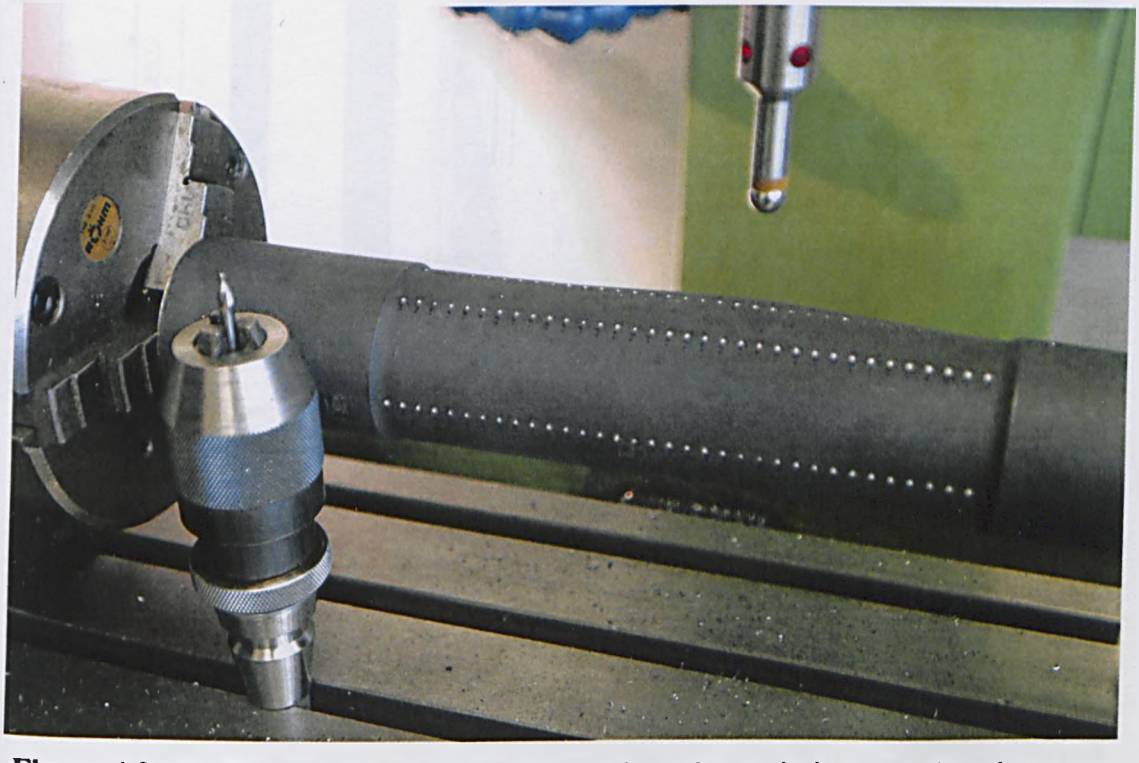

Figure 4.3-15: The measurements are fewer where the strain is lower (location more distant from the fracture).

4.4 Internally Pressurized Tube Testing - Figures

4.4 Internally Pressurized Tube Testing - Tables

2.25Cr-1Mo steel and consumable												
		C	Si	Mn	P	S	Cr	Mo	Ni	Al	Cu	Sn
BM	Nom.	0.14	0.18	0.59	0.004	0.003	2.25	1.05	0.14	0.01	0.07	0.006
	EPMA	-	0.18	0.62	-	-	2.09		0.13	-	0.08	-
Cons.	Nom.	0.10	.11	0.75	.009	0.002	2.37	1.01	0.11	-	-	0.002
	EPMA	-	0.11	0.77	-	-	2.03	1.09	0.14	-	0.09	-

Table 4.4-1: Nominal composition of the test 2.25Cr-1Mo steel and consumable compared with EPMA.

2.25Cr-1Mo and V-modified 2.25Cr-1Mo													
Material		C	Si	Mn	P	S	Cr	Mo	Ni	Al	Cu	Sn	V
1	BM	0.14	0.18	0.59	0.004	0.003	2.25	1.05	0.14	0.01	0.07	0.006	-
	WM	0.10	0.11	0.75	0.009	0.002	2.37	1.01	0.11	-	-	0.002	-
2	BM	0.12	0.26	0.43	0.004	0.002	2.36	1.02	0.73	0.02	0.062	0.005	0.28
	WM	0.11	0.10	0.63	0.007	0.003	2.60	1.05	0.07	-	0.032	0.005	0.29

Table 4.4-2: Nominal composition of the test 2.25Cr-1Mo (steel 1) and V-modified 2.25Cr-1Mo (steel 2) steels and consumables.

4.5 The Specimen preparation - Figures

Figure 4.5-1: Drawing of the uniaxial sample.

Figure 4.5-2: The tube.

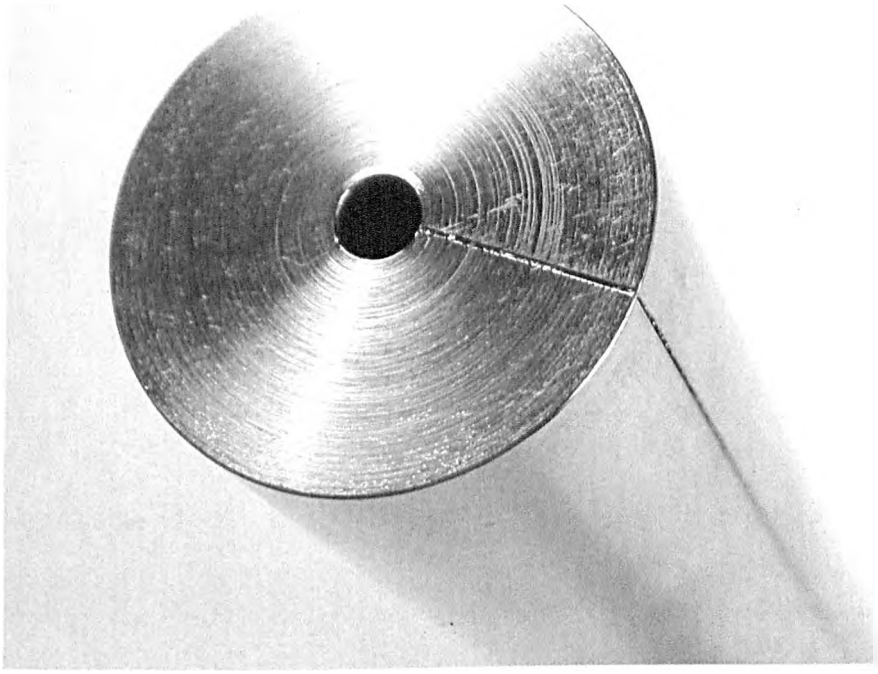

Figure 4.5-3: The filler bar, obtained via wire-erosion.

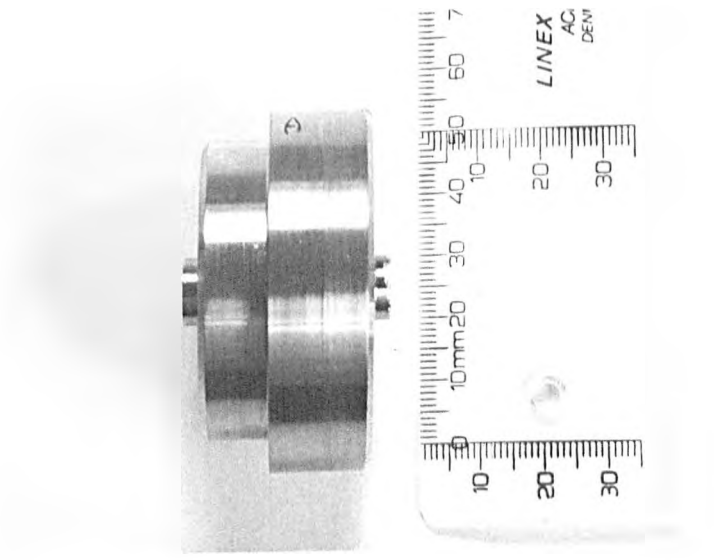

Figure 4.5-4: End cap total diameter.

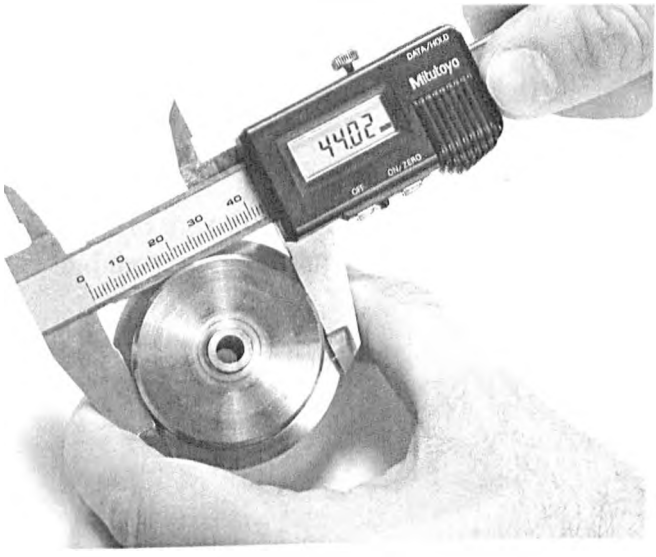

Figure 4.5-5: End cap internal diameter (of the part that entries in the tube)

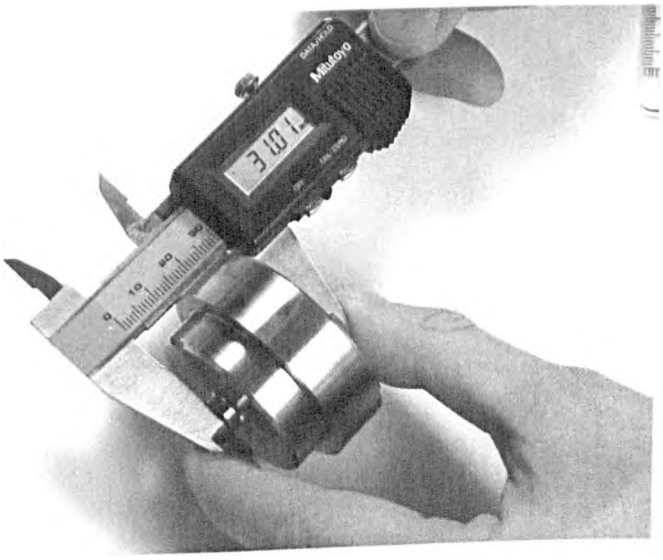

Figure 4.5-6: End cap thickness.

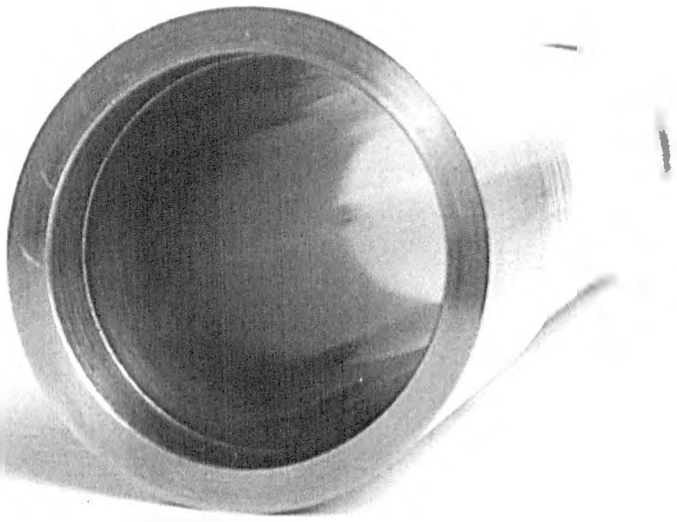

Figure 4.5-7: Groove close to the tube opening, conceived to permit the easy insert and the perfect fitting of the end caps.

Figure 4.5-8: Complete set: tube, filler bars and end caps.

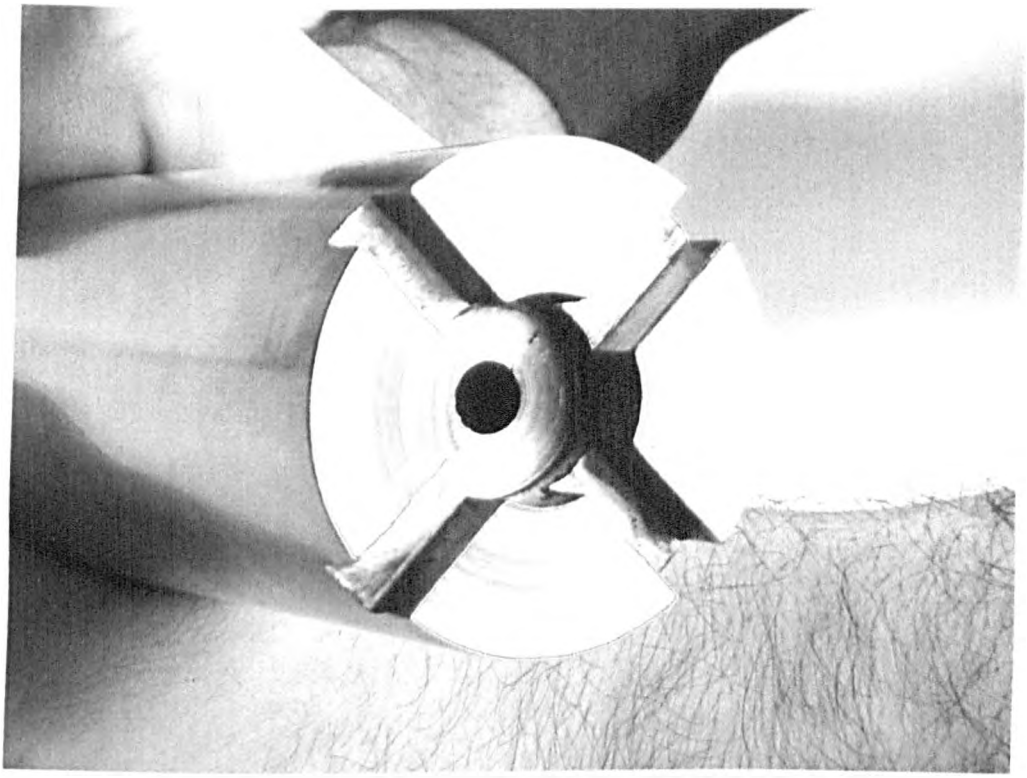

Figure 4.5-9: Special feature of the filler bar: the small chamber and the grooves for the flow of the pressurising gas.

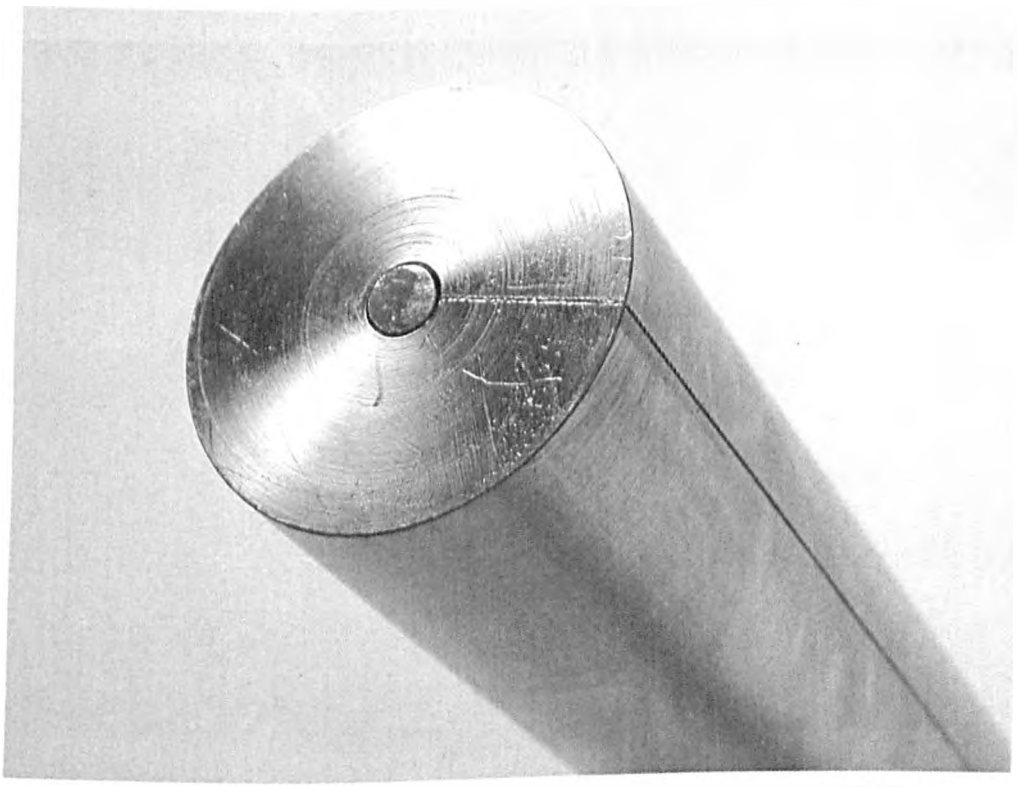

Figure 4.5-10: Closure of the filler bar. The purpose is that the pressurising gas does not enter in the filler bar via the cuts due to wire erosion, but flows along its external surface, In this way it is possible to study the effect of the radial penetration of hydrogen in the steel and eventual gradient of damage.

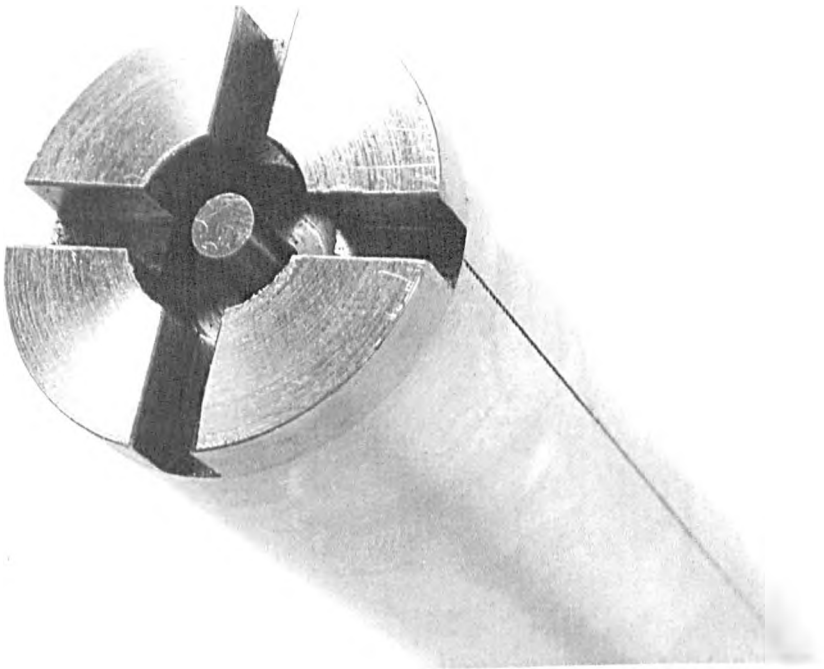

Figure 4.5-11: Closure of the hole due to wire erosion, with a manufactured pin.

Figure 4.5-12: Hole in the end cap for the gas flow. The hole introduces the gas in the filler bar chamber. The gas is transferred via a supply pipe.

Figure 4.5-13: From the filler bar chamber the gas flows externally, via the machined grooves.

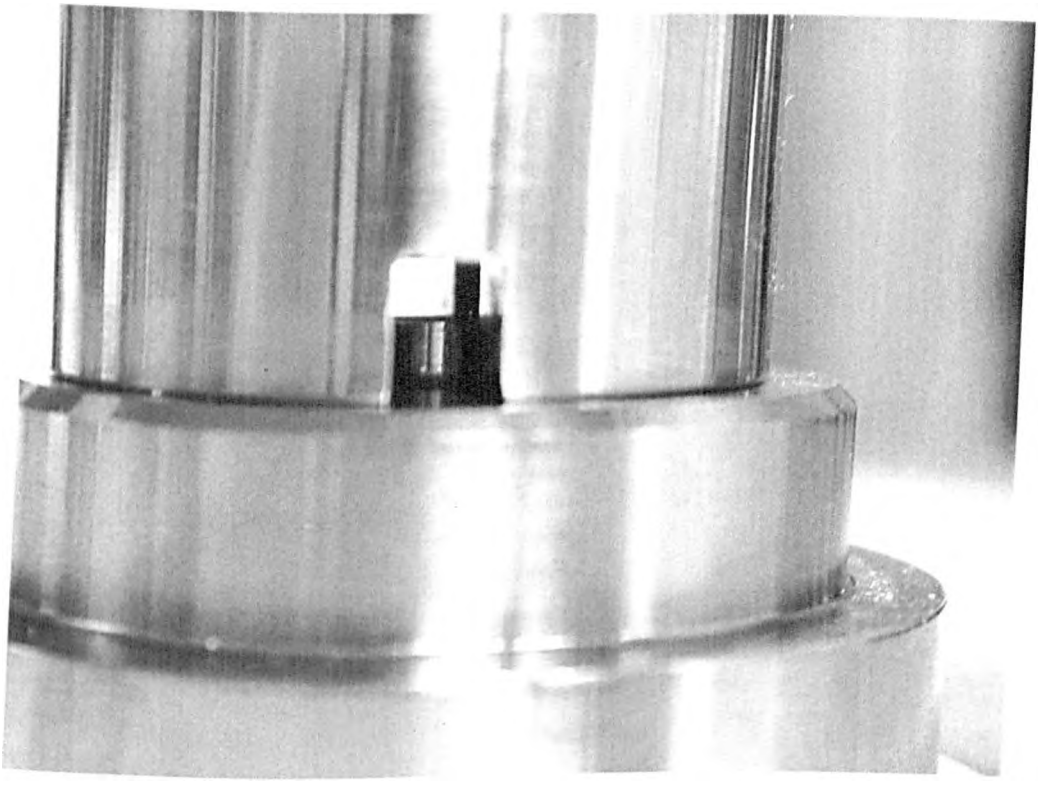

Figure 4.5-14: Detail of the design feature.

Figure 4.5-15: Starting of the assembly of the tubular specimen

Figure 4.5-16: Mounting of the tubular specimen.

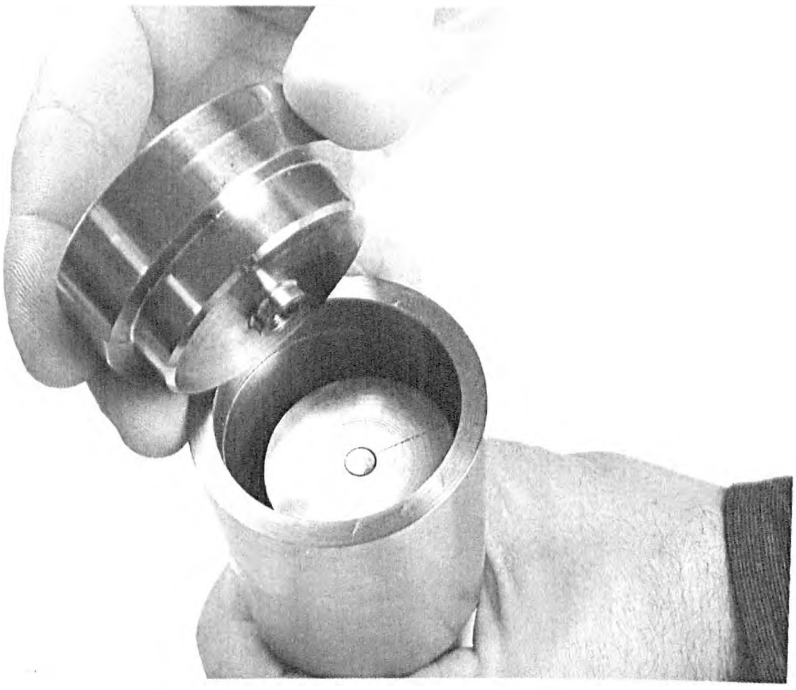

Figure 4.5-17: Closure of the tubular specimen. The filler bar occupies the most of the internal volume of the tube.

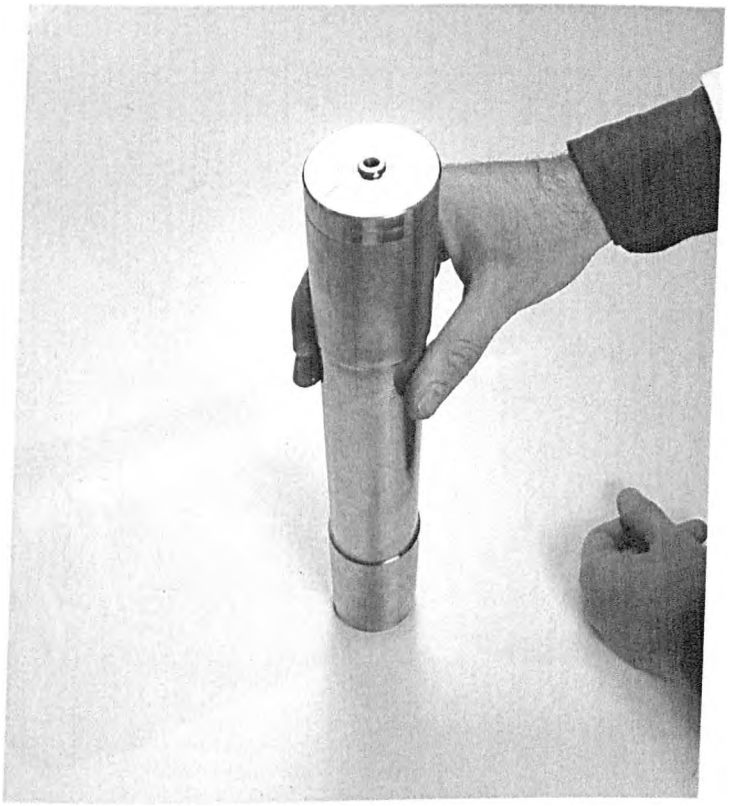

Figure 4.5-18: The tubular specimen assembled.

Figure 4.5-19: The tubular specimens for pressurizing tests with argon and hydrogen

Figure 4.5-20: Mounting of the gas supply pipe and closure of the tubular specimen by means of multi-pass weldment.

4.5 The Specimens Preparation - Tables

Dimensional Feature	Recommended ratios/relations
Gauge length	$l \geq \sqrt{100 D_m t_1}$
Thickness ratio	$t_2/t_1 = 1.2$
Transition radius	$r = 2t_1$
End-cap length/diameter ratio	$L/D_0 = 2$

2.25Cr-1Mo Tube		
Dimensional ratios	**Recommended**	**Actual tube dimensions**
$l \geq \sqrt{100 D_m t_1}$	$l \geq 130$	$l = 170$
t_2/t_1	1.2	1.5
$r = 2t_1$	$r = 8.8$	$r = 7.7$
L/D_0	2	1.58

2.25Cr-1Mo-V Tube		
Dimensional ratios	**Recommended**	**Actual tube dimensions**
$l \geq \sqrt{100 D_m t_1}$	$l \geq 130$	$l = 167$
t_2/t_1	1.2	1.5
$r = 2t_1$	$r = 8.8$	$r = 7$
L/D_0	2	1.58

Table 4.5-1: Adopted and recommended design ratios for the tubular specimens respectively made of 2.25Cr-1Mo steel and its V-modified grade.

Materials	Reference tests (air and argon)						
	Test type						
		Stress- free (air)		Uniaxial load (air)		Multiaxial load (Ar)	
	Batch	Exposure Temperat.	Exposure Time (h)	Test Temperat.	Stress (MPa)	Weld type	MDHS (MPa)
Welded 2.25Cr-1Mo		843K (570°C)	1000	843K (570°C)	100		
			2000				
			4000	873K (600°C)	100		
Welded 2.25Cr-1Mo-V	(1st batch)	873K (600°C)	500	873K (600°C)	120		
			1000		140		
			2000				
			4000		170		
	(2nd batch)	873K (600°C)	447	873K (600°C)	100	Single Arc Longitudinal Weldment	120
			1526		120		
			3035		140		
3Cr-1Mo–V (without Nb)				873K (600°C)	100		
					120		
					140		
					170		

Table 4.6-1: Table of the tests performed in air or argon.

Materials	Batch	Tests in H_2						
		Test type						
		Stress-free		Uniaxial load		Multiaxial load		
		Exposure Conditions	Exposure Time (h)	Test Conditions	Stress (MPa)	Test Conditions	Weld type	MDHS (MPa)
Welded 2.25Cr-1Mo		843K (570°C) P=18MPa	1000	873K (600°C) P=18MPa	100	843K (570°C) P=18MPa	Single Arc Circumf. Weldment	100
			2000					
			3230					
			4000					
Welded 2.25Cr-1Mo-V	(1st batch)	T=600 °C P=18MPa	500	873K (600°C) P=22MPa	120			
			1000					
			2000	873K (600°C) P=18MPa	140			
	(2nd batch)	T=600 °C P=18MPa	382	873K (600°C) P=18MPa	100	873K (600°C) P=18MPa	Single Arc Longitudinal Weldment	120
			1431					
			2987		120			
					140			
3Cr-1Mo–V (without Nb)				873K (600°C) P=18MPa	100			
					140			

Table 4.6-2: Matrix of the tests performed in hydrogen.

5.2 Testing on the Stand. 2.25Cr-1Mo Steel - Figures

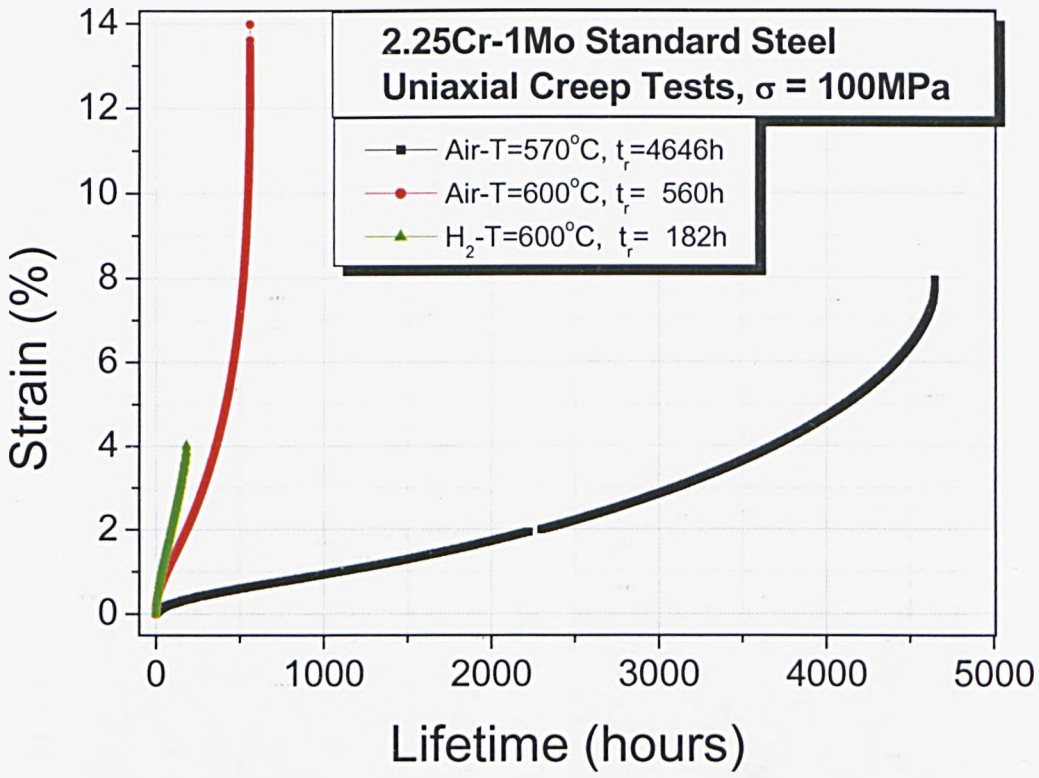

Figure 5.2-1: Uniaxial constant-load creep curves of cross-welded 2.25Cr-1Mo standard steel, tested both in air and in hydrogen (P_{H2}=18MPa).

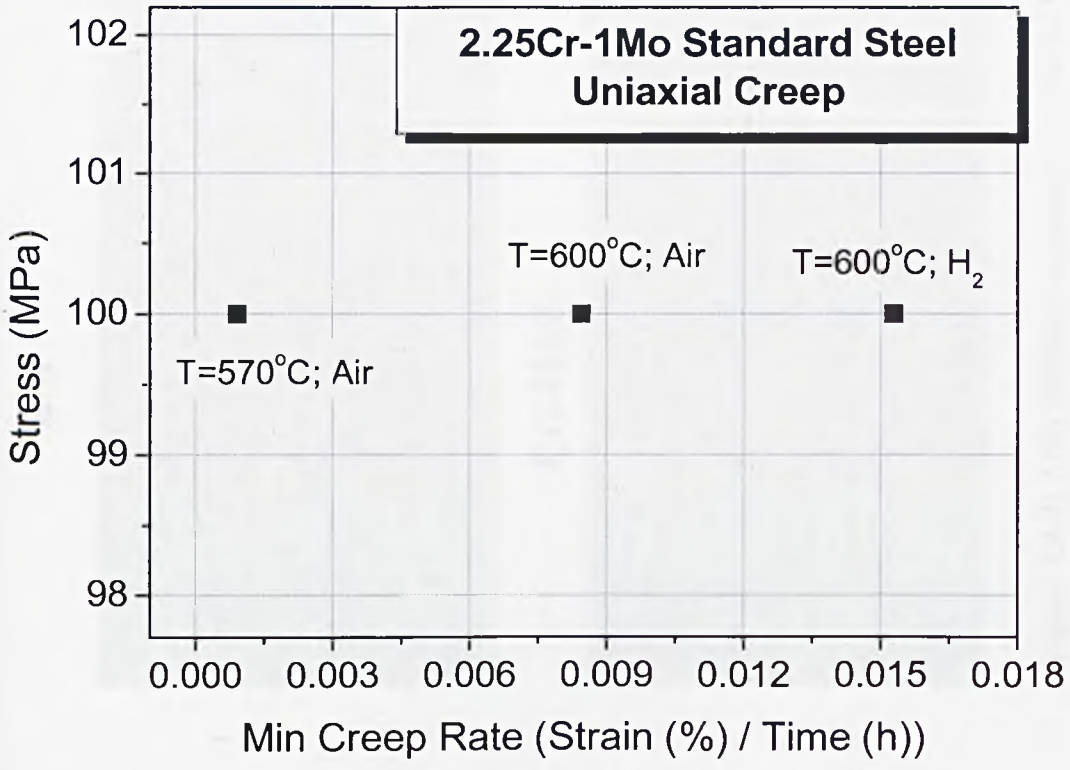

Figure 5.2-2: Plot of minimum creep rate vs stress for the cross-welded 2.25Cr-1Mo standard steel, under constant uniaxial load.

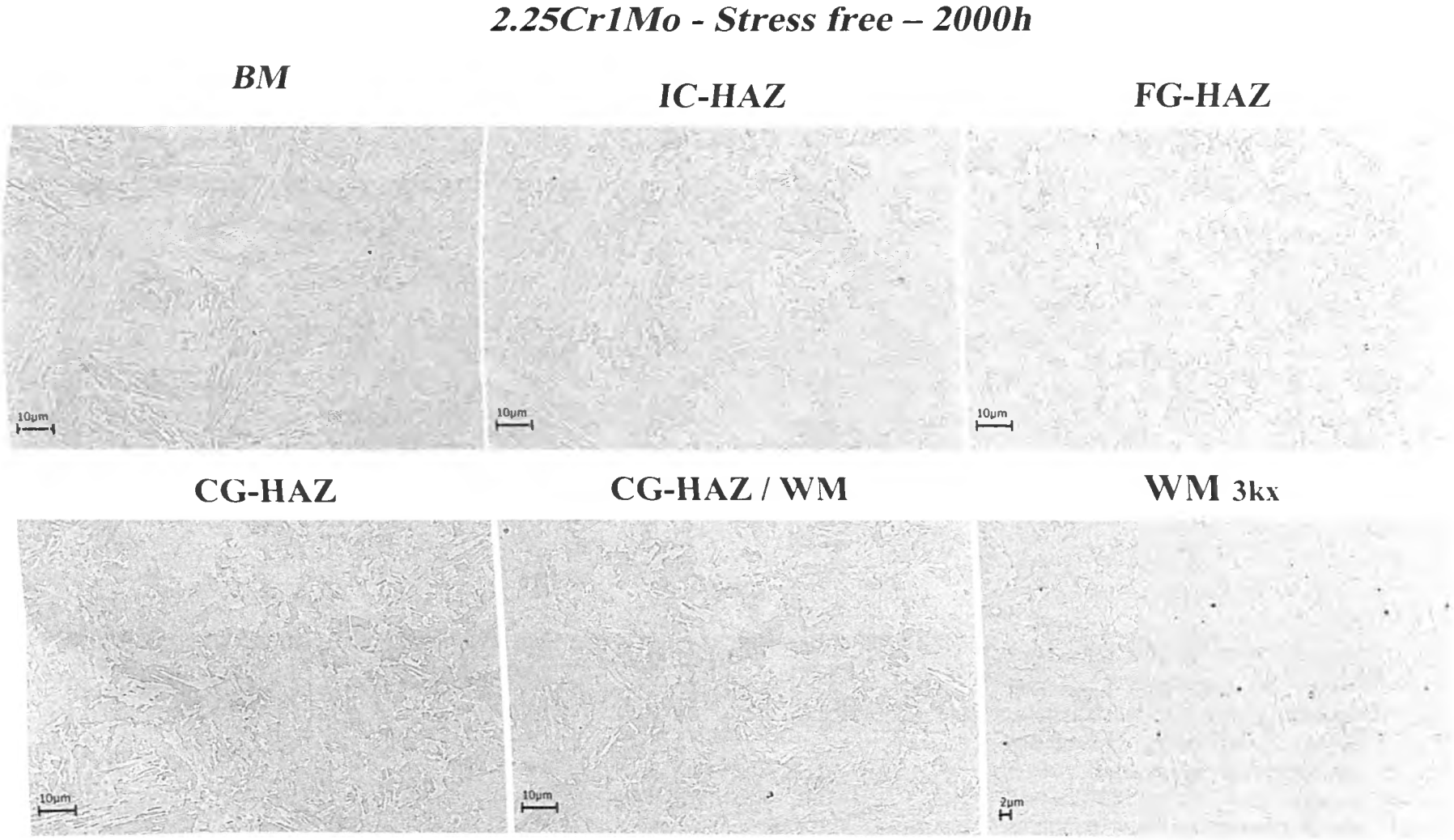

Figure 5.2-3: After 2000h of exposure, only the weld metal (WM) appears cavitated. The other regions, in particular CGHAZ and base metal (BM), can be considered practically not cavitated. The micrographs have been taken at a magnification of 2kx, with the only exception of the micrograph referred to the WM, which had been taken at 3kx.

2.25Cr1Mo - Stress free – 4000h

BM

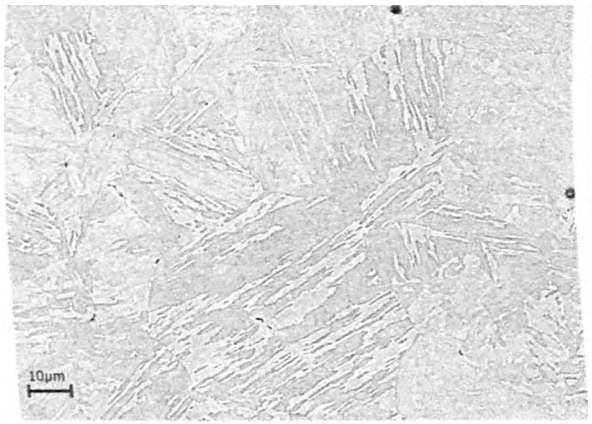

IC-HAZ

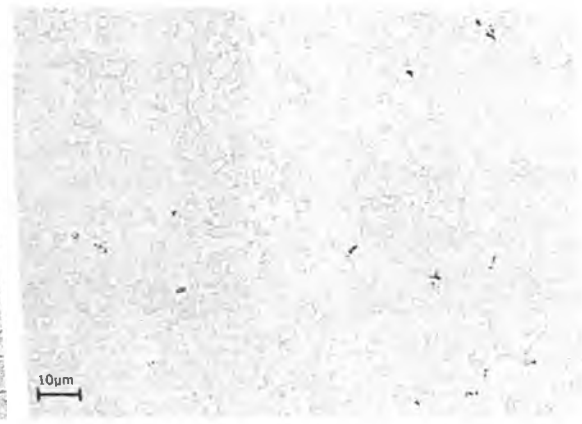

FG-HAZ

CG-HAZ

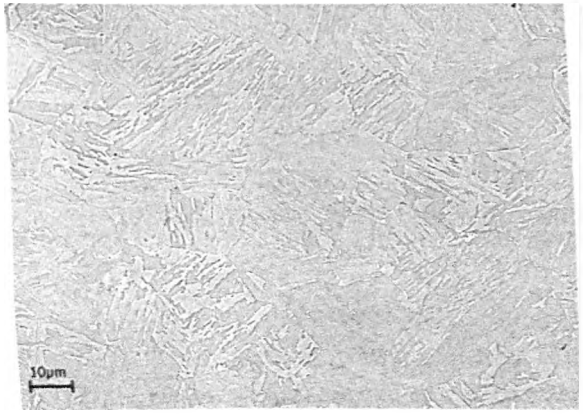

WM

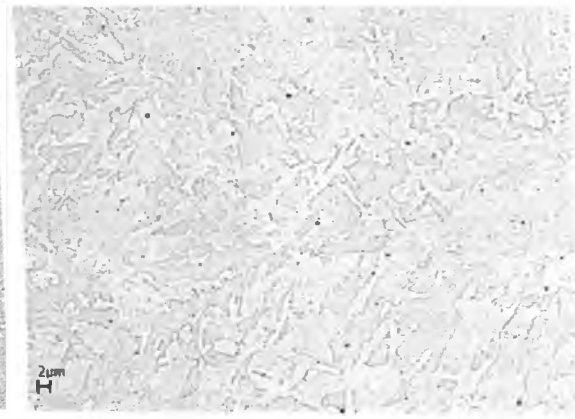

Figure 5.2-4: After 4000h of exposure, the FGHAZ presents marked cavitation, the WM is less cavitated and the BM present light cavitation mainly along the grain boundaries. The CGHAZ is still practically uncavitated. The micrographs have a magnification of 2kx, with the only exception of the micrograph referred to the weld metal (WM), which had been taken at 3kx.

2.25Cr1Mo - Stress free – 3230h (Filler Bar)

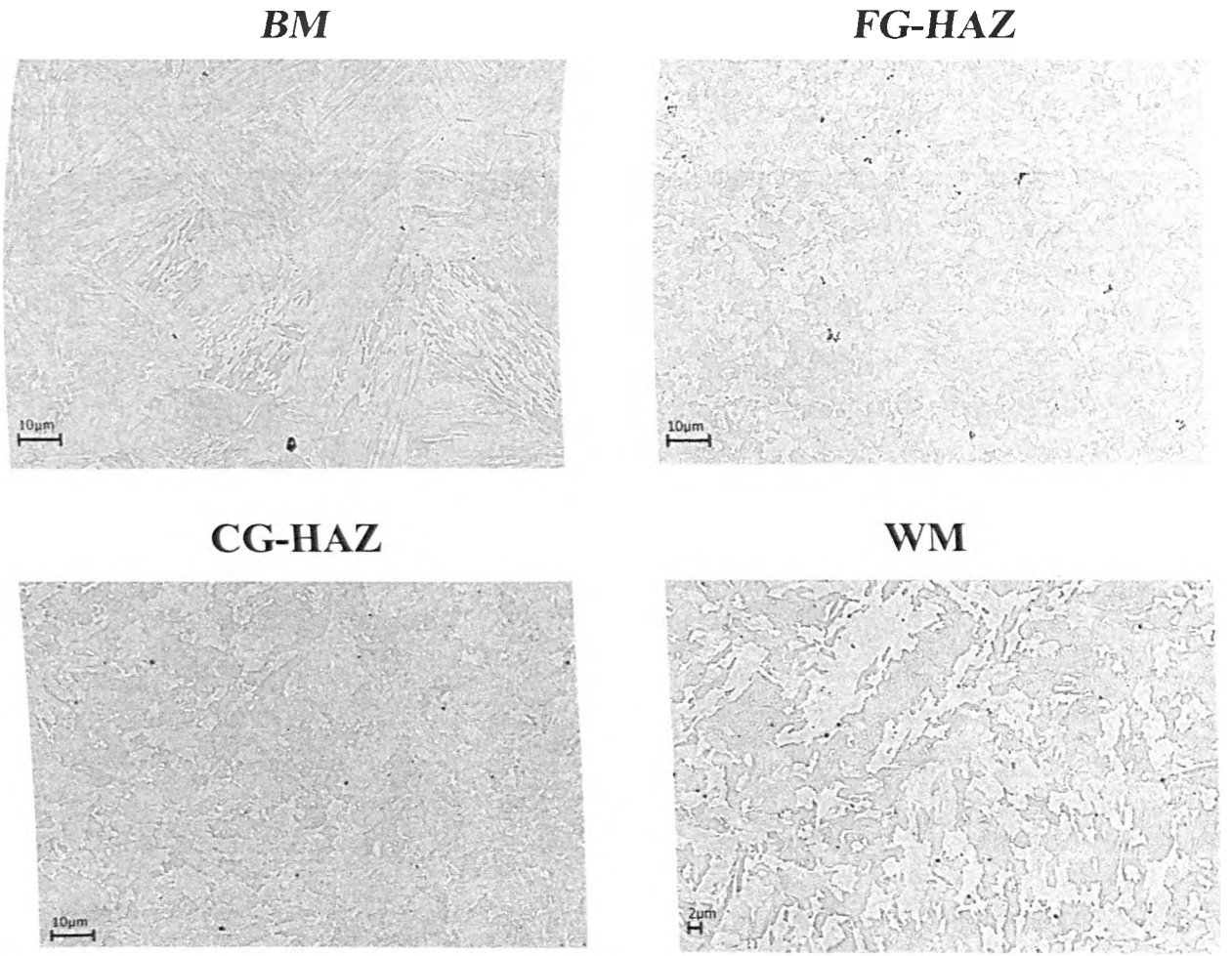

Figure 5.2-5: After 3230 hours of exposure, the FGHAZ, the CGHAZ and the weld metal (WM) of the filler bar of the pressurized tube, exhibit cavitation. Less damage is detected in the base metal (BM), where cavities are formed especially along grain boundaries. The micrographs had been taken at a magnification of 2kx, with the only exception of the micrograph representing the WM, which had been taken at 3kx.

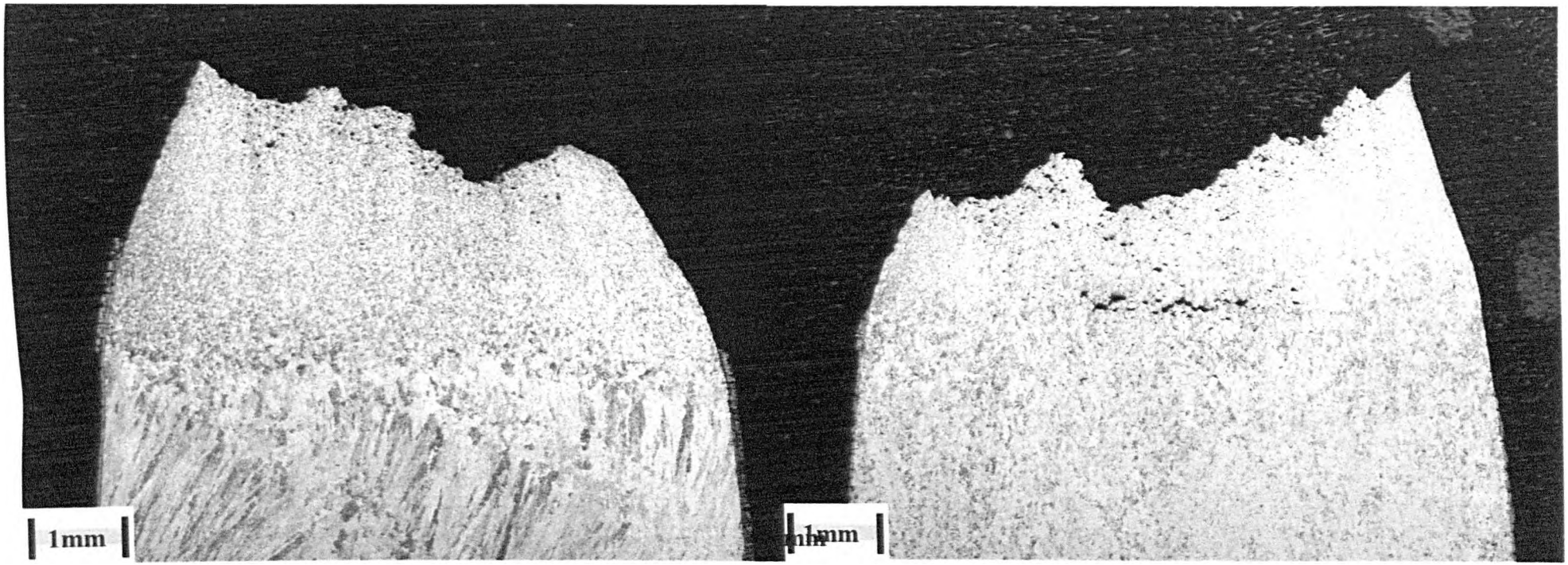

Figure 5.2-6a: Standard 2.25Cr-1Mo steel, welded joint tested in air at 843K (570°C) and in presence of an applied initial stress of 100MPa. Both halves. The test lasted 4646h.

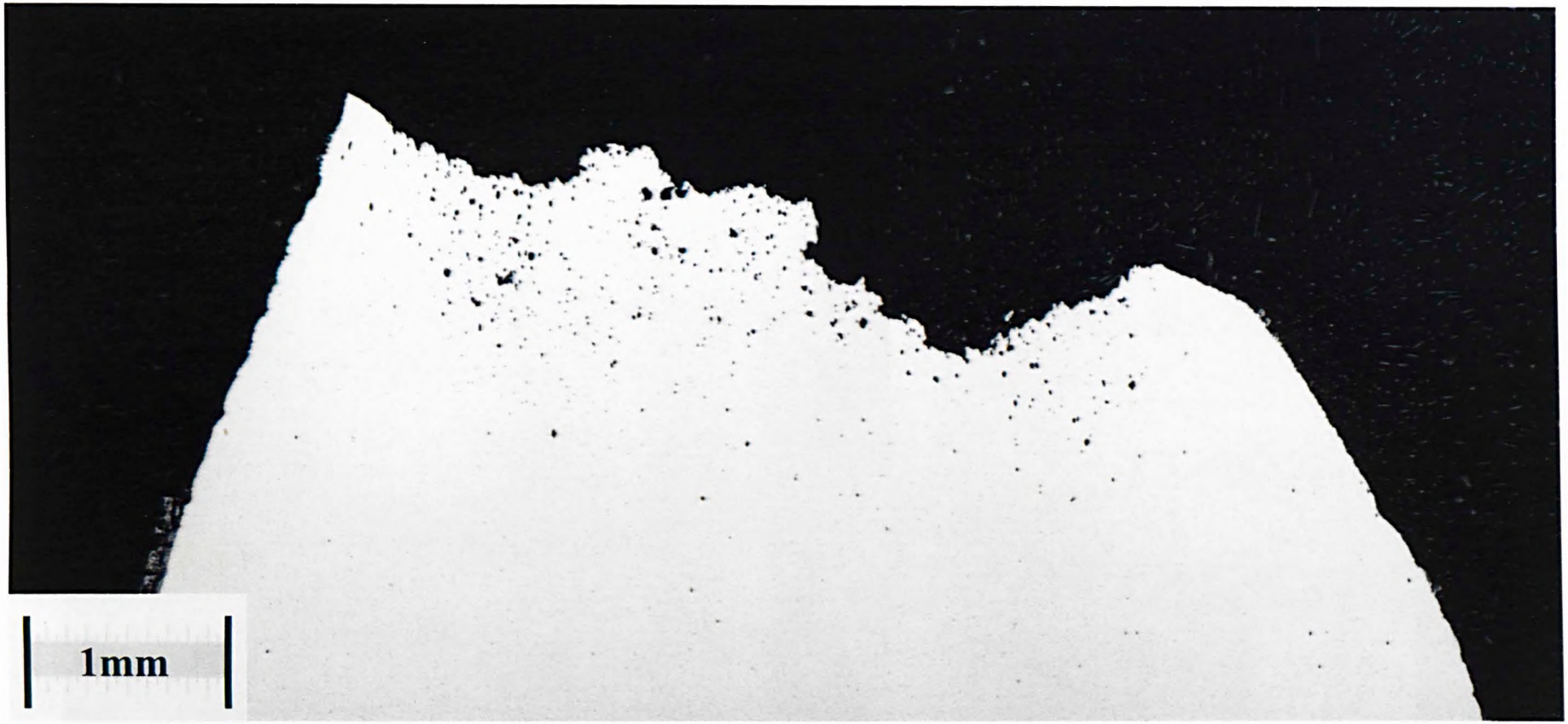

Figure 5.2-6b: *Material*: standard 2.25Cr-1Mo welded joint. *Test*: uniaxial creep in air. *Conditions*: T=843K (570°C); σ = 100MPa (initial stress); t = 4646h. One half. Not etched.

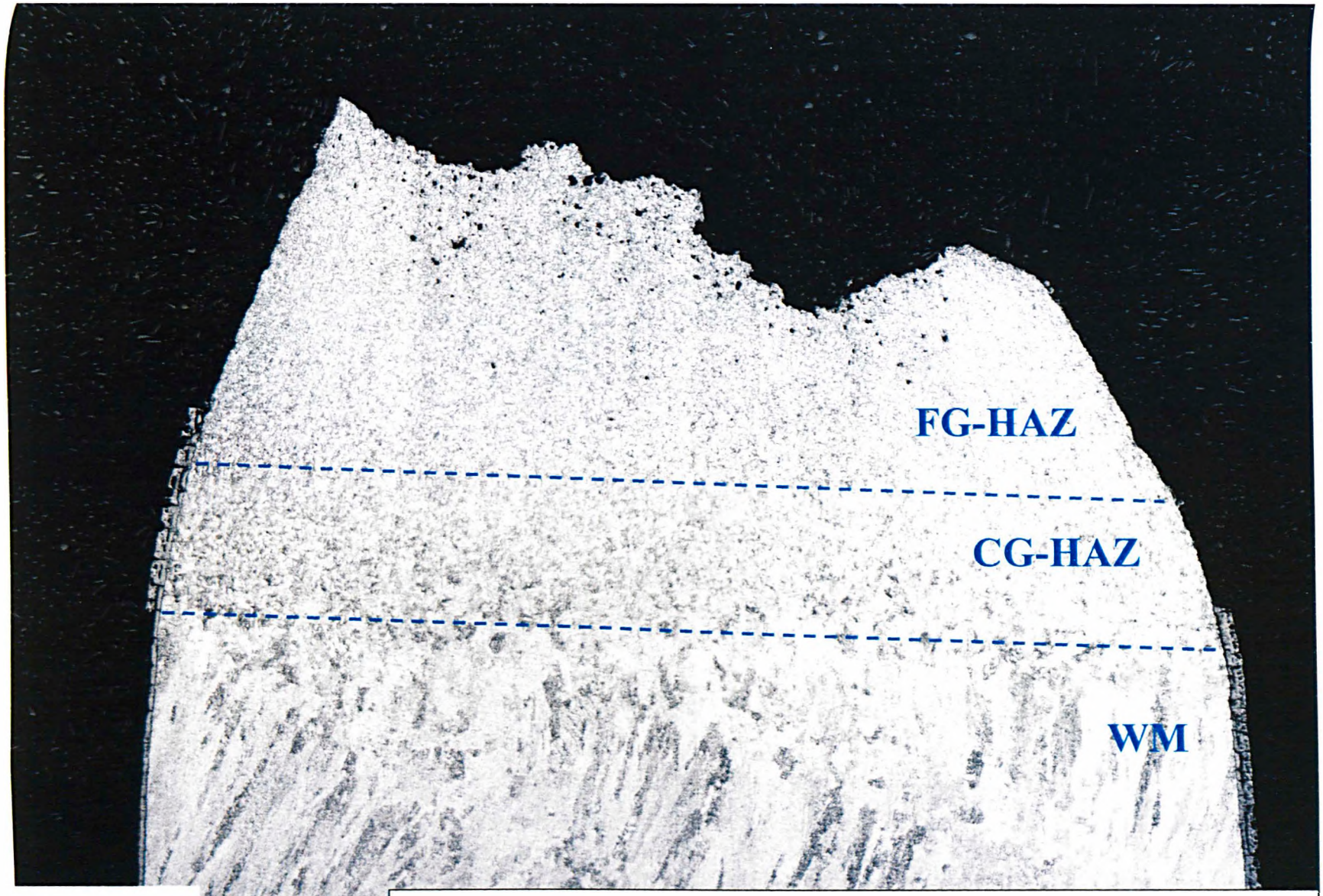

Figure 5.2-6c: *Material*: standard 2.25Cr-1Mo welded joint. *Test*: uniaxial creep in air. *Conditions*: T=843K(570°C); σ = 100MPa (initial stress); t = 4646h. One half. Etched with Nital 3%

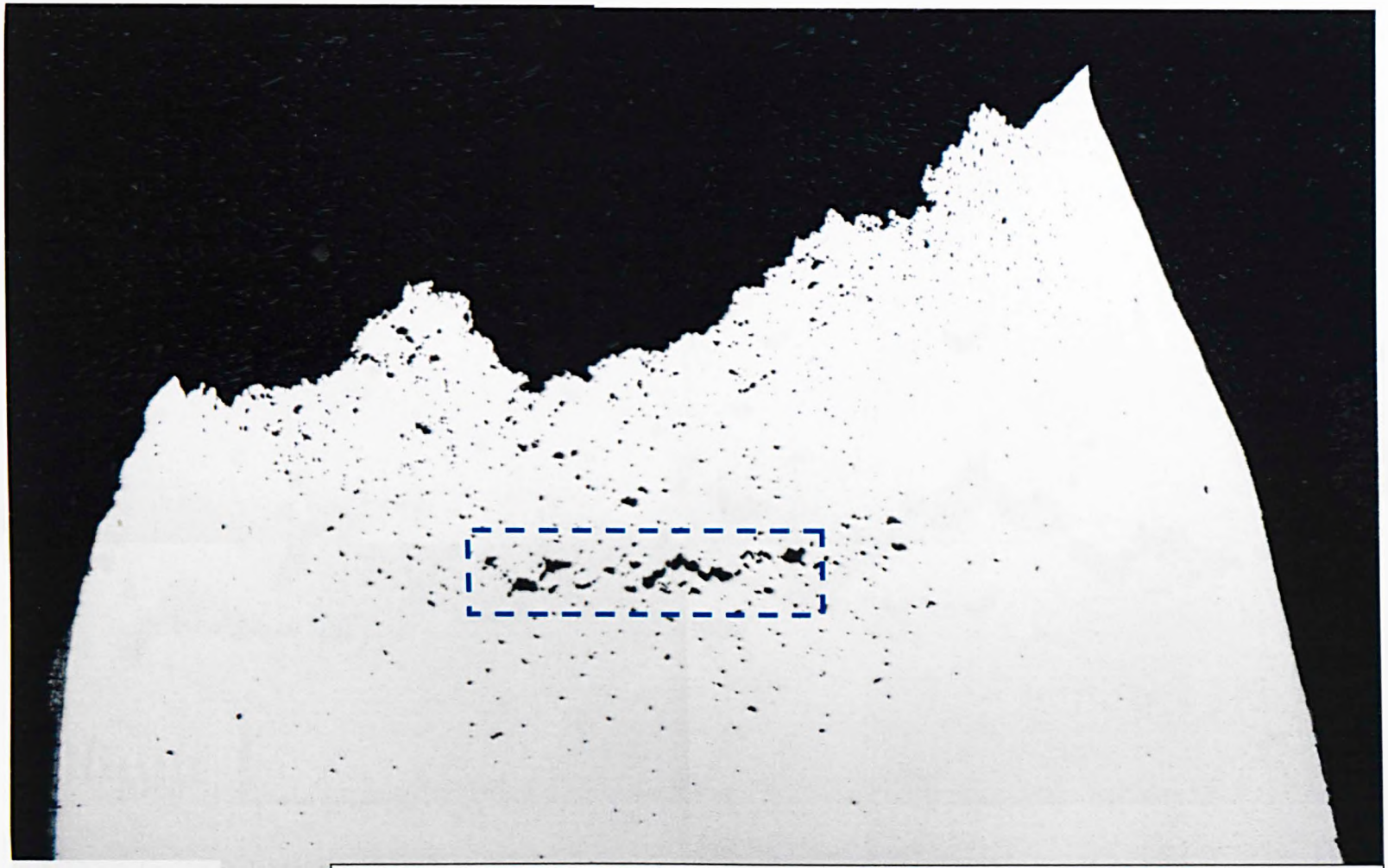

Figure 5.2-6d: *Material*: standard 2.25Cr-1Mo welded joint. *Test*: uniaxial creep in air. *Conditions*: T=843K (570°C); σ = 100MPa (initial stress); t = 4646h. Other half. Not etched

Figure 5.2-6e: Detail of Fig. 5.2-6d. Small cavities, void formation and coalescence of voids which leads to the formation of cracks.

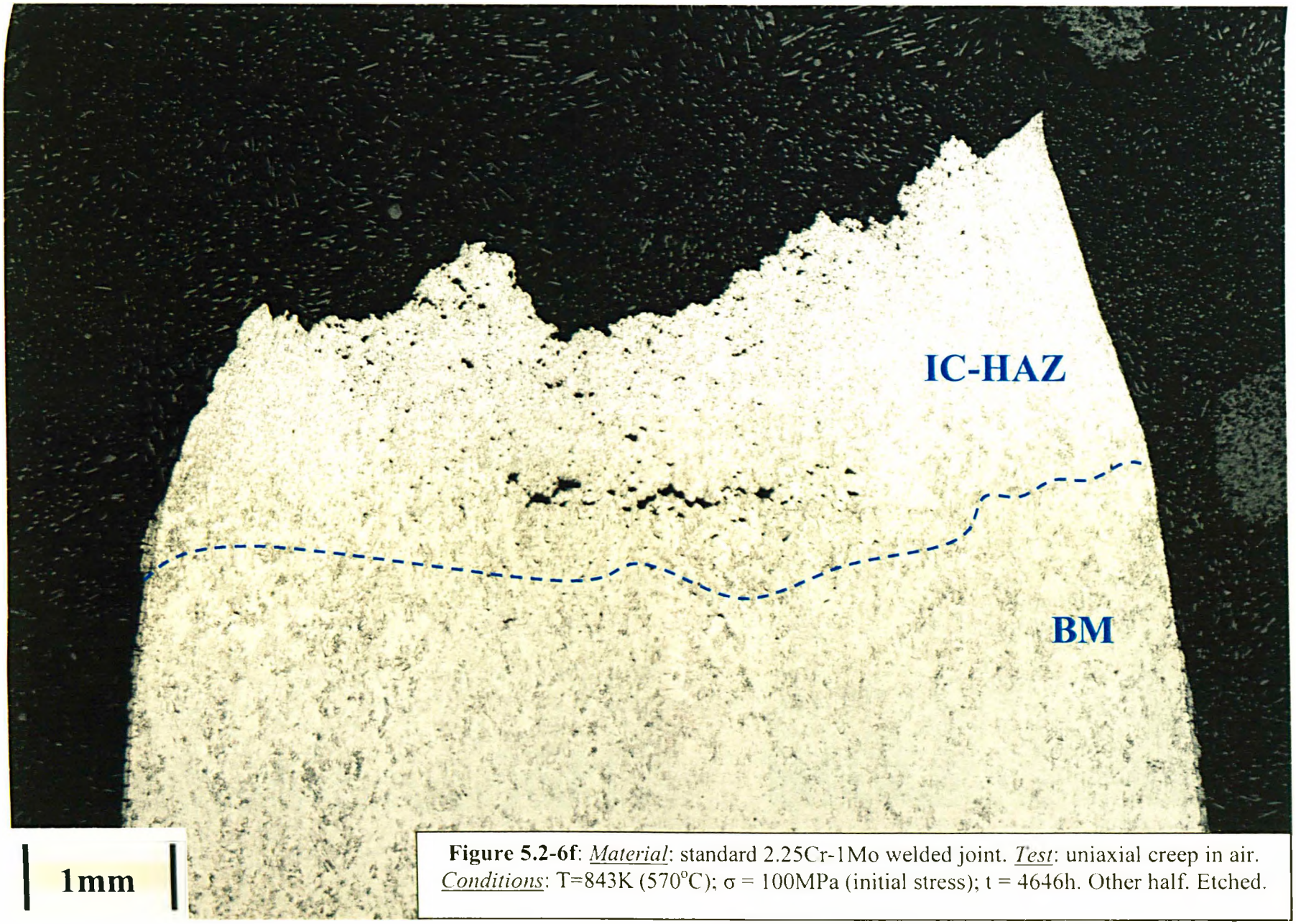

Figure 5.2-6f: *Material*: standard 2.25Cr-1Mo welded joint. *Test*: uniaxial creep in air. *Conditions*: T=843K (570°C); σ = 100MPa (initial stress); t = 4646h. Other half. Etched.

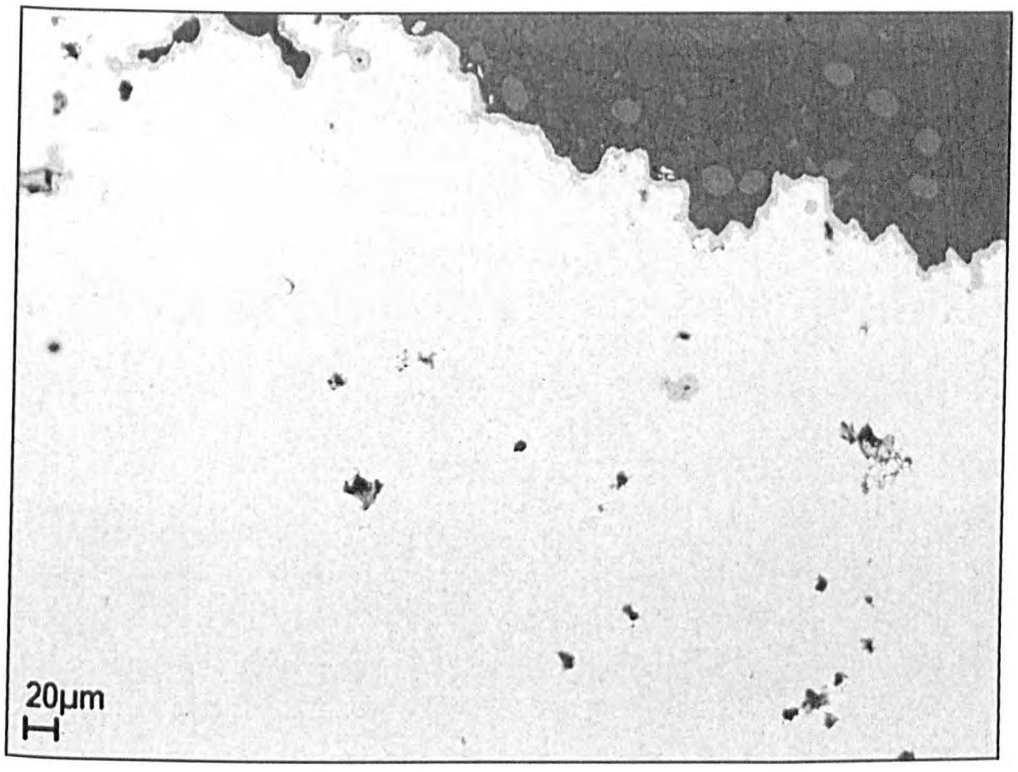

Figure 5.2-6g: 2.25Cr-1Mo welded joint tested in air at 843K (570°C), σ= 100MPa (initial stress). ICHAZ close to the Fracture Surface.

Figure 5.2-6h: Detail of Fig.5.2-6f. Damage in the zone. Sub-micron sized cavities.

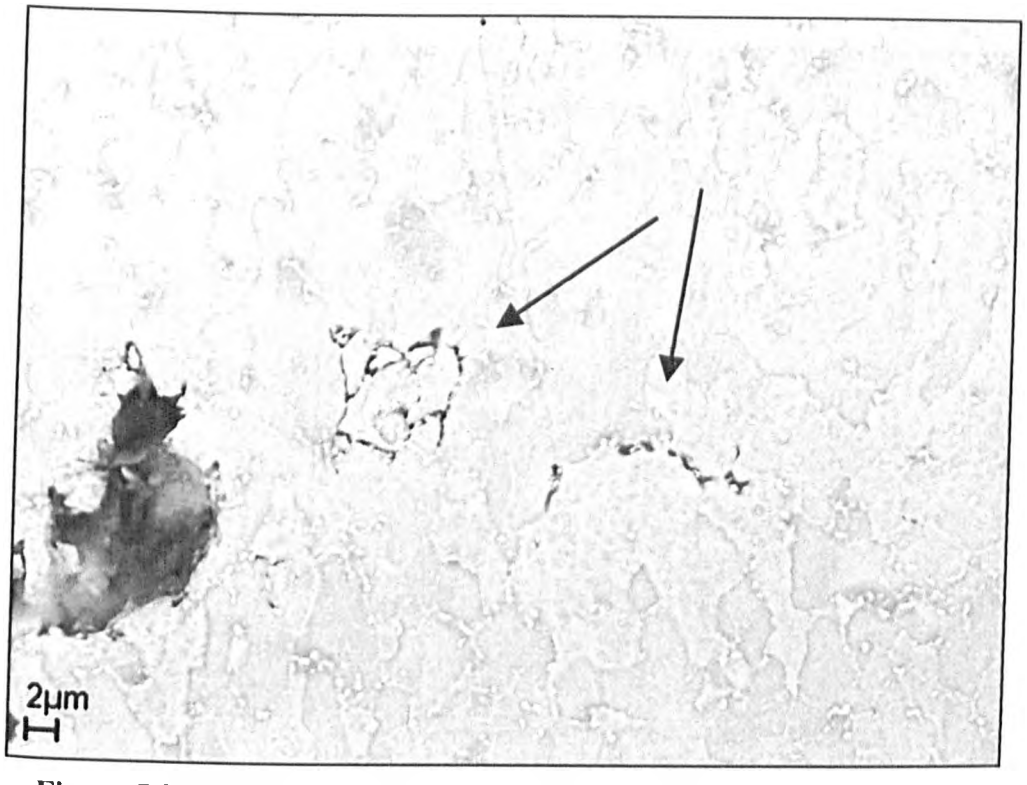

Figure 5.2-6i: ICHAZ. Cavitation at interfaces. Link-up of cavities which forms narrow cracks which develop locally along circuital paths.

Figure 5.2-6j: ICHAZ. Cavitation at interfaces. Narrow circuital cracks.

Figure 5.2-6k. Sub-micron cavities at interfaces and close to carbides.

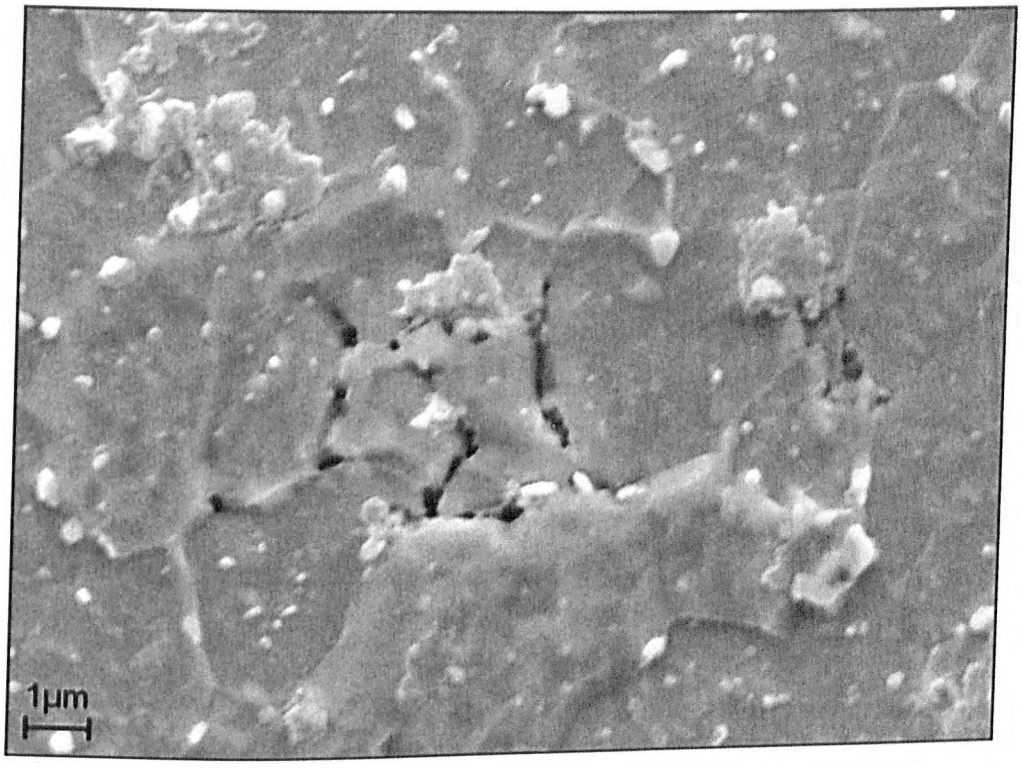

Figure 5.2-6l. Cavitation mainly at interfaces. (Secondary electrons)

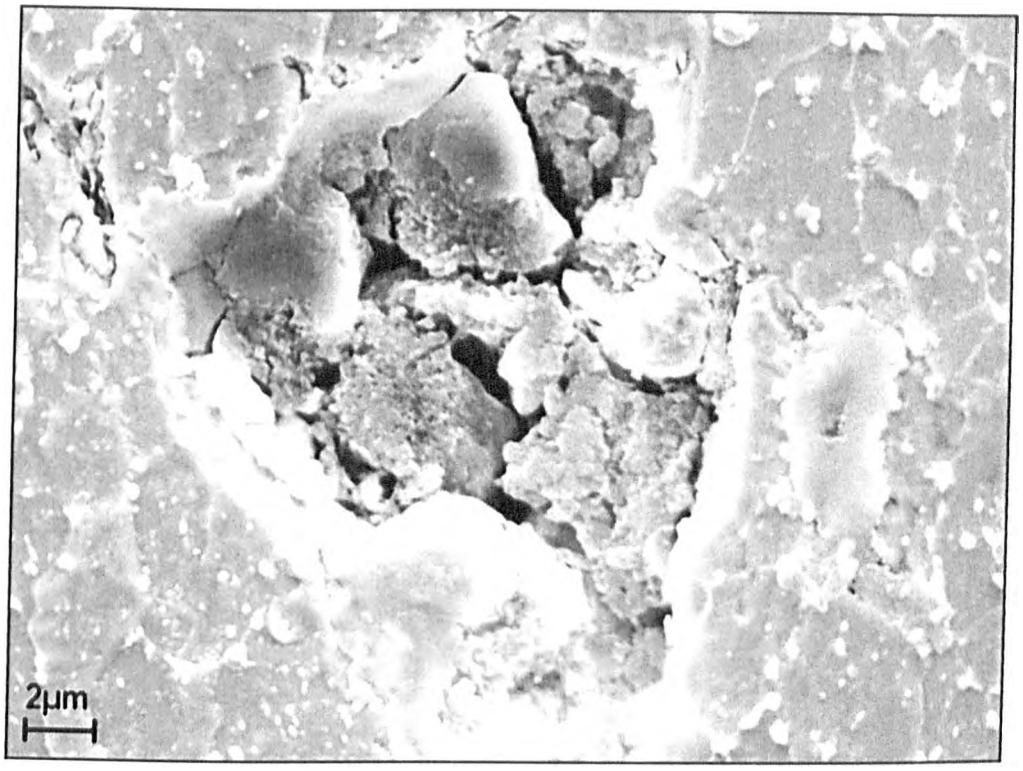

Figure 5.2-6m. Detail. The bottom of a void shows intergranular fracture due to grain boundary cavitation.

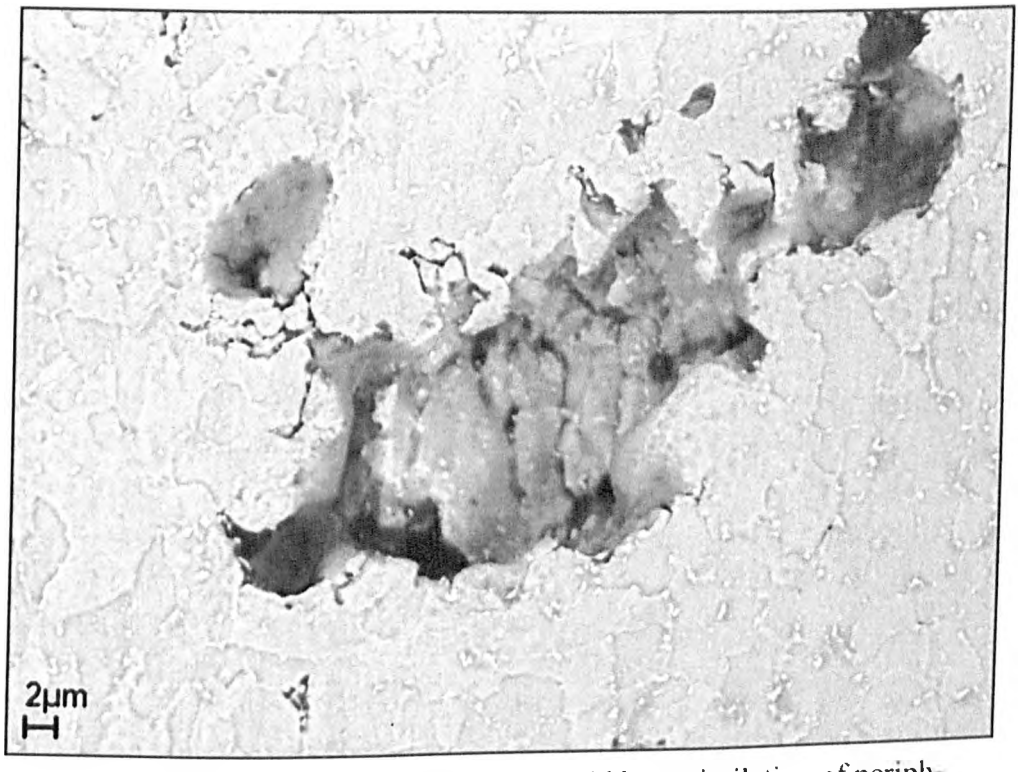

Figure 5.2-6n. Detail. Enlargement of a void by assimilation of peripheral cavities and microcracks.

Figure 5.2-6o. The same welded joint: weld metal. Very low or even absent cavitation.

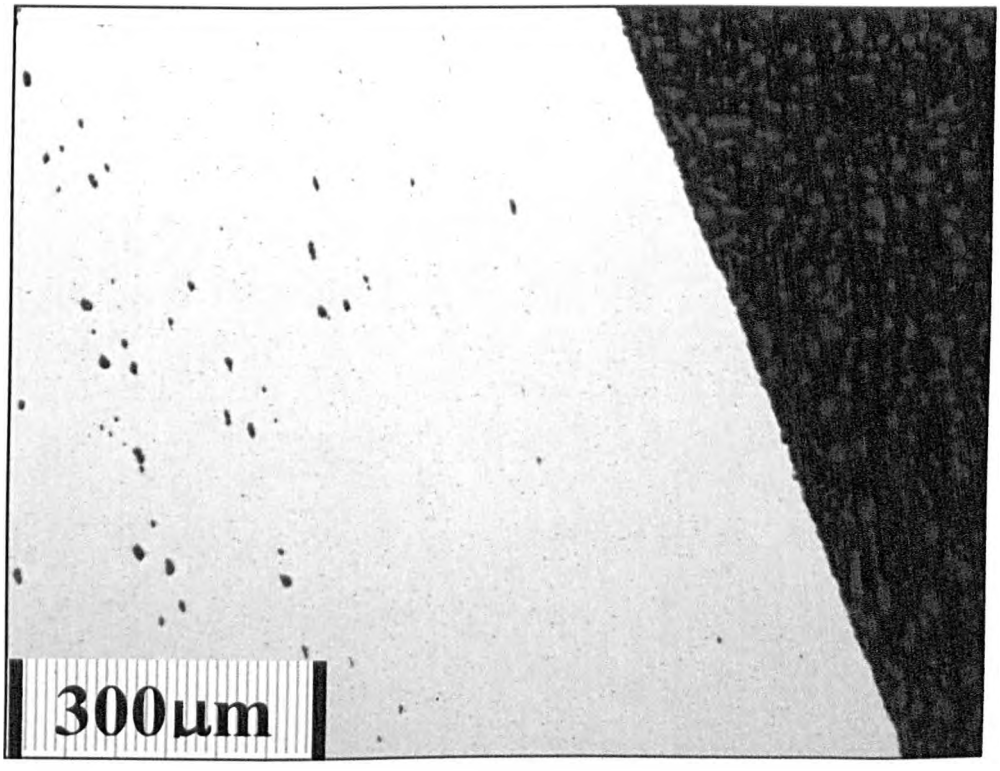

Figure 5.2-6p. The same welded joint: Less cavitation at the surface layer. Similar to the decarburised layer of samples tested in hydrogen.

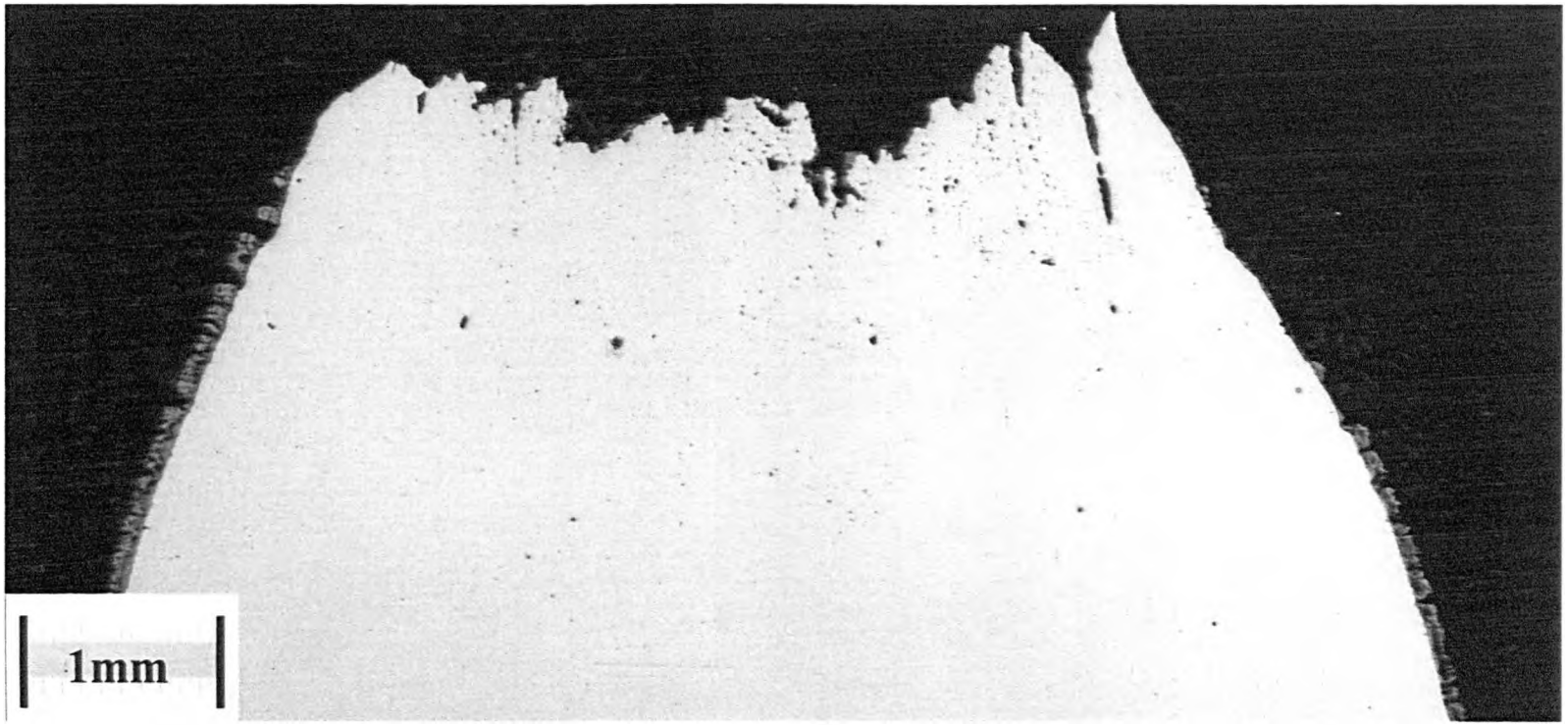

Figure 5.2-7a: *Material*: standard 2.25Cr-1Mo welded joint. *Test*: uniaxial creep in air. *Conditions*: T= 873K (600°C); σ = 100MPa (initial stress); t = 560h. Sample not etched.

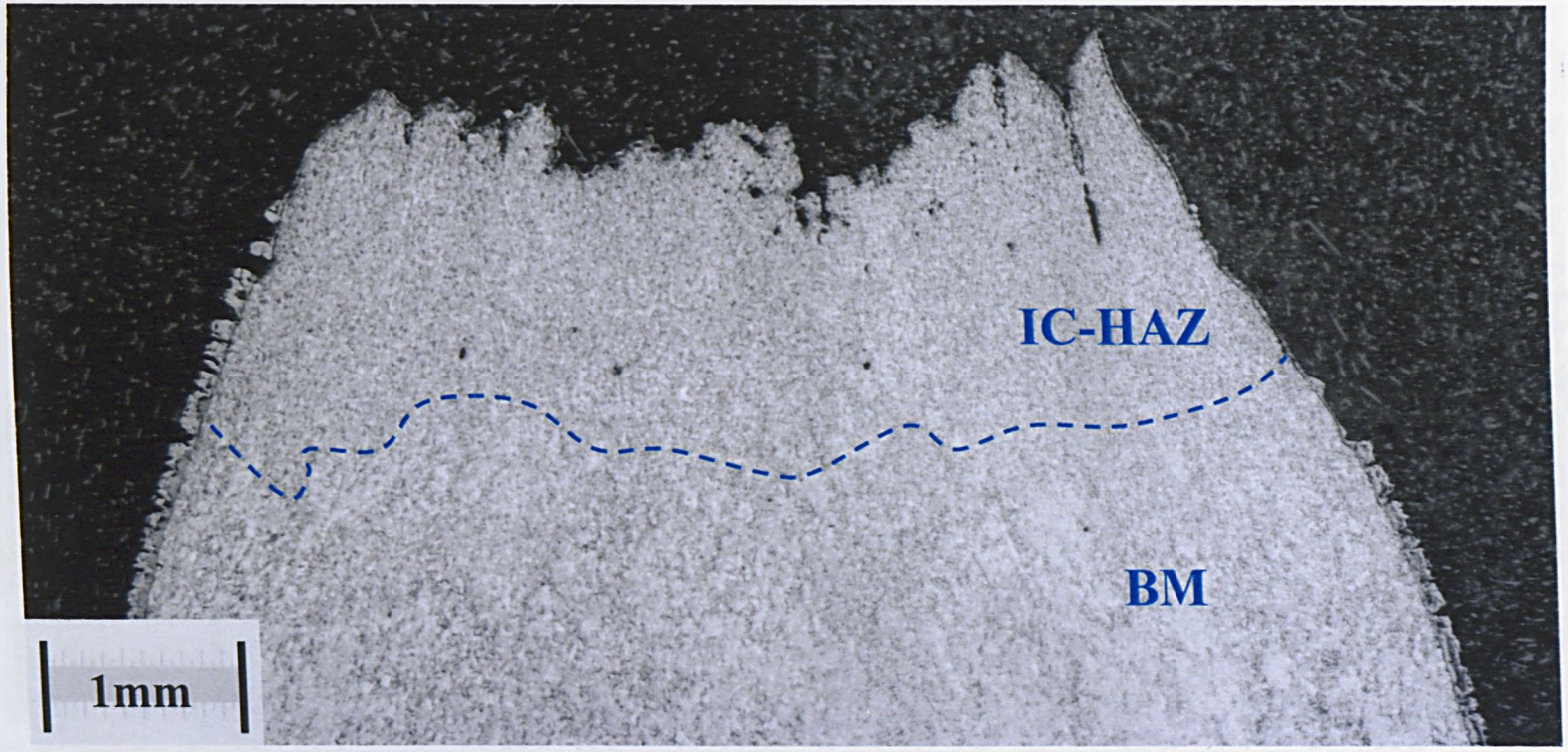

Figure 5.2-7b: *Material*: standard 2.25Cr-1Mo welded joint. *Test*: uniaxial creep in air. *Conditions*: T= 873K (600°C); σ = 100MPa (initial stress); t = 560h. Sample etched with Nital.

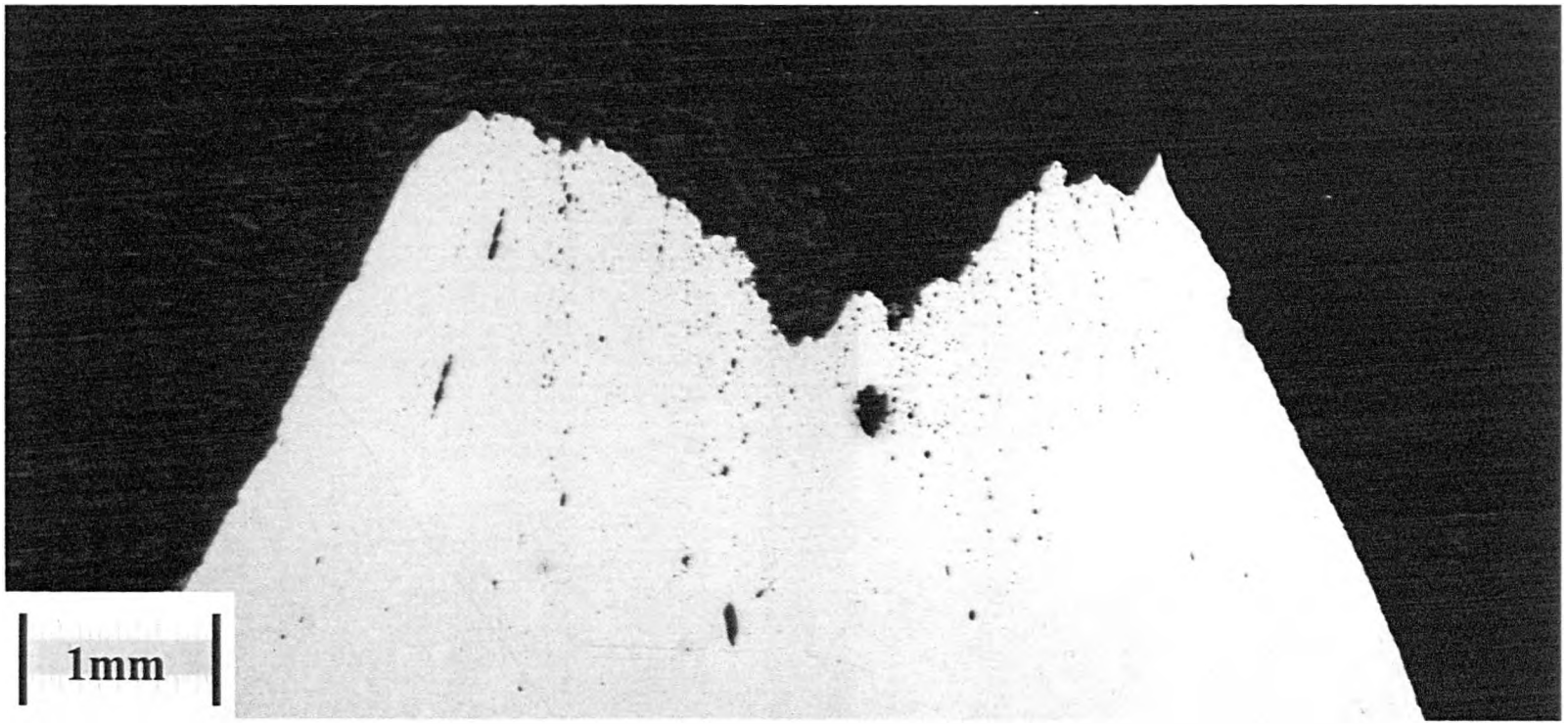

Figure 5.2-7c: *Material*: standard 2.25Cr-1Mo welded joint. *Test*: uniaxial creep in air. *Conditions*: T= 873K (600°C); σ = 100MPa (initial stress); t = 560h. Other half. Sample not etched.

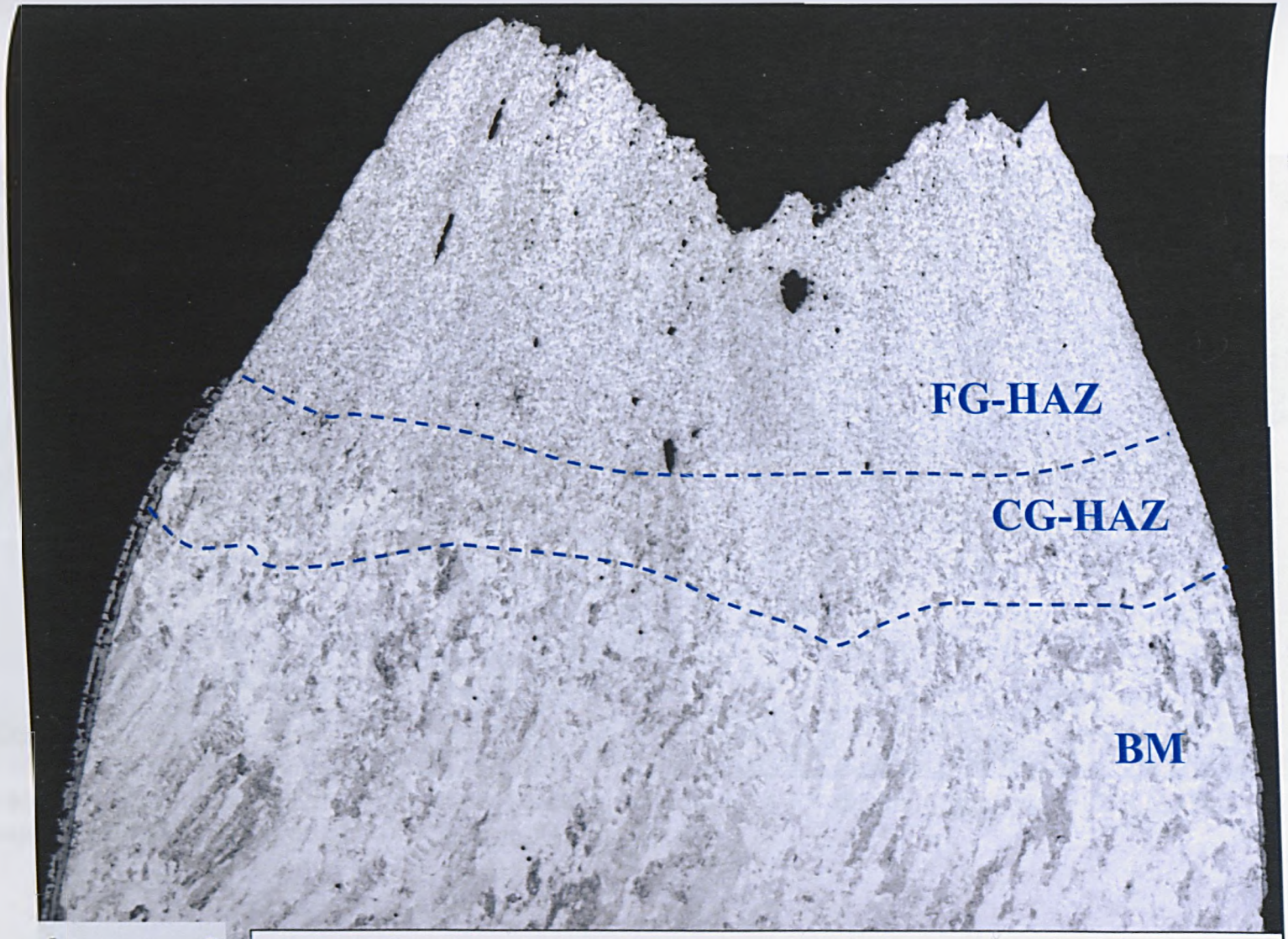

Figure 5.2-7d: *Material*: standard 2.25Cr-1Mo welded joint. *Test*: uniaxial creep in air. *Conditions*: T= 873K (600°C); σ = 100MPa (initial str.); t = 560h. Sample etched with Nital.

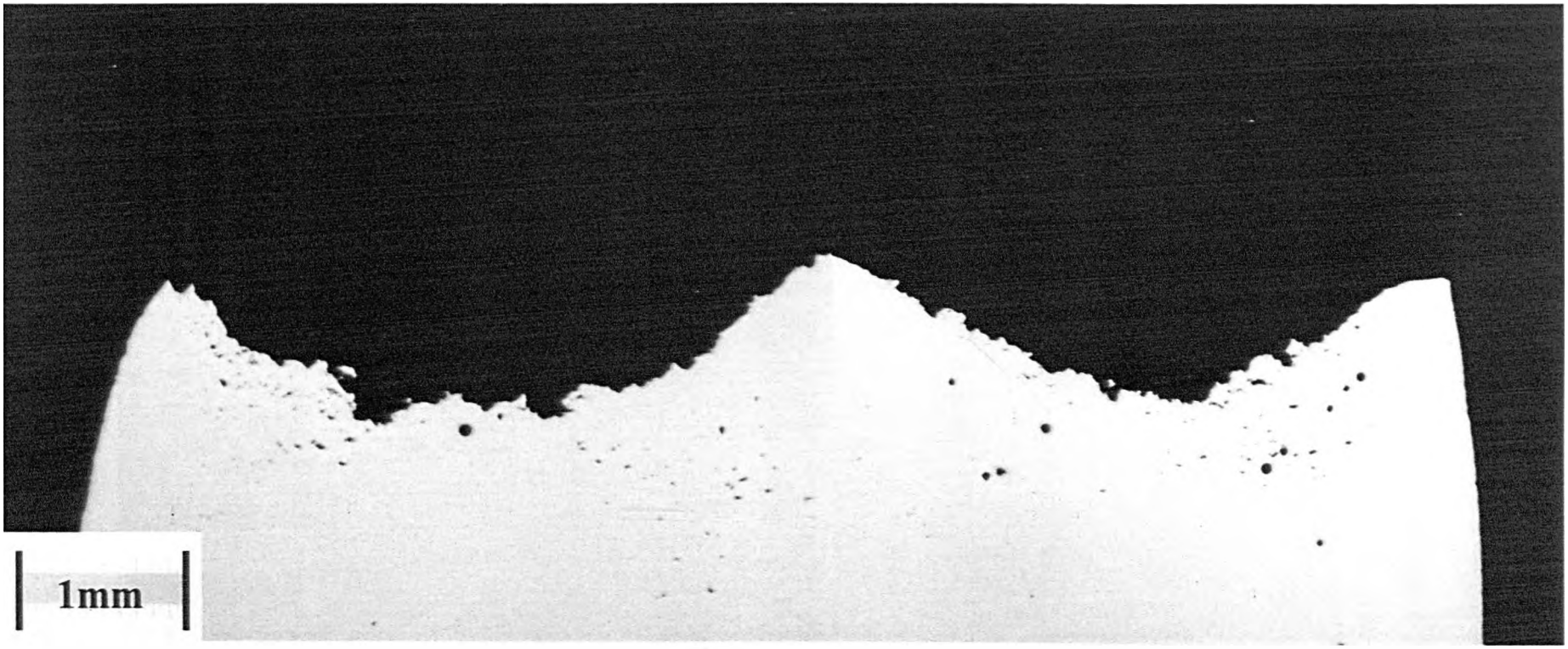

Figure 5.2-8a: *Material*: standard 2.25Cr-1Mo welded joint. *Test*: uniaxial creep in hydrogen. *Conditions*: T=873K (600°C); P=18MPa (180bars); σ = 100MPa (initial stress); t = 182h. Sample not etched.

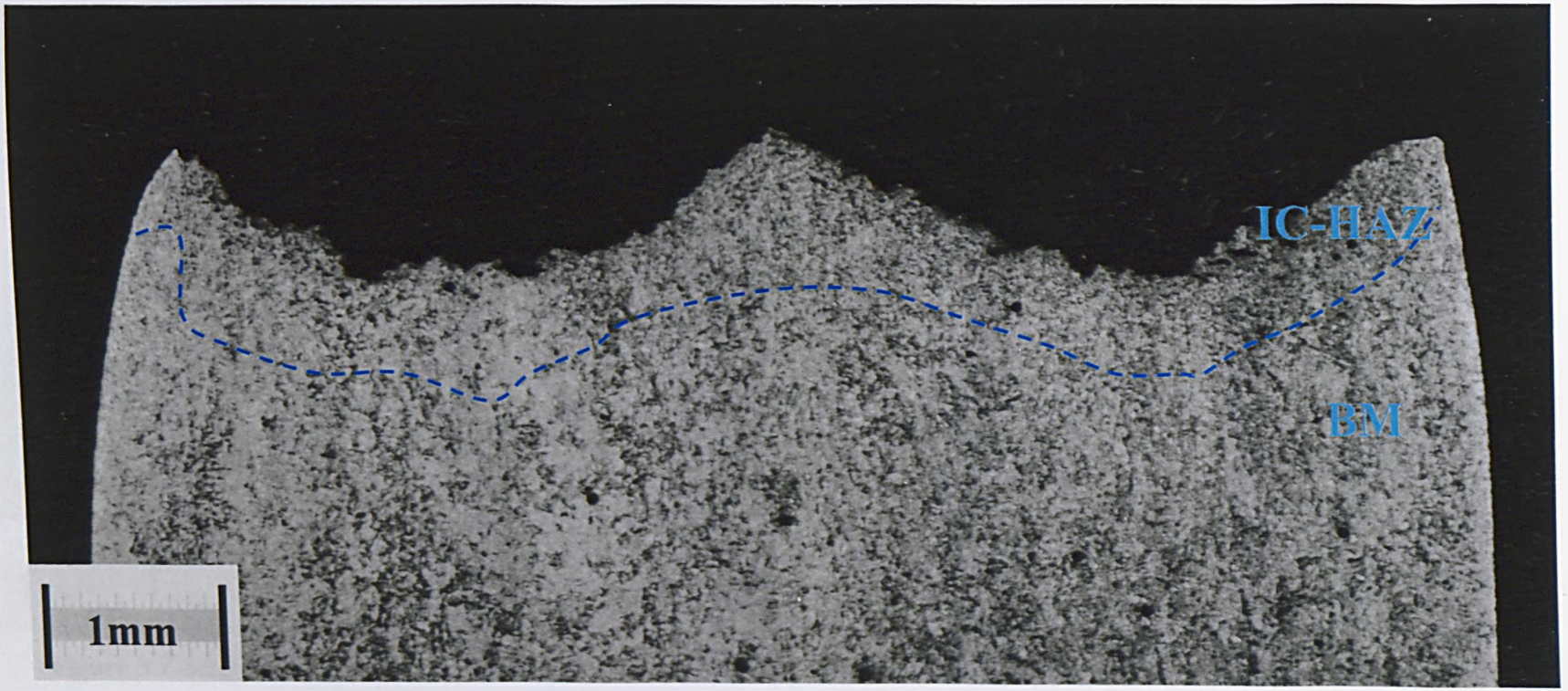

Figure 5.2-8b: *Material*: standard 2.25Cr-1Mo welded joint. *Test*: uniaxial creep in hydrogen. *Conditions*: T=873K (600°C); P=18MPa (180bars); σ = 100MPa (initial stress); t = 182h. Sample etched with Nital.

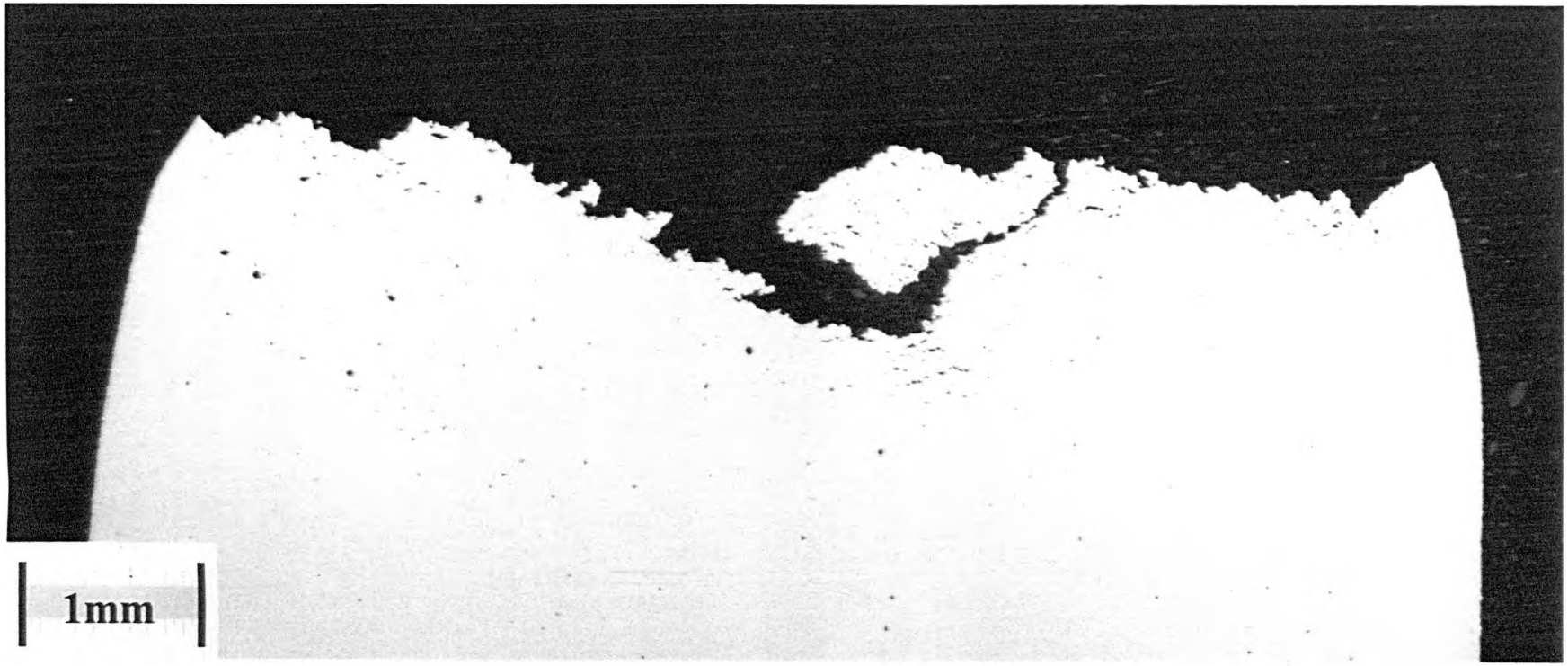

Figure 5.2-8c: *Material*: Standard 2.25Cr-1Mo welded joint. *Test*: Uniaxial Creep in Hydrogen. *Conditions*: T=600°C; P=180bars; σ = 100MPa (initial stress); t = 182h. Sample not etched.

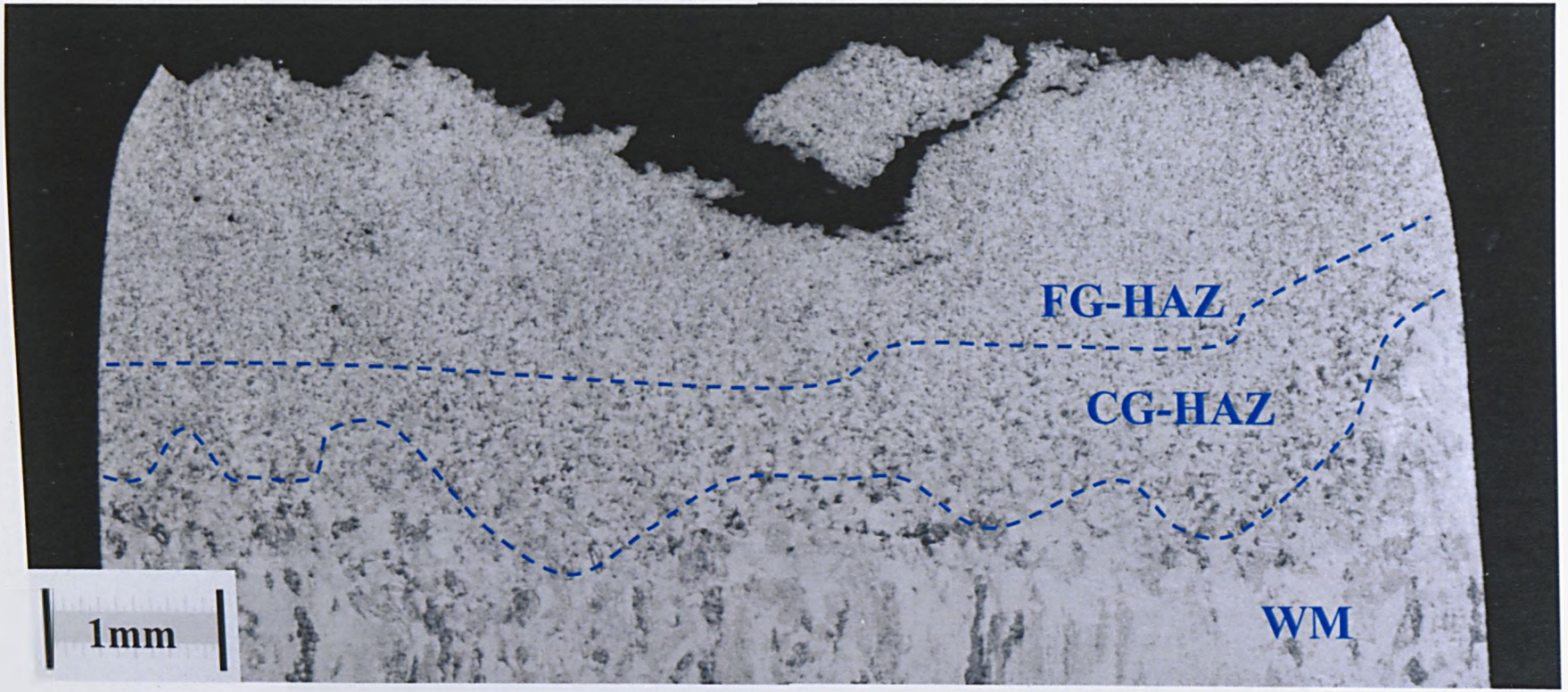

Figure 5.2-8d: *Material*: Standard 2.25Cr-1Mo welded joint. *Test*: Uniaxial Creep in Hydrogen. *Conditions*: T=600°C; P=180bars; σ = 100MPa (initial stress); t = 182h. Sample etched with Nital.

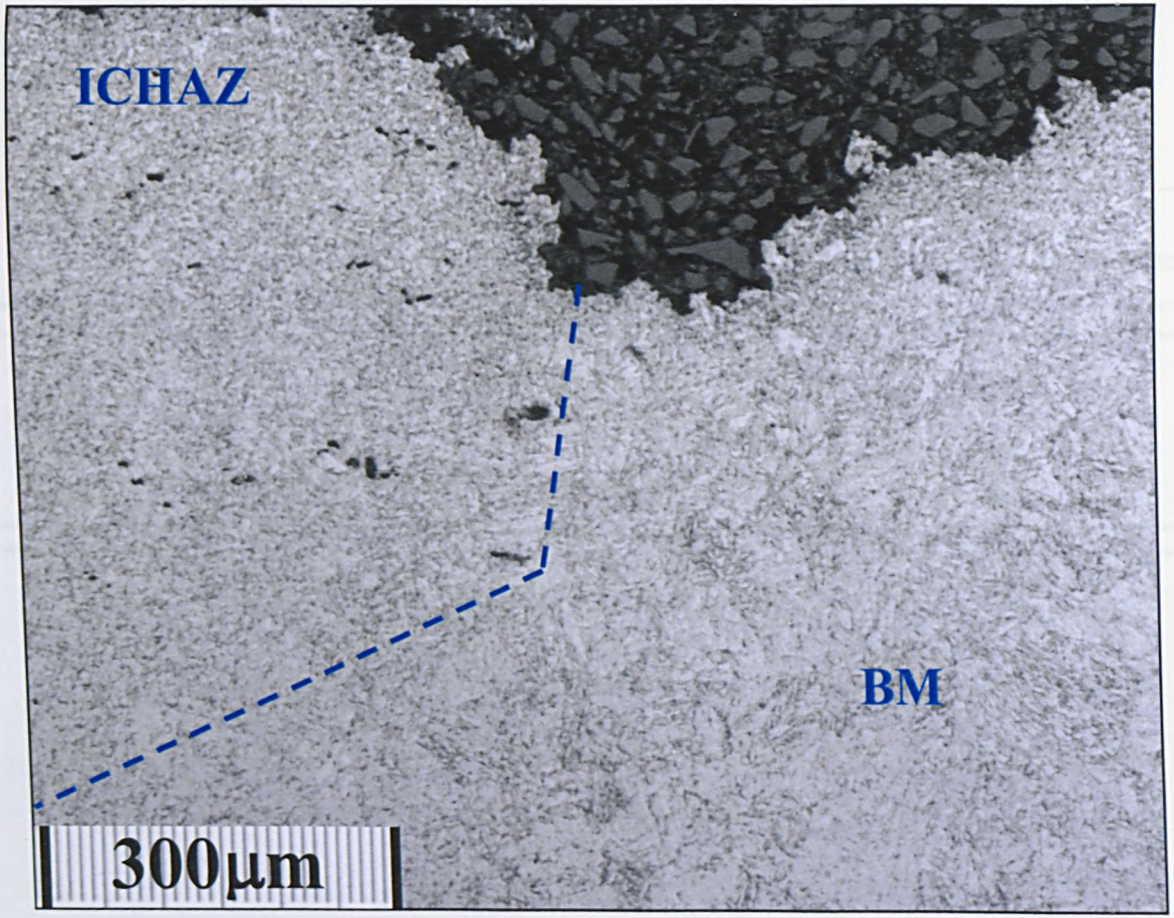

Figure 5.2-8e: Detail of Fig. 3 showing two zones: the base metal (BM) and the ICHAZ. Voids are prevalently present in the ICHAZ.

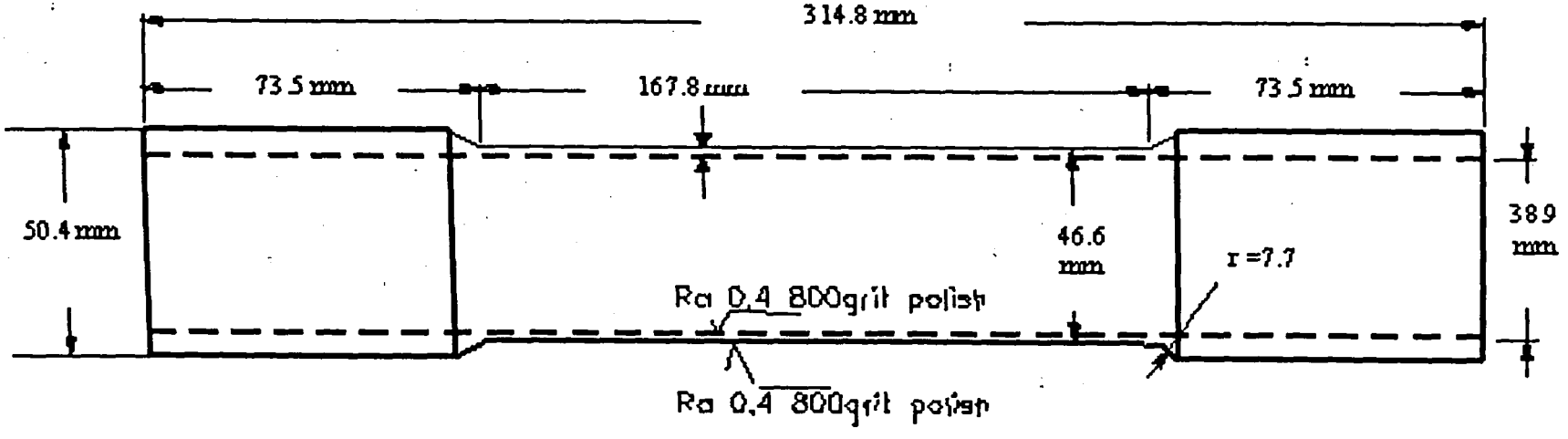

Fig. 5.2-9a: Drawing of the pressurized tube, with measurements.

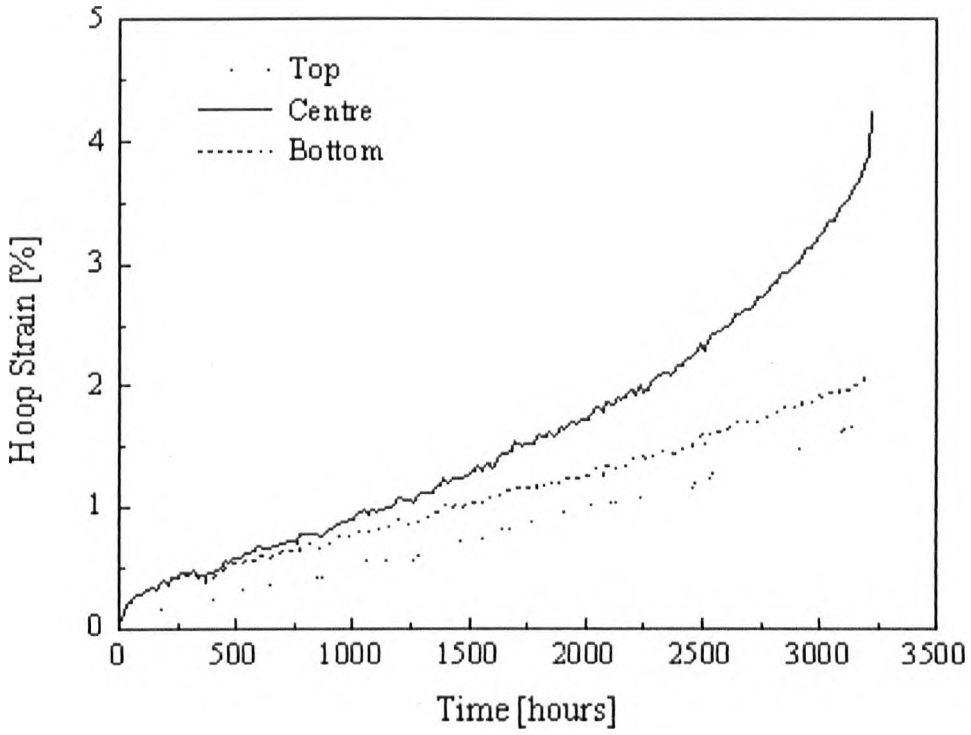

Fig. 5.2-9b: Creep curves registered by means of the sensors placed respectively in the Top, Centre and Bottom positions of the gauge length of the pressurized Tube made of cross-welded 2.25Cr-1Mo steel.

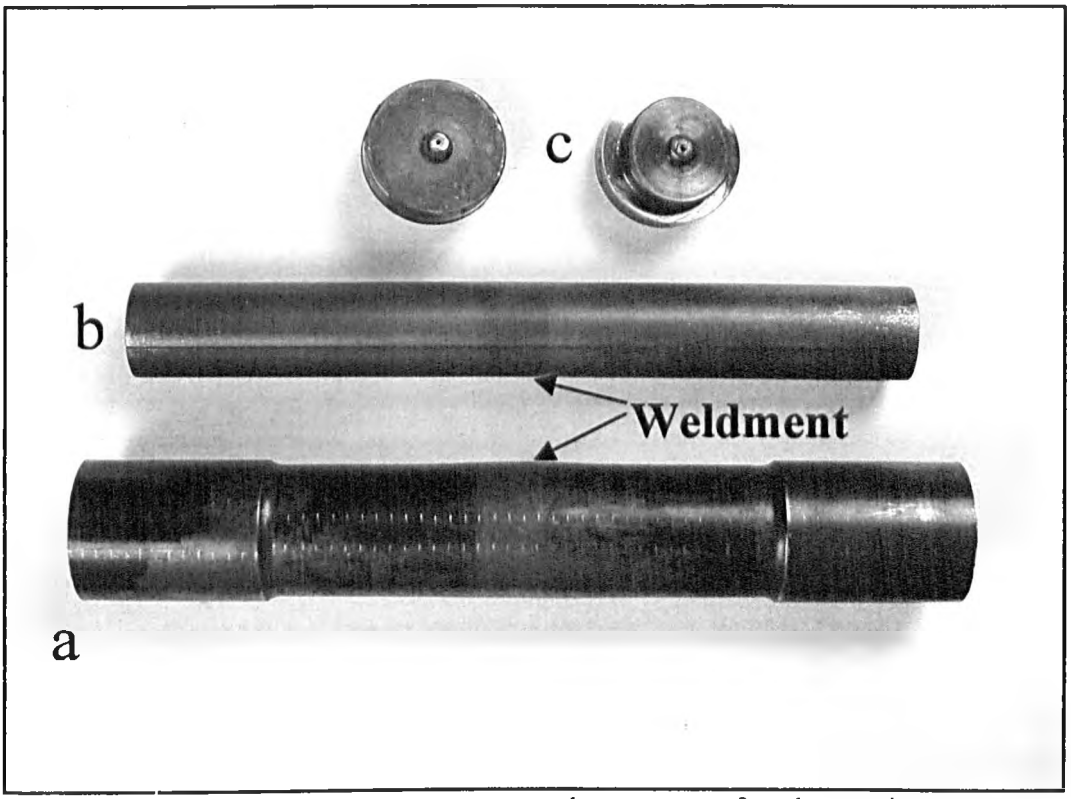

Figure 5.2-10: All the tube components, as they appear after the test in hydrogen. **a:** Tube **b:** Filler Bar; **c:** End Caps. After the test, strain measurements have been carried out on the tube (See the markers of the positions of measurement).

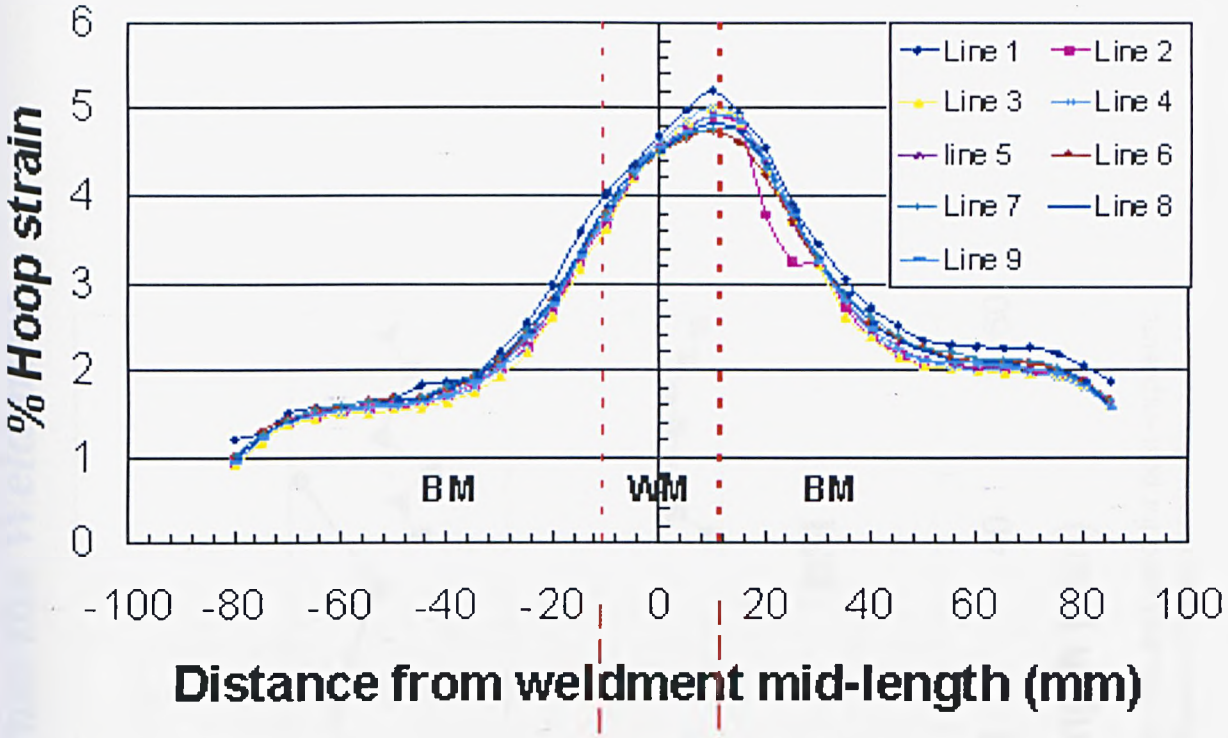

Fig. 5.2-11: The measurements of the tube gauge diameter, by means of calliper, every 5 mm along the whole gauge length and following 9 parallel lines.

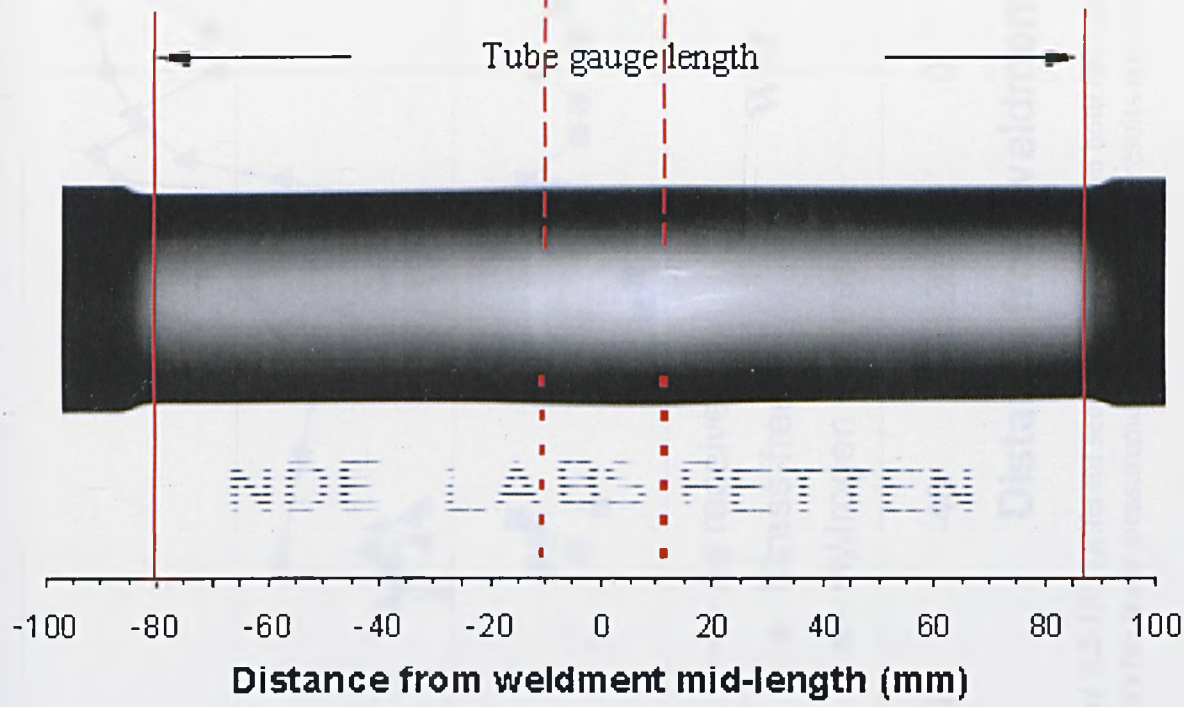

Fig 5.2-12: Results of the inspection performed by means of X-rays. It gives evidence of the presence of two main cracks in the part of the welded joint more affected by bulging. The cracks appear to propagate from the HAZ into the base metal (BM).

(Figure 5.2-11 and 5.2-12 have been published in the *Annual Report 2001* of the Institute for Energy)

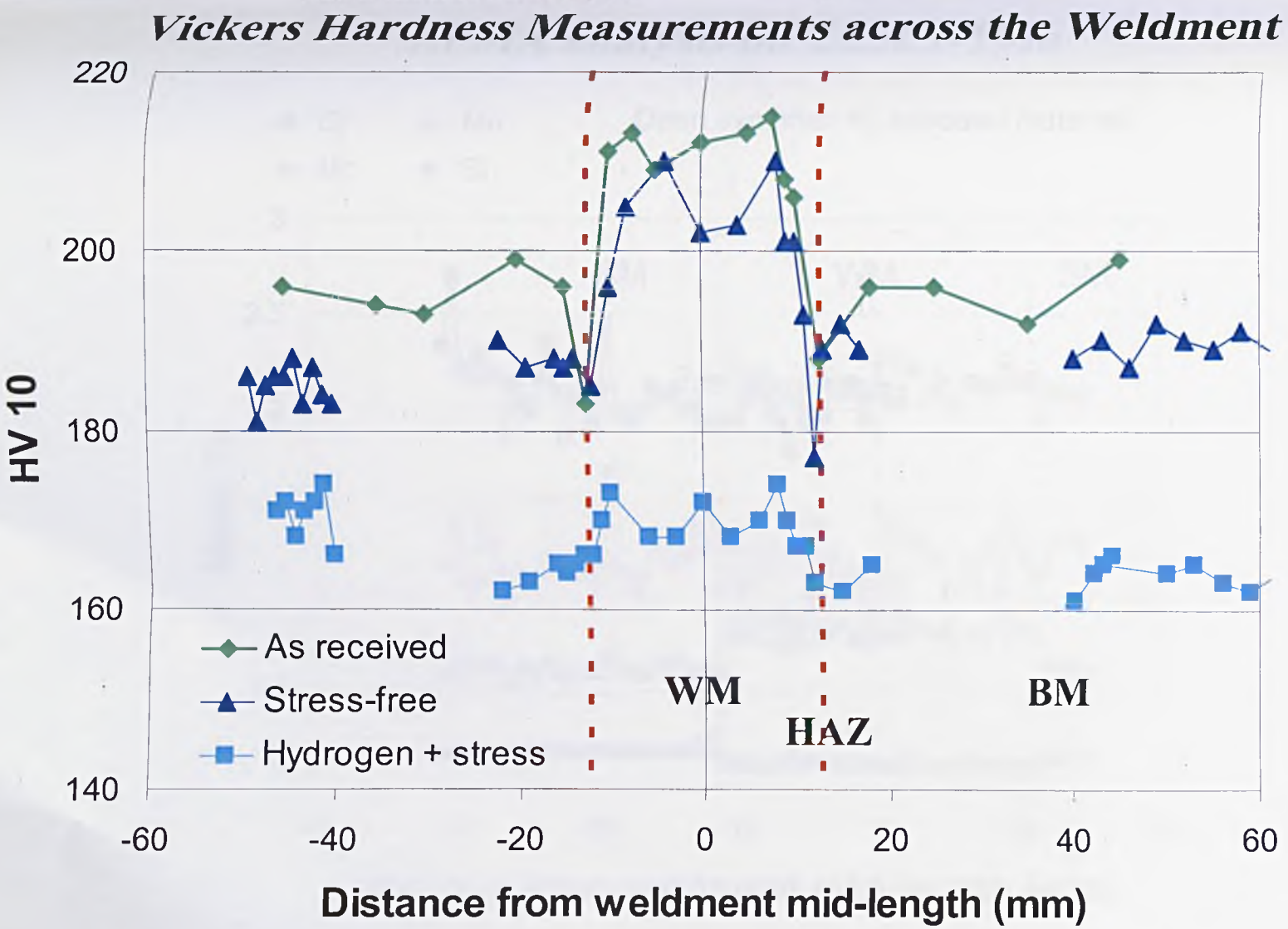

Figure 5.2-13: Different sections were cut from both the tube and the filler bar, and used for post-exposure Vickers hardness measurements. The hardness results are compared with those of the as received material.

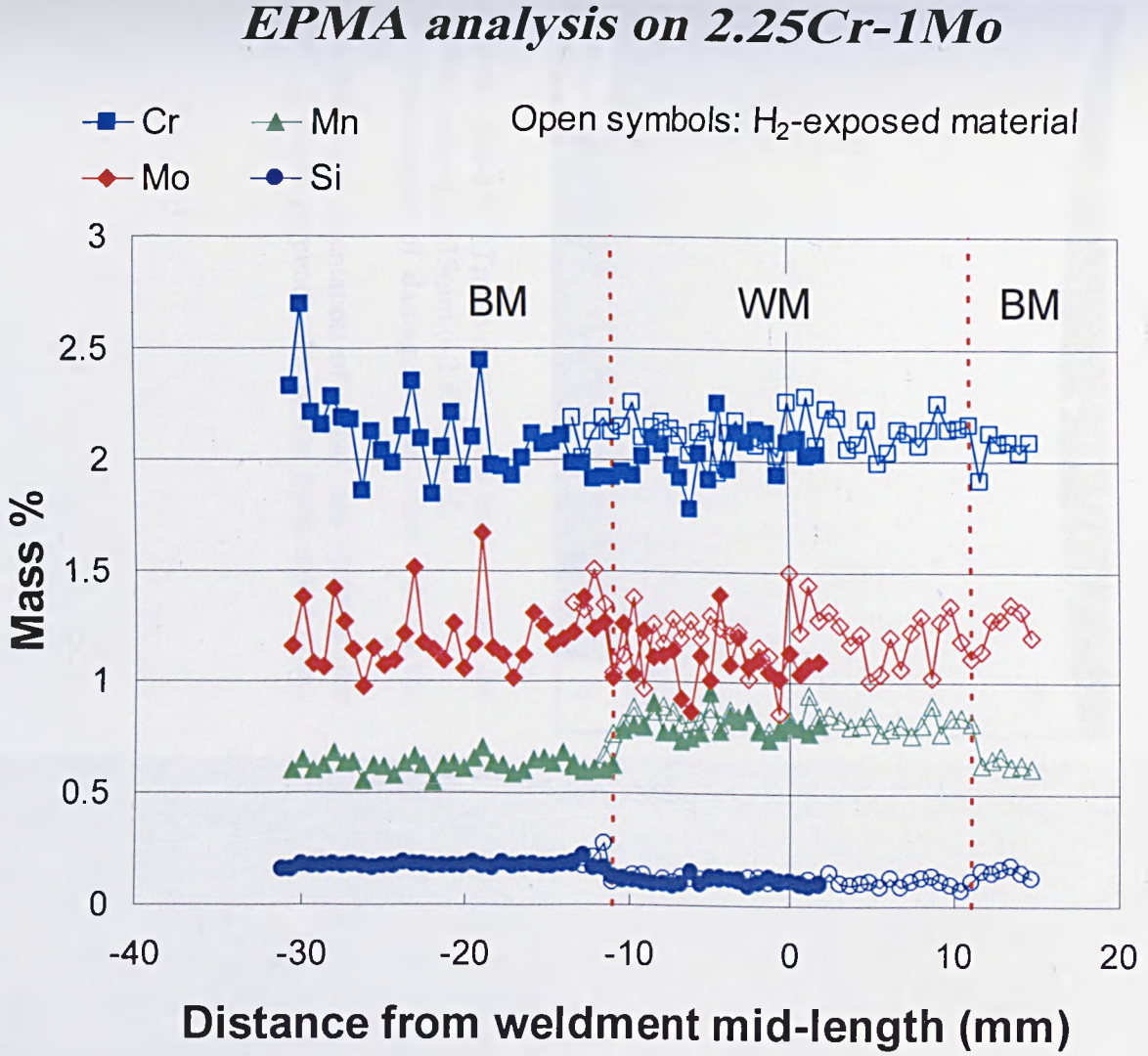

Figure 5.2-14: EPMA Linescan profiling of the cross-weld region in the as-received state and after H_2 exposure.

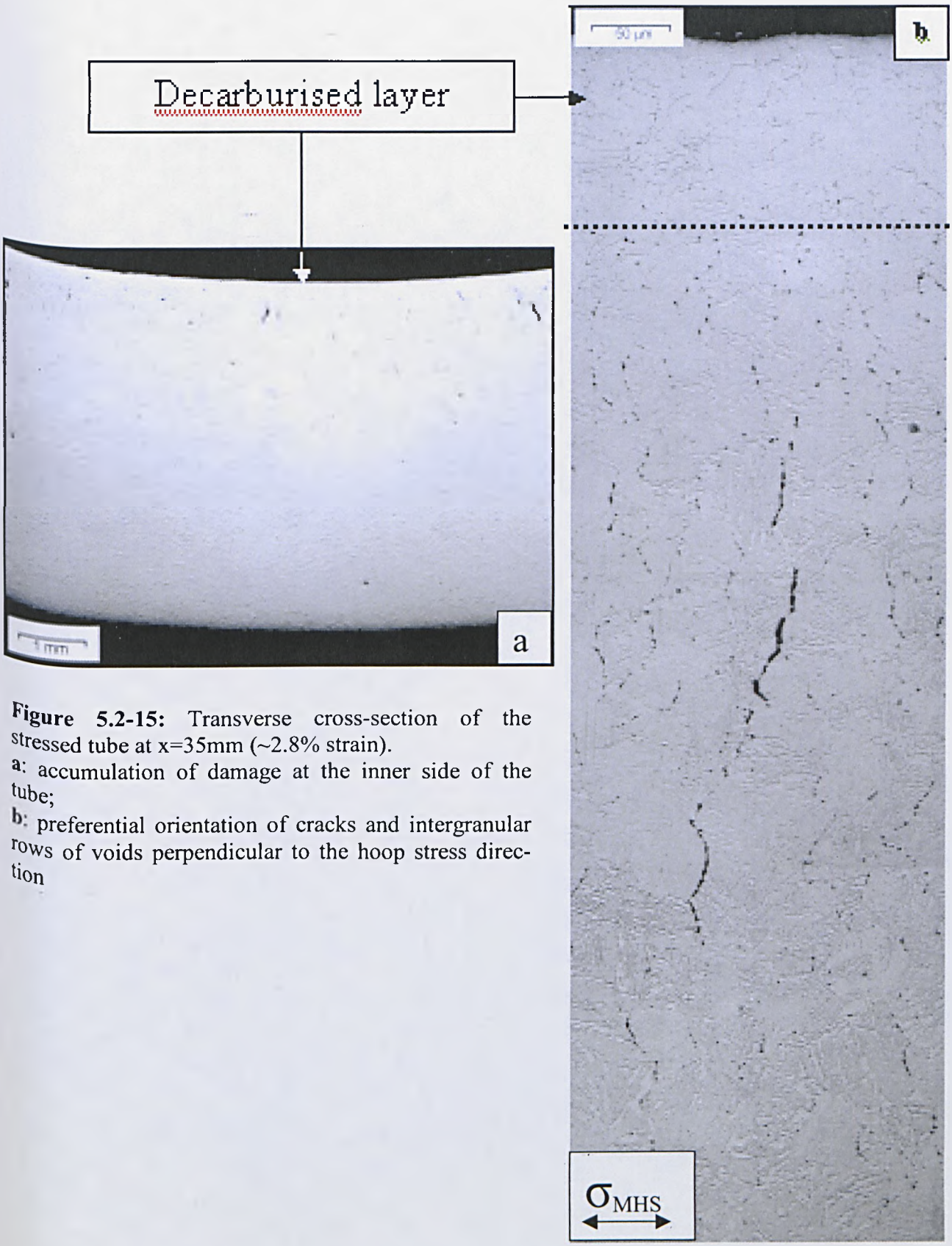

Figure 5.2-15: Transverse cross-section of the stressed tube at x=35mm (~2.8% strain).
a: accumulation of damage at the inner side of the tube;
b: preferential orientation of cracks and intergranular rows of voids perpendicular to the hoop stress direction

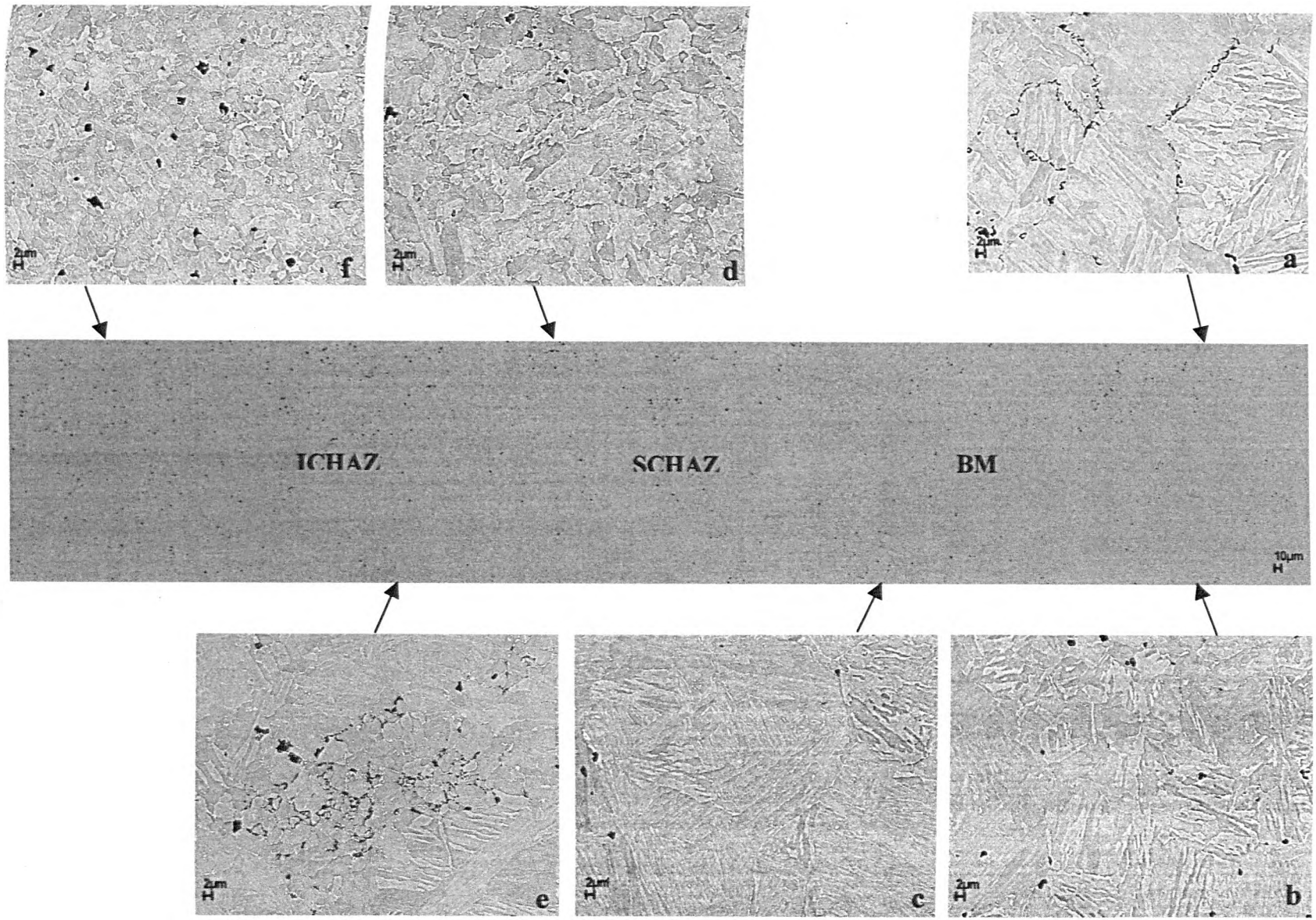

Fig. 5.2-16: Slice B. Welded joint perpendicular to the hoop stress. **a, b, c:** BM; **d, e:** SCHAZ; **f:** ICHAZ

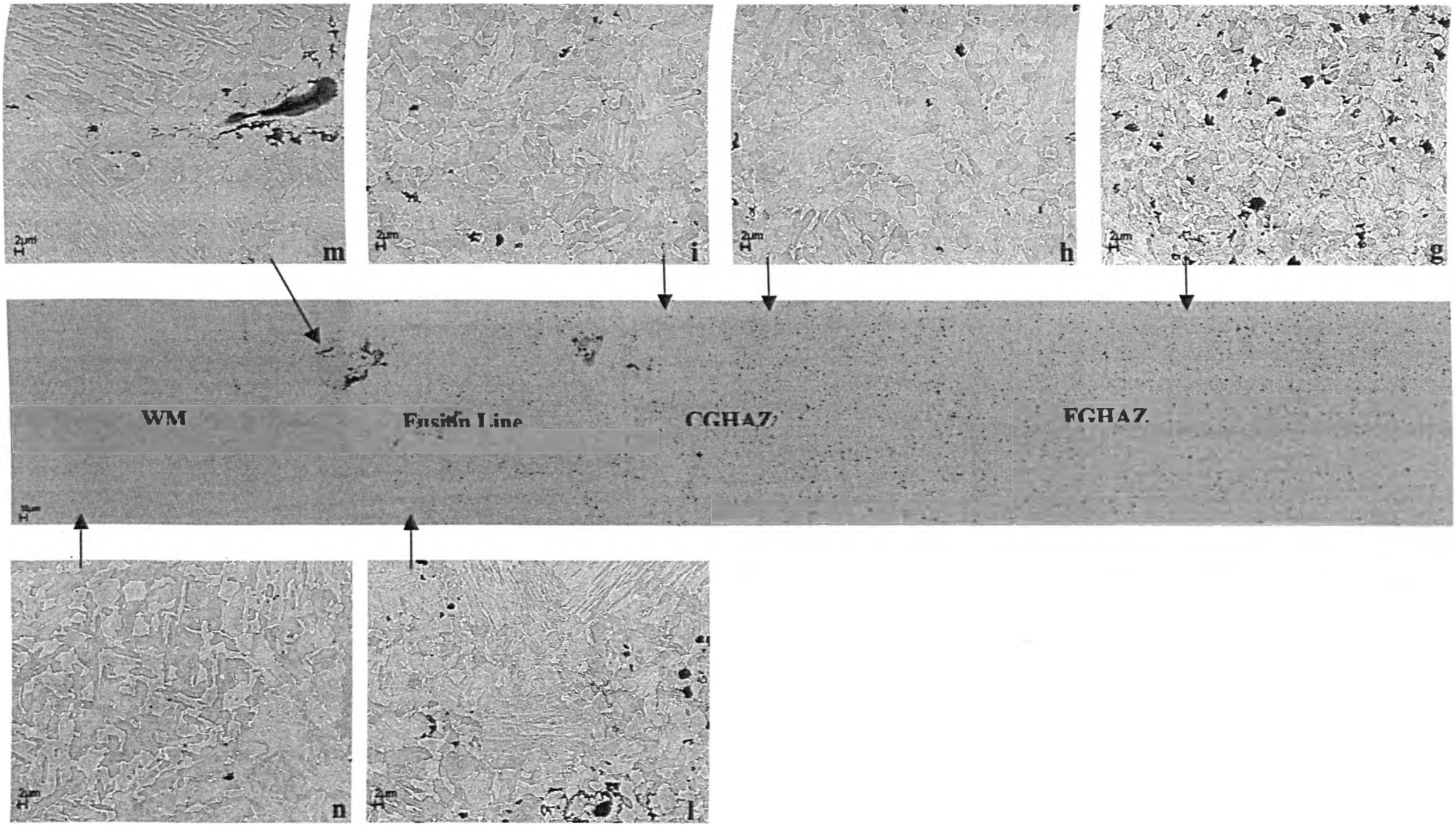

Figure 5.2-16': Slice B. **g:** FGHAZ, **h, i:** CGHAZ; **l, m:** Fusion Line; **n:** WM

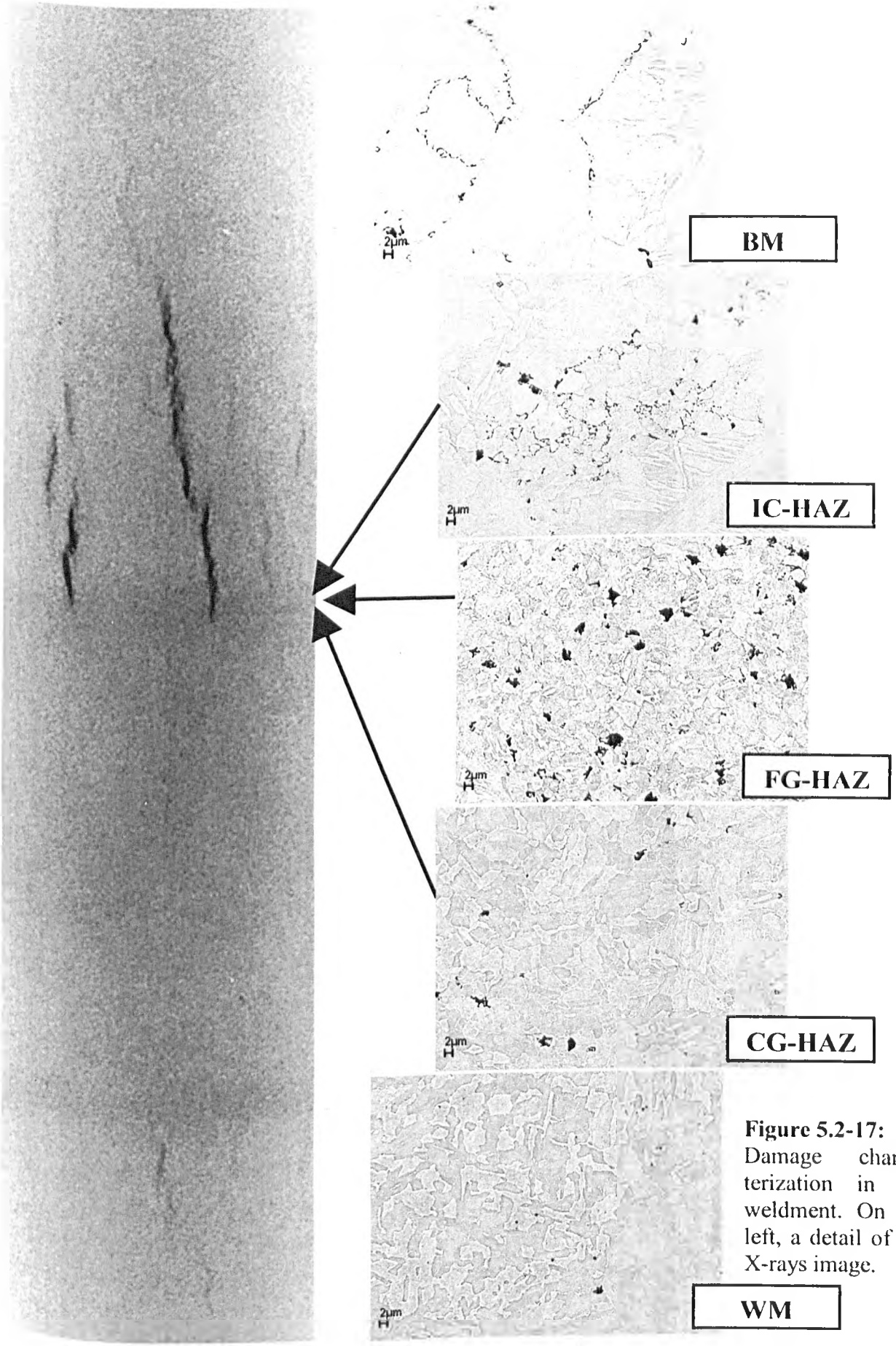

Figure 5.2-17: Damage characterization in the weldment. On the left, a detail of the X-rays image.

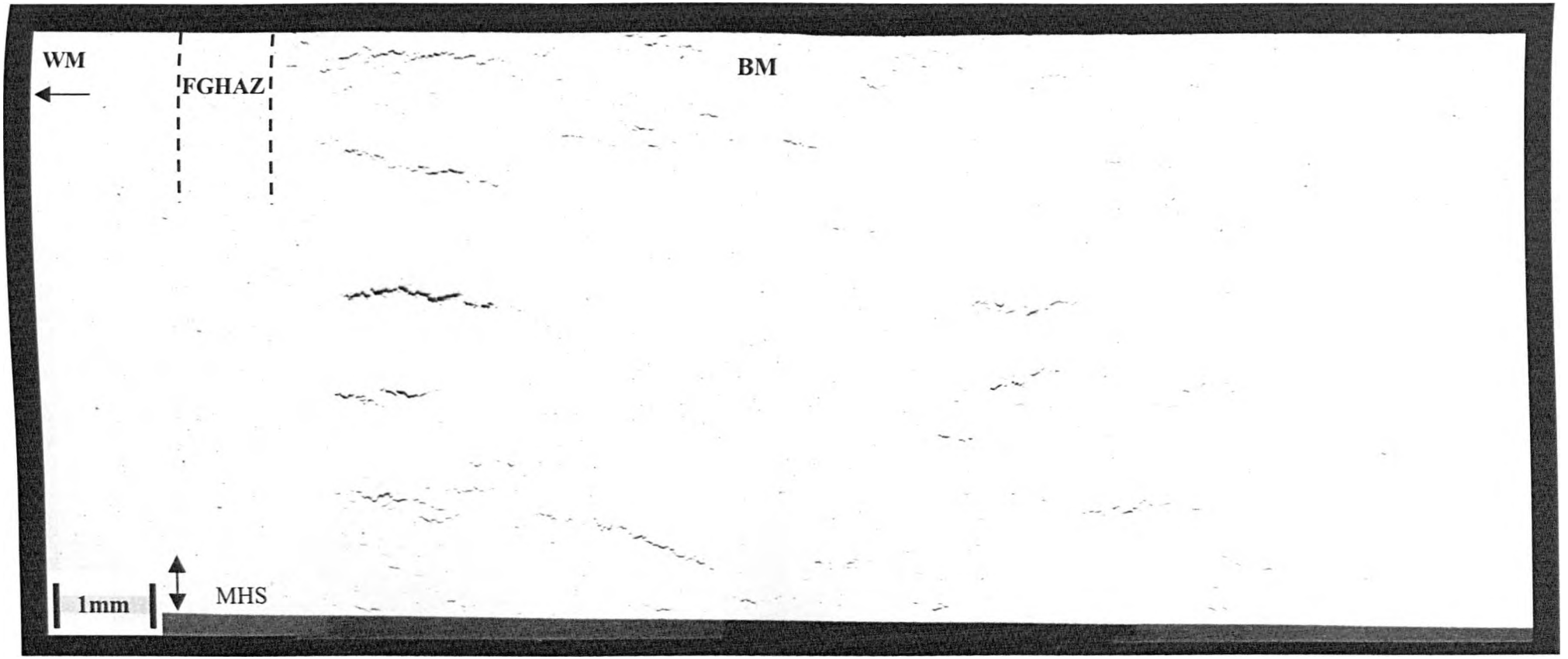

Figure 5.2-18a: Slice C. The image –taken before etching- shows part of the welded joint surface that had been directly exposed to hydrogen

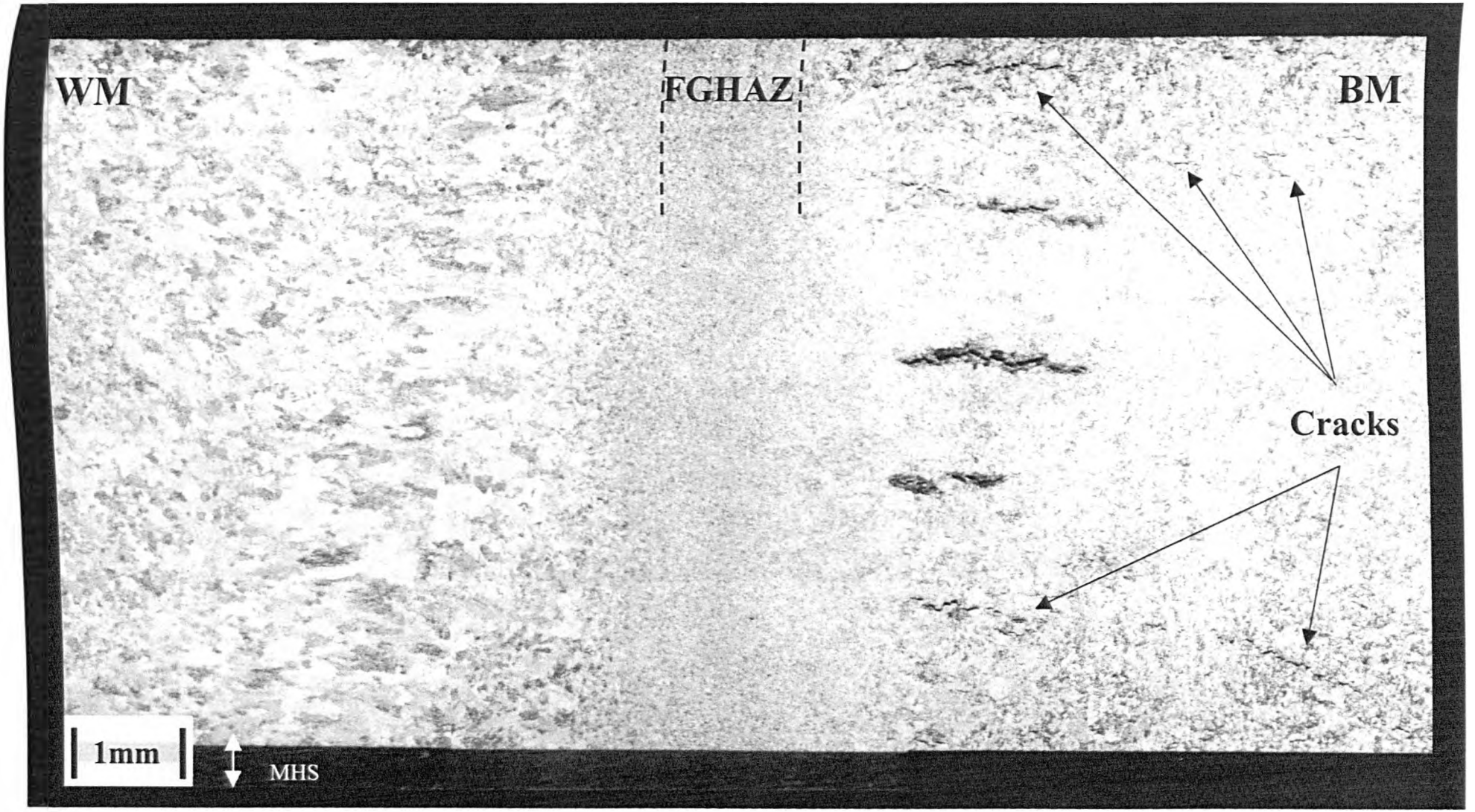

Figure 5.2-18b: Slice C. Image taken after etching with Nital 3%. It is evident that cracks are mainly present in the ICHAZ and in the part of the base metal close to it. No cracks are detected in the FGHAZ and in the weld metal (WM).

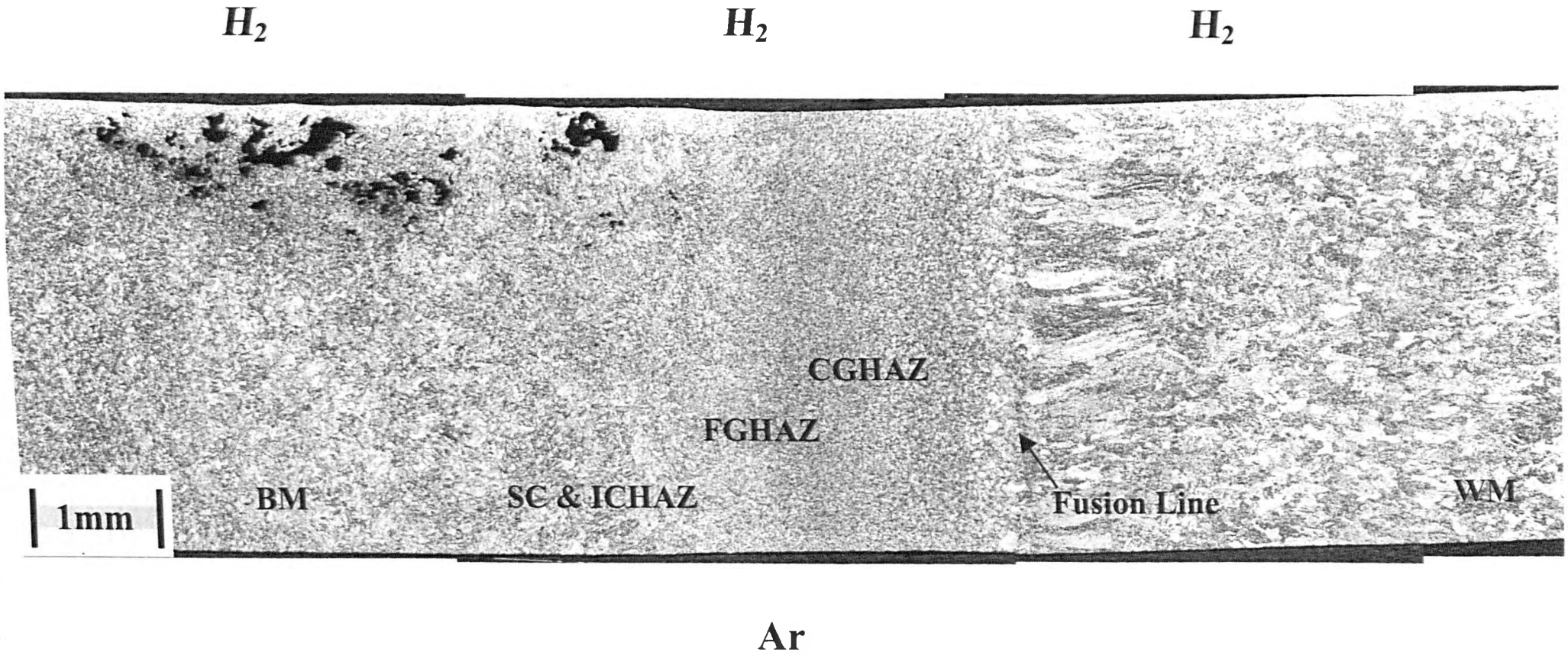

Figure 5.2-19: Slice A. It is a cross-section of the tube wall. In this case, the surface is perpendicular to the hoop stress direction. The top layer had been directly exposed to hydrogen; the bottom layer, instead, to argon.

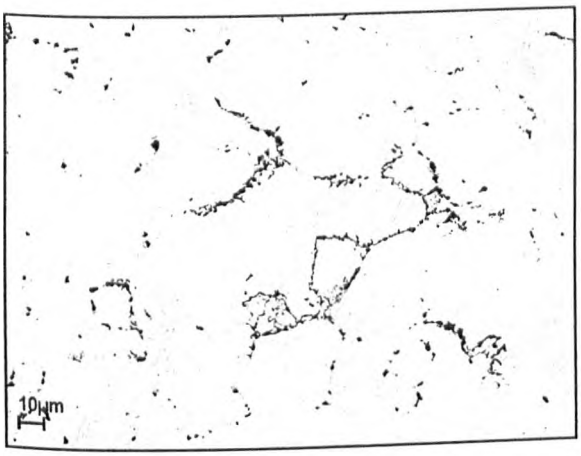

Fig. 20a: Base Metal

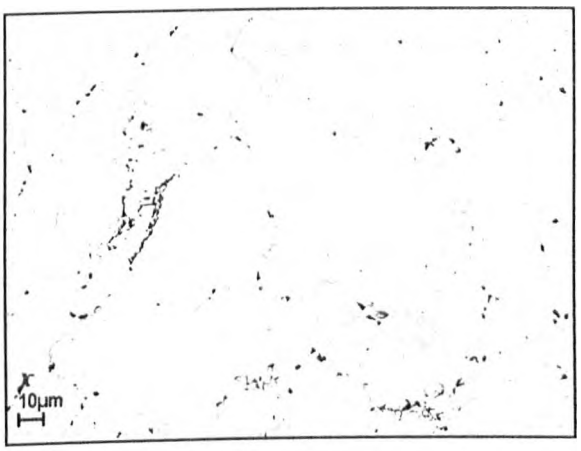

Fig. 20b: SCHAZ

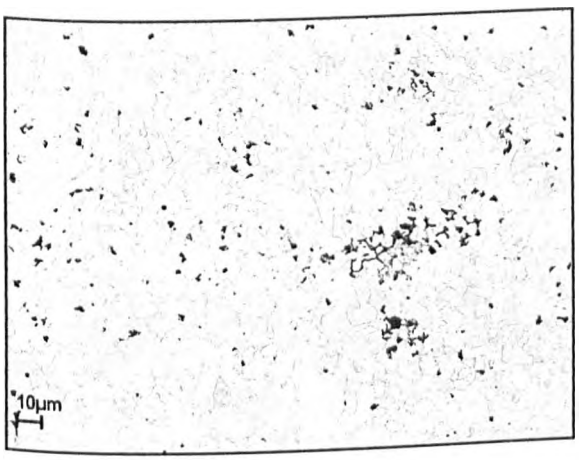

Fig. 20c: ICHAZ

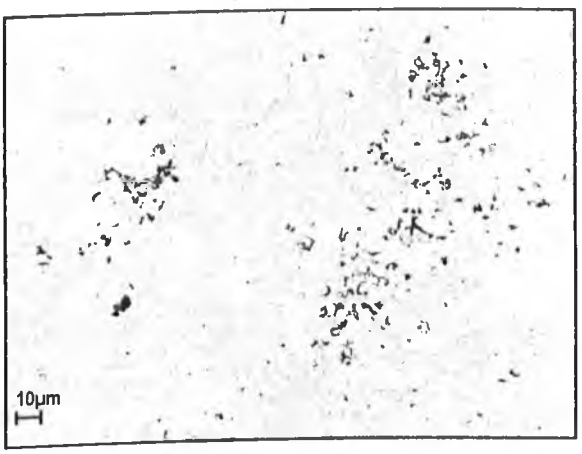

Fig. 20d: ICHAZ

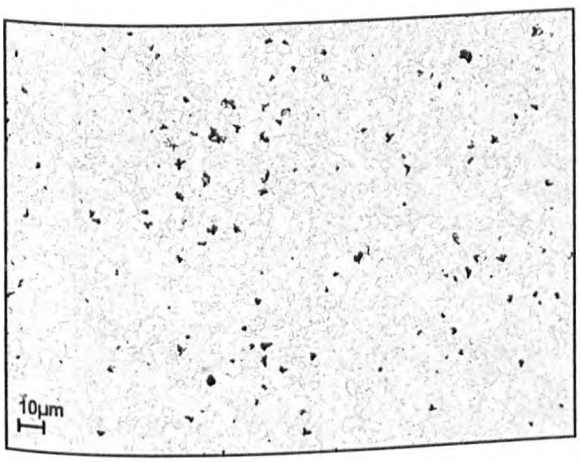

Fig. 20e: FGHAZ

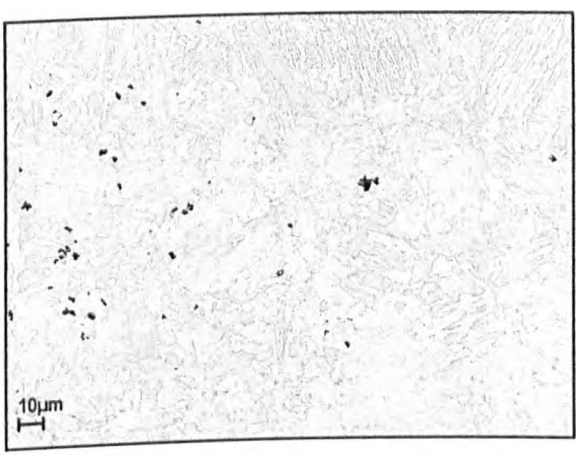

Fig. 20f: CGHAZ

Figure 5.2-20: Slice A. SEM micrographs, by means of back-scattered electrons, of the different metallurgical zones. The ICHAZ exhibit clusters of cavities.

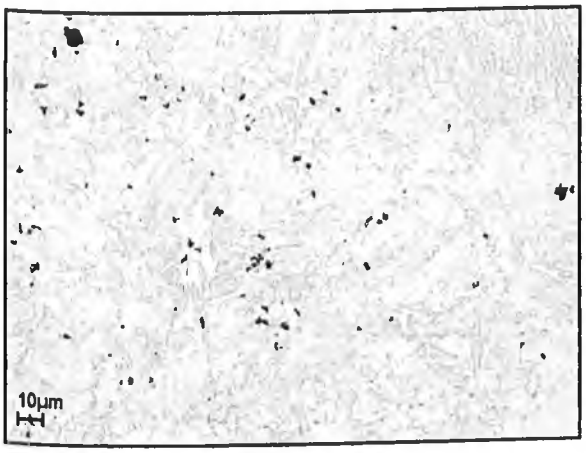

Fig. 20g: CGHAZ

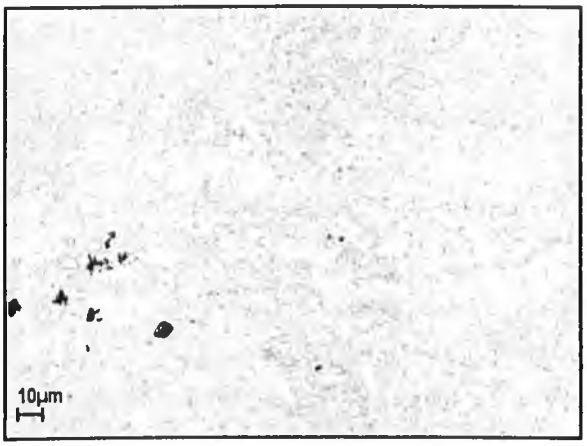

Fig. 20h: Weld Metal

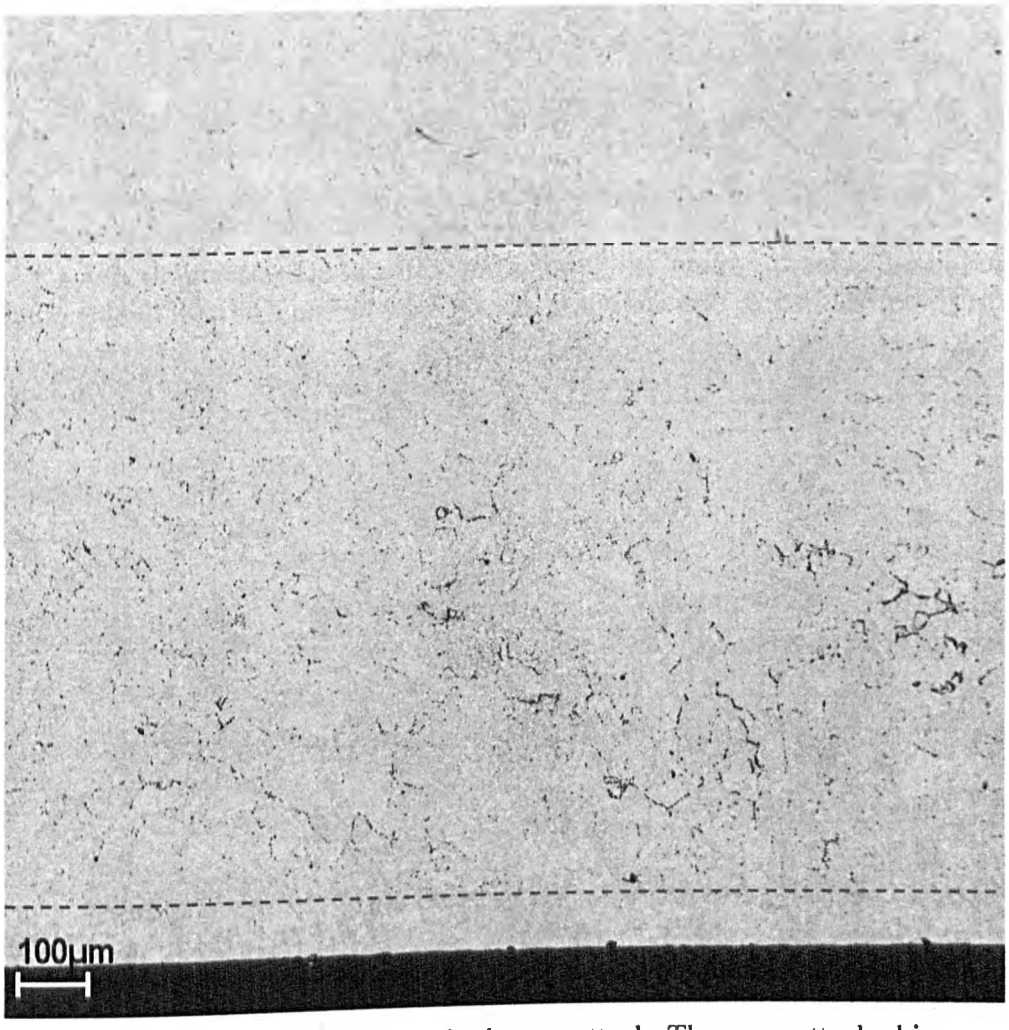

Figure 5.2-21: Gradient of the hydrogen attack. The zone attacked is about 800 µm thick, whilst the decarburised layer is about 100 µm thick.

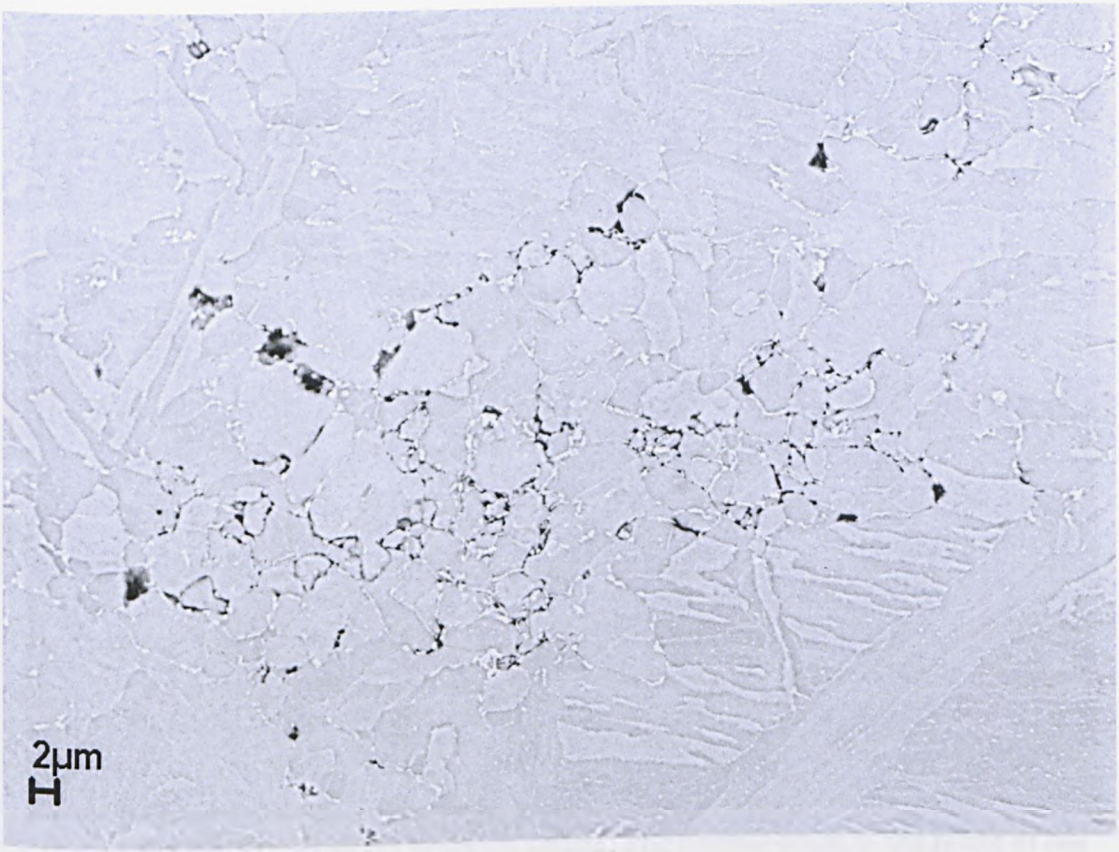

Figure 5.2-22: Slice B, ICHAZ. SEM micrographs exhibit a typical feature of the damage: sub-micron sized cavities mainly at interfaces (e.g. carbide/matrix)

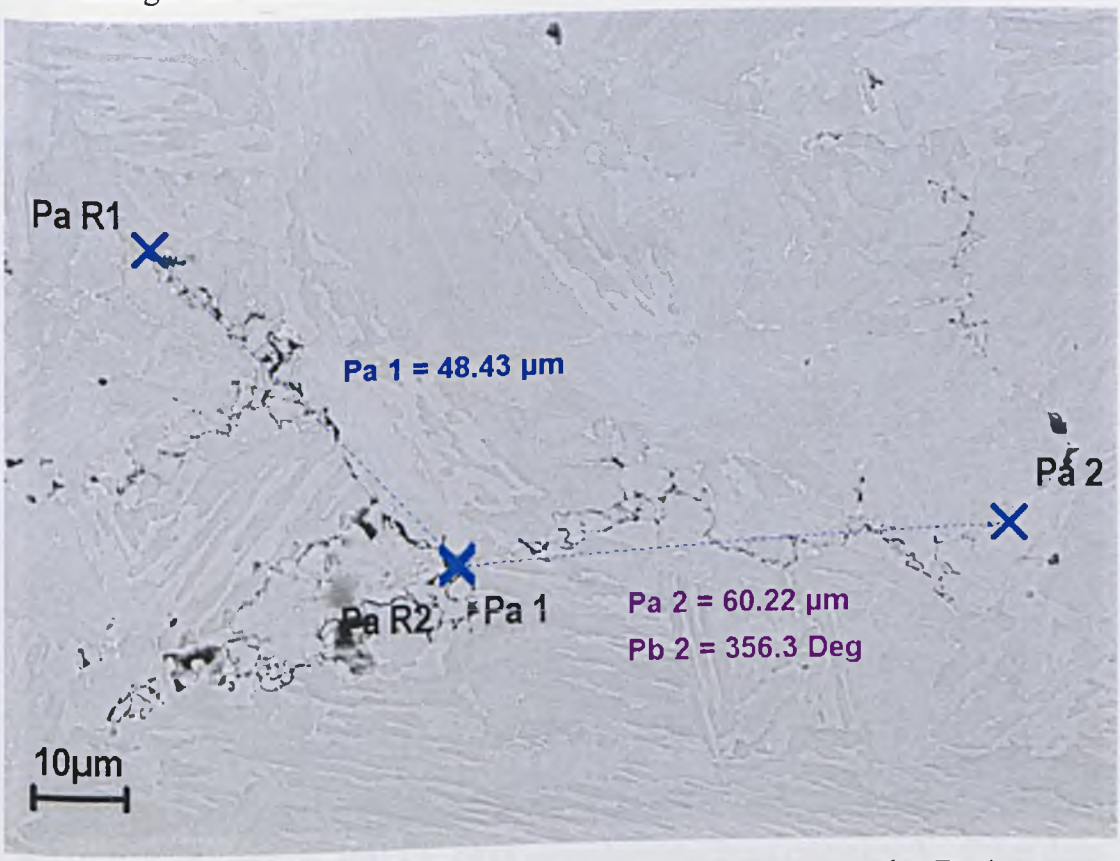

Figure 5.2-23: Slice B. ICHAZ. Damage feature: long narrow cracks. For instance, the crack branch considered is longer than 100µm.

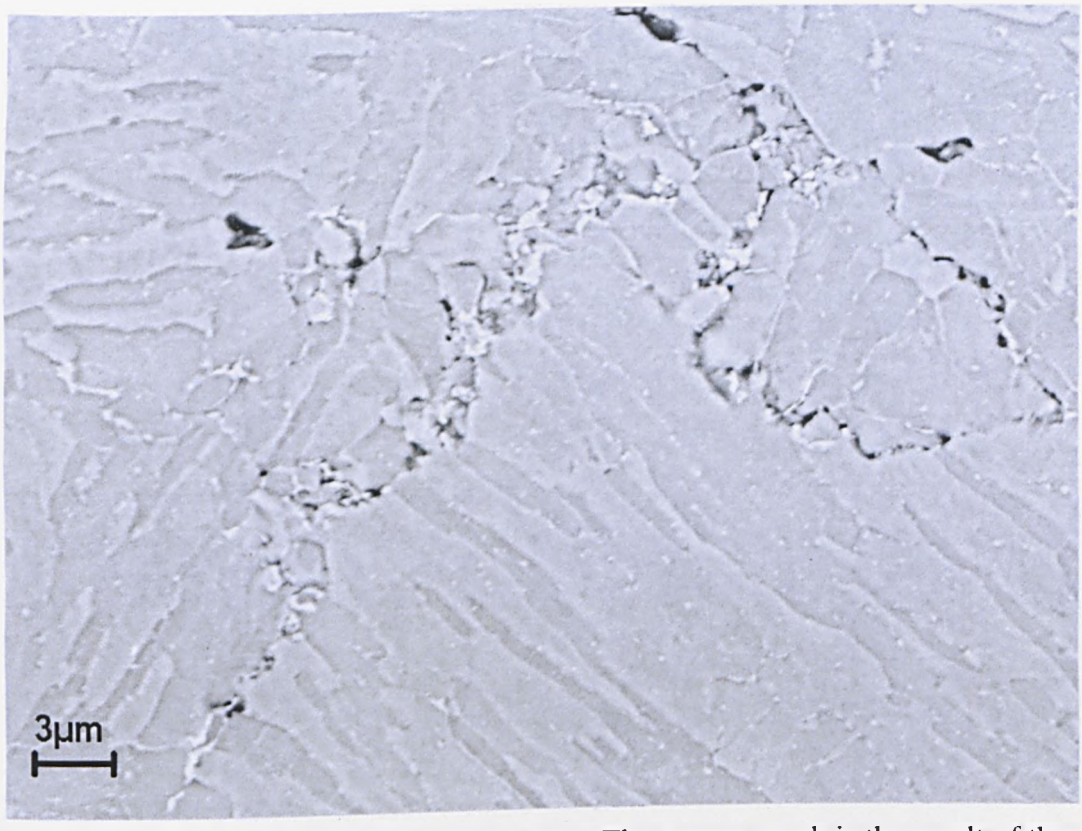

Figure 5.2-24: Detail of the previous image. The narrow crack is the result of the linking of small cavities. Again, the cavities form mainly close to carbides.

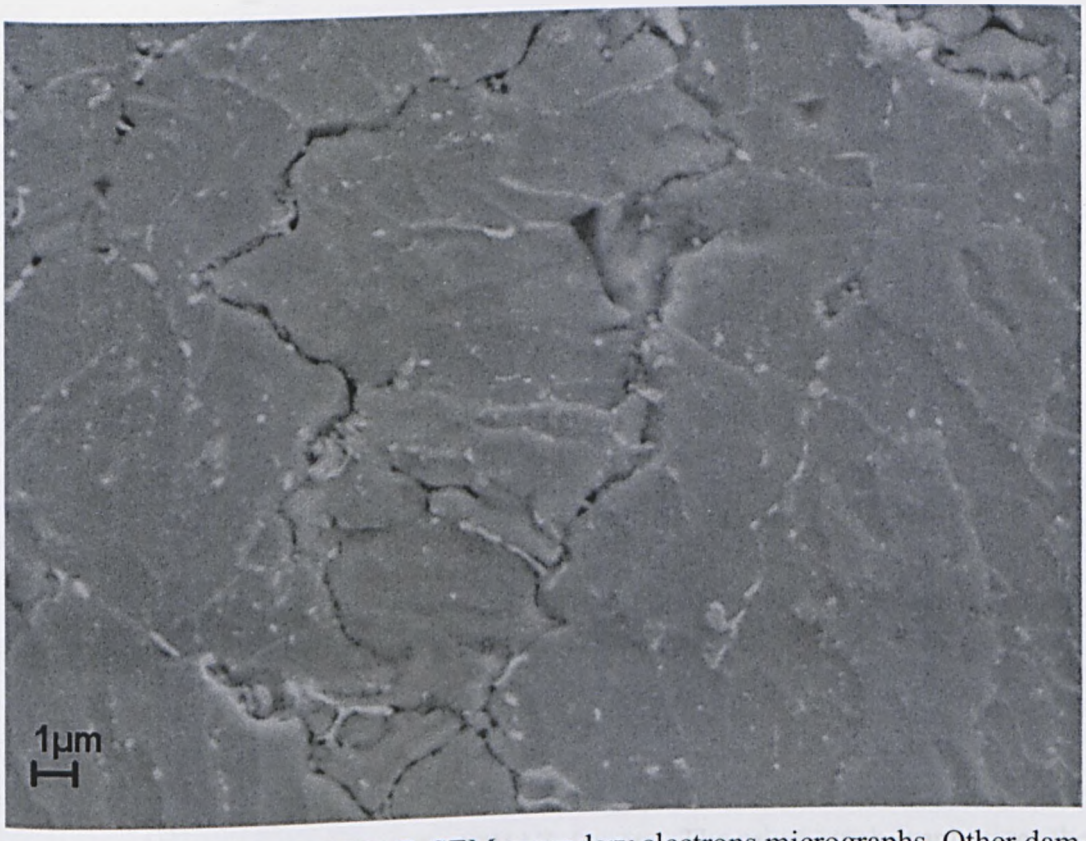

Figure 5.2-25a: Slice B. ICHAZ. SEM secondary electrons micrographs. Other damage features: the narrow cracks are due to cavities link-up. Presence of long carbides.

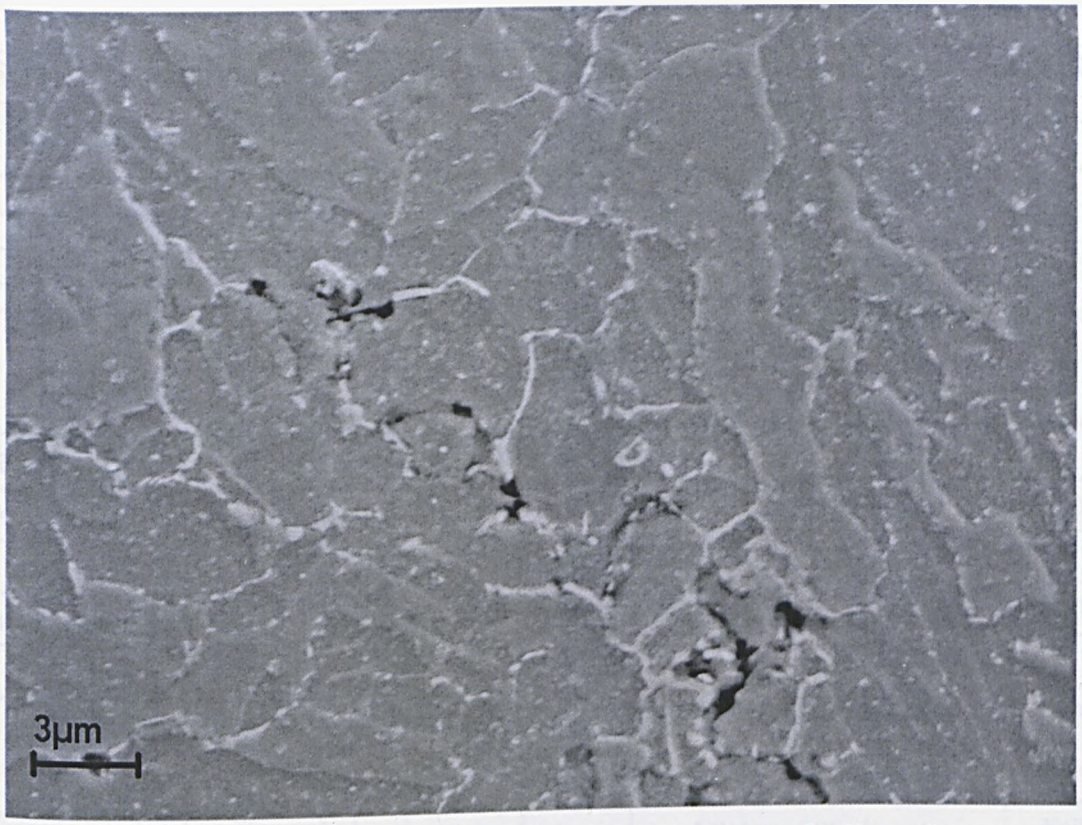

Figure 5.2-25b: Slice B.ICHAZ. The long carbides seem to facilitate the narrow cracks formation.

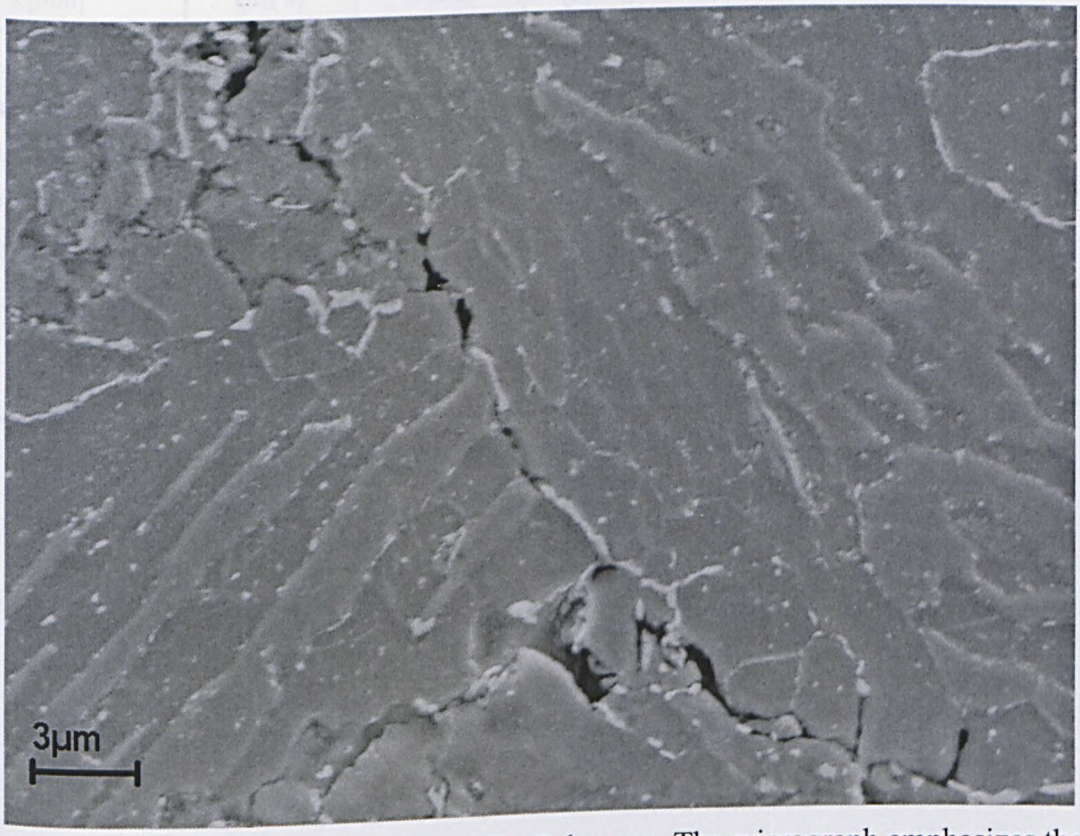

Figure 5.2-25c: Other detail of the ICHAZ damage. The micrograph emphasizes the role of the long carbides in the formation of narrow cracks. (SEM Second. Electrons)

Stress (MPa)	Temperature (°C)	Environment	Lifetime (h)	Rupture Strain (%)	RA (%)	MCR (%/h)
100	570	Air	4646	8	28	9E-4
100	600	Air	560	14	48	8E-3
100	600	Hydrogen	182	4	9	15E-3

Table 5.2-1: Summary of the uniaxial creep test results on the standard 2.25Cr-1Mo welded joint

St. 2.25Cr-1Mo		C	Si	Mn	P	S	Cr	Mo	Ni	Al	Cu	Sn
BM	Nom.	0.14	0.18	0.59	0.004	0.003	2.25	1.05	0.14	0.01	0.07	0.006
	EPMA	-	0.18	0.62	-	-	2.09		0.13	-	0.08	-
Cons.	Nom.	0.10	.11	0.75	.009	0.002	2.37	1.01	0.11	-	-	0.002
	EPMA	-	0.11	0.77	-	-	2.03	1.09	0.14	-	0.09	-

Table 5.2-2: Nominal composition of the test steel and consumable compared with EPMA.

Sample Geometry* [mm]		Mean Diameter Hoop stress (MPa)	Skeletal Point Von Mises stress (MPa)	Test time [h]	Minimum Strain-rate [s^{-1}]			Failure Hoop strain** %
					Top	Centre	Bottom	
t =	3.8	100	86.5	3230	8×10^{-10}	2.7×10^{-9}	8×10^{-10}	4.3
Dmax =	50.4							
D_0 =	46.6							
D_I =	38.9							
$(D_o+D_i)/2$=	42.8							
L =	167.8							
l =	73.5							
r =	7.7							

Table 5.2-3: Sample geometry, stress conditions and creep results

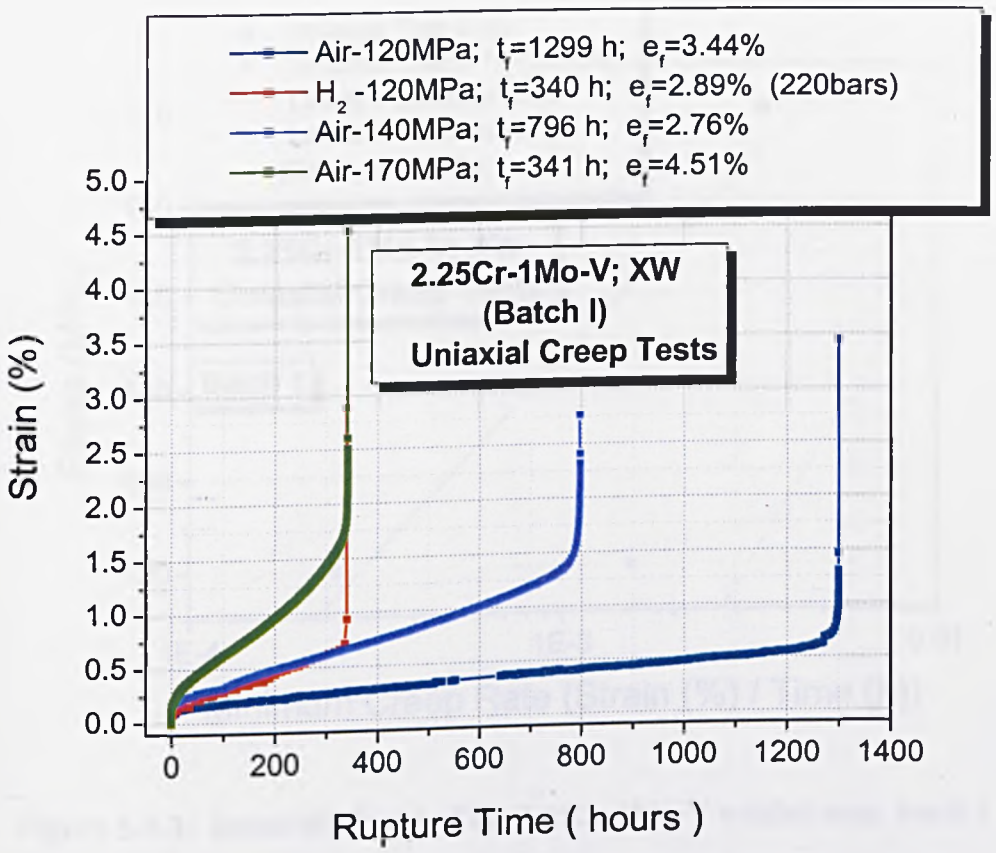

Figure 5.3-1: Uniaxial creep curves of the 2.25Cr-1Mo-V welded joint, batch 1.

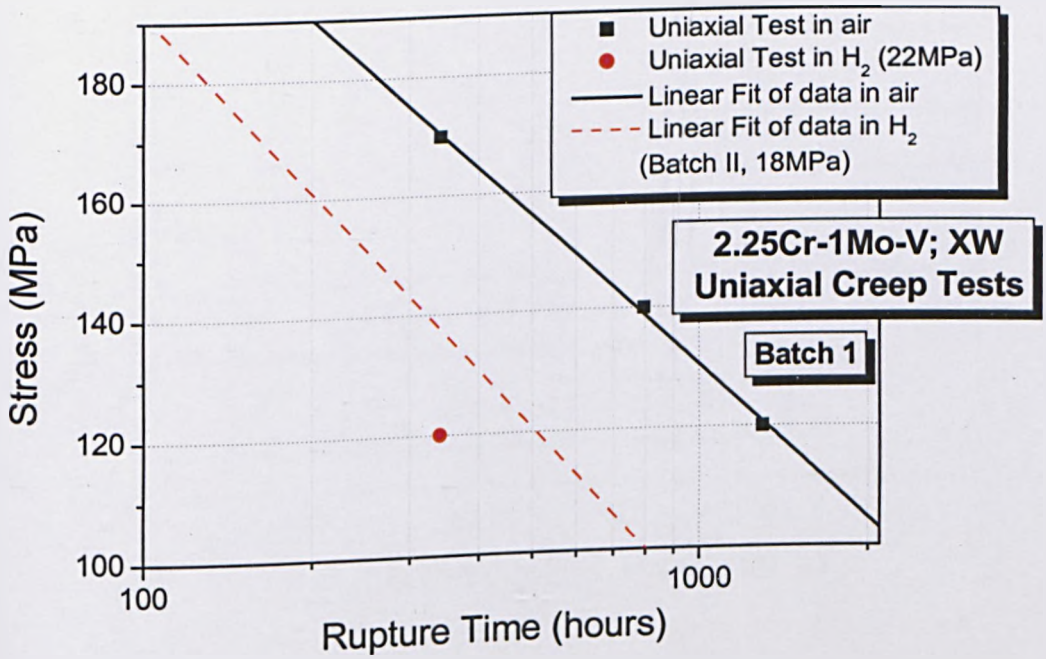

Figure 5.3-2: Stress-rupture curves of the 2.25Cr-1Mo-V welded joint, batch 1.

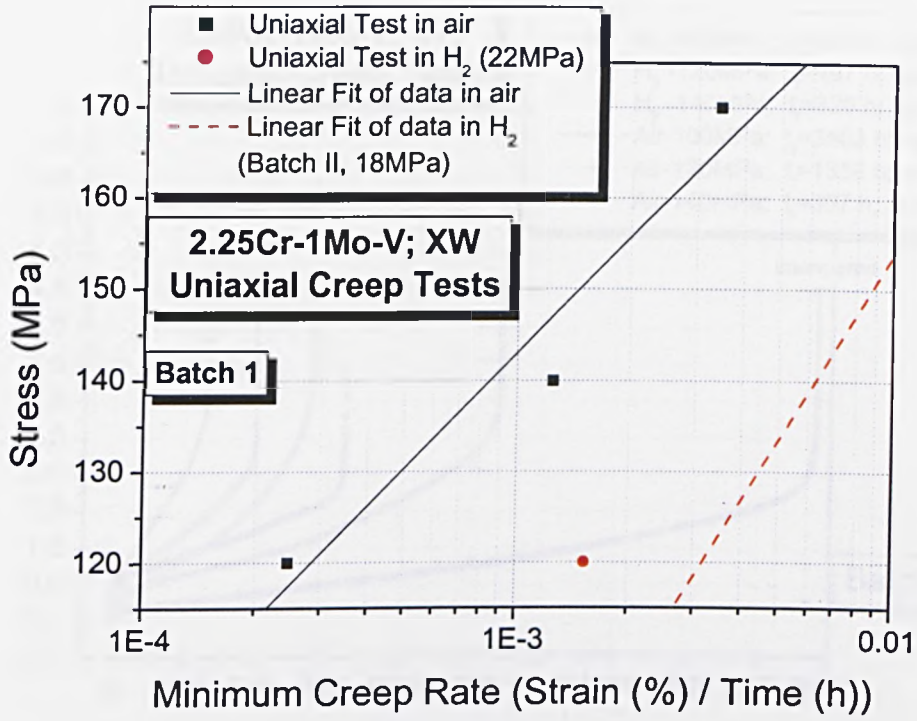

Figure 5.3-3: Stress/MCR plot of the 2.25Cr-1Mo-V welded joint, batch 1.

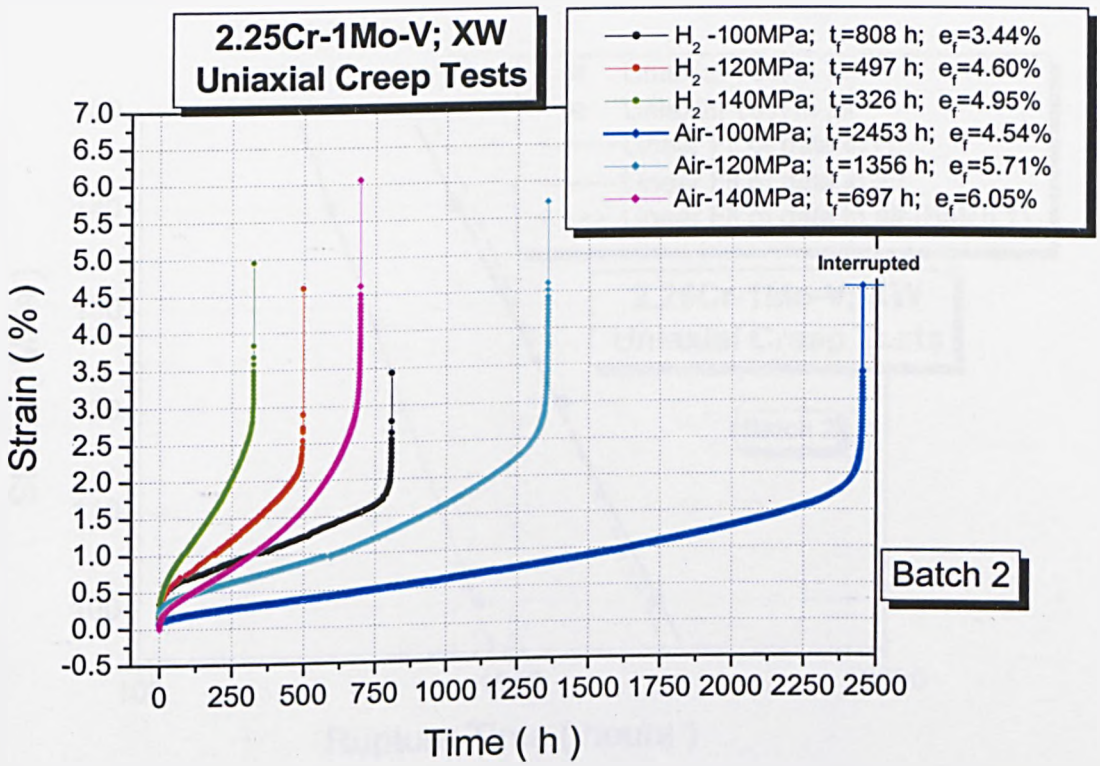

Figure 5.3-4: Uniaxial creep curves of the 2.25Cr-1Mo-V welded joint, batch 2.

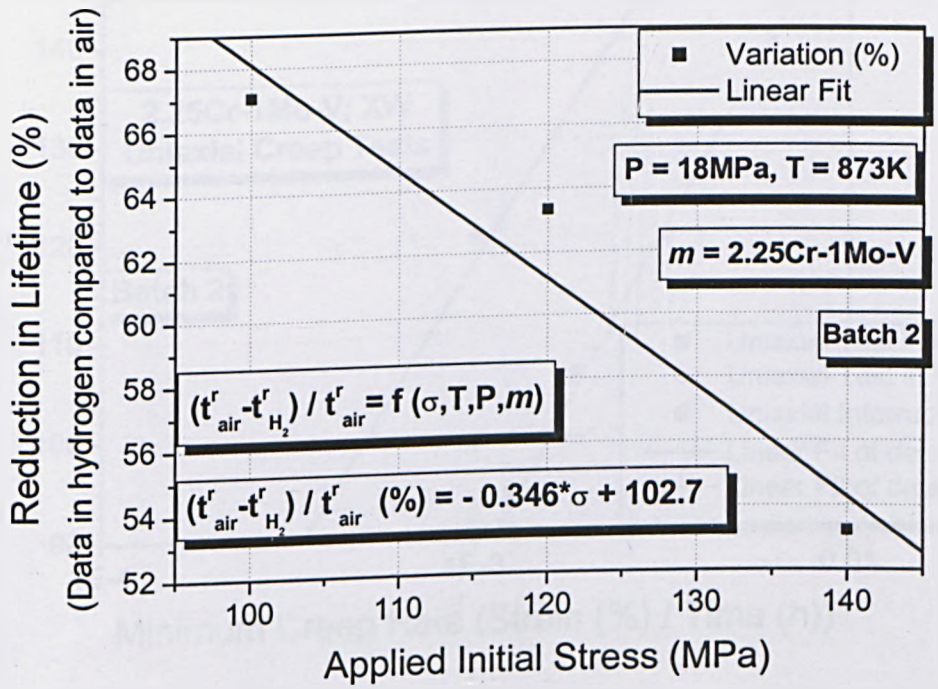

Figure 5.3-5: Variation of lifetime, as function of the applied initial stress, of the 2.25Cr-1Mo-V welded joint, batch 2.

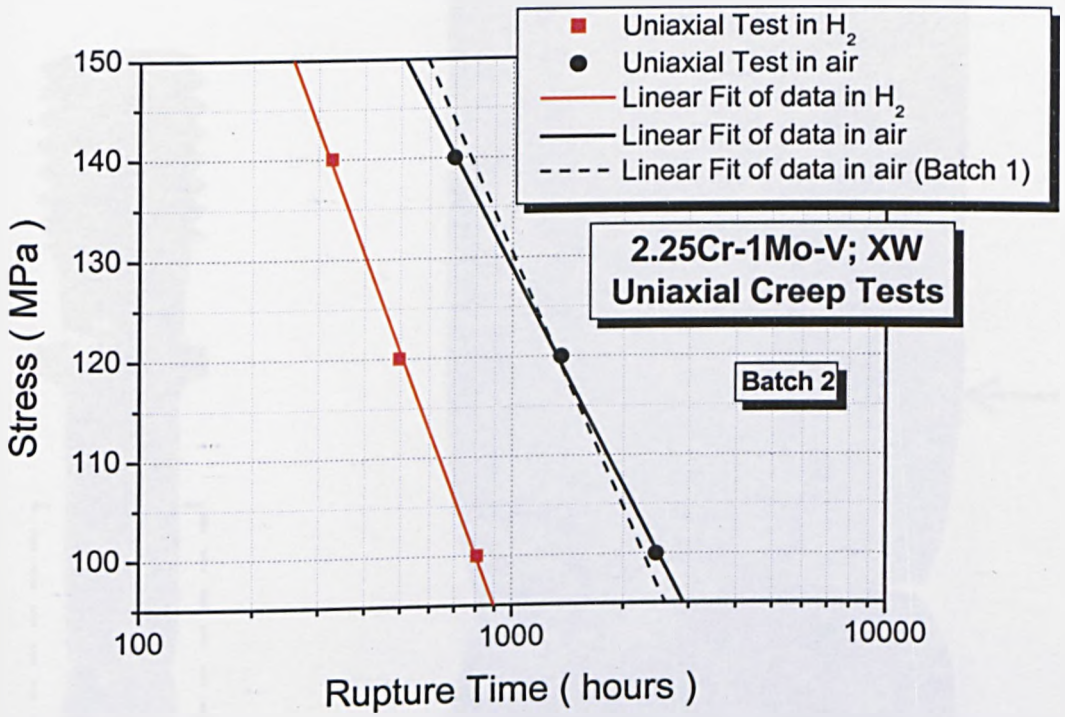

Figure 5.3-6: Uniaxial stress/rupture plot of the 2.25Cr-1Mo-V welded joint, batch 2.

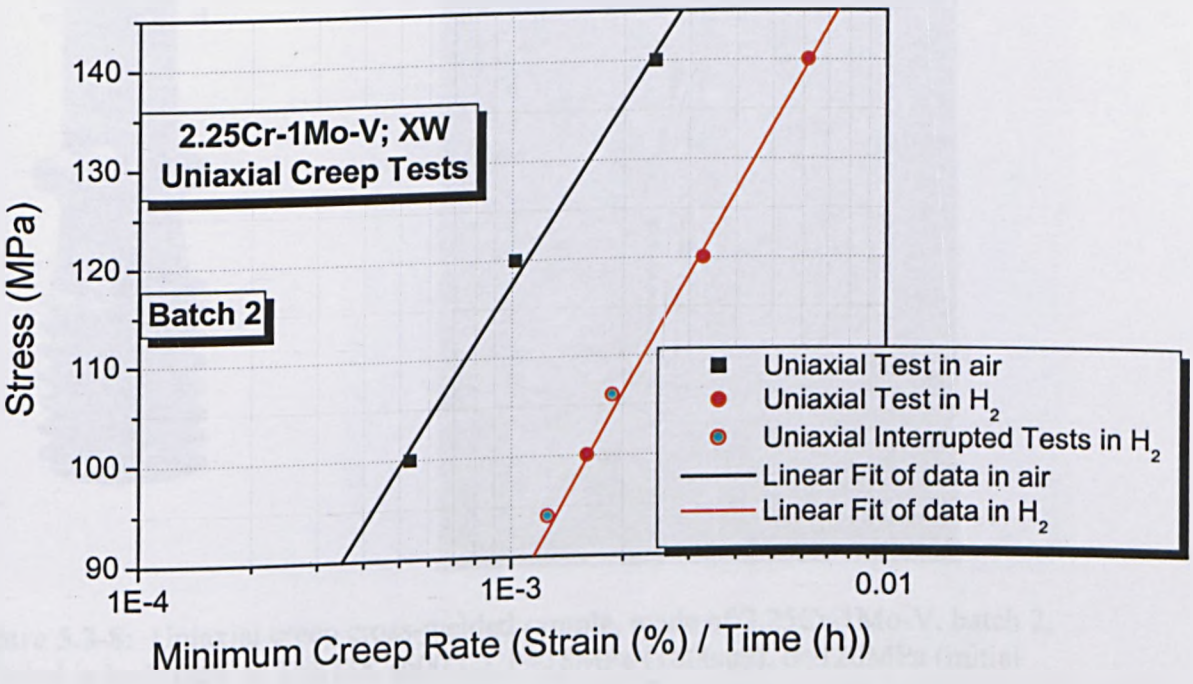

Figure 5.3-7: Uniaxial Stress/MCR plot of the 2.25Cr-1Mo-V welded joint, batch 2.

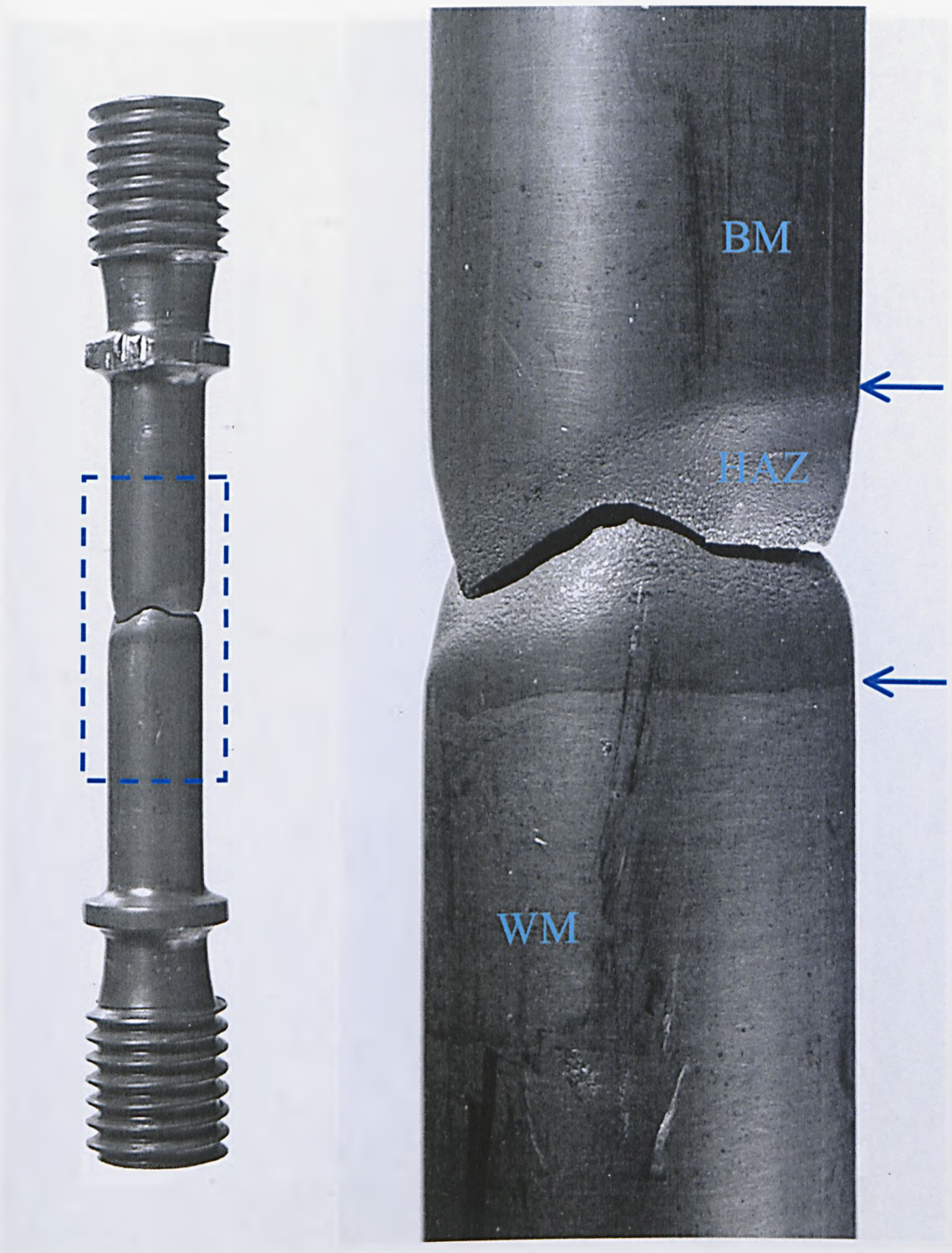

Figure 5.3-8: Uniaxial creep cross-welded sample, made of 2.25Cr-1Mo-V, batch 2, tested in hydrogen, at T=873K (600°C), P=18MPa (180bars), σ=120MPa (initial stress).

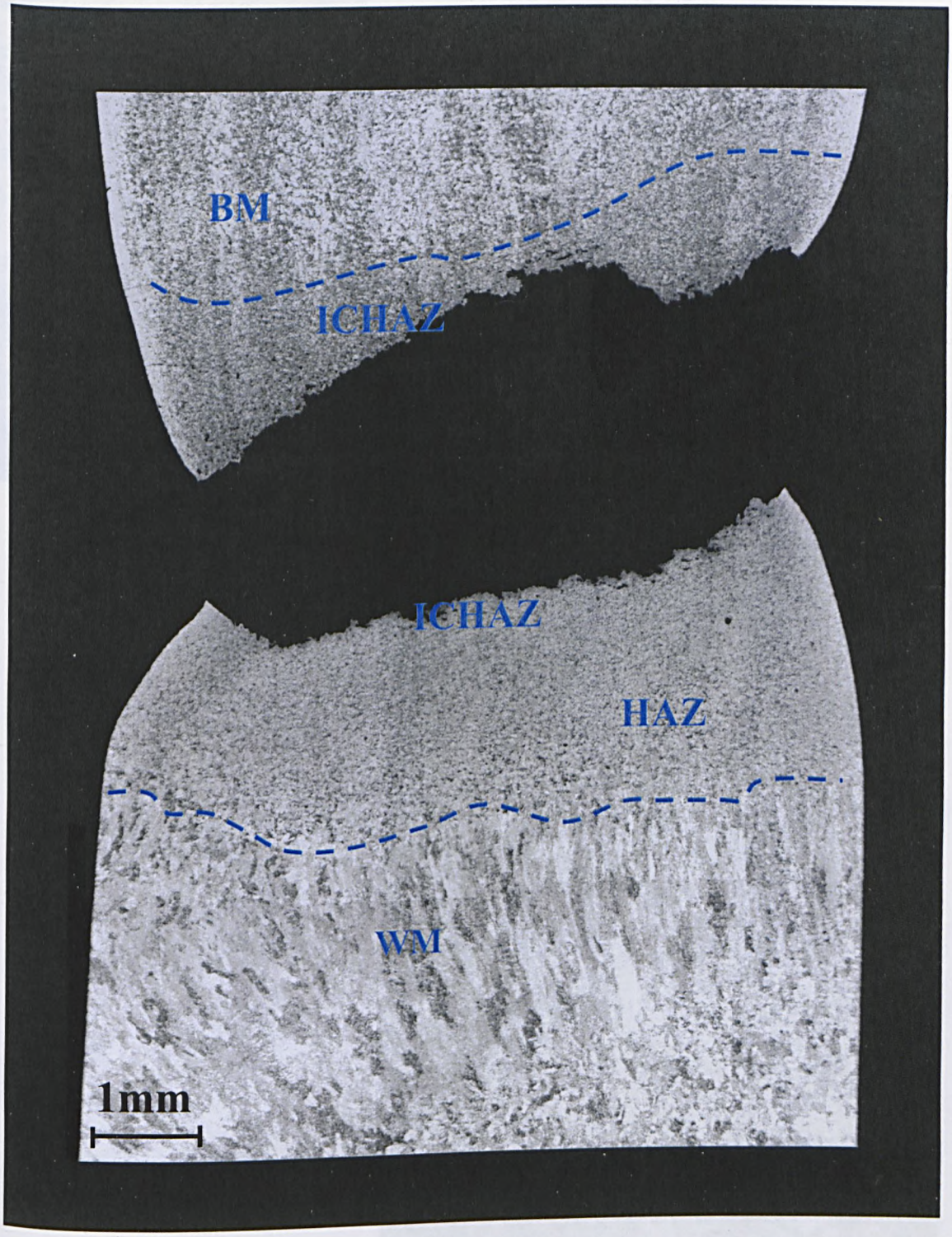

Figure 5.3-9: Cross-section of the uniaxial creep cross-welded sample, made of 2.25Cr-1Mo-V, batch 2, tested in hydrogen, at T=873K (600°C), P=18MPa (180bars), σ=120MPa (applied initial stress). The surface had been etched with Nital 3%.

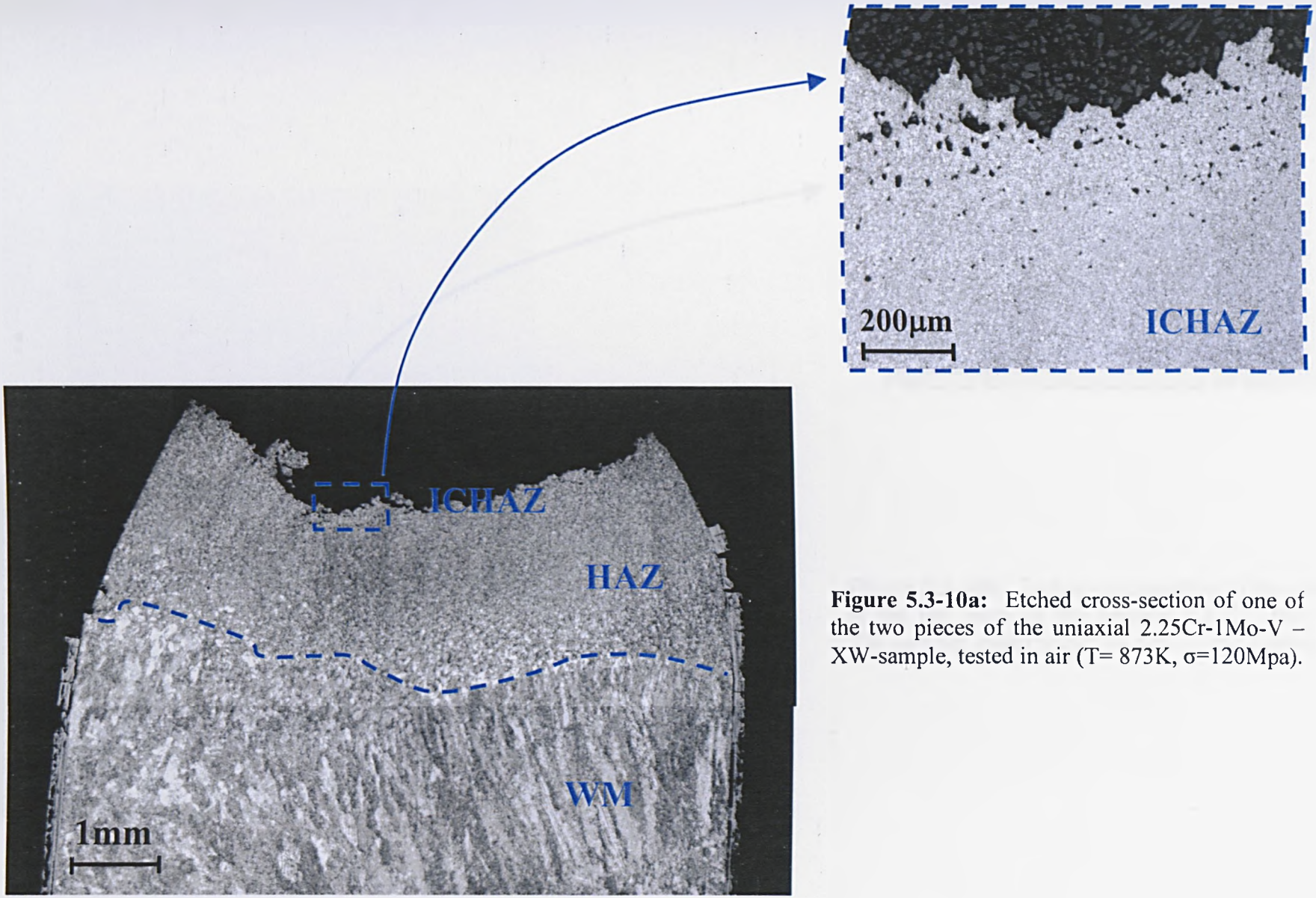

Figure 5.3-10a: Etched cross-section of one of the two pieces of the uniaxial 2.25Cr-1Mo-V – XW-sample, tested in air (T= 873K, σ=120Mpa).

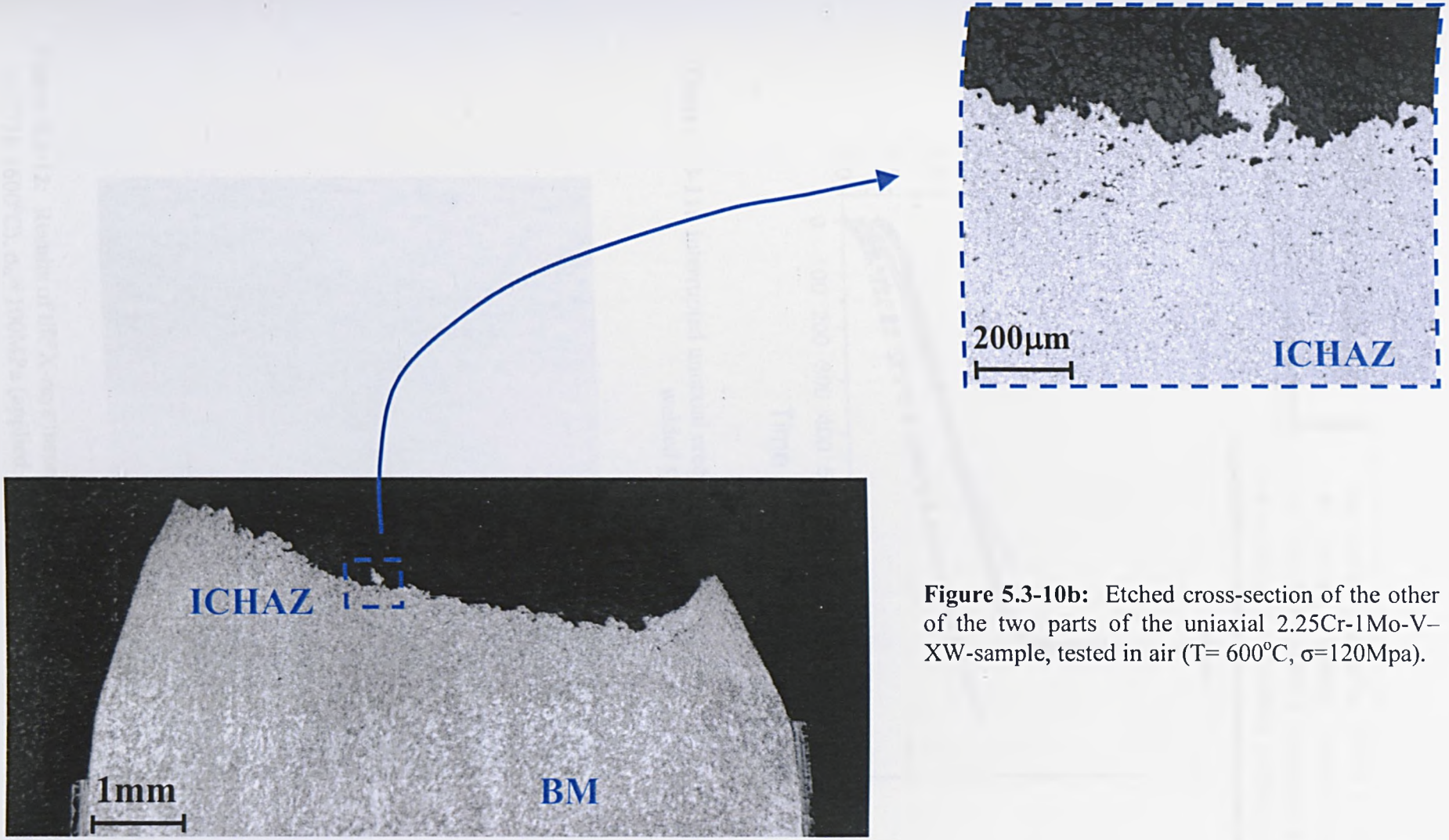

Figure 5.3-10b: Etched cross-section of the other of the two parts of the uniaxial 2.25Cr-1Mo-V–XW-sample, tested in air (T= 600°C, σ=120Mpa).

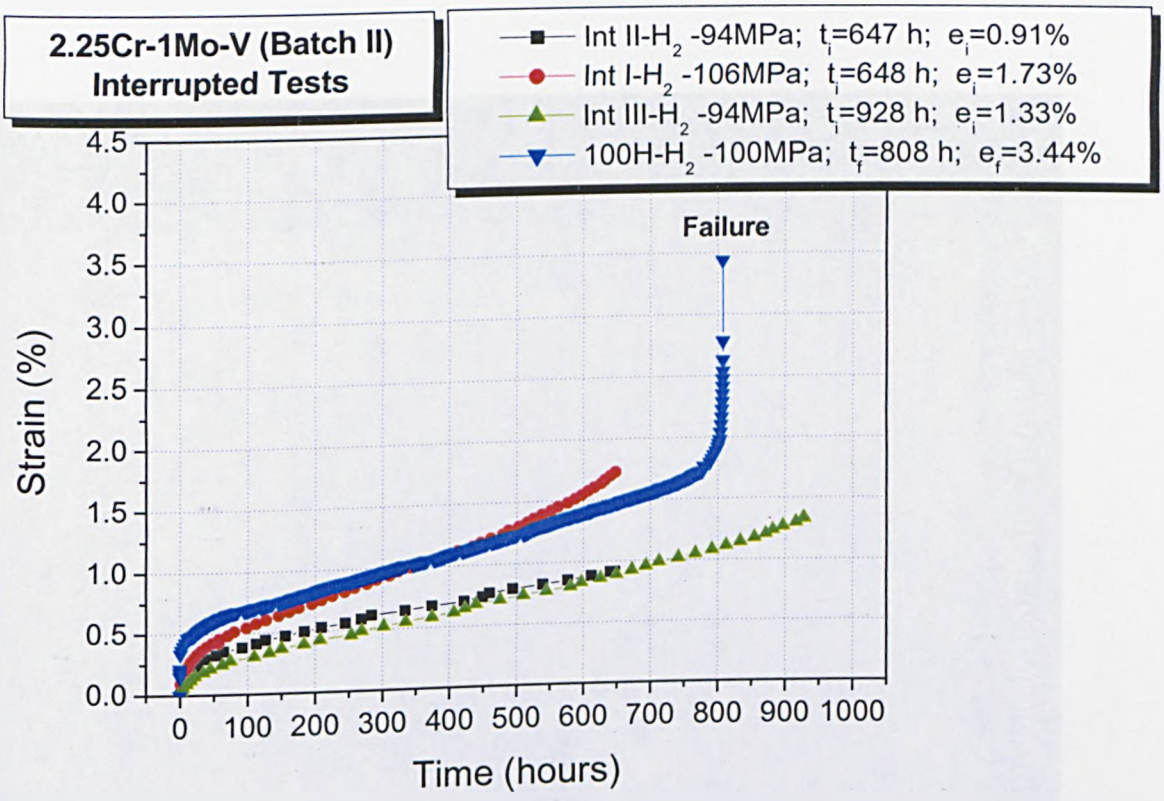

Figure 5.3-11: Interrupted uniaxial creep tests on the V-mod. 2.25Cr-1Mo cross-welded specimens

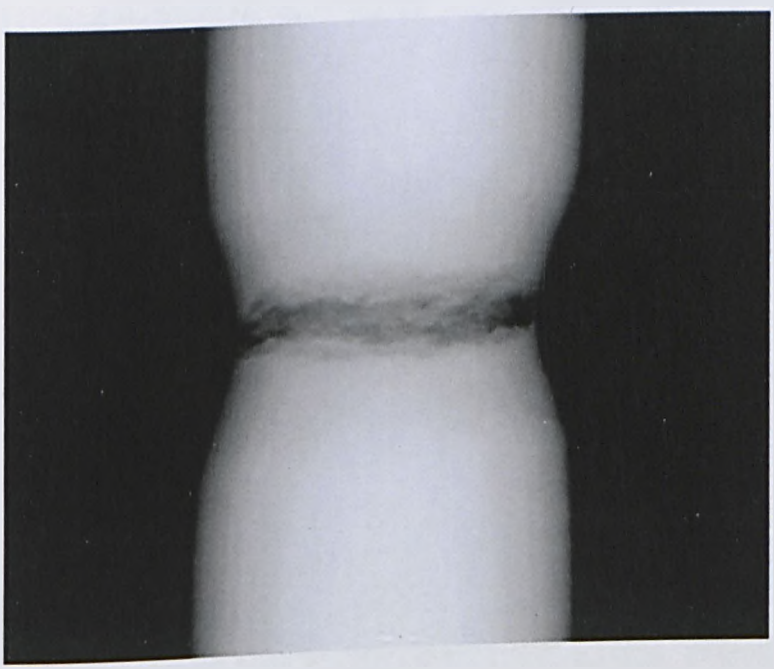

Figure 5.3-12: Results of the X-rays inspection carried out on the sample tested in air at 873K (600°C), σ_o= 100MPa (applied initial stress), t=2453h (Interrupted test).

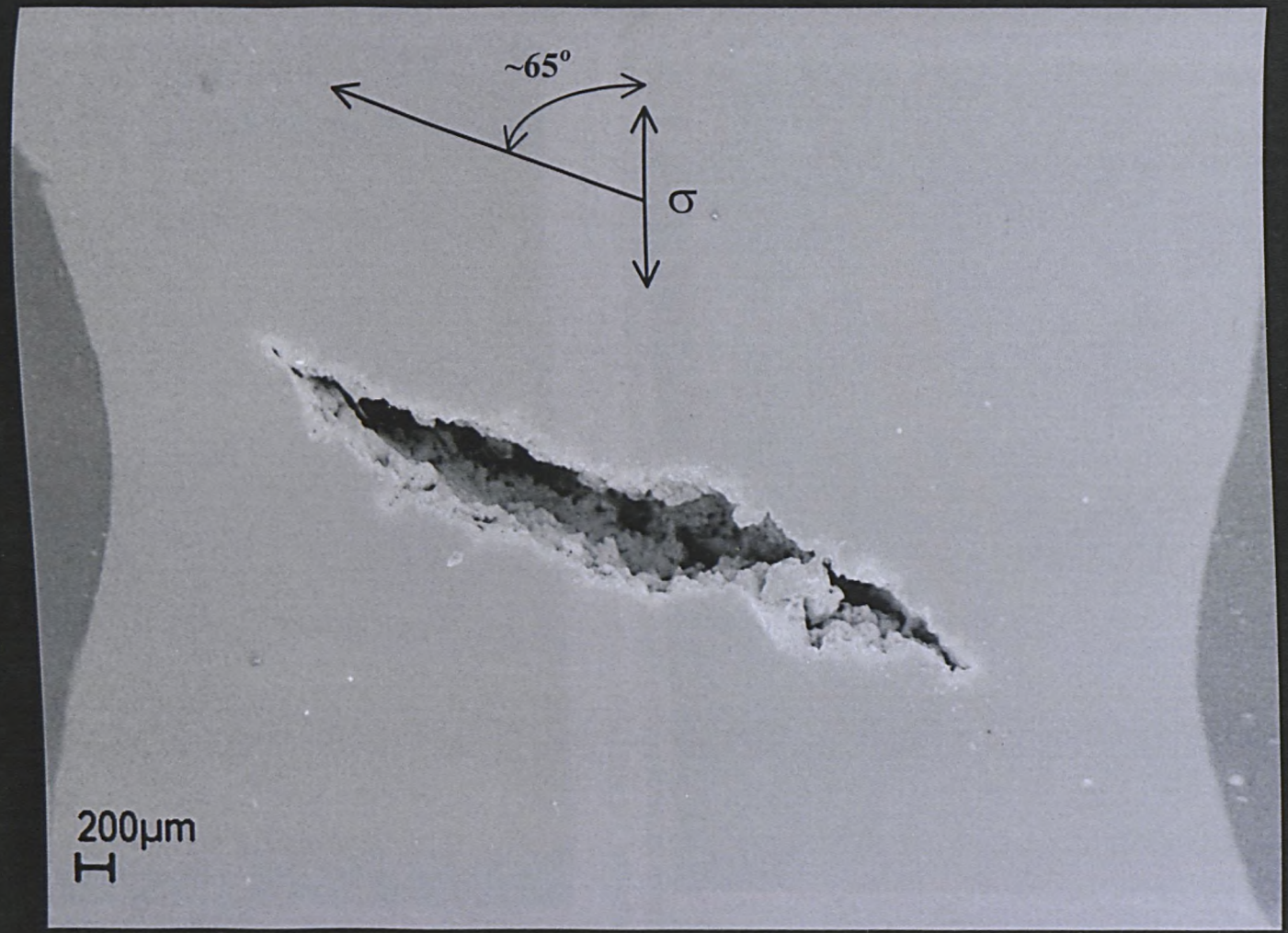

Figure 5.3-13: SEM image of the fracture of the sample tested in air at 873K (σ_o= 100MPa, t=2453h)

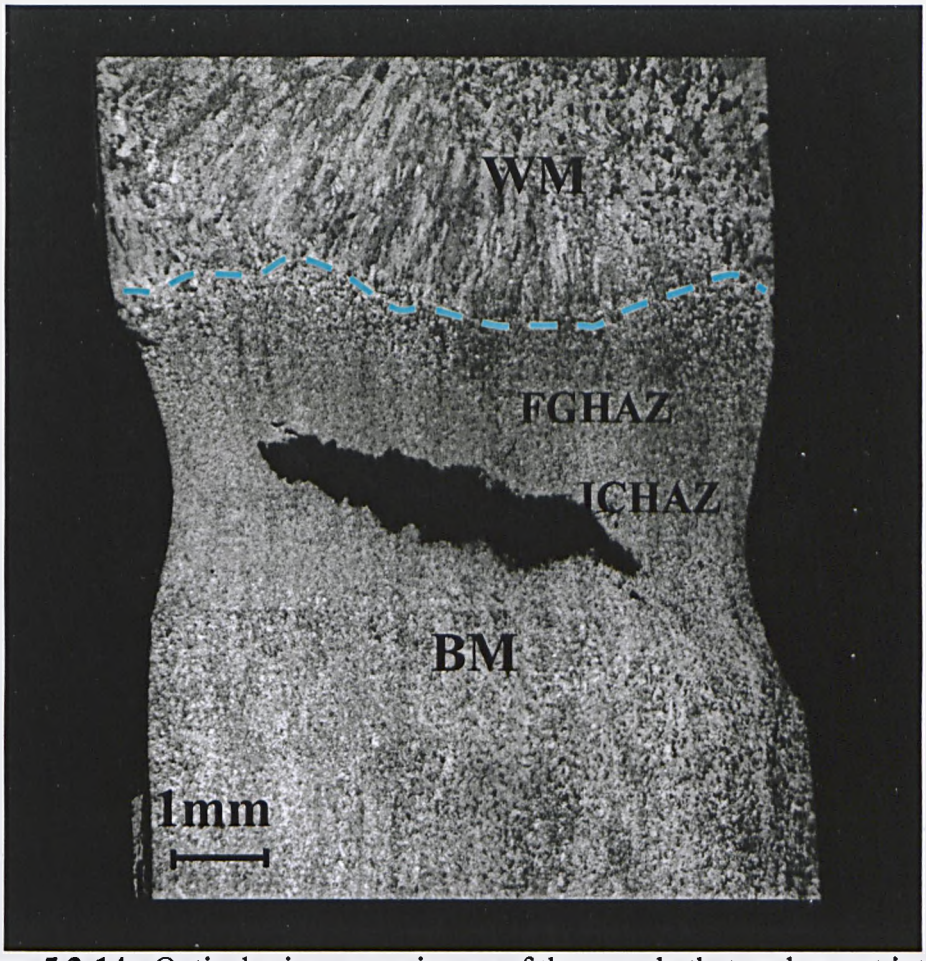

Figure 5.3-14: Optical microscope image of the sample that underwent interrupted testing in air at 873K (600°C), σ_o= 100MPa (applied initial stress), t=2453h.

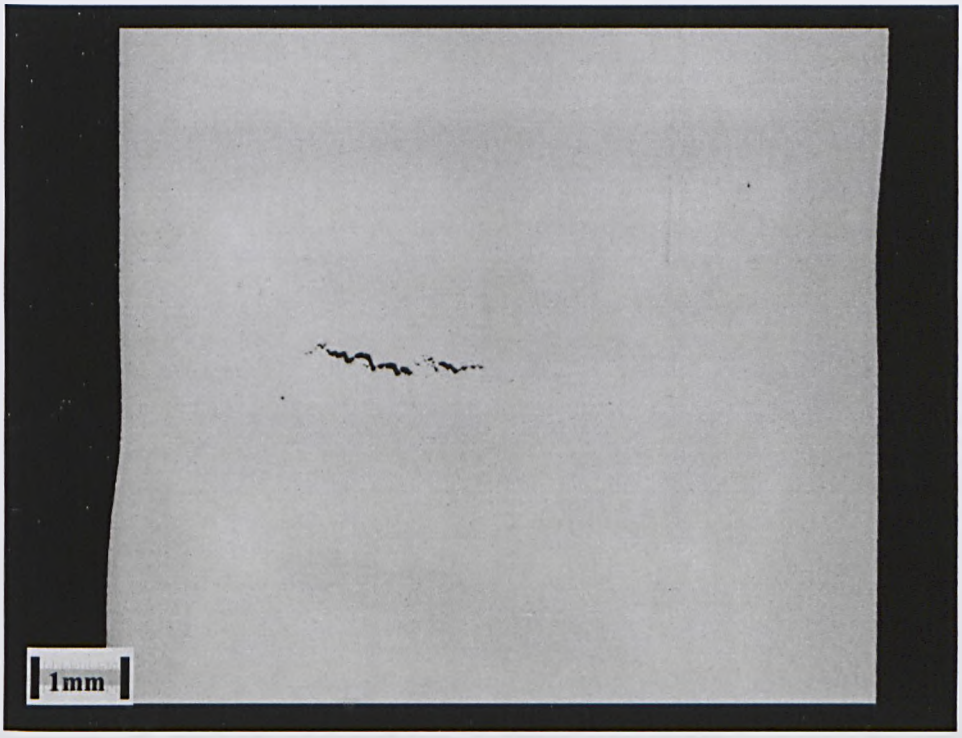

Figure 5.3-15: Optical microscope image of the sample that underwent interrupted testing in H_2 at 873K, σ_o= 106MPa (applied initial stress), t=647h.

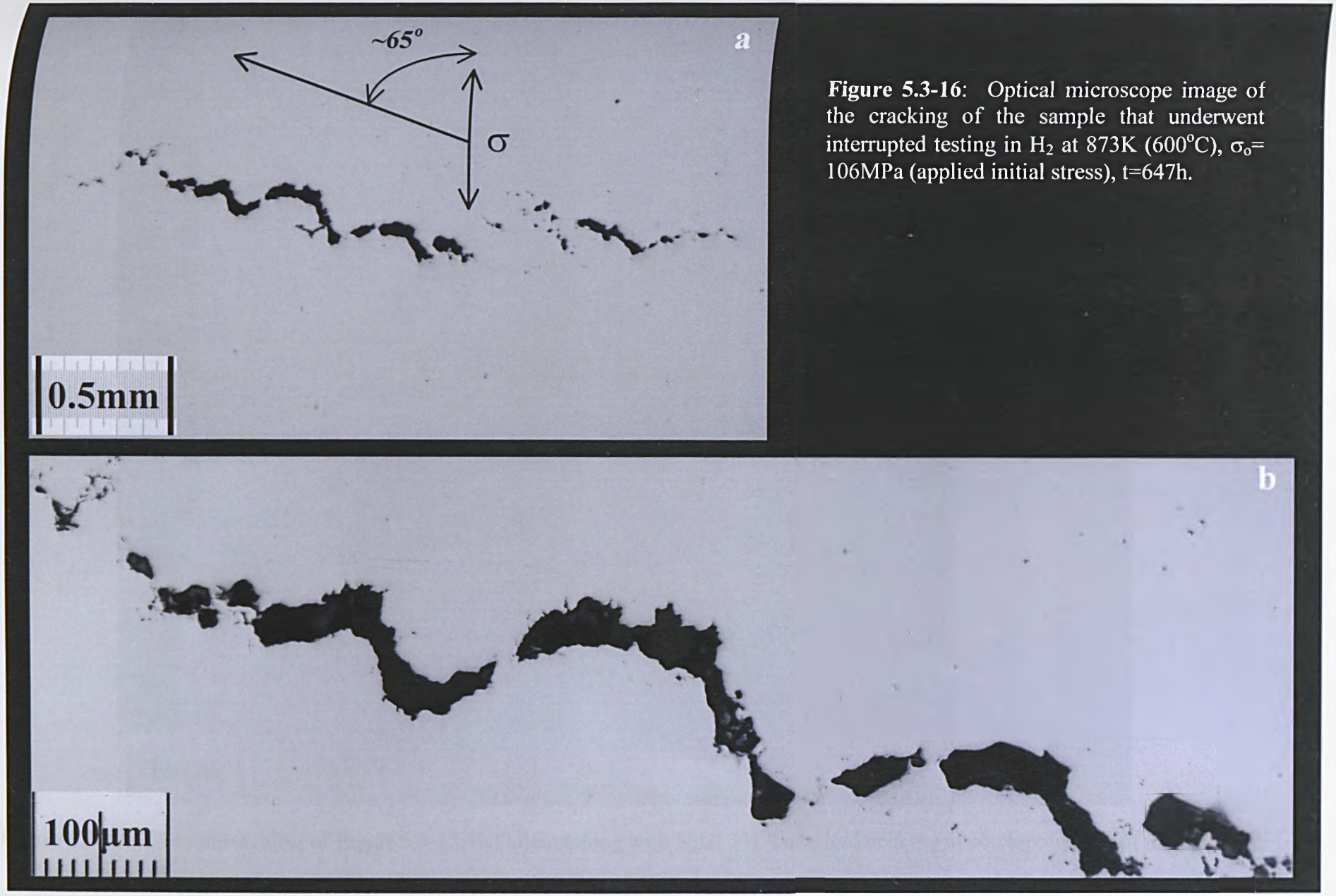

Figure 5.3-16: Optical microscope image of the cracking of the sample that underwent interrupted testing in H_2 at 873K (600°C), σ_o= 106MPa (applied initial stress), t=647h.

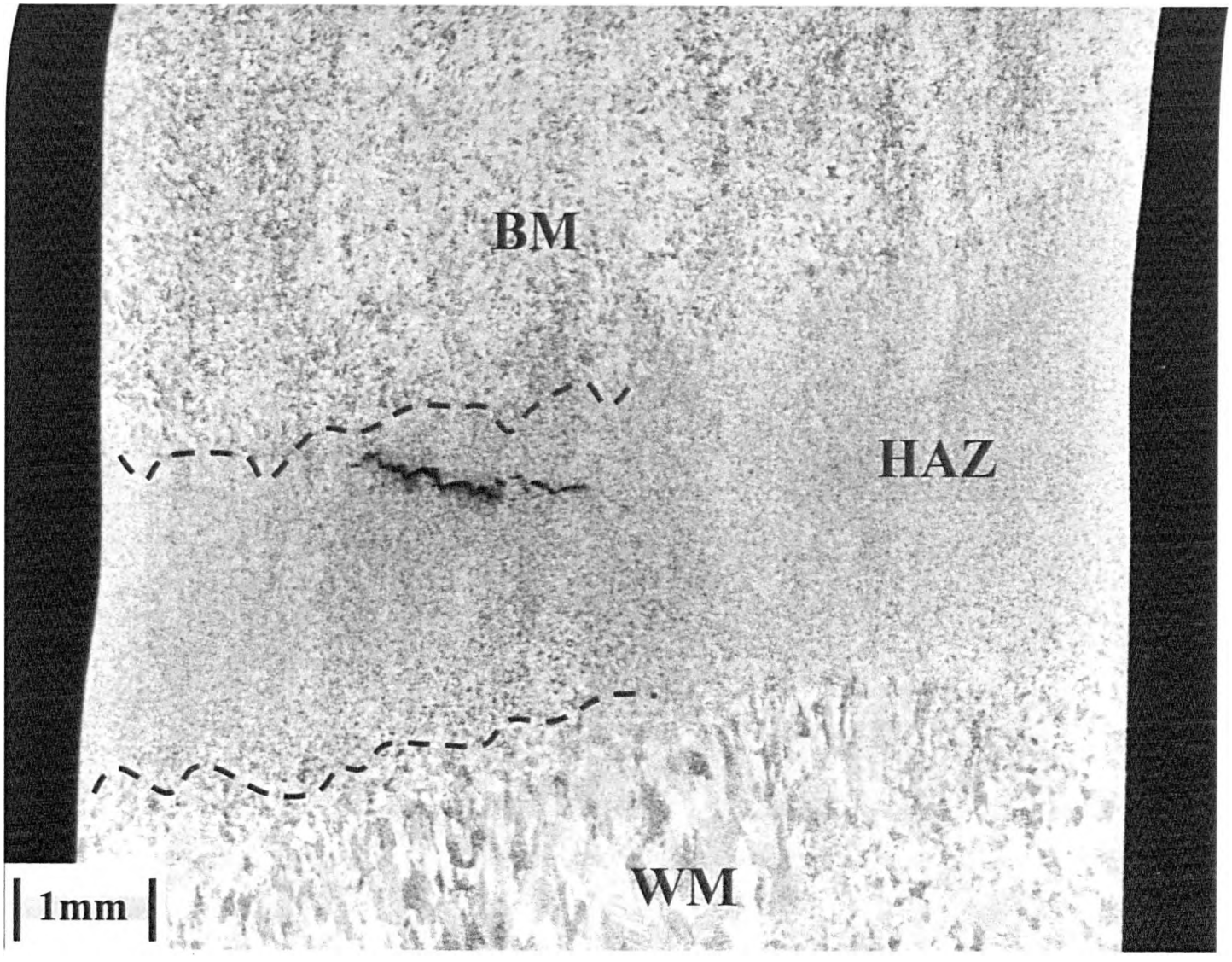

Figure 5.3-17: The same subject of Figure 5.3-15, but after etching with Nital 3%. Localized necking in correspondence of the ICHAZ.

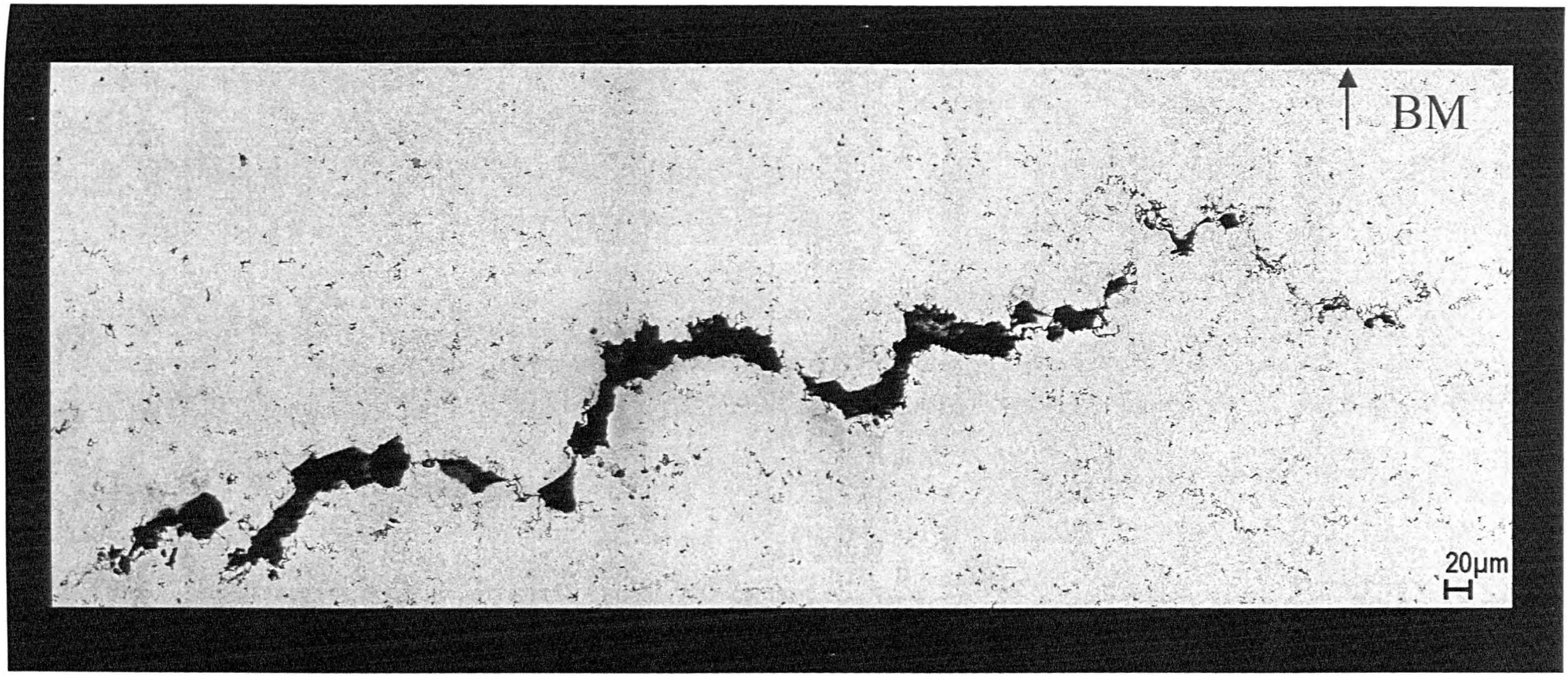

Figure 5.3-18: Image of the cracking of the sample that underwent interrupted testing in H_2 at 873K (600°C), σ_o= 106MPa (applied initial stress), t=647h, taken at the SEM (Back-Scattered Electrons)

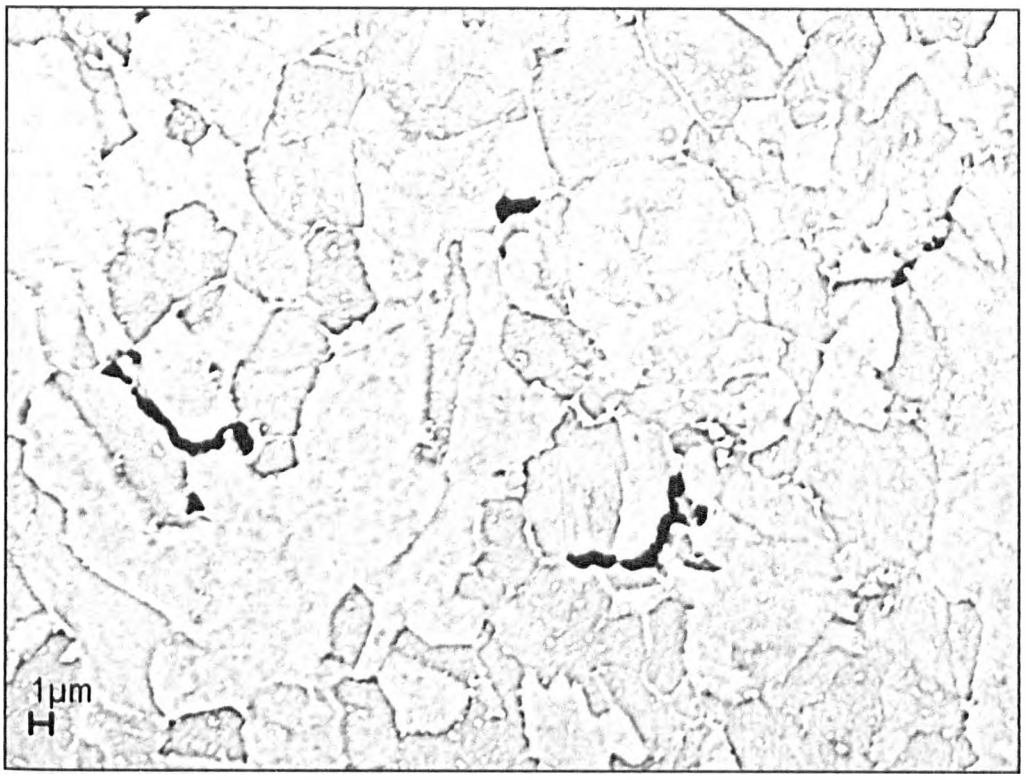

Figure 5.3-19a: Sample tested in hydrogen (T=873K, P=18MPa, σ_o=106MPa, t=647h). Cavitation and Link-up of cavities. The Link-up is facilitated by the formation of very narrow cracks at the interface Bainite/Martensite, and along grain boundaries.

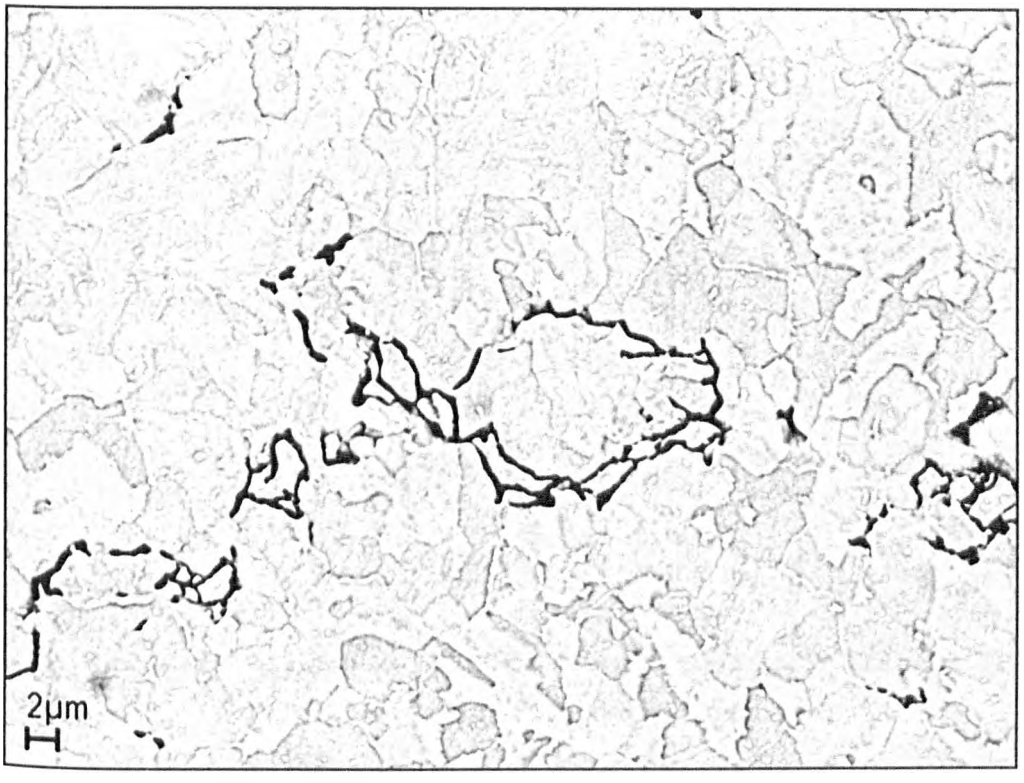

Figure 5.3-19b: Sample as in figure –19a. Microcracking phase.

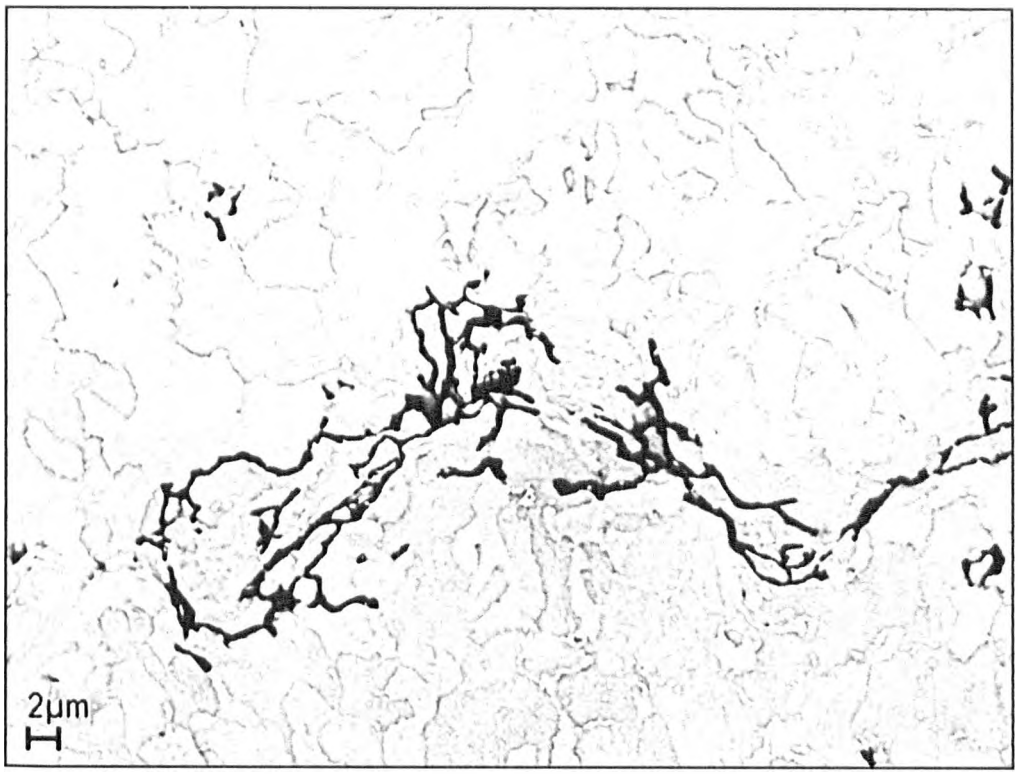

Figure 5.3-19c: Idem. Mosaicing phase.

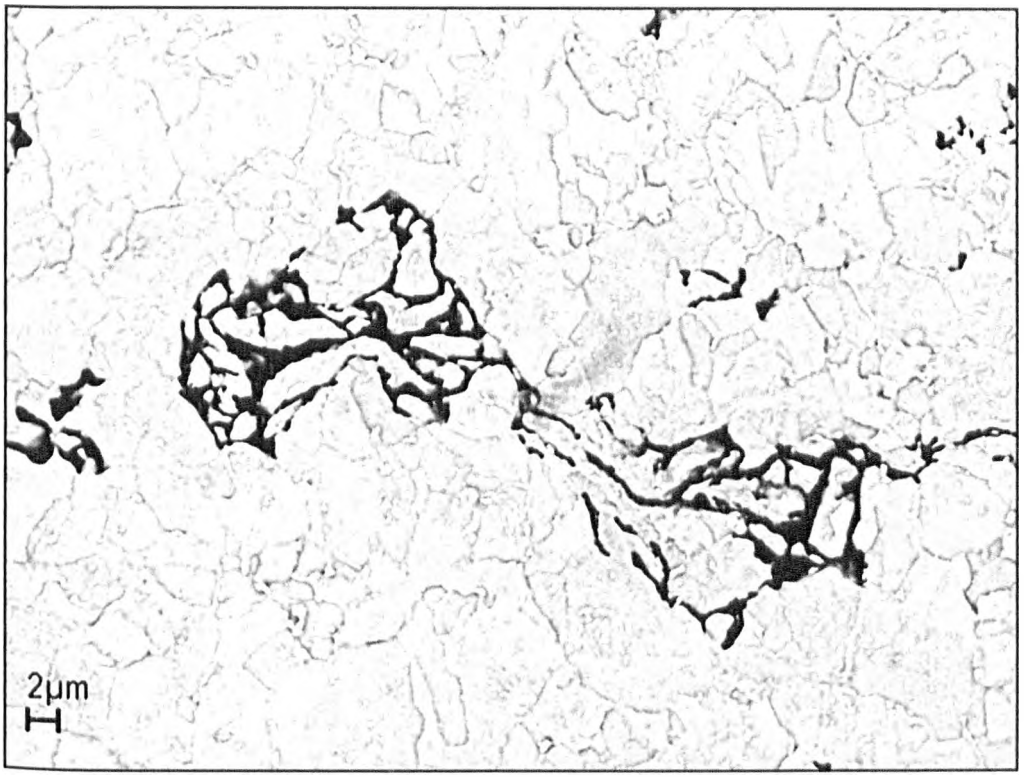

Figure 5.3-19d: Idem. Fragmentation phase.

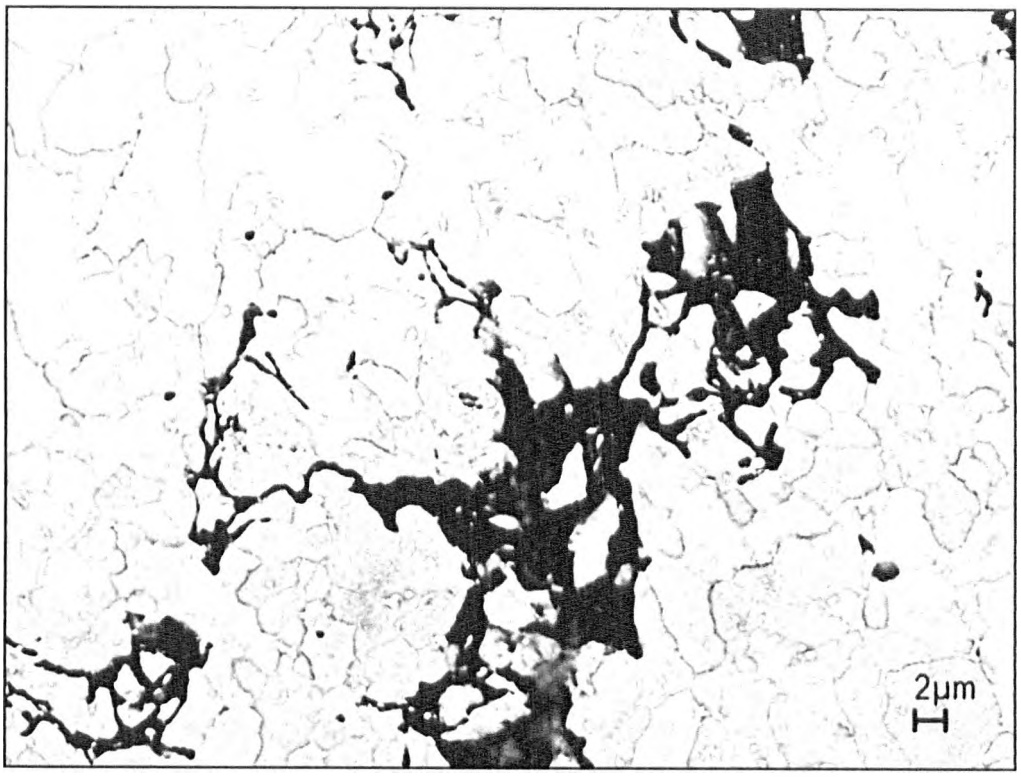

Figure 5.3-19c: Idem. Voidation phase.

Figure 5.3-20: Sample as in figure –19a. Area of the ICHAZ distant from the fracture. It appears cavitated, and more cavitated than the FGHAZ.

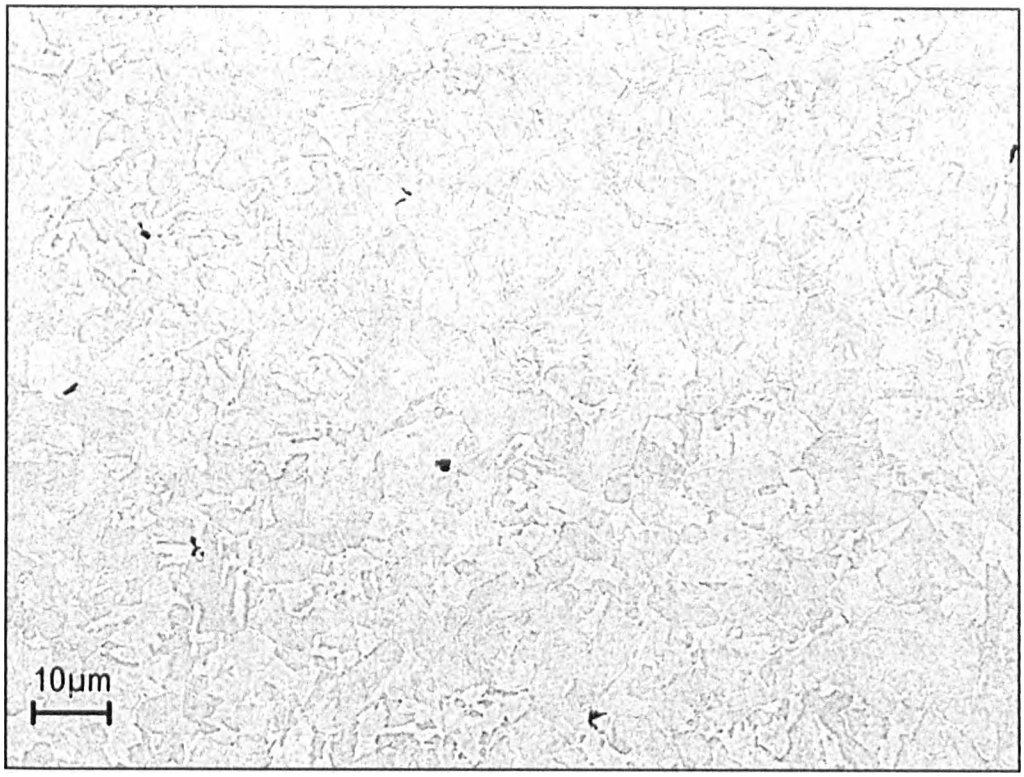

Figure 21: Sample as in figure –19a. FGHAZ of the sample. It exhibits lower cavitation than the ICHAZ.

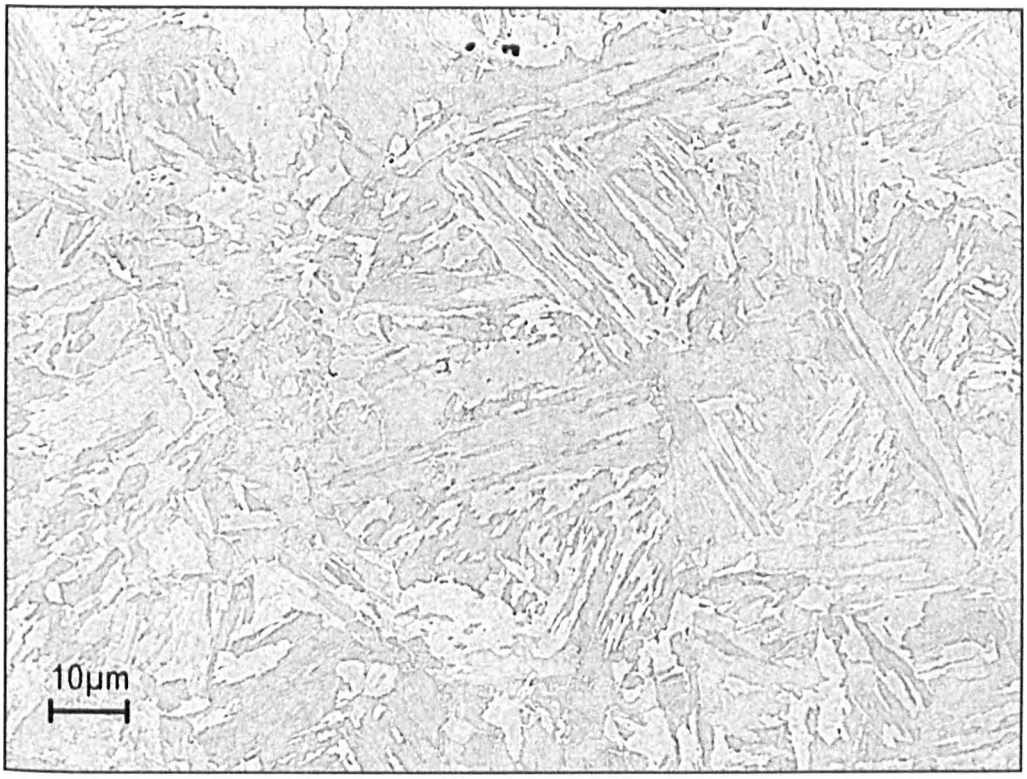

Figure 5.3-22: Idem. Fusion Line. Practically, no cavitation is detected

Figure 5.3-23: Sample as in figure –19a. The weld metal (WM) is populated by a non-uniform distribution of small cavities – if compared to the ICHAZ - round-shaped and isolated.

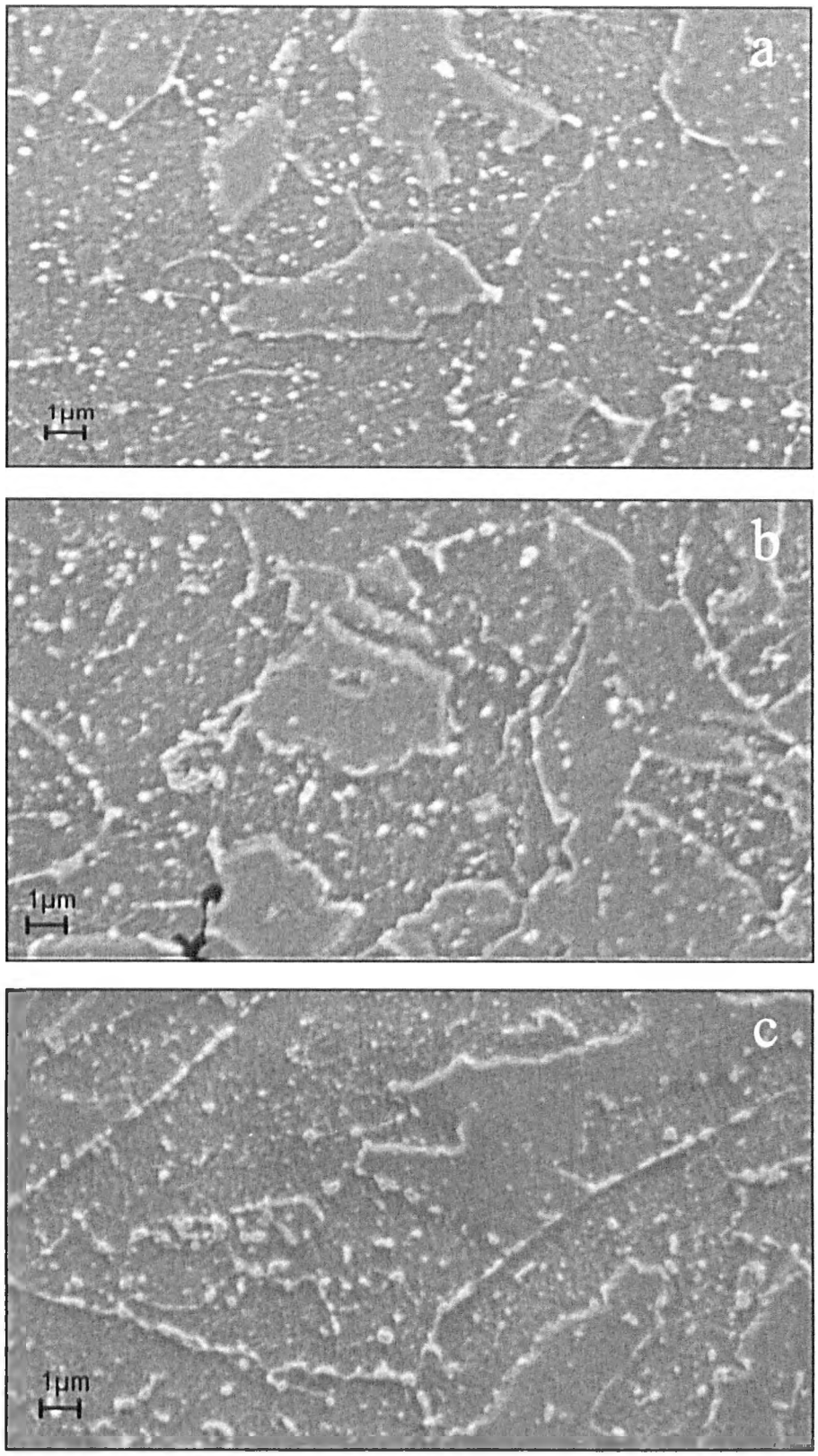

Figure 5.3-24: Distribution of carbides respectively in the ICHAZ (a), FGHAZ(b), BM(c), observed by means of SEM in Secondary Electrons mode. The ICHAZ shows a distribution of relatively fine carbides dispersed in the matrix, whilst the carbides of the FGHAZ seem of bigger dimension. In the BM, carbides of big dimension are found both in the matrix and along grain boundaries

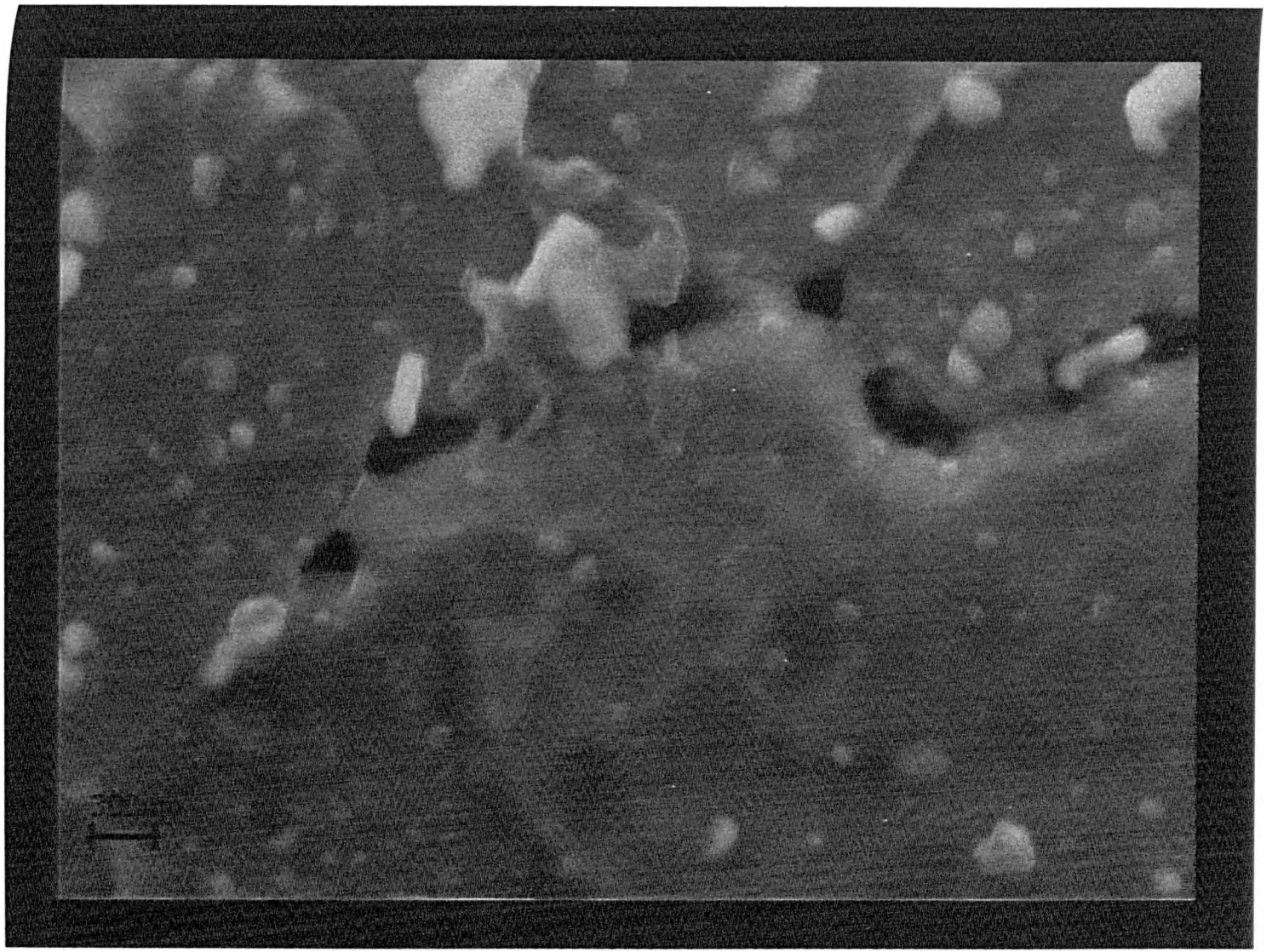

Figure 5.3-25: Sample as in fig.-19a. ICHAZ. The interface carbide/matrix is a preferential site for cavity nucleation

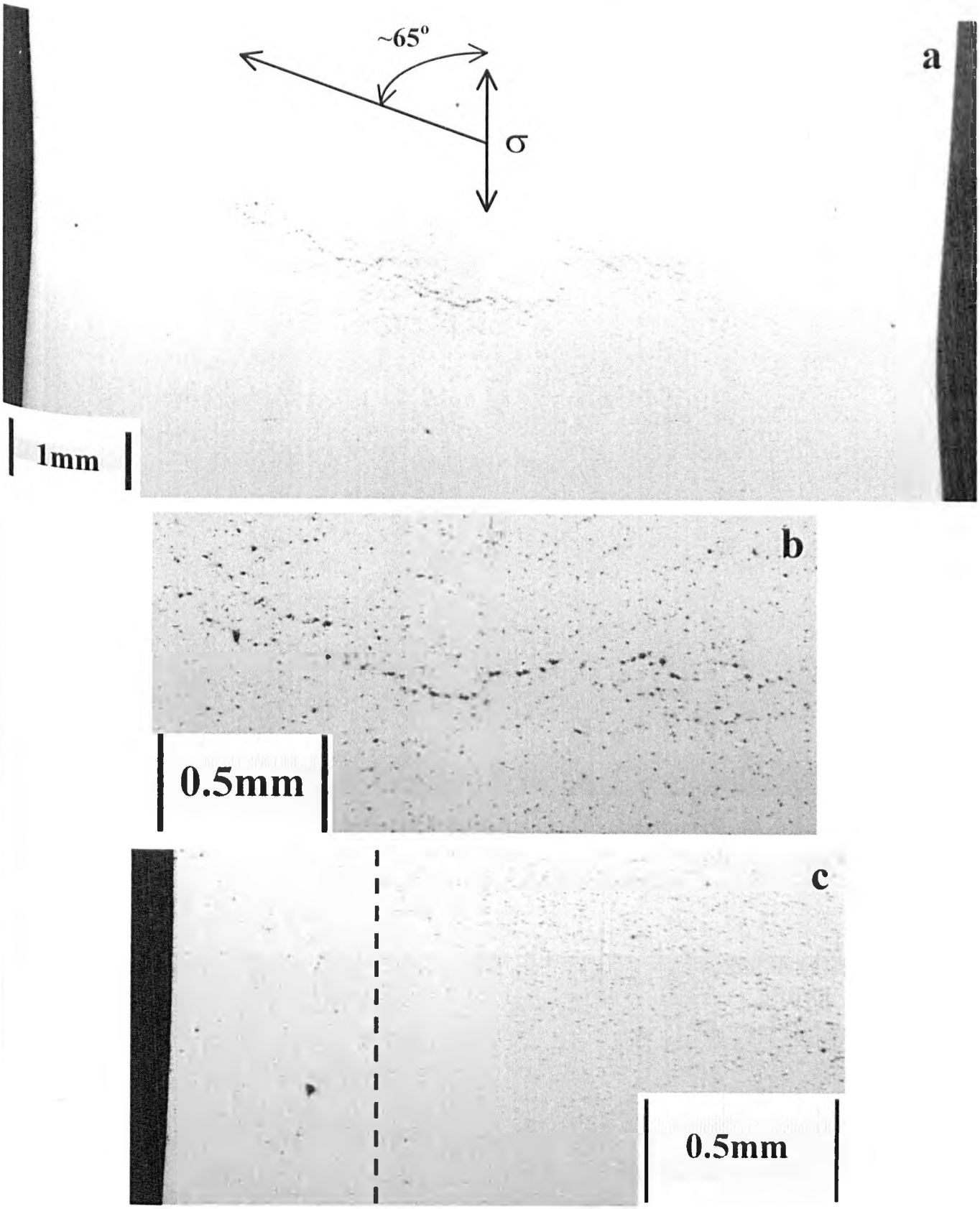

Figure 5.3-26: Cross-welded sample, made of 2.25Cr-1Mo-V steel, tested in hydrogen at T=873K, P= 18MPa, σ_o=94MPa (applied initial stress) and for t=928h. **a**: distributed cavitation inside the sample; **b**: detail of fig.*a*.; it shows the link-up of cavities and the formation of voids; **c**: lower presence of cavities in the surface layer.

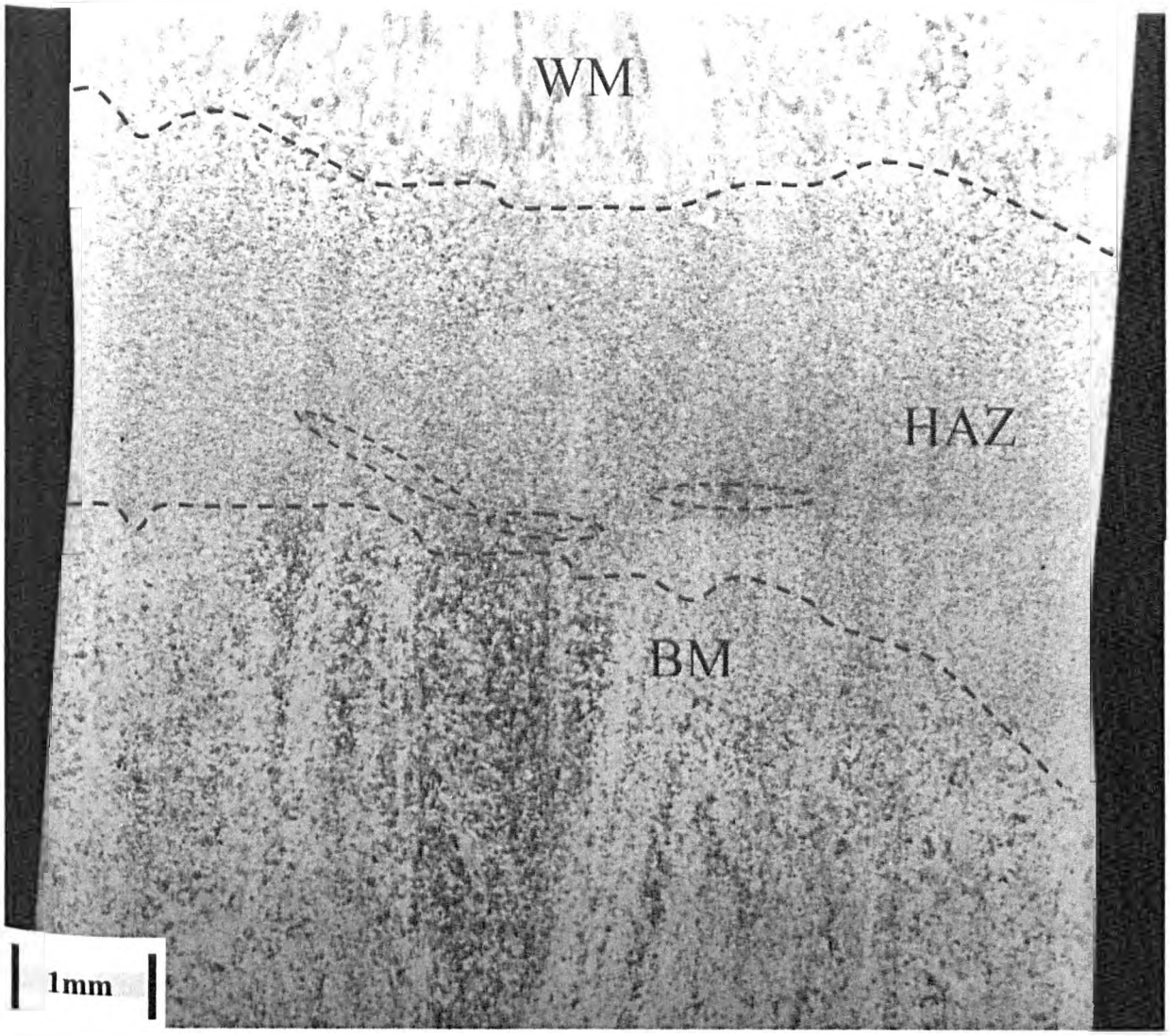

Figure 5.3-27: Cross-welded sample as in figure –26, etched by means of Nital 3%. After etching, it is evident that the damage is located mainly in the ICHAZ, in correspondence of which the sample necks.

Figure 5.3-28: Cross-welded sample as in figure –26. Link-up of cavities is also registered in the weld metal (WM) along grain boundaries

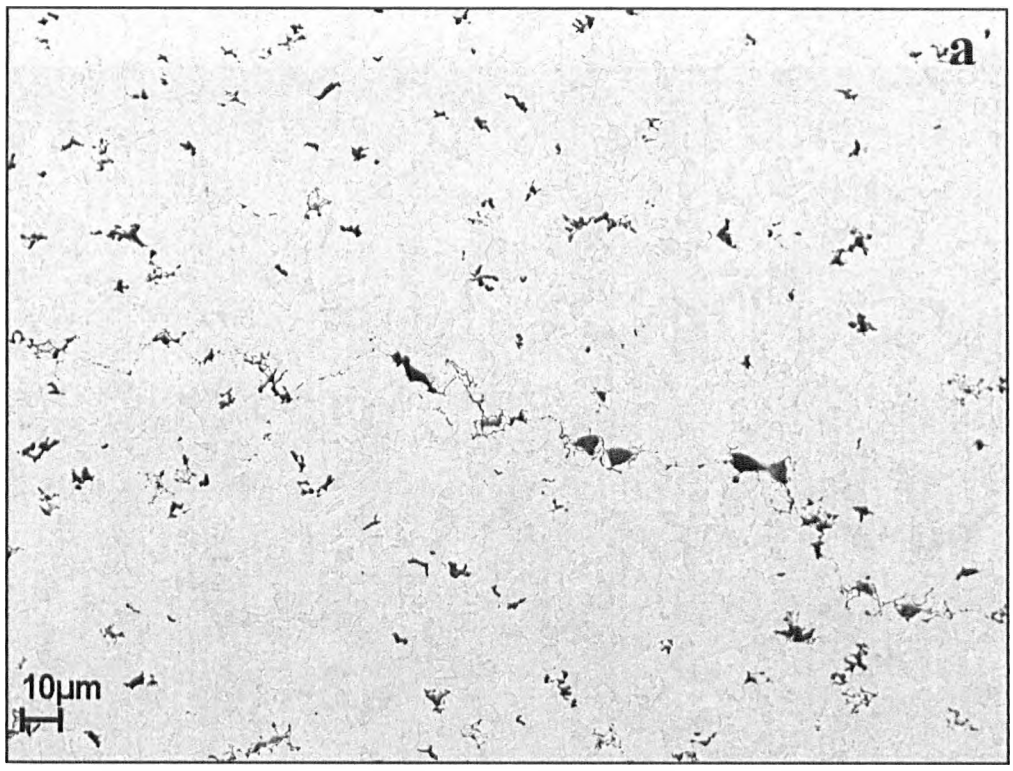

Figure 5.3-29a: Sample as before. At the SEM, the ICHAZ appears as the most damaged zone, with link-up of cavities extended for several hundreds of microns.

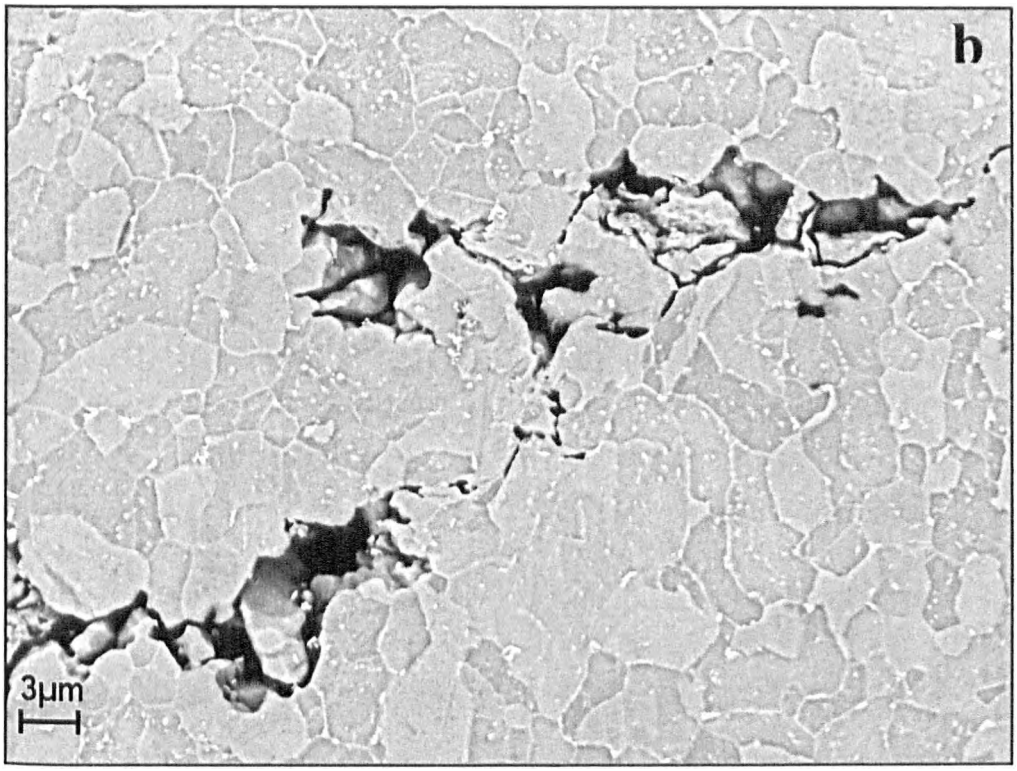

Figure 5.3-29b: Detail of Fig. –29a. The voids of the ICHAZ present irregular shapes. They appear linked by narrow microcracks. Presence of cavities of sub-micron size is also detected: they appear as "initiators" of the macroscopic damage.

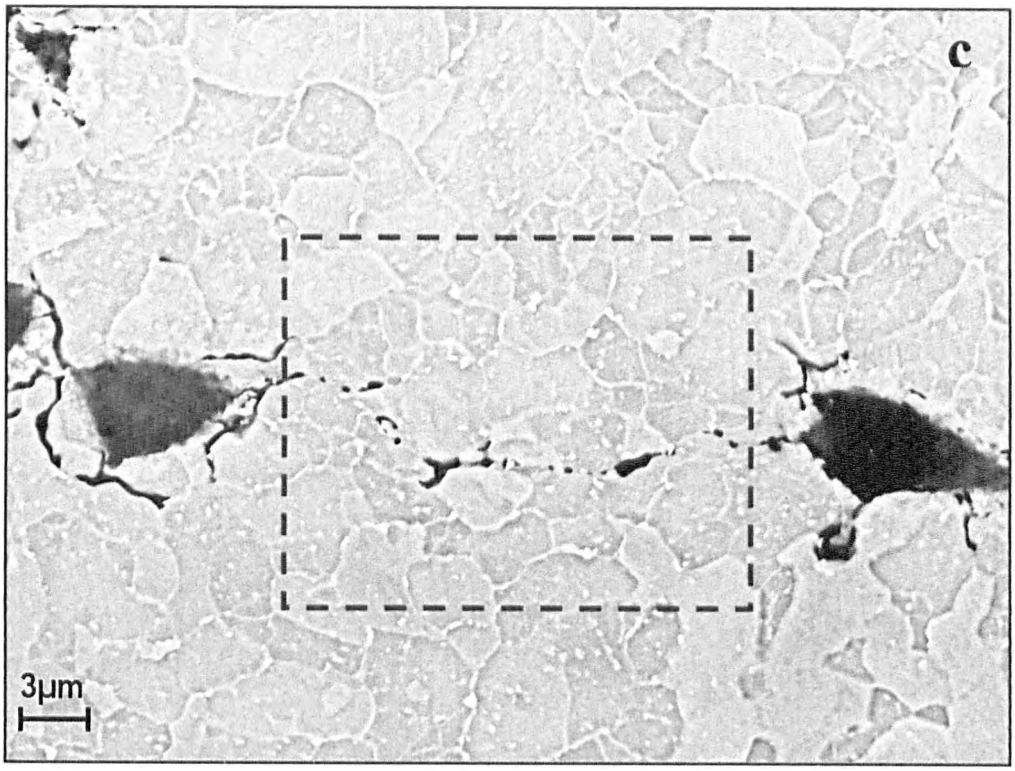

Figure 5.3-29c: Other detail of fig.-29a. Small cavities of sub-micron size, which facilitate the propagation of the micro-crack.

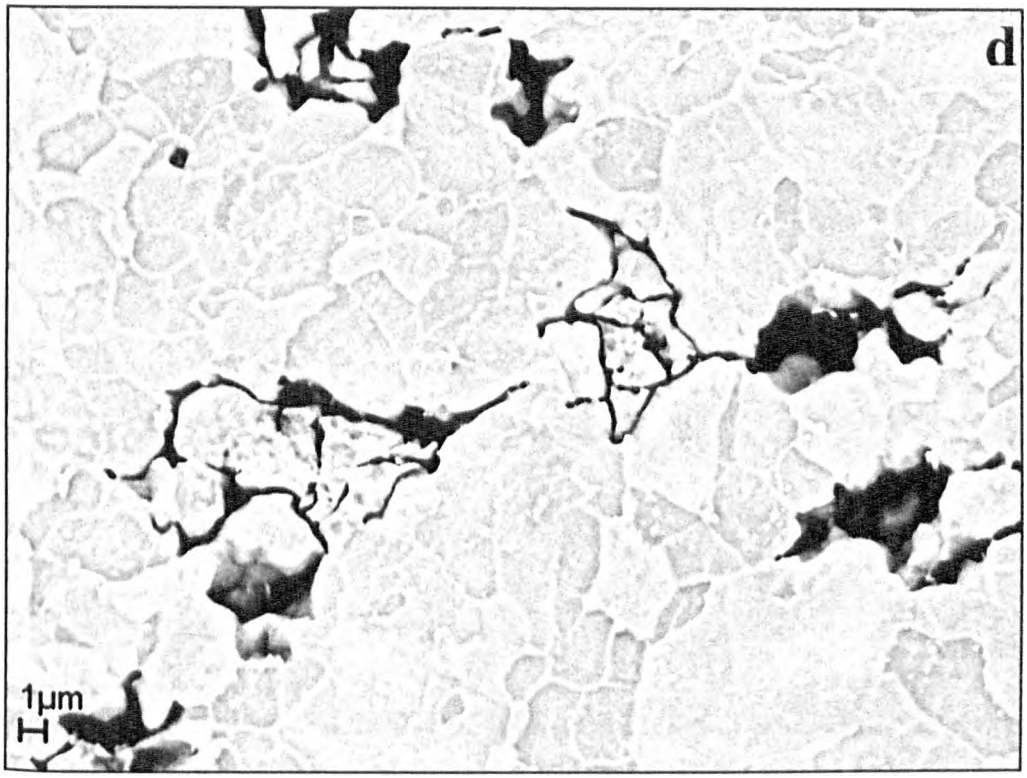

Figure 5.3-29d: Detail of fig. –29a. Beginning of the *Mosaicing* phase.

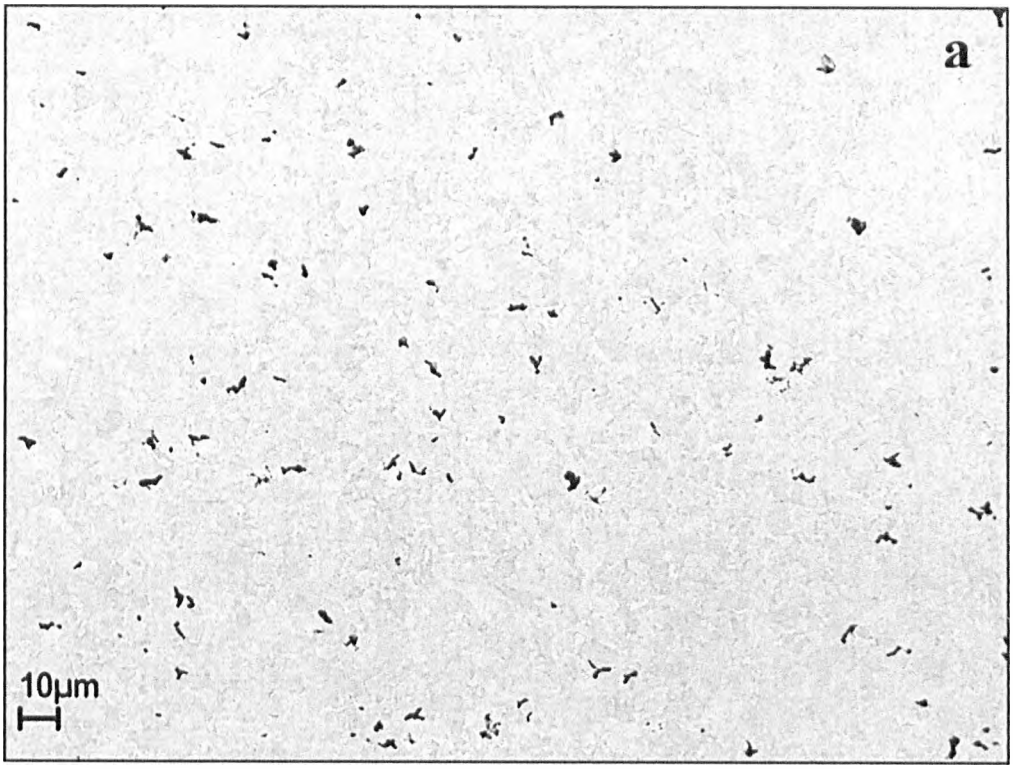

Figure 5.3-30a: Sample as before (tested in hydrogen at T=873K, P= 18MPa, σ_0=94MPa and for t=928h). FGHAZ. The zone is highly cavitated.

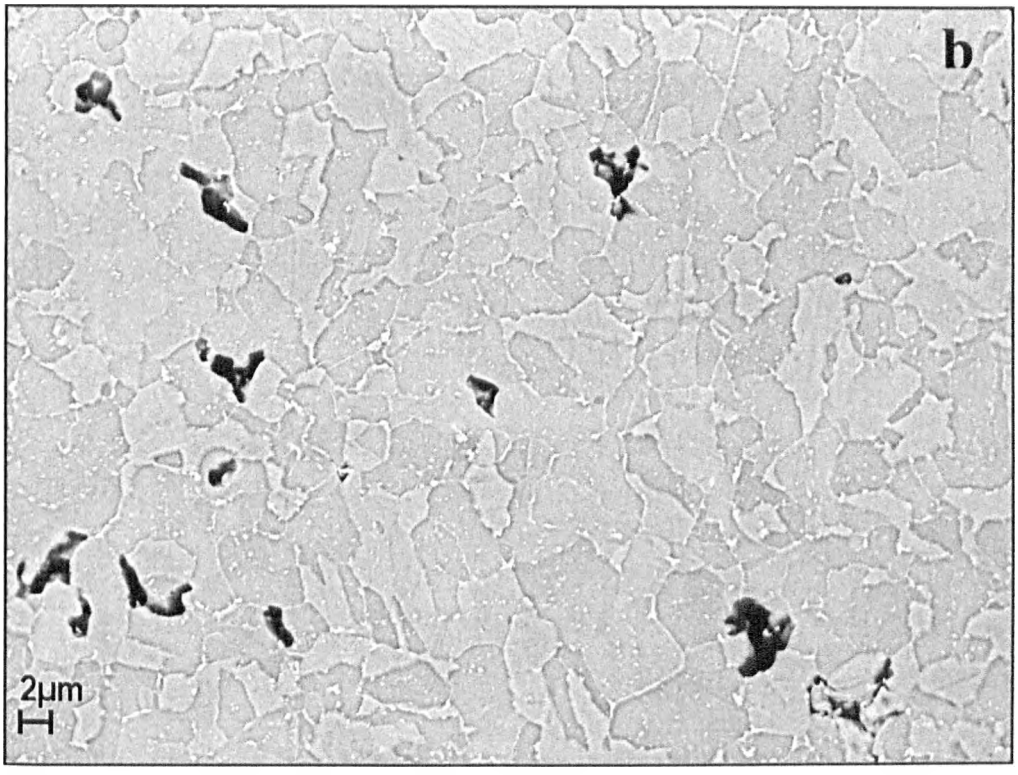

Figure 5.3-30b: Detail of the FGHAZ. The voids present irregular shape and no presence of link-up is detected.

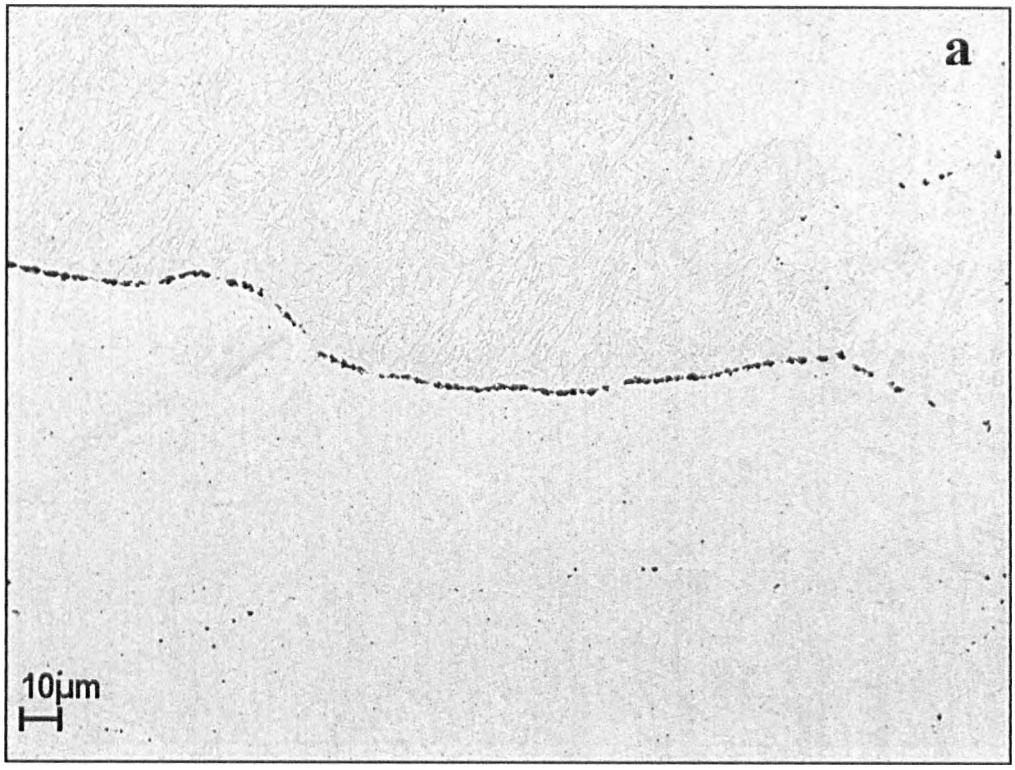

Figure 5.3-31a: Sample as before. Weld metal. Link-up of cavities along grain-boundaries, observed in some areas.

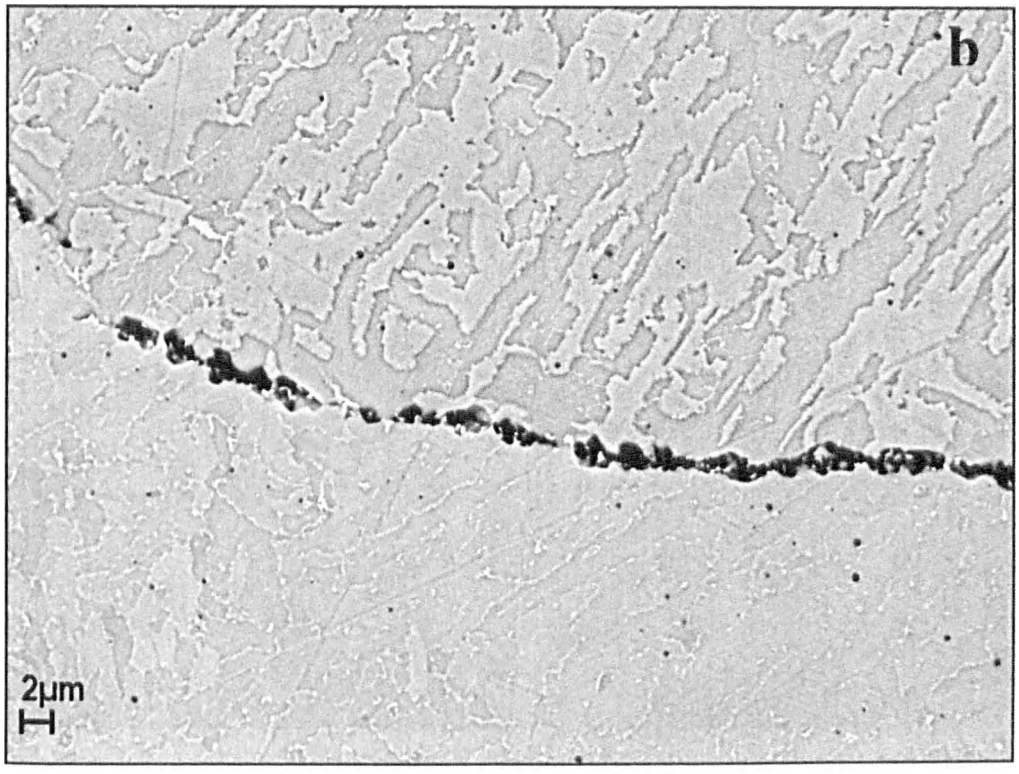

Figure 5.3-31b: Detail of figure –31a. Weld metal.

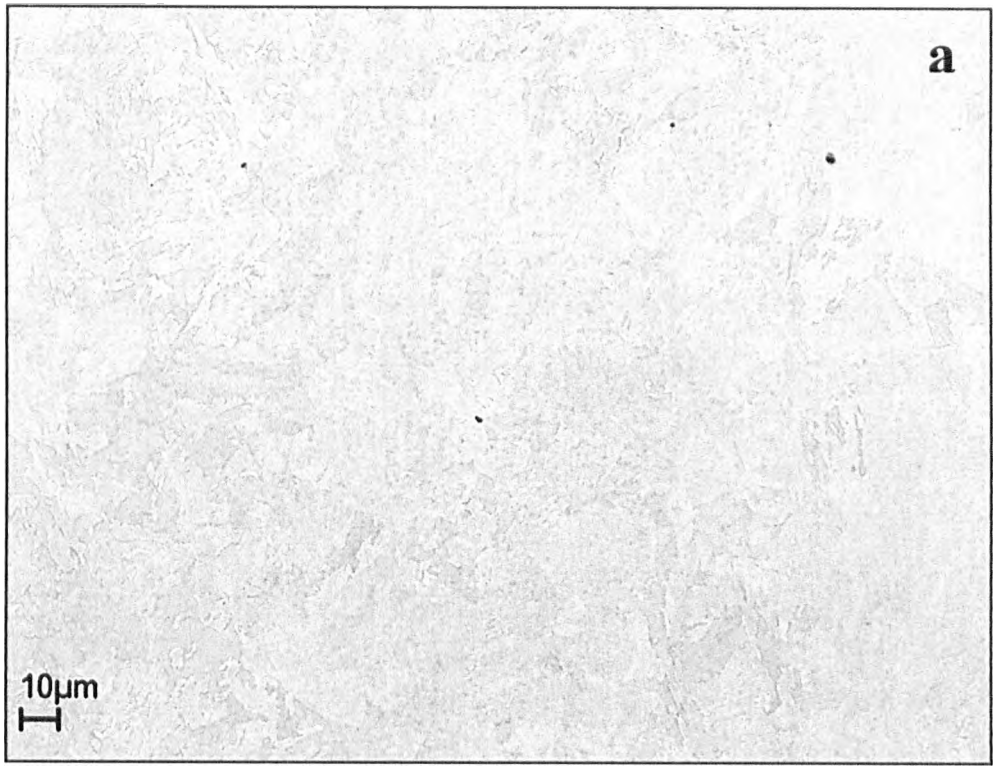

Figure 5.3-32a: Sample as before. Base metal. Practically no damage is detected even at the SEM.

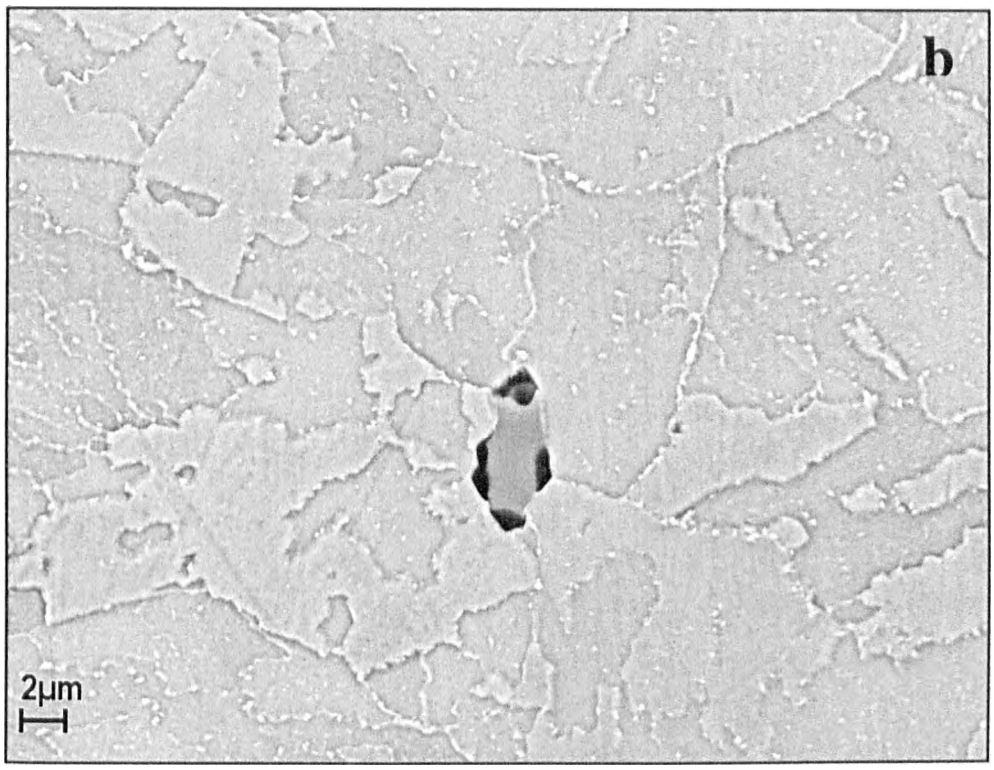

Figure 5.3-32b: Rare presence of the attack is found in preferential places, as grain boundaries and interfaces inclusion/matrix.

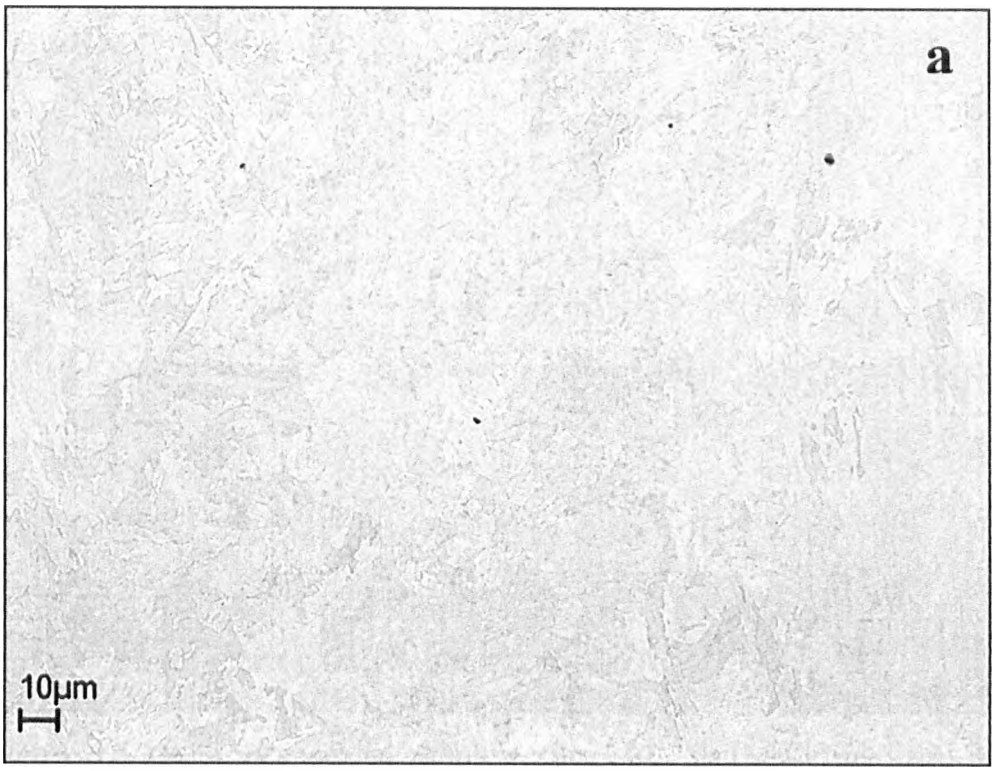

Figure 5.3-32a: Sample as before. Base metal. Practically no damage is detected even at the SEM.

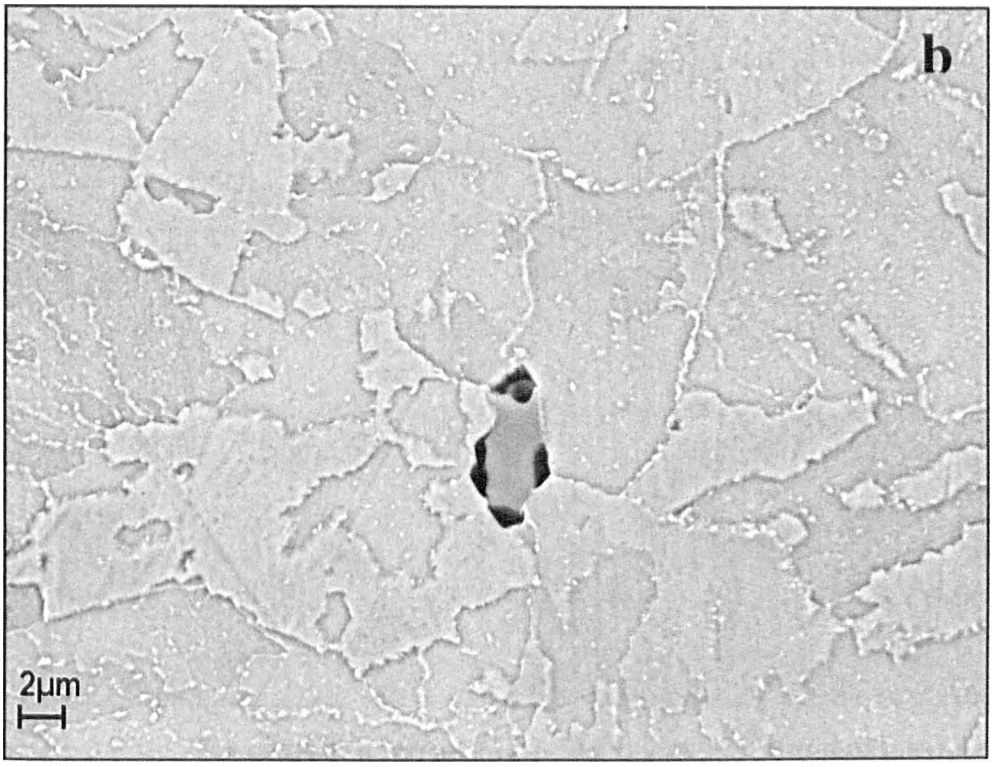

Figure 5.3-32b: Rare presence of the attack is found in preferential places, as grain boundaries and interfaces inclusion/matrix.

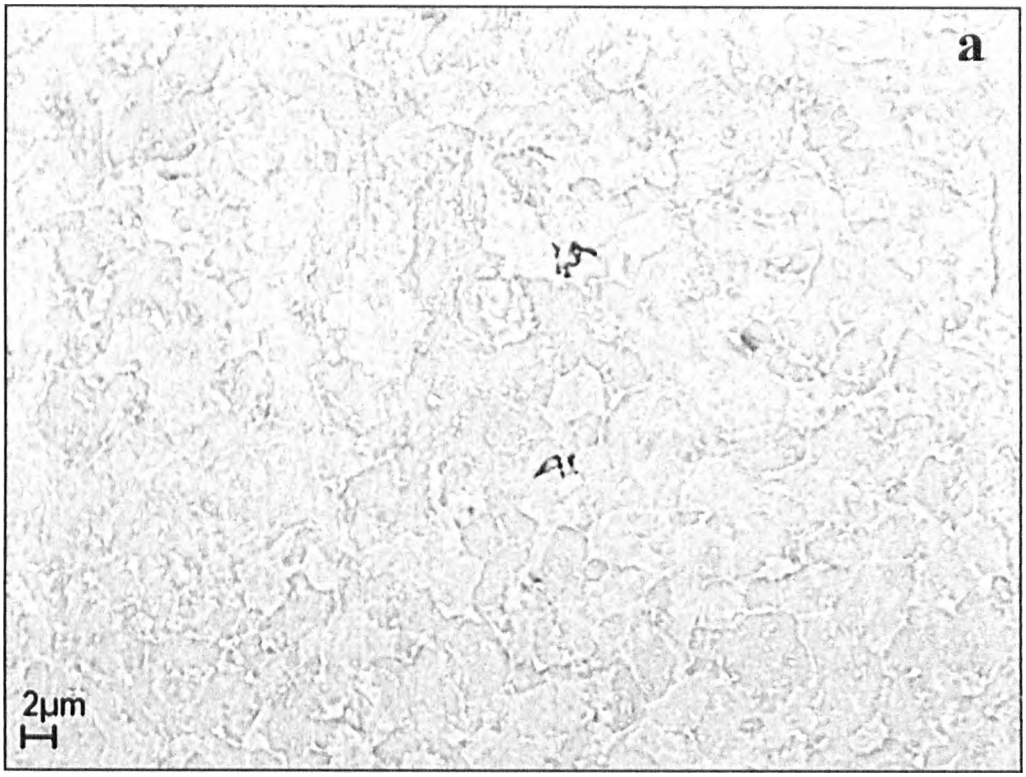

Figure 5.3-33a: Cross-welded sample, made of 2.25Cr-1Mo-V steel, tested in hydrogen at T=873K, P= 18MPa, σ_0=94MPa and for t=648h. Traces of damage are detected only in the ICHAZ. The damage consists of cavities at the interfaces.

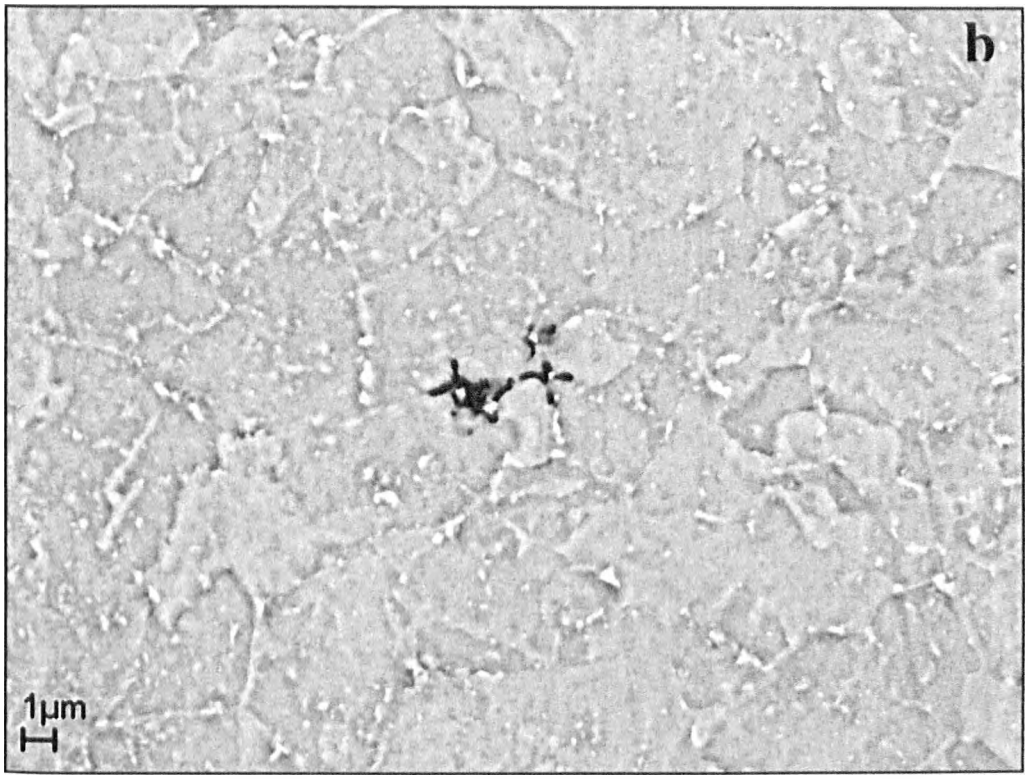

Figure 5.3-33b: The same zone as for Fig. –33a, but at higher magnification. The cavities link each other along the interfaces.

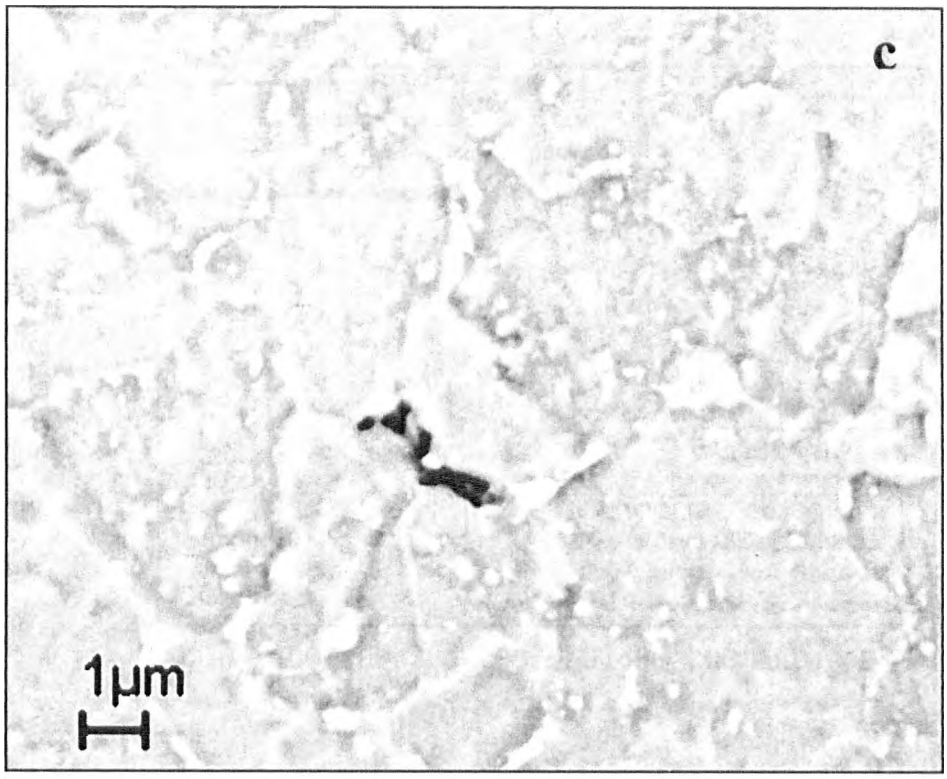

Figure 5.3-33c: Idem as for Figure –33b.

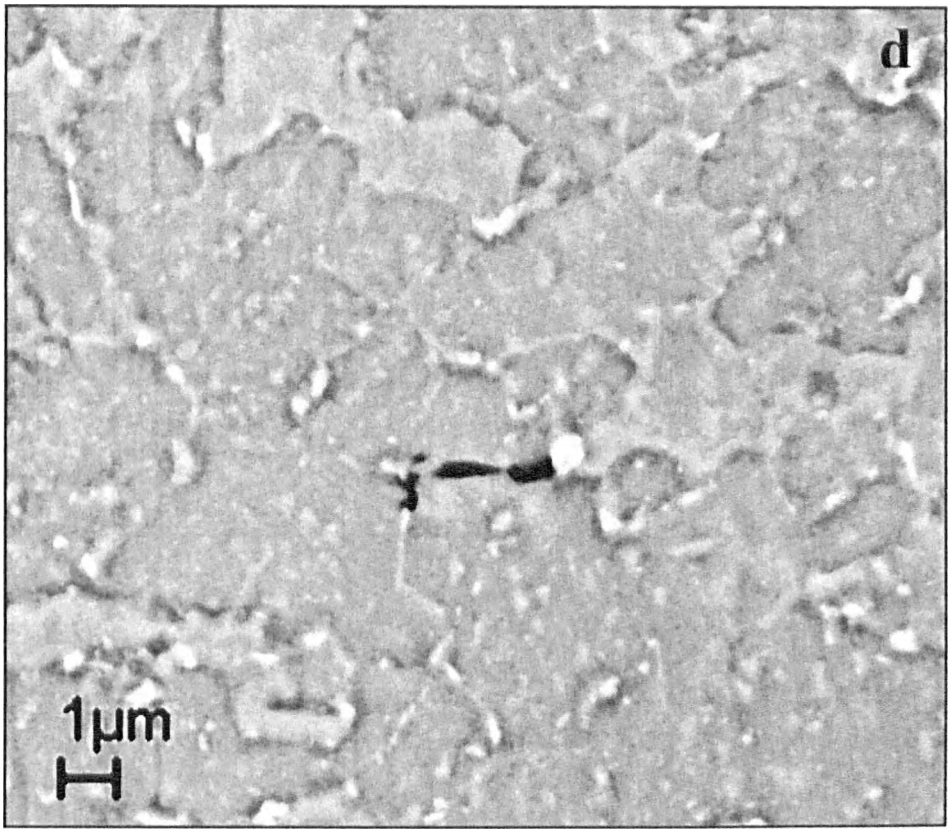

Figure 5.3-33d: Same zone as for Figure –33a. The damage consists of small cavities, mainly of sub-micron size. The micrograph shows cavities mainly of sub-micron size, linking each other.

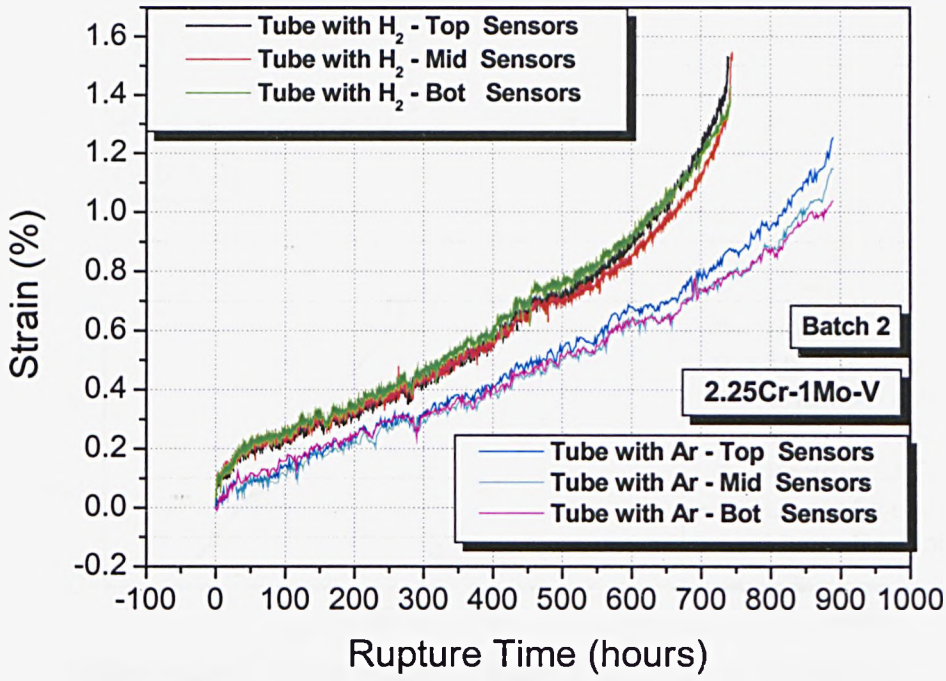

Figure 5.3-34: Creep-rupture curves of the tubular specimens, made of V-mod. 2.25Cr-1Mo steel, longitudinally welded, pressurized by means of hydrogen or argon

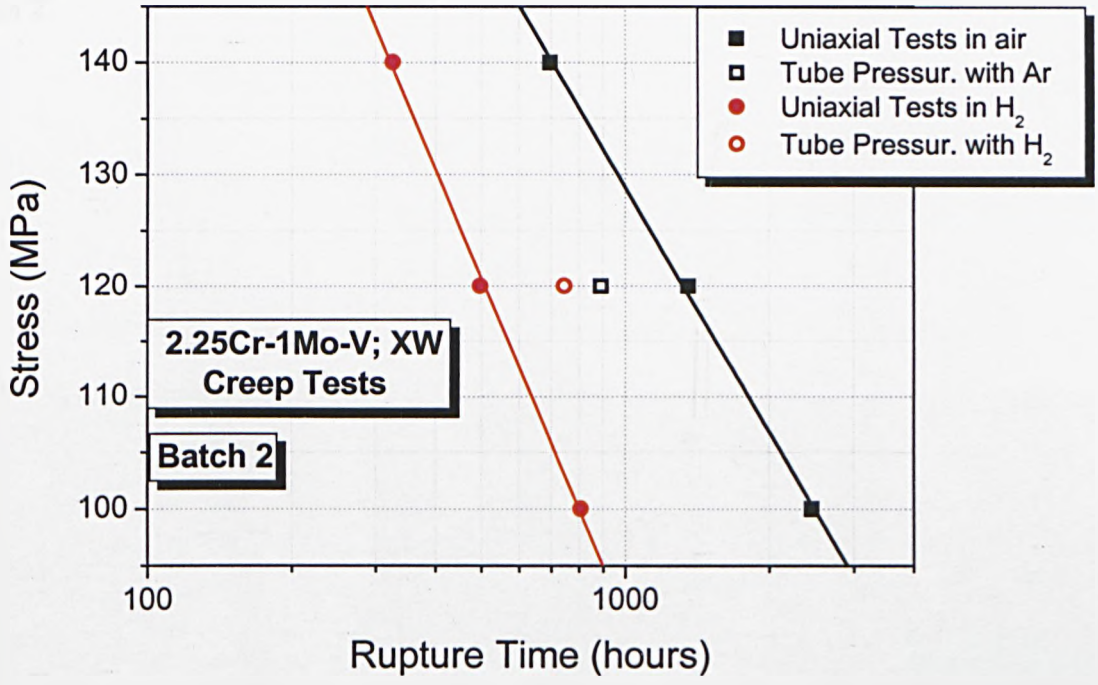

Figure 5.3-35: Stress/Rupture plot of the creep tests, performed in uniaxial as well as in more complex state of stress, on the welded V-mod. 2.25Cr-1Mo steel, batch 2.

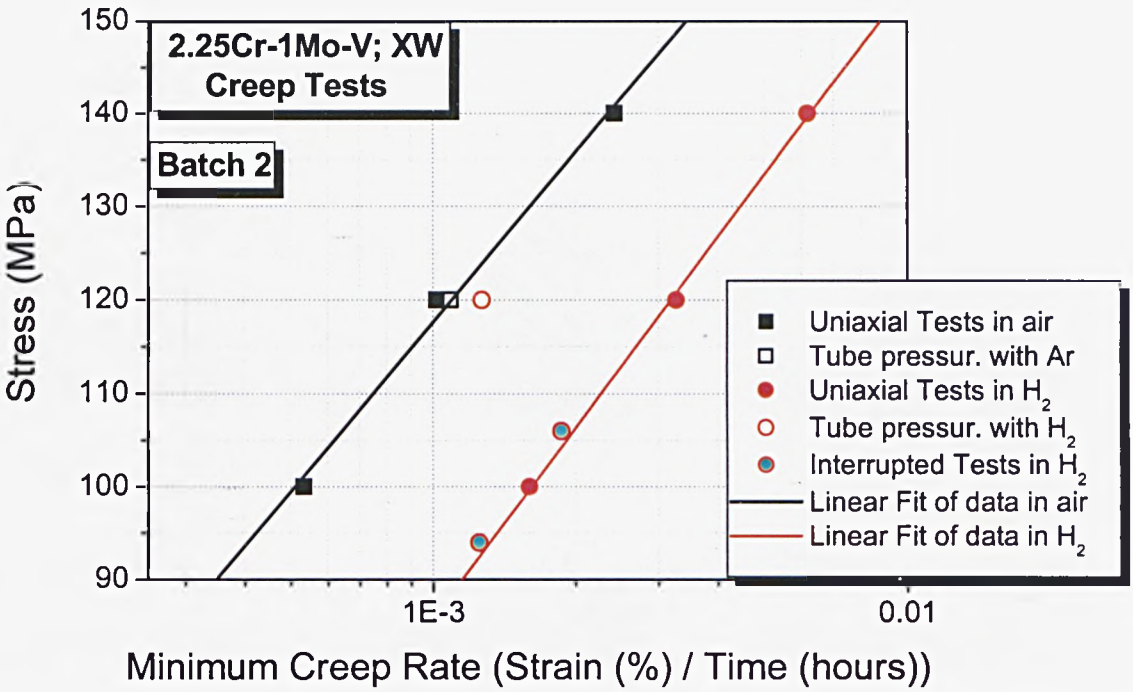

Figure 5.3-36: Stress versus MCR of the creep-rupture tests performed, in uniaxial as well as in more complex state of stress, on the welded V-mod. 2.25Cr-1Mo steel, batch 2.

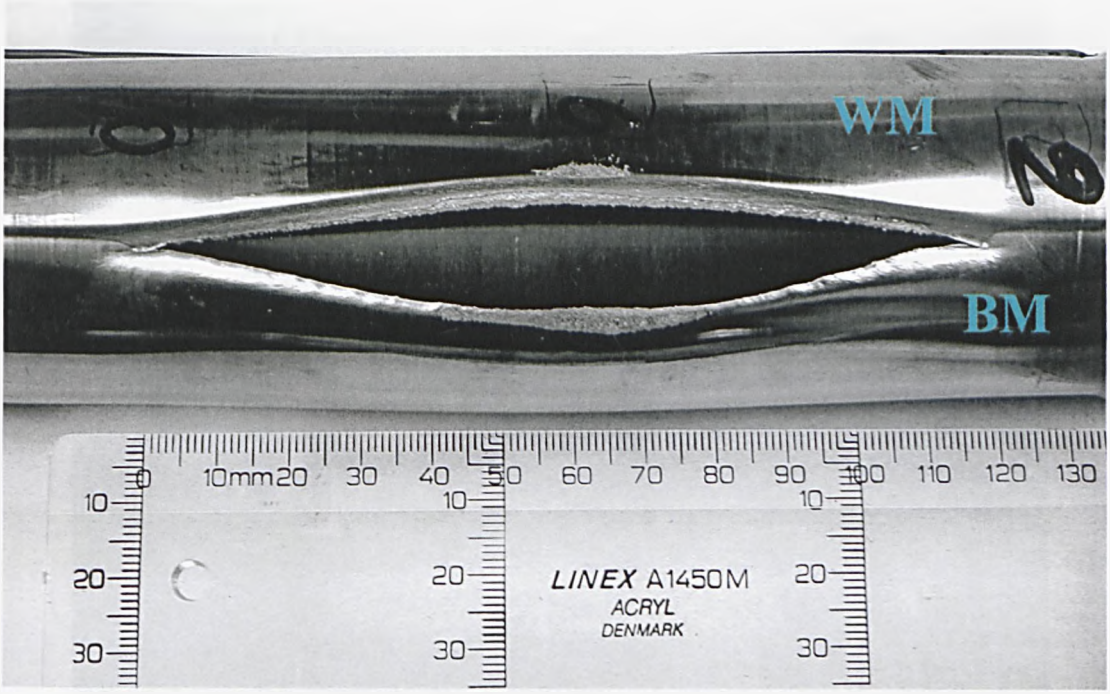

Figure 5.3-37: With the naked eye, the failure of the tubular specimen, pressurized by means of hot hydrogen, at 873K and a pressure of 18MPa, is registered between the weld metal (WM) and the base metal (BM).

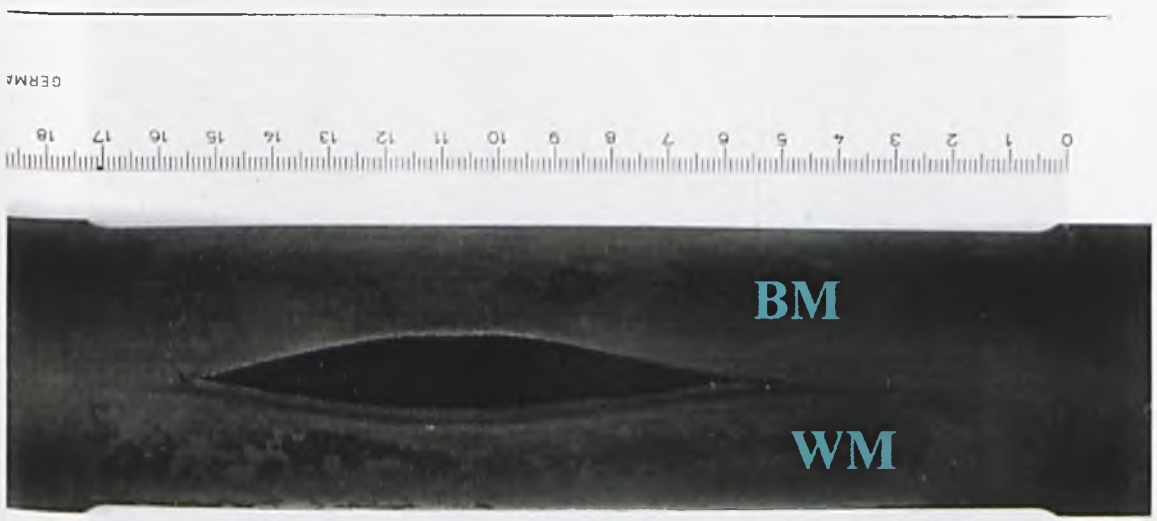

Figure 5.3-38: With the naked eye, also the failure of the tubular specimen, pressurized by means of hot argon, at 873K and with a pressure of 18MPa, is registered between the weld metal (WM) and the base metal (BM).

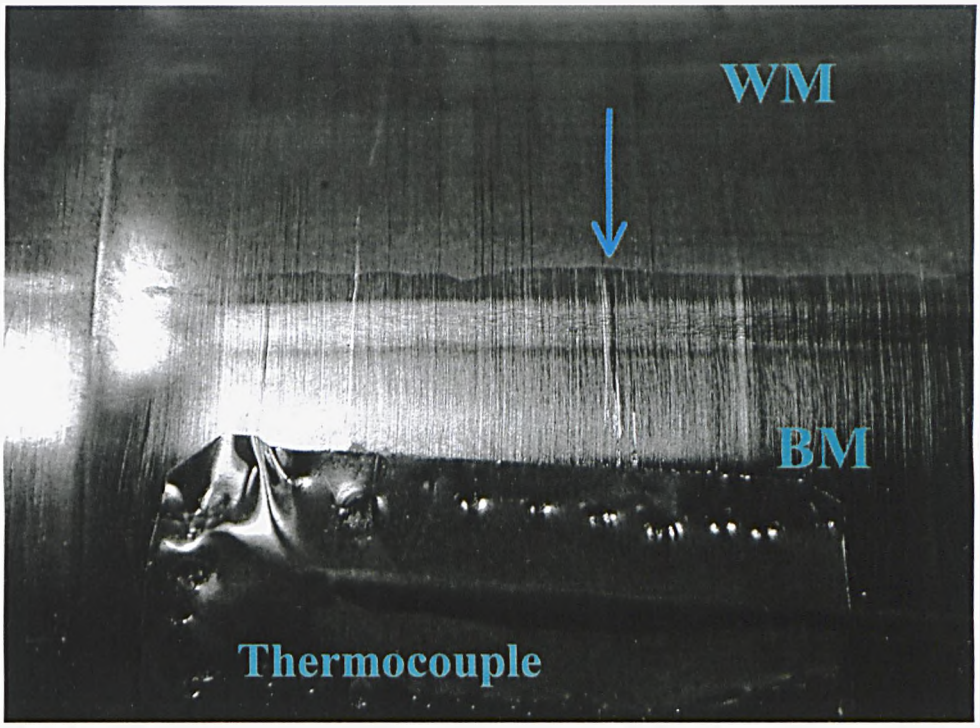

Figure 5.3-39: As a consequence of the pressurization, the WM exhibits an outward movement, which originates a "step" on the external surface of the tube. This step is just perceivable in areas close to the shoulder of the tube.

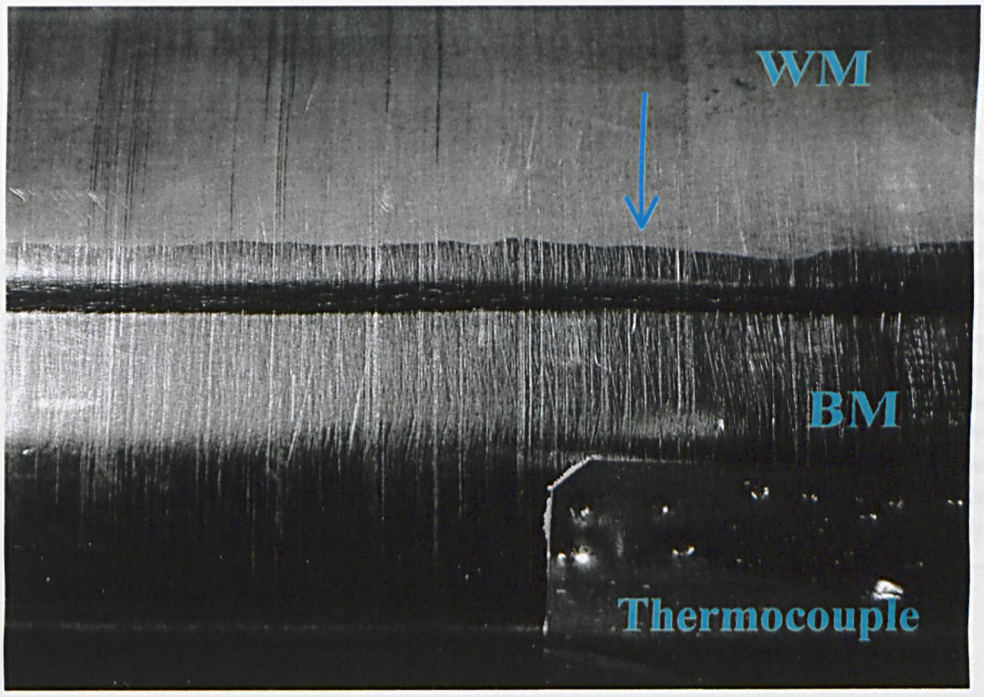

Figure 5.3-40: The 'step' produced by the outward movement of the WM becomes more pronounced going towards the middle of the gauge-length. Note that in hot high-pressurized hydrogen the onset of the WM become visible by naked eye (blue arrow).

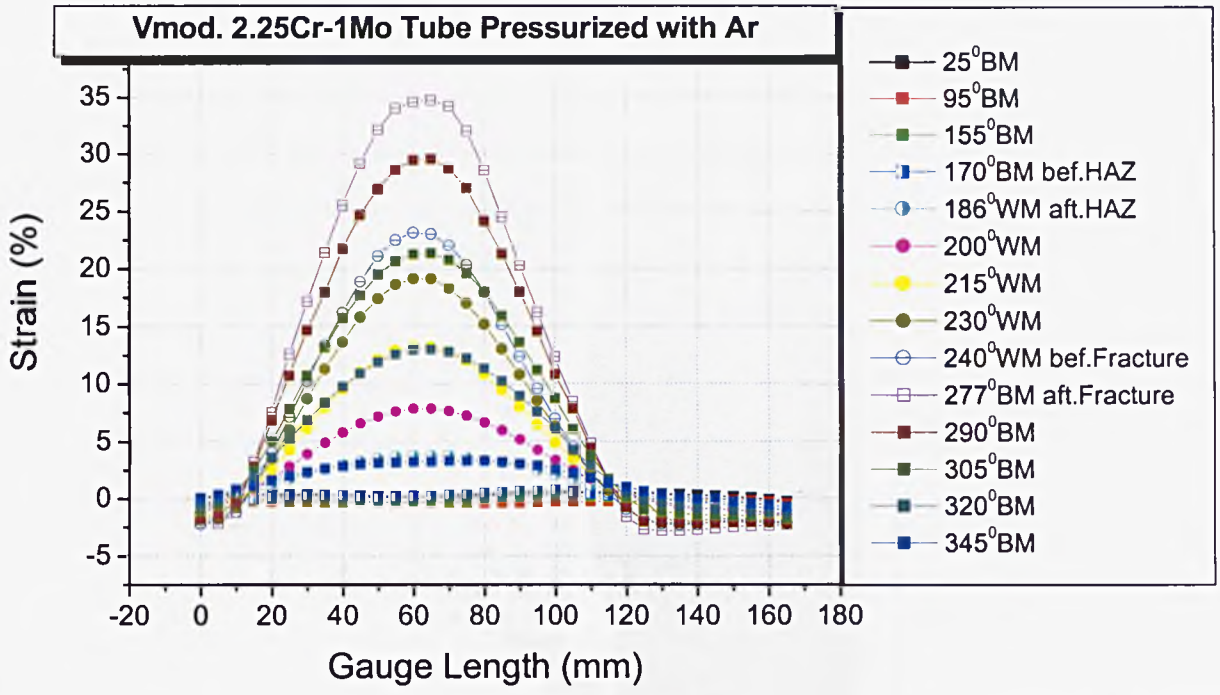

Figure 5.3-41: Results of the strain measurement carried out, after test, on the tube, made of welded V-modified 2.25Cr-1Mo, pressurized with argon

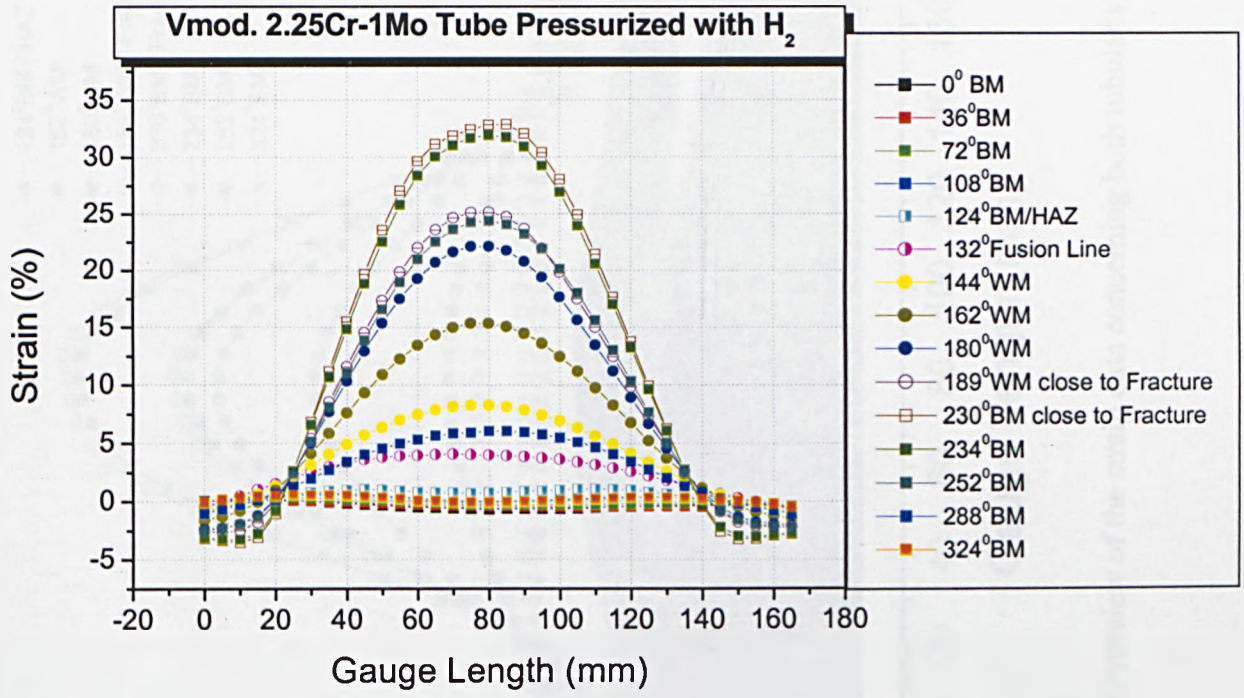

Figure 5.3-42: Results of the strain measurements carried out, after test, on the tube ,made of welded V-modified 2.25Cr-1Mo, pressurized with hydrogen.

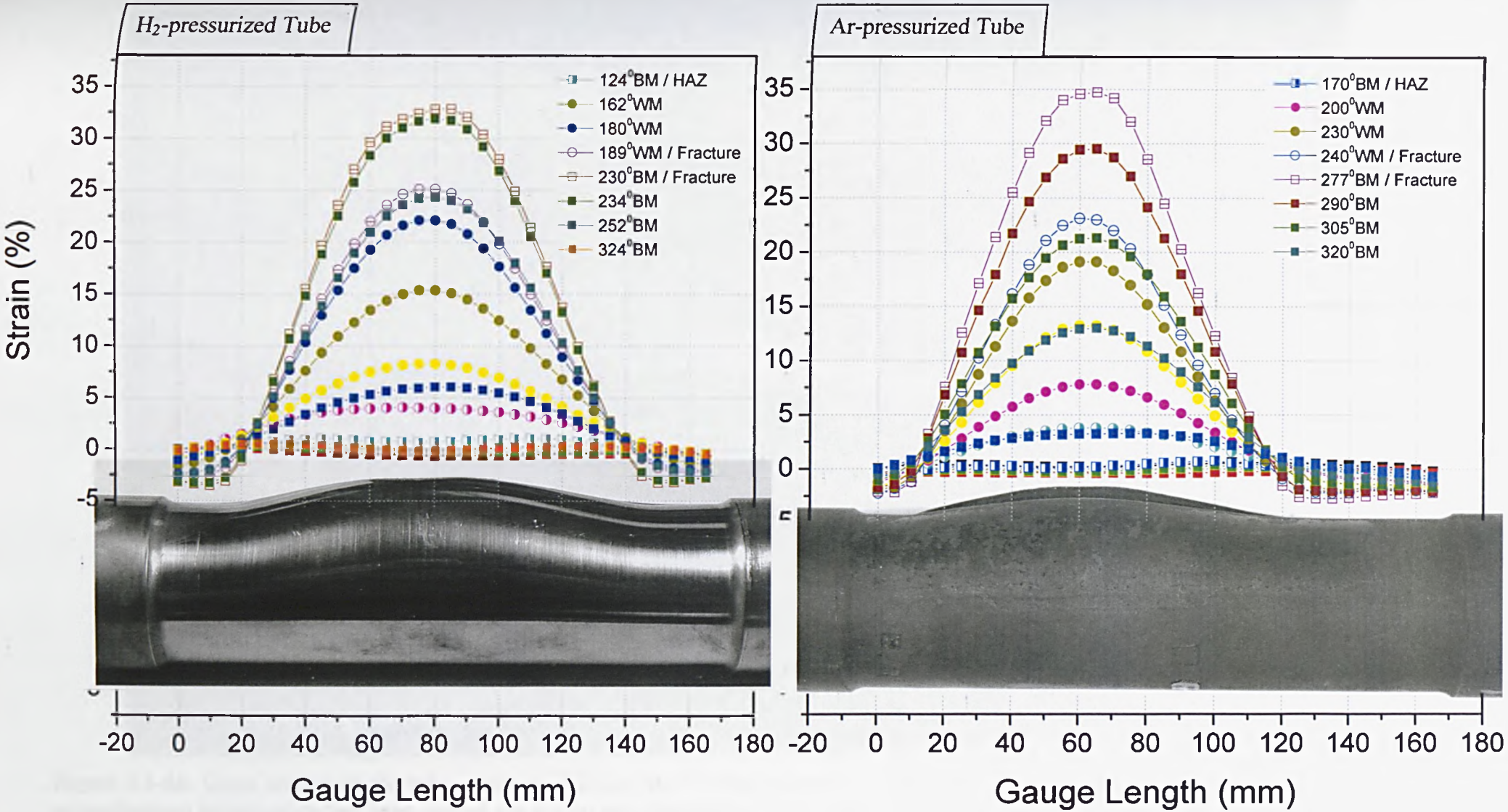

Figure 5.3-43: Overview of the strain data concerning both tubular specimens made of V-mod. 2.25Cr-1Mo welded steel.

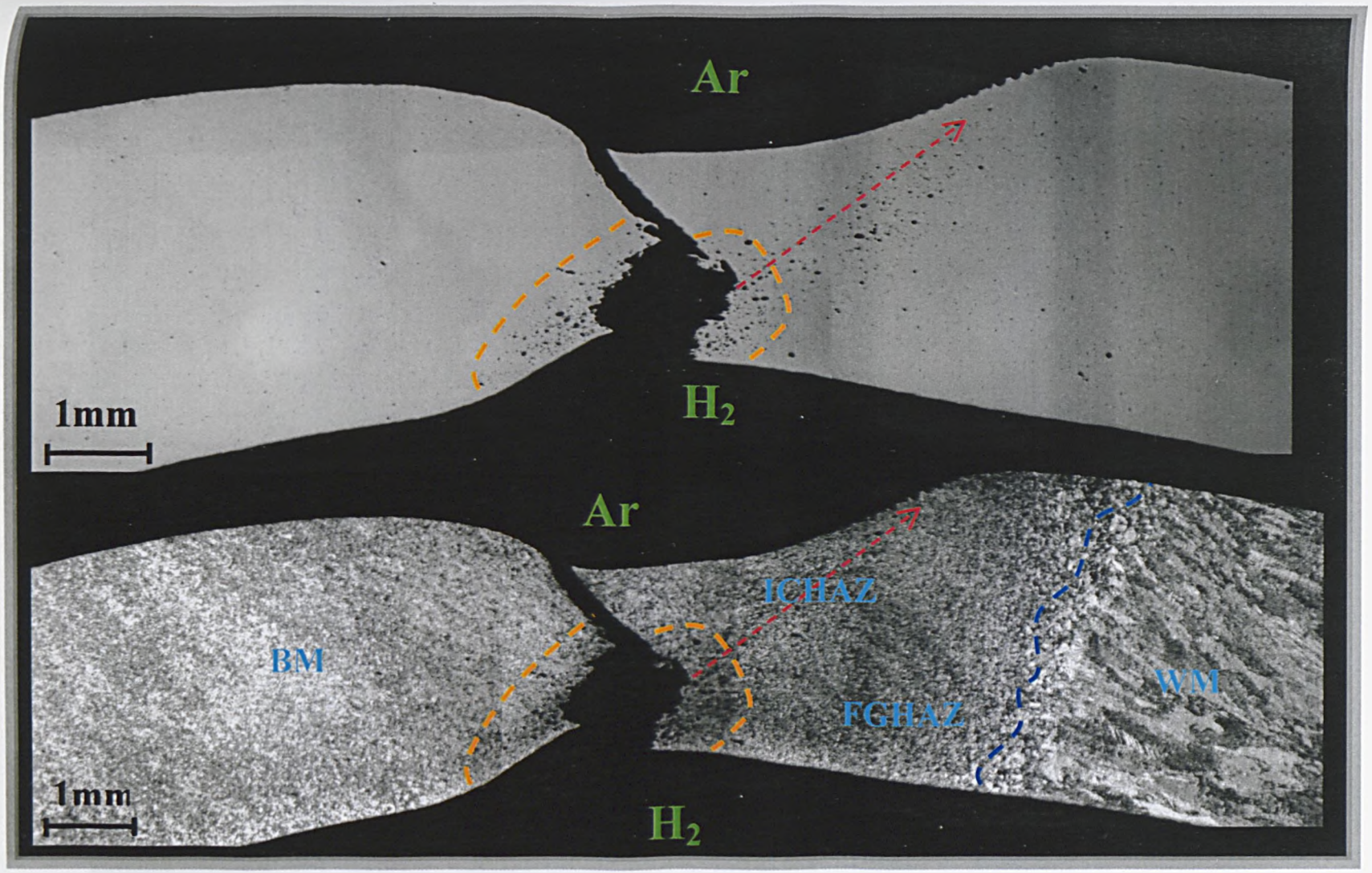

Figure 5.3-44: Cross section of the tube, made of 2.25Cr-1Mo-V, longitudinally welded, pressurized with hydrogen at 873K (600°C). The microstructural investigation had been carried out before and after etching with Nital. The cavitation is registered mainly in the ICHAZ, and is more marked close to the surface exposed to hydrogen.

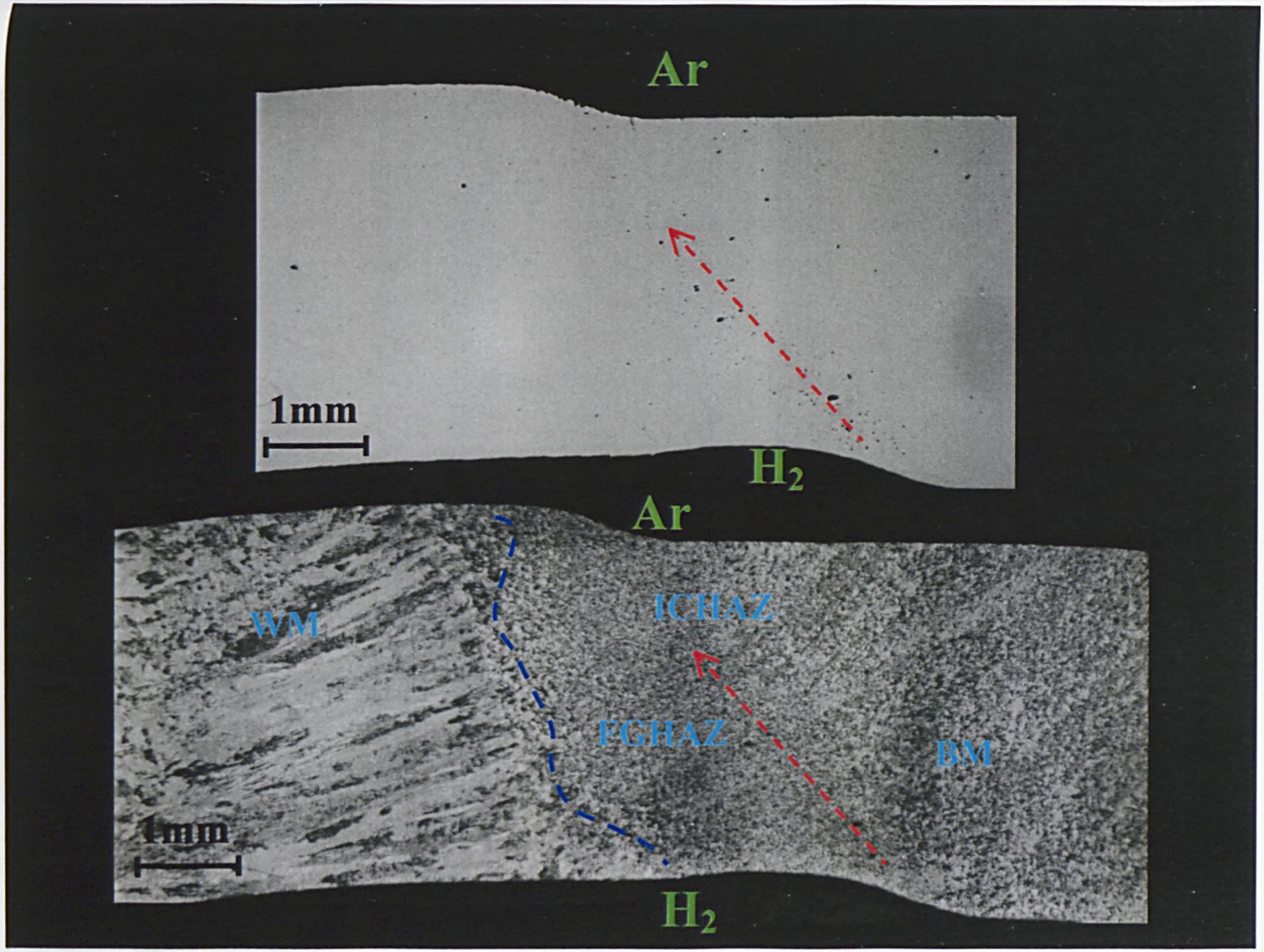

Figure 5.3-45: Cross-section of the tube made of 2.25Cr-1Mo-V, pressurized with hydrogen. The observed welded joint experienced a strain of ~5%.

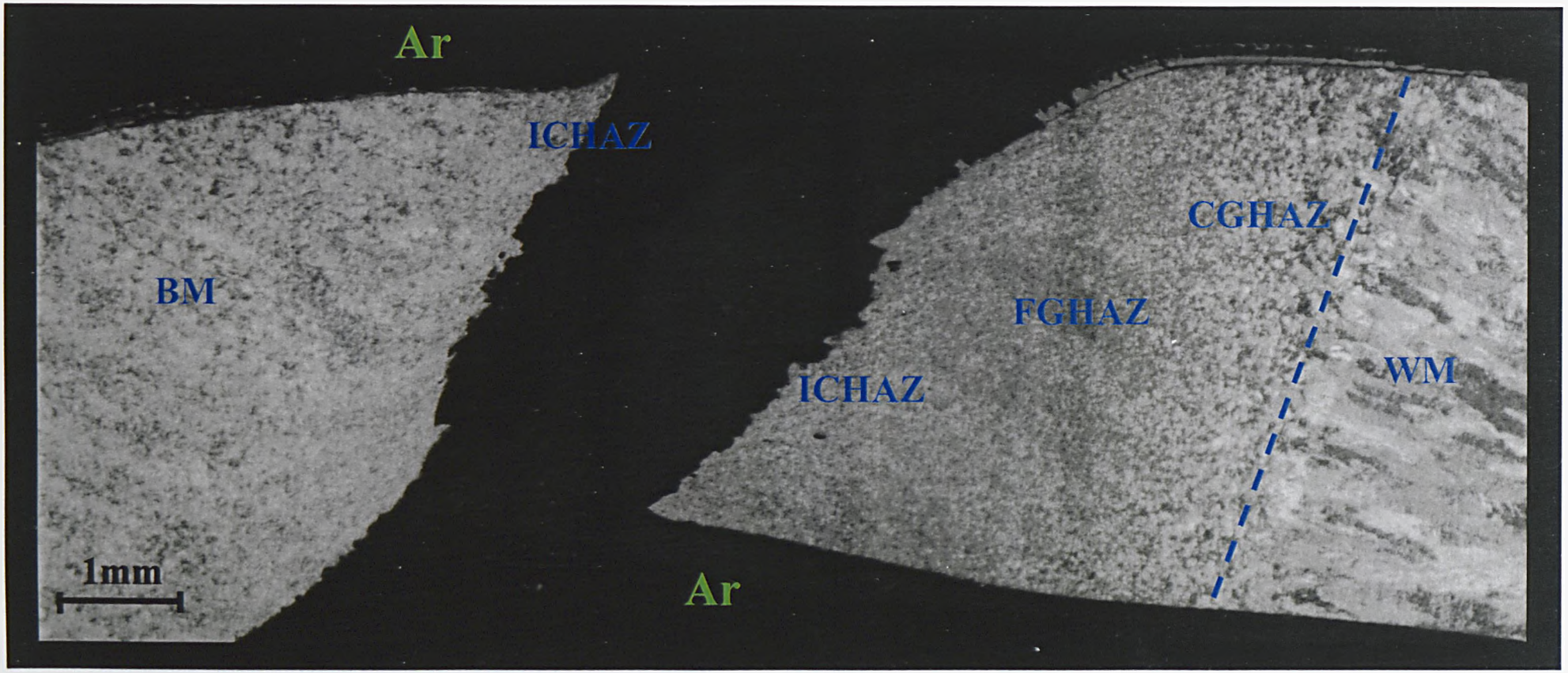

Figure 5.3-46: Cross-section of the tube pressurized with argon, at a temperature of 873K (600°C) and a pressure of 18MPa (180bars). The test lasted 900 hours and ended with the failure of the test piece in the ICHAZ.

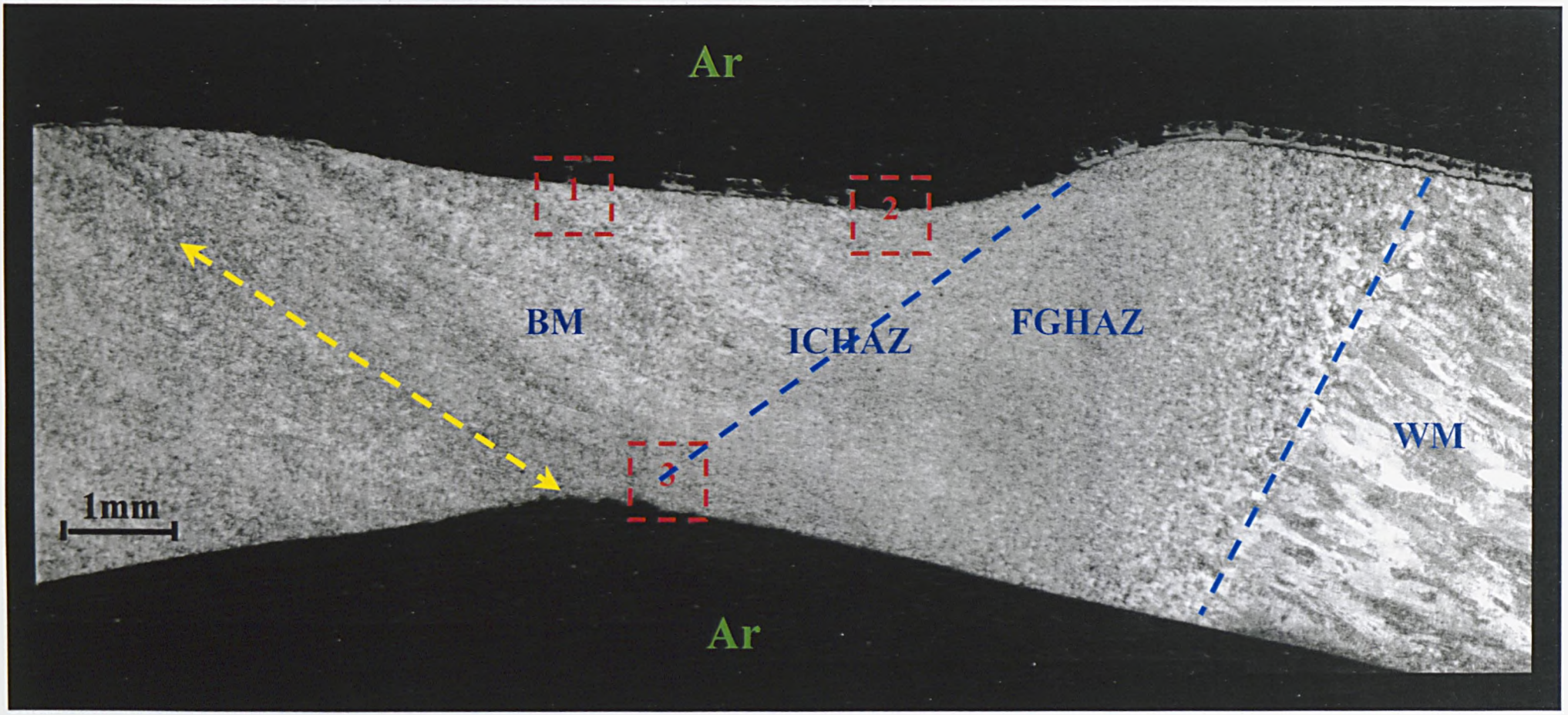

Figure 5.3-47: Cross-section extracted from part of the tube which experienced a radial strain of about 6%. The ICHAZ and the near base metal (BM) are the metallurgical zones which experience accumulation of strain. The areas enumerated as 1,2,3 are observed at higher magnification. The results are showed in the following figures.

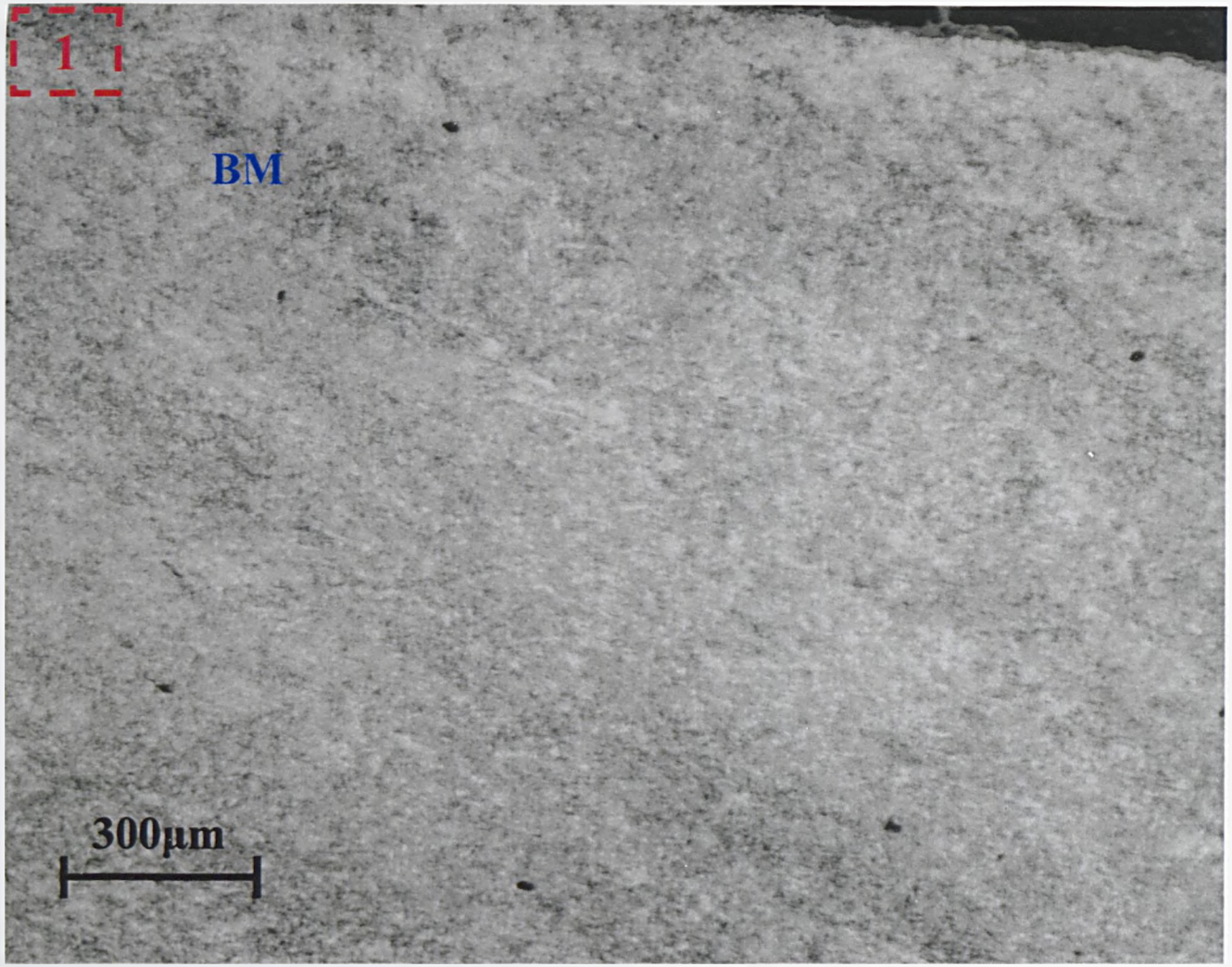

Figure 5.3-48: The base metal exhibits a light cavitation.

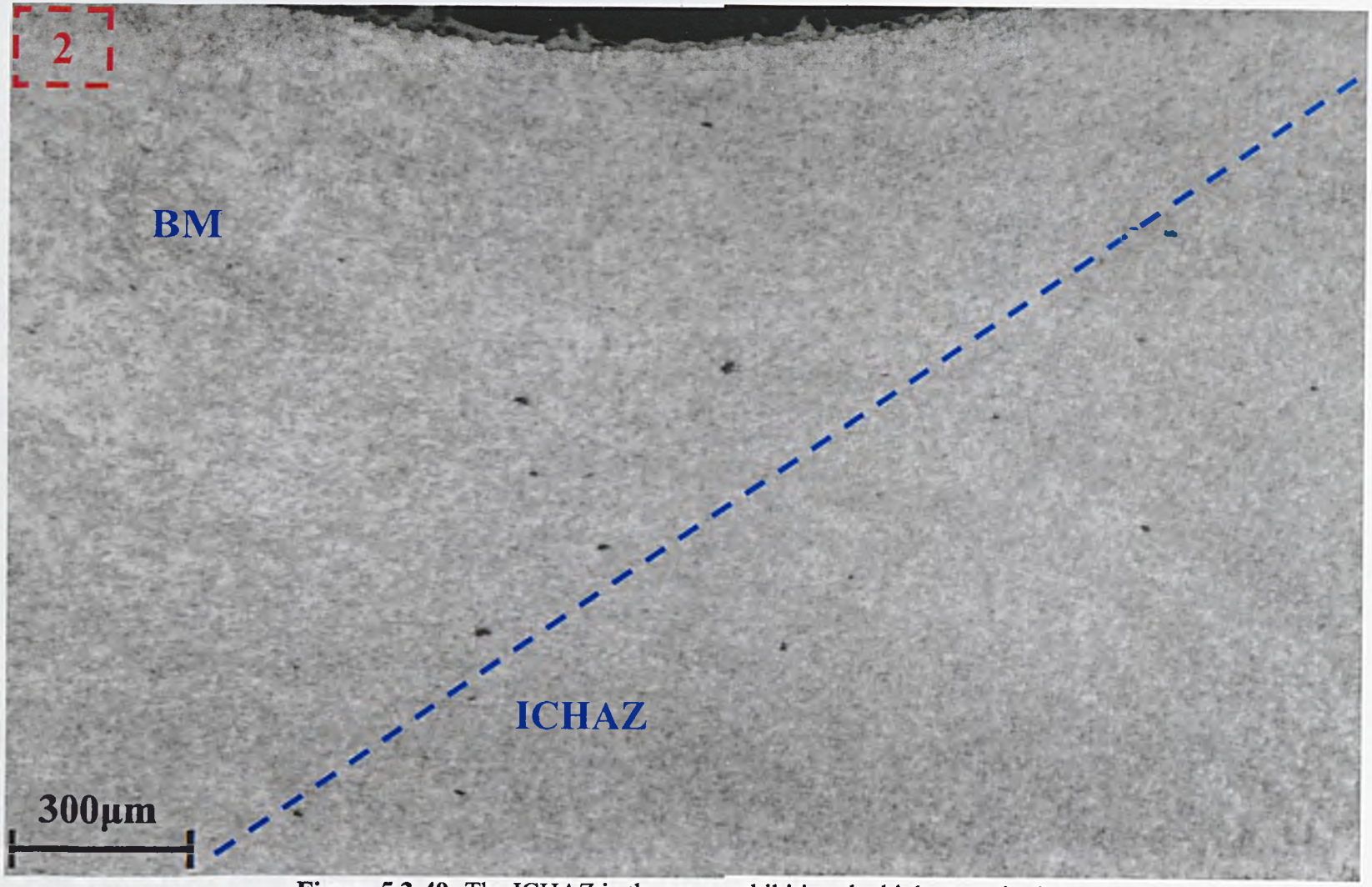

Figure 5.3-49: The ICHAZ is the zone exhibiting the highest cavitation.

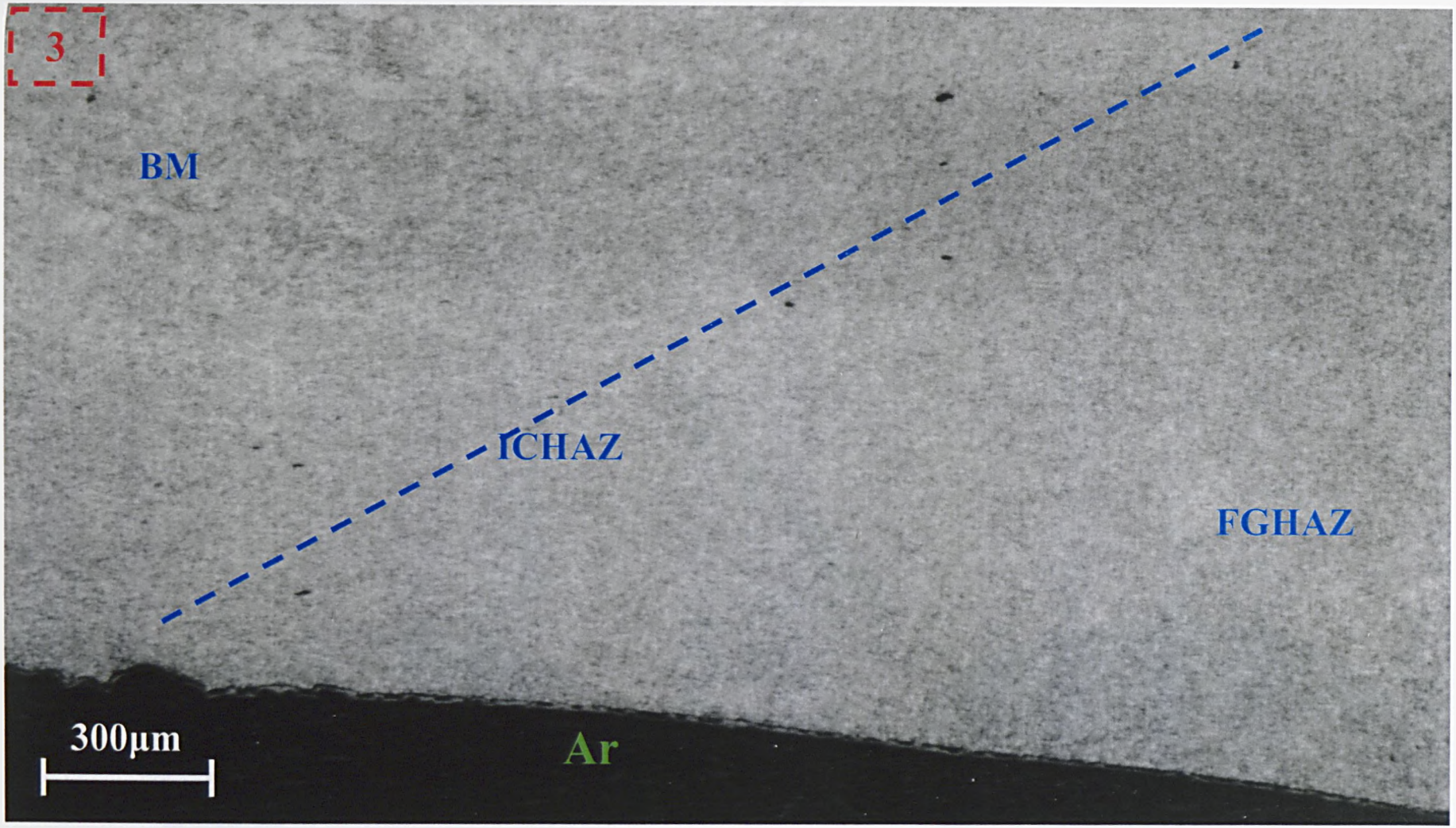

Figure 5.3-50: The ICHAZ close to the internal surface of the tube exhibits a cavitation lower than that of the ICHAZ in figure –49. Also the neighbouring BM and FGHAZ show very small traces of cavitation. The reason significantly might be the high strain that the welded joint experiences in this area.

Aims of the Investigation on Carbides

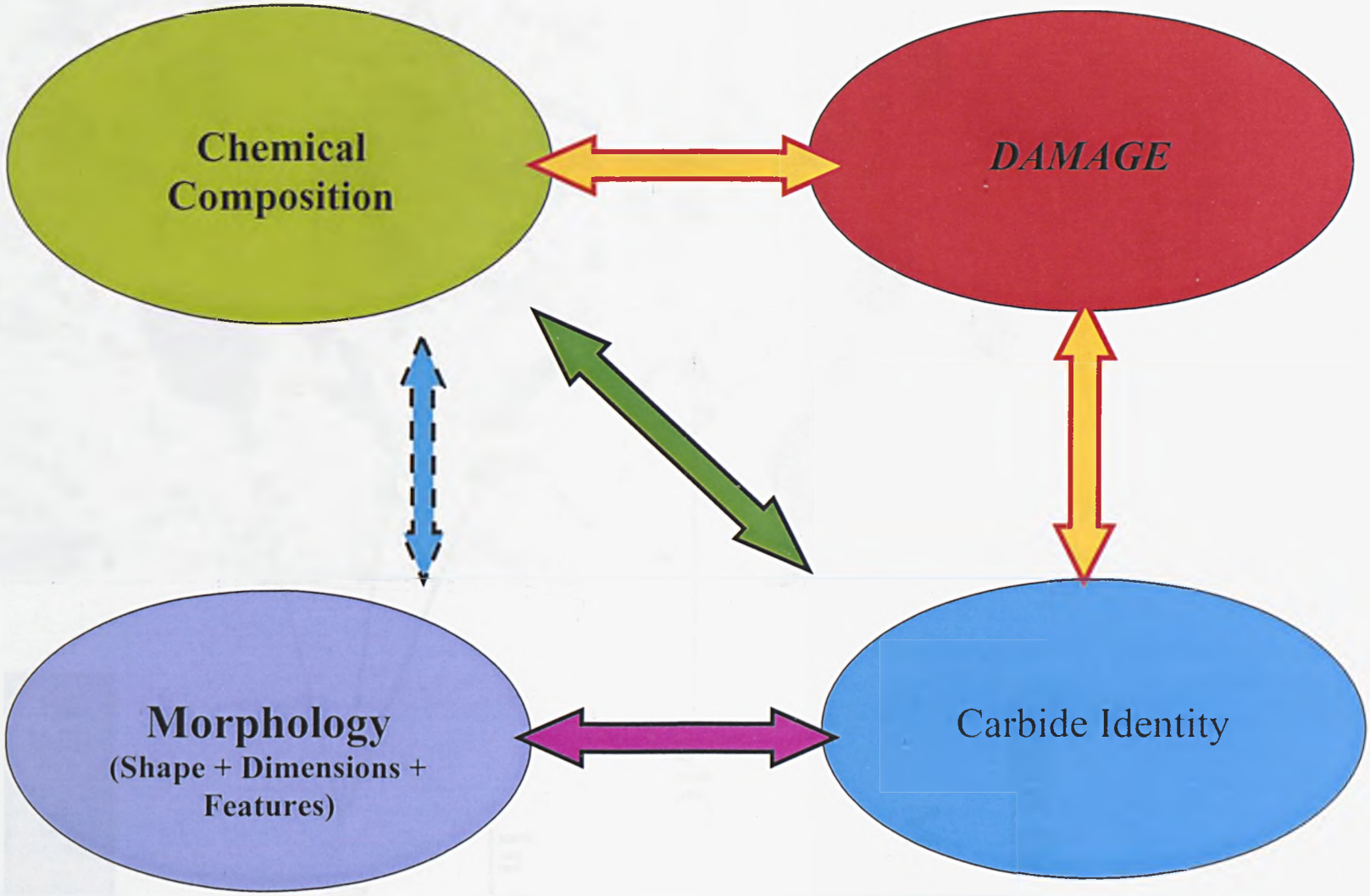

Figure 5.3-51: Schematic representation of the aims of the investigation on the carbides of the V-modified 2.25Cr-1Mo welded joint.

2.25Cr-1Mo-V - Base Metal

(Batch I – as received)

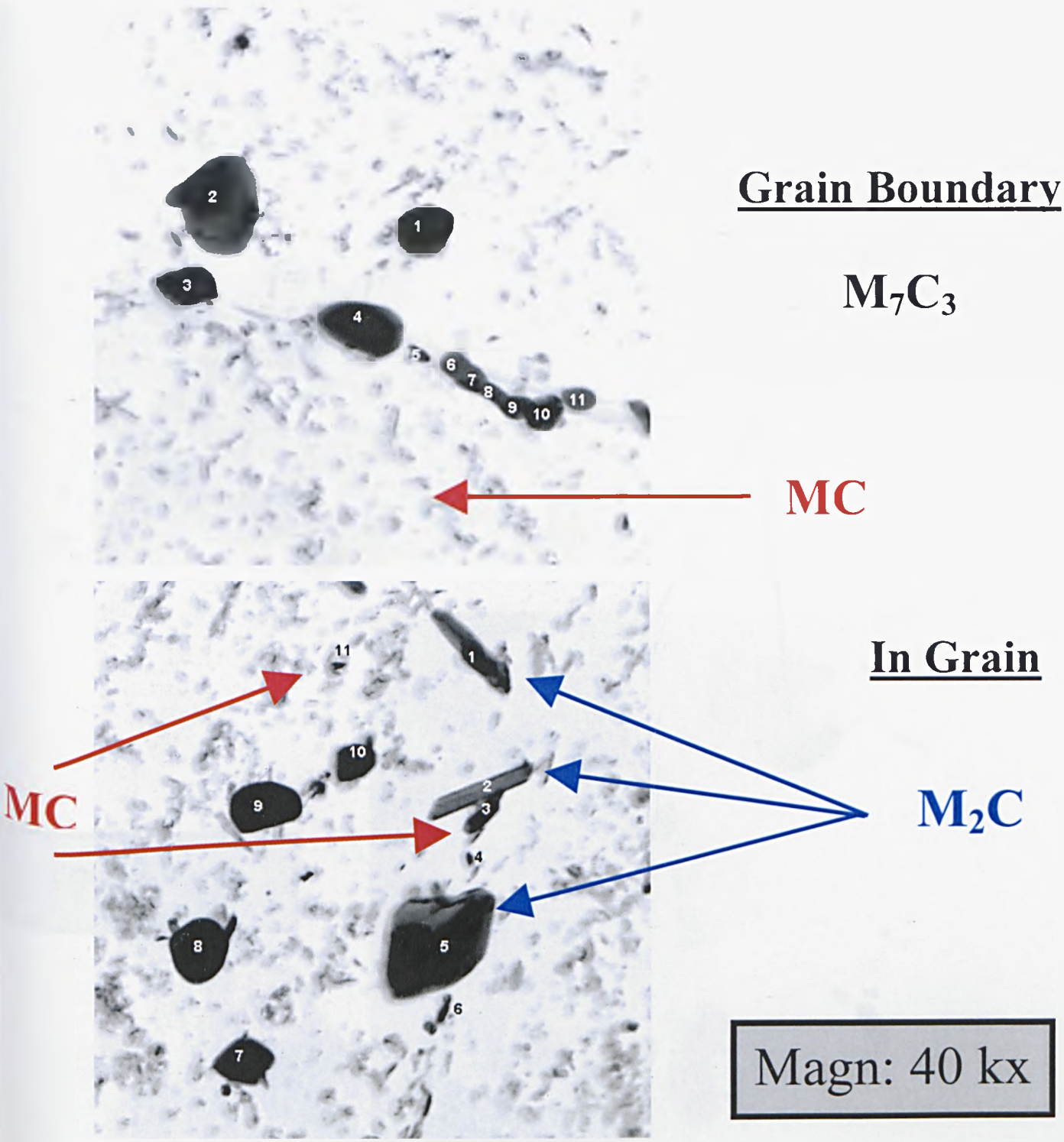

Figure 5.3-52: Carbides in the Base Metal.

2.25Cr-1Mo-V – FG-HAZ
(Batch I – as received)

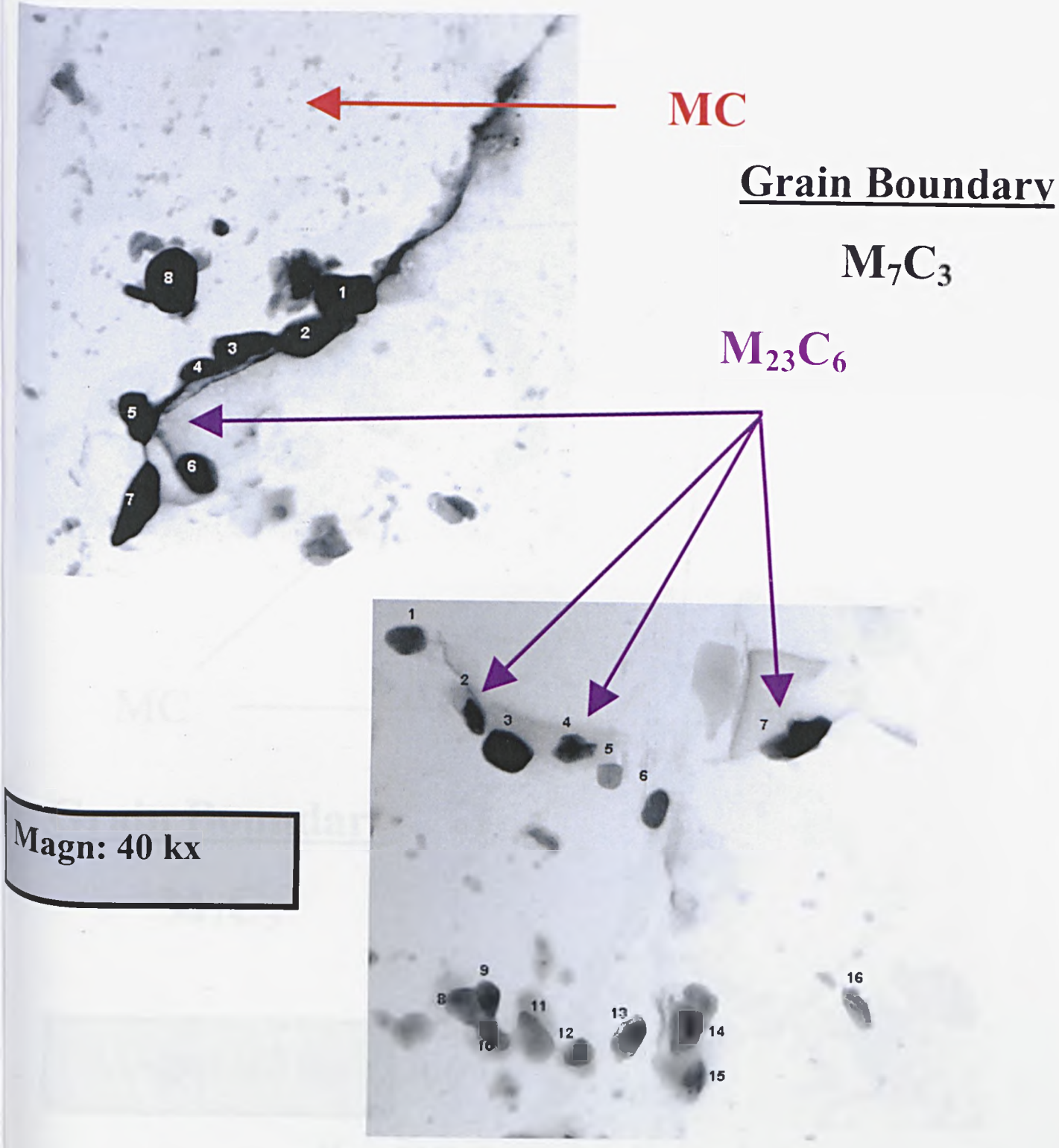

Figure 5.3-53: Carbides in the FGHAZ.

2.25Cr-1Mo-V - Weld Metal
(Batch I – as received)

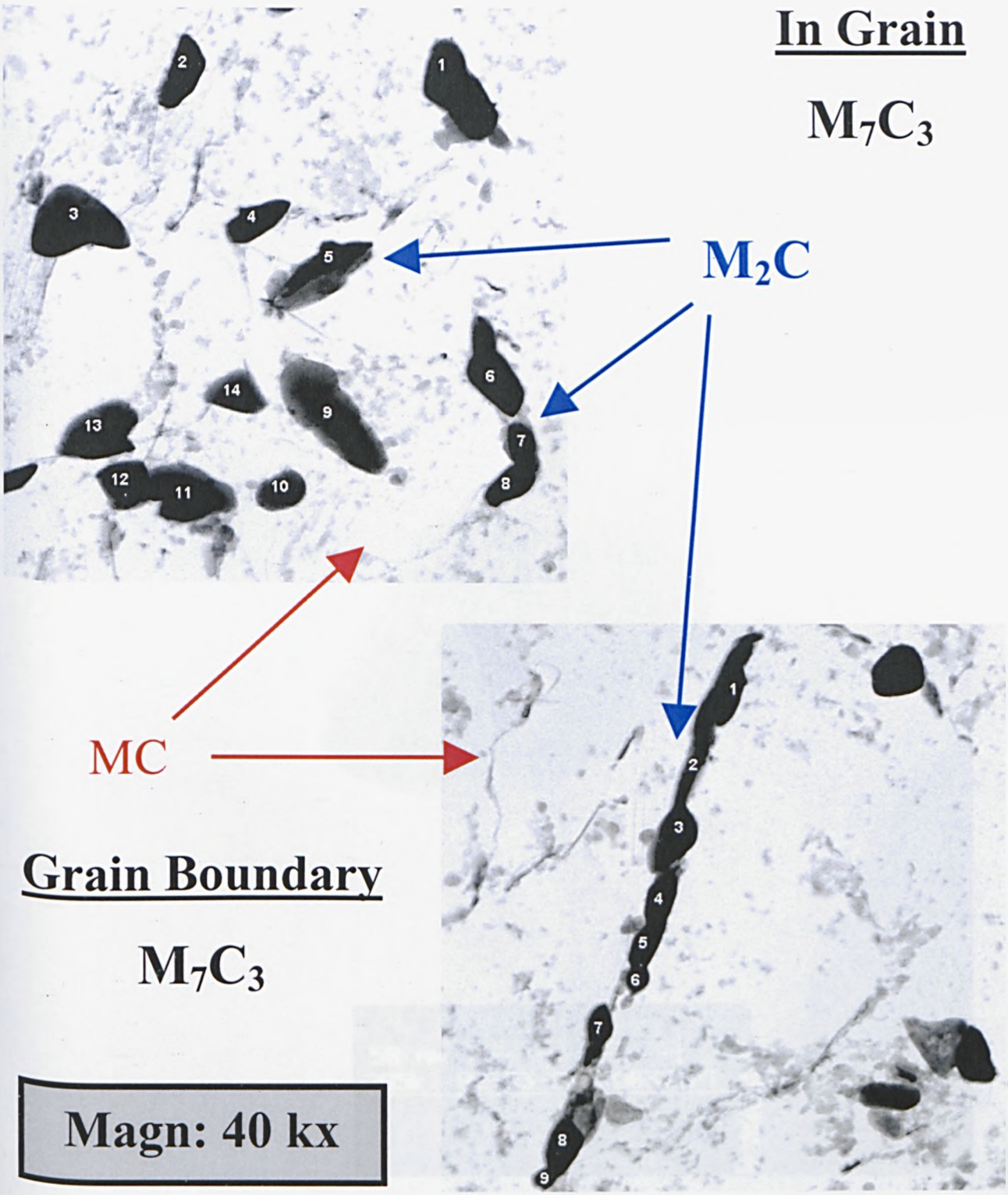

Figure 5.3-54: Carbides in the Weld Metal.

MC Carbide

Figure 5.3-55: Morphology of the MC-type carbide.

2.25Cr-1Mo-V (as received): Spectra of Carbides

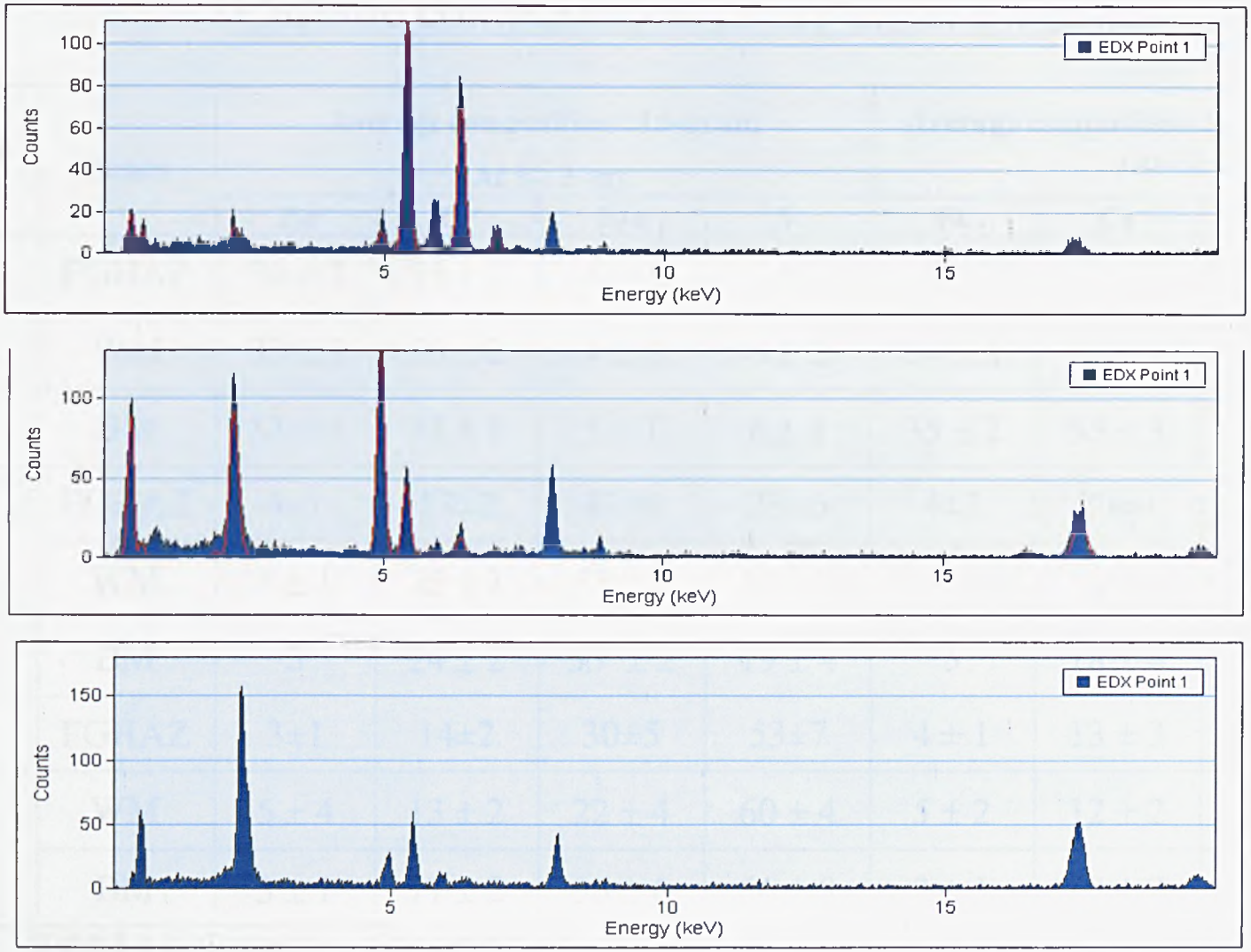

M_7C_3

M_2C

MC

Figure 5.3-56: Examples of EDS spectra for different types of carbides

2.25Cr-1Mo-V – (Batch 1, as received)
Carbide compositions in the different zones

Carbide type	Zones	Average composition : In-grain (At % ± σ)				Average composition : At grain boundary (At % ± σ)			
		Fe	Cr	Mo	V	Fe	Cr	Mo	V
M_7C_3	FGHAZ	34 ± 1	55 ± 1	4 ± 1	6 ± 1	35±2	55±2	4±1	6±2
	WM	33 ± 2	56 ± 2	4 ± 1	6 ± 2	34 ± 2	56 ± 2	4 ± 2	6 ± 2
	BM	33 ± 1	57 ± 1	5 ± 1	6 ± 1	35 ± 2	55 ± 3	5 ± 1	6 ± 1
M_2C	FGHAZ	4±1	17±2	47±4	33±6	4±2	20±4	46±6	30±7
	WM	4 ± 1	25 ± 3	53 ± 7	19 ± 6	3 ± 1	23 ± 6	58 ± 6	16 ± 3
	BM	3	24 ± 2	53 ± 2	19 ± 4	3	18 ± 4	55 ± 7	24 ± 7
MC	FGHAZ	3±1	14±2	30±5	53±7	4 ± 1	13 ± 3	32 ± 4	52 ± 5
	WM	5 ± 4	13 ± 2	22 ± 4	60 ± 4	5 ± 2	12 ± 2	32 ± 5	51 ± 5
	BM	3 ± 1	11 ± 2	30 ± 6	56 ± 8	3 ± 1	10 ± 2	33 ± 7	55 ± 8

Table 5.3-1: Composition of the carbides in the different metallurgical zones of the 2.25Cr-1Mo-V welded joint.

2.25Cr-1Mo-V: Microstructural Investigations

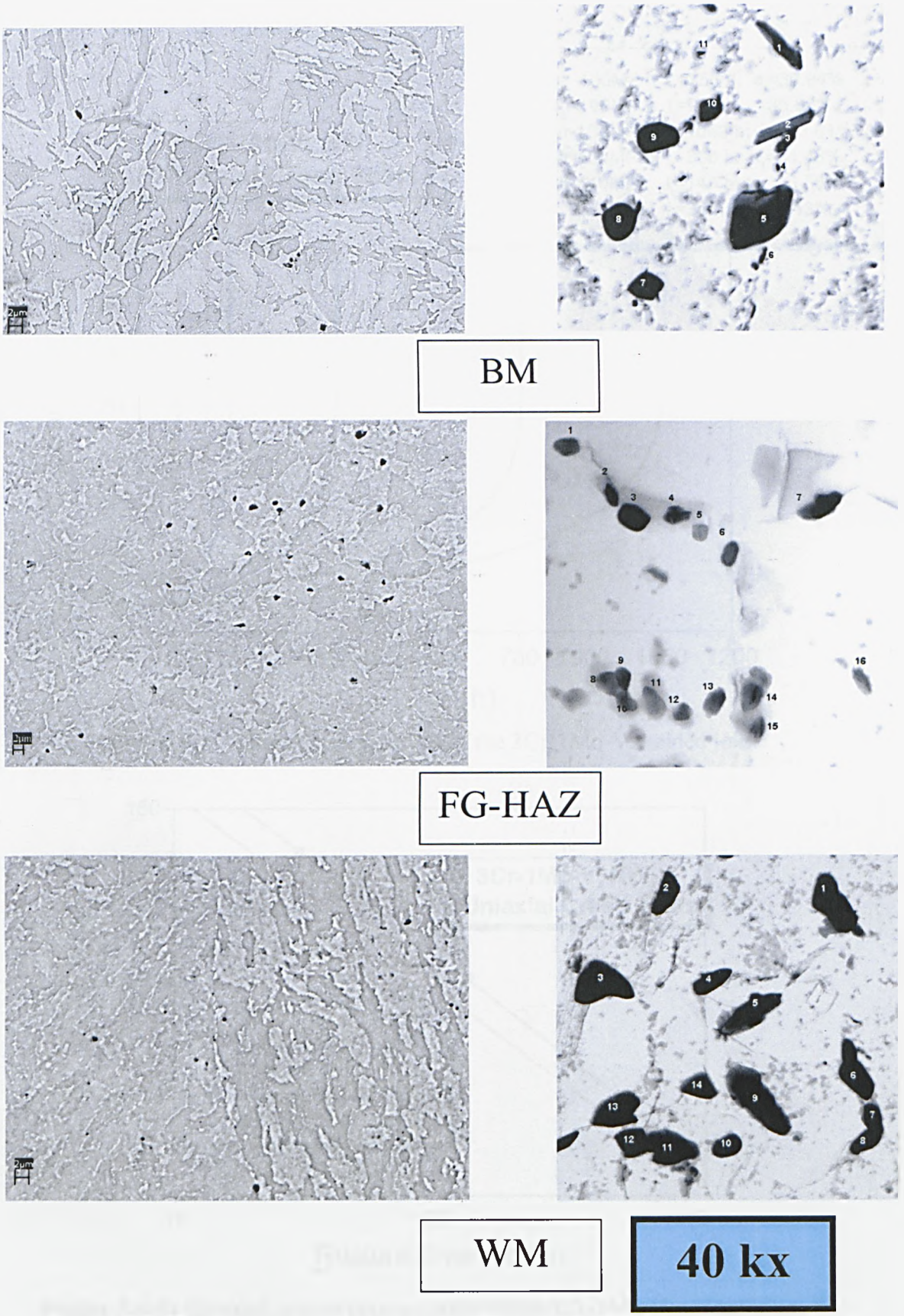

Figure 5.3-57 : Comparison between the SEM and the TEM results concerning the different metallurgical zones.

5.4 Testing of the 3Cr-1Mo-V Steel - Figures

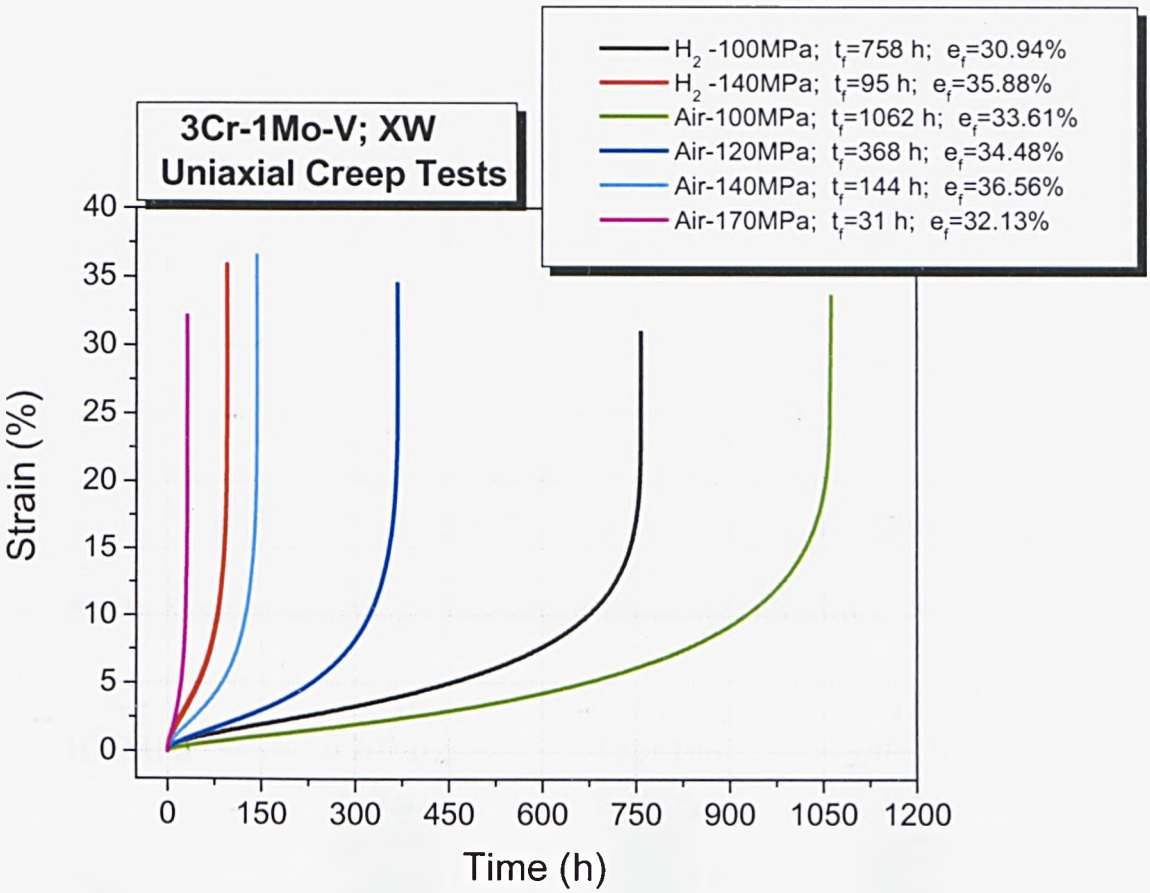

Figure 5.4-1: Uniaxial creep curves of the 3Cr-1Mo-V welded joint

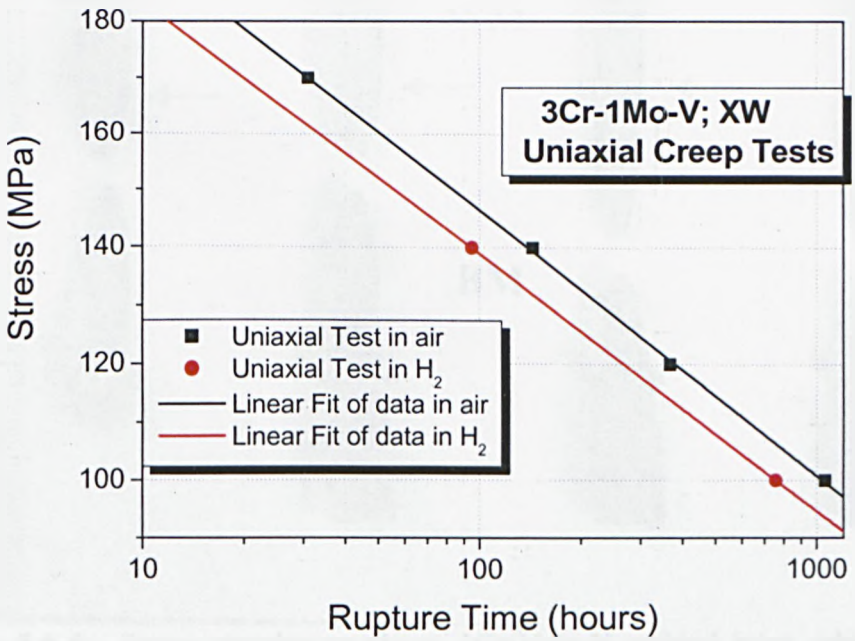

Figure 5.4-2: Uniaxial stress-rupture curves of the 3Cr-1Mo-V welded joint.

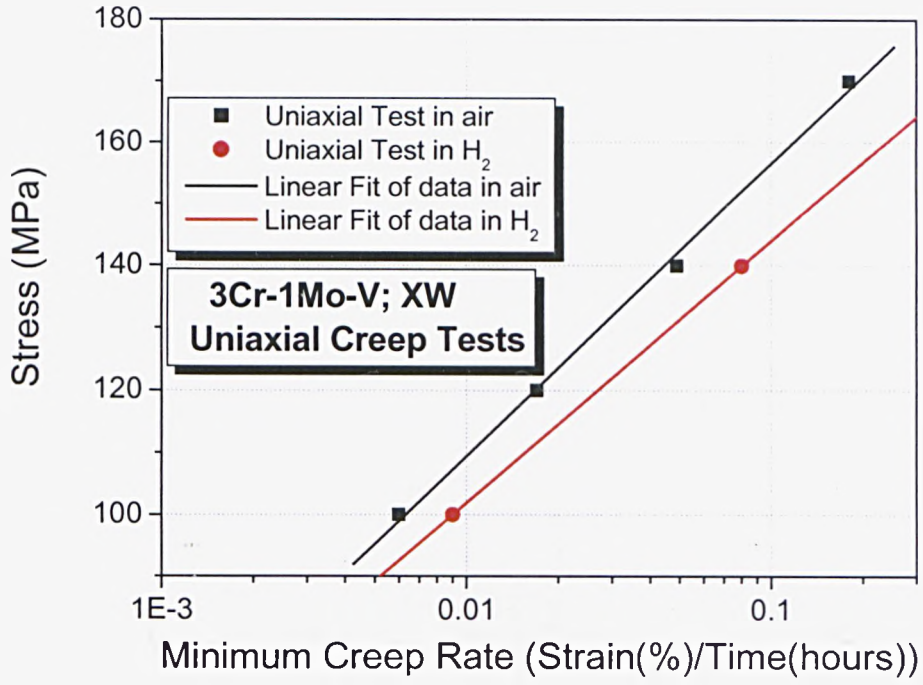

Figure 5.4-3: Stress vs minimum creep rate curves for the 3Cr-1MoV welded joint

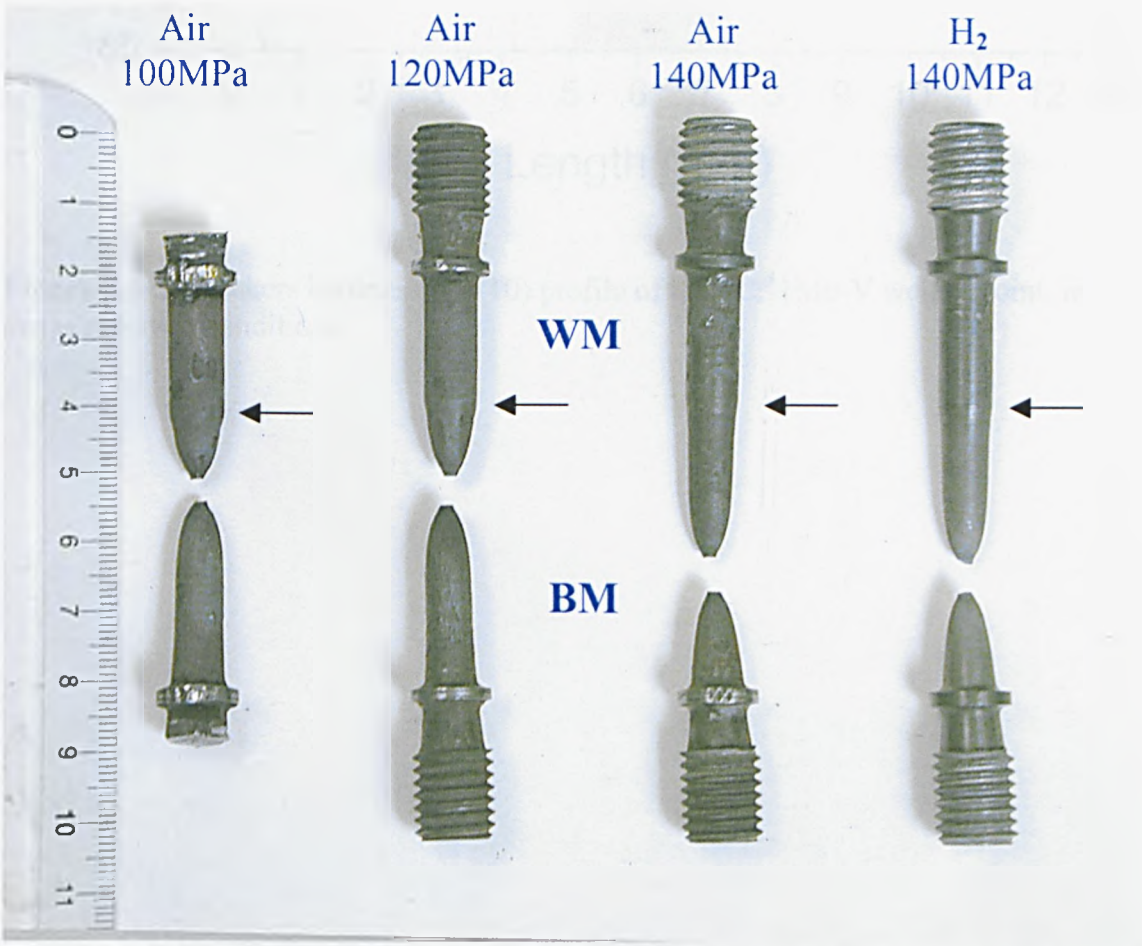

Figure 5.4-4: Some samples, made of 3Cr-1Mo-V welded joint, which underwent uniaxial creep testing. Immediately above the arrow there is the WM, below the BM and the arrow roughly indicates the HAZ, where the restriction starts to appear.

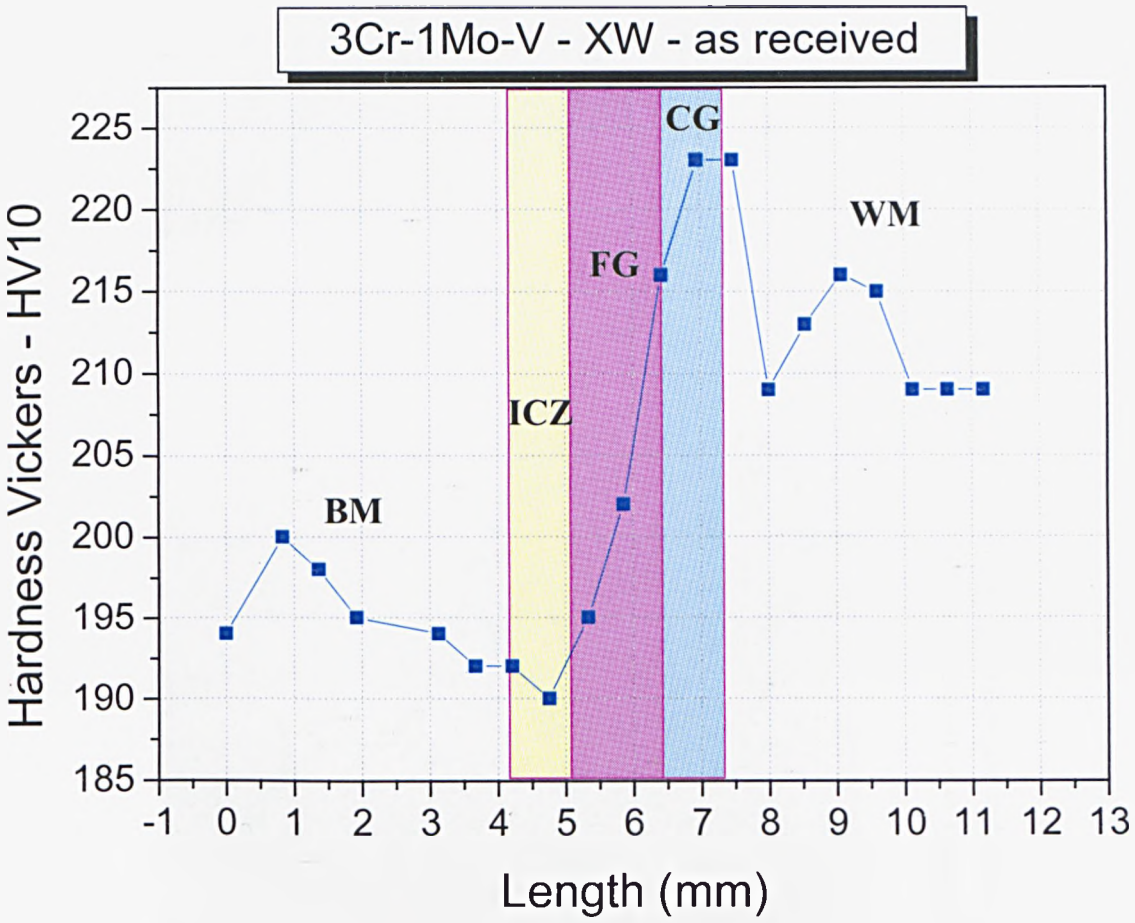

Figure 5.4-5: Vickers hardness (HV10) profile of the 3Cr-1Mo-V welded joint, in the as received conditions.

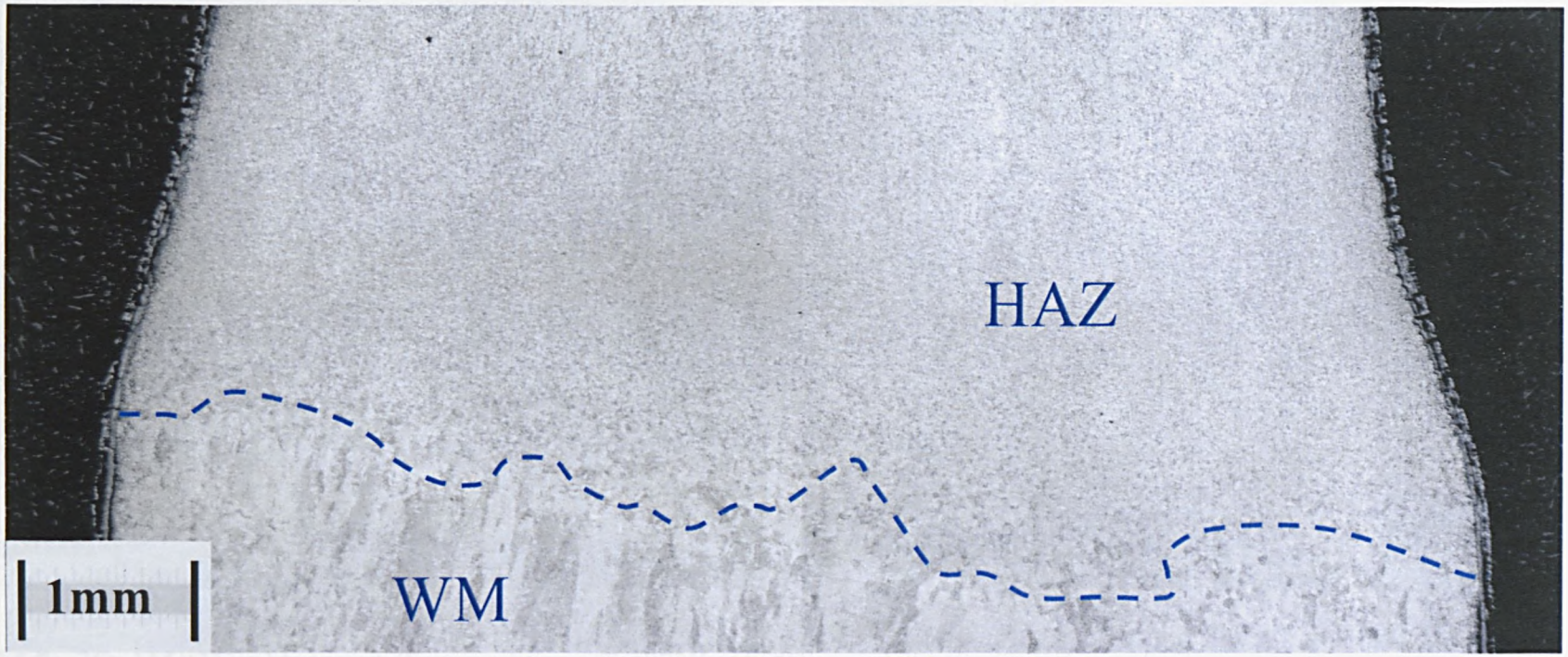

Figure 5.4-6: 3Cr-1Mo-V welded joint. Test conditions: T= 873K (600°C), σ = 100MPa (initial stress), Environment = air. No crack is detected in the weld metal (WM) and in the heat-affected zone (HAZ). The sample exhibits big reduction in area (RA) at fracture. The WM is the metallurgical zone that experiences the lowest reduction in area.

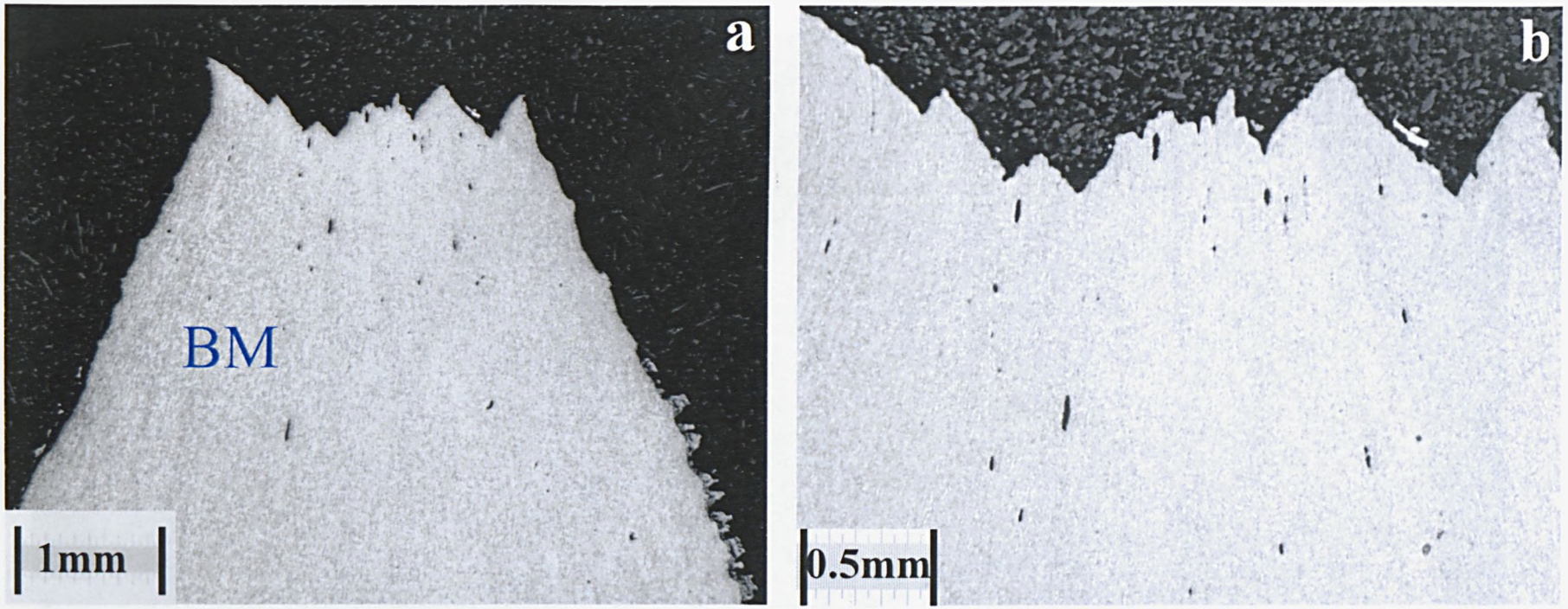

Figure 5.4-7: 3Cr-1Mo-V welded joint. Test conditions: T= 873K (600°C), σ = 100MPa (initial stress), Environment= air. The fracture happens in the base metal (BM) (Fig. **a**). The BM is the zone that experiences the more pronounced reduction in area. Rather close to the fracture surface are observed voids of large dimensions elongated in the direction of application of the stress. The fracture surface shows traces of wide and deep dimples (Fig **b**, detail of Fig **a**).

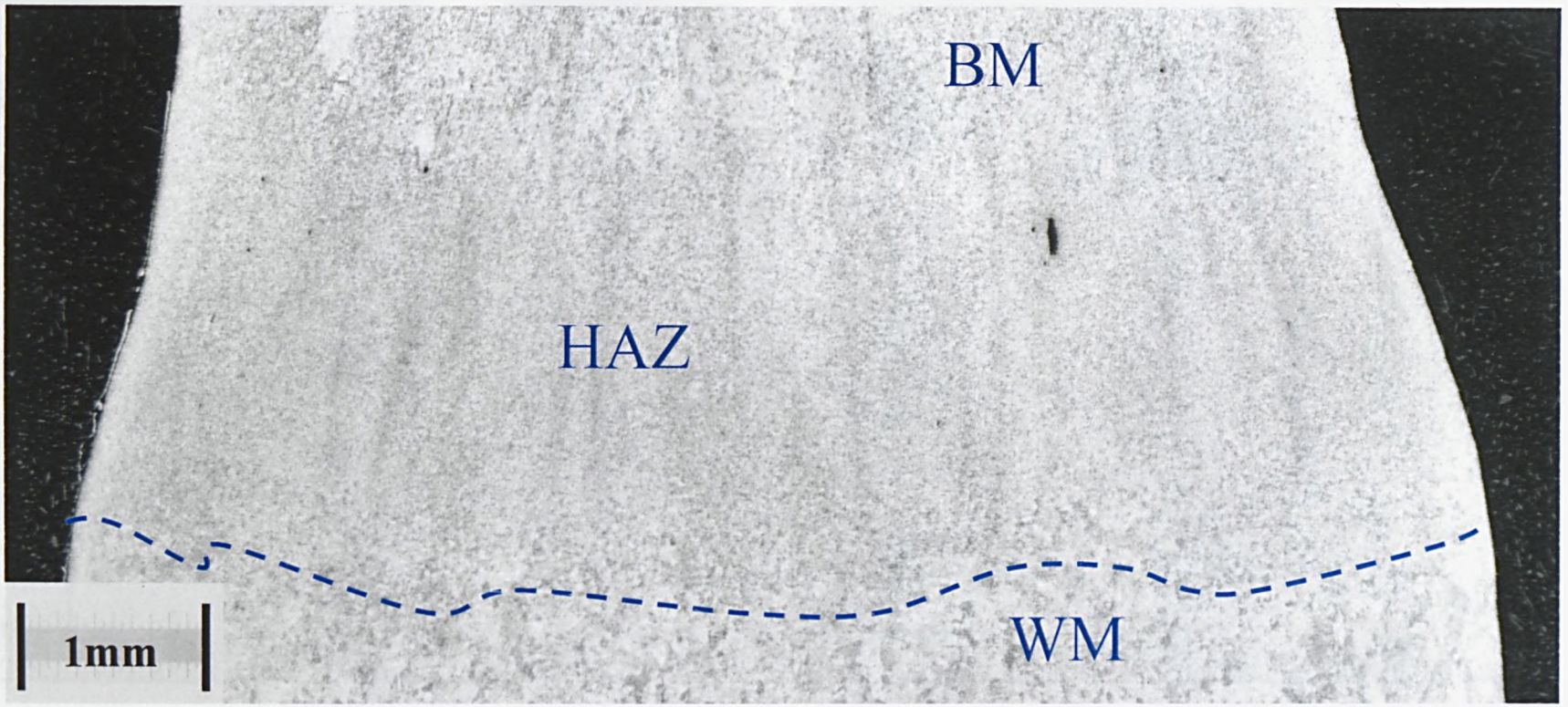

Figure 5.4-8: 3Cr-1Mo-V welded joint. Test Conditions: T= 600°C, σ = 100MPa, Environment= hydrogen, P = 180 bars. The welded joint tested in hydrogen, as the welded joint tested in air, does not present macroscopic fractures in the WM and in the HAZ. The WM is the zone which registers the lowest reduction in area.

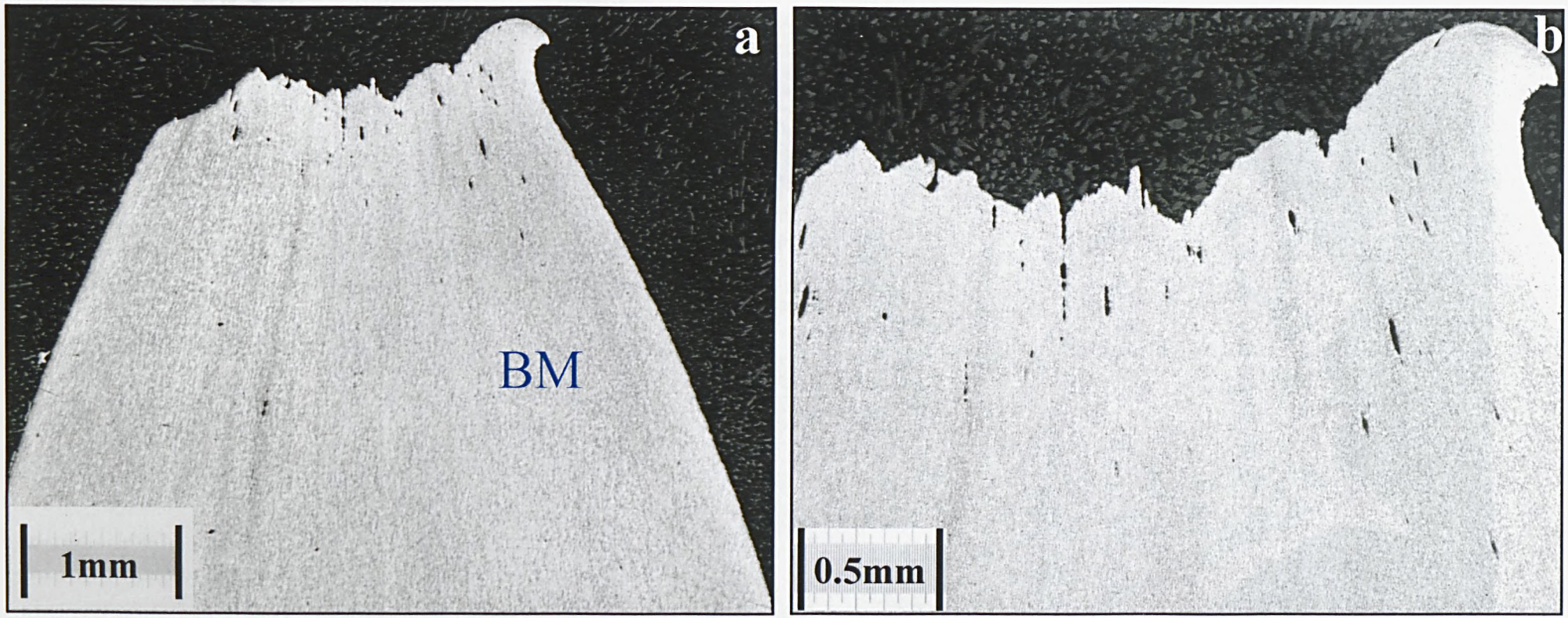

Figure 5.4-9: 3Cr-1Mo-V welded joint. Test conditions: T= 873K (600°C), σ = 100MPa (initial stress), Environment= hydrogen, P = 18MPa (180 bars). Analogously to the test in air, also in case of testing in hydrogen the failure is registered in the BM (Fig. **a**). Before of failing, the zone experiences high reduction in area. Also in this case are detected large voids, close to the fracture surface and elongated in the direction of the applied stress.

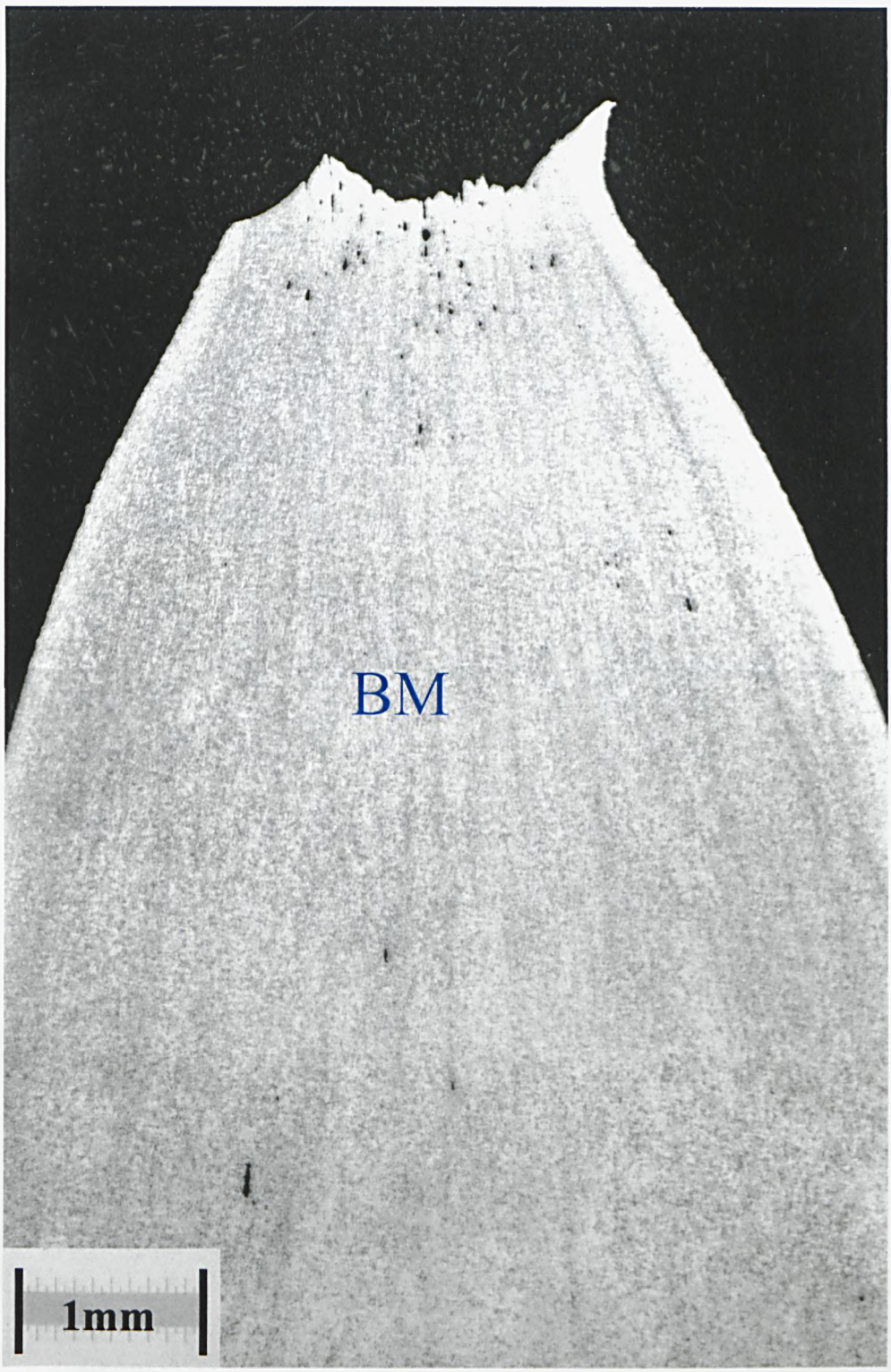

Figure 5.4-10: 3Cr-1Mo-V welded joint. Test conditions: T= 873K (600°C), σ = 100MPa (initial stress), hydrogen, P = 18MPa (180 bars). The figure gives an idea of the extent of the necking and of the elongation of the base metal (BM), before fracture.